MOSCOW CENTER
FOR DIAGNOSTICS & TELEMEDICINE

ISSN 2712-8490 (Print)
ISSN 2712-8962 (Online)

DIGITAL DIAGNOSTICS

A peer-reviewed scientific medical journal

4 Volume 3 Issue

2023

ECO•VECTOR
https://journals.eco-vector.com/DD

УЧРЕДИТЕЛИ
- ГБУЗ «Научно-практический клинический центр диагностики и телемедицинских технологий ДЗМ»
- ООО «Эко-Вектор»

Свидетельство о регистрации СМИ ПИ
№ ФС 77 - 74099 от 19.10.2018

ИЗДАТЕЛЬ
ООО «Эко-Вектор»
Адрес: 191186, Санкт-Петербург, Аптекарский переулок, д. 3, литера А, помещение 1Н
E-mail: info@eco-vector.com
WEB: https://eco-vector.com

РЕКЛАМА
Отдел рекламы
Тел.: +7 (968) 545 78 20
E-mail: adv2@eco-vector.com

РЕДАКЦИЯ
Зав. редакцией
Елена Андреевна Филиппова
E-mail: ddjournal@eco-vector.com
Тел: +7 (965) 012 70 72
Адрес: 127051, Москва, ул. Петровка, д. 24, стр. 1

ПОДПИСКА
Подписка на печатную версию через интернет:
www.journals.eco-vector.com/
www.akc.ru
www.pressa-rf.ru

OPEN ACCESS
В электронном виде журнал распространяется бесплатно —
в режиме немедленного открытого доступа

ИНДЕКСАЦИЯ
- SCOPUS
- РИНЦ
- Google Scholar
- Ulrich's International Periodicals Directory
- WorldCat

Оригинал-макет
подготовлен в издательстве «Эко-Вектор».
Литературный редактор: *М.Н. Шошина*
Корректор: *М.Н. Шошина*
Вёрстка: *Ф.А. Игнащенко*
Обложка: *Е.Д. Бугаенко*

Сдано в набор 04.09.2023.
Подписано в печать 12.09.2023. Формат 60 × 88⅛.
Печать офсетная. Печ. л. 25,5. Усл. печ. л. 23,7.
Уч.-изд. л. 13,9. Тираж 5000 экз. Заказ 3-7813-lv.
Цена свободная.

Отпечатано в ООО «Типография Фурсова».
196105, Санкт-Петербург, ул. Благодатная, 69.
Тел.: +7 (812) 646-33-77

16+

ISSN 2712-8490 (Print)
ISSN 2712-8962 (Online)

Digital Diagnostics

Том 4 | Выпуск 3 | 2023

ЕЖЕКВАРТАЛЬНЫЙ РЕЦЕНЗИРУЕМЫЙ НАУЧНЫЙ МЕДИЦИНСКИЙ ЖУРНАЛ

ЭКО • ВЕКТОР

FOUNDERS
- Moscow Center for Diagnostics and Telemedicine
- Eco-Vector

PUBLISHER
Eco-Vector
Address: 3 liter A, 1H, Aptekarsky pereulok, 191186, Saint Petersburg, Russian Federation
E-mail: info@eco-vector.com
WEB: https://eco-vector.com

ADVERTISE
Adv. department
Phone: +7 (968) 545 78 20
E-mail: adv2@eco-vector.com

EDITORIAL OFFICE
Executive editor
Elena A. Philippova
E-mail: ddjournal@eco-vector.com
Phone: +7 (965) 012 70 72

SUBSCRIPTION
For print version:
www.journals.eco-vector.com/

PUBLICATION ETHICS
Journal's ethic policies are based on:
- ICMJE
- COPE
- ORE
- CSE
- EASE

OPEN ACCESS
Immediate Open Access is mandatory for all published articles

INDEXATION
- SCOPUS
- Russian Science Citation Index
- Google Scholar
- Ulrich's International Periodicals Directory
- WorldCat

TYPESET
Completed in Eco-Vector
Copyeditor: *M.N. Shoshina*
Proofreader: *M.N. Shoshina*
Layout editor: *Ph. Ignashchenko*
Cover: *E. Bugaenko*

16+

ISSN 2712-8490 (Print)
ISSN 2712-8962 (Online)

Digital Diagnostics

Volume 4 | Issue 3 | 2023

QUARTERLY PEER-REVIEW MEDICAL JOURNAL

ECO•VECTOR

СОДЕРЖАНИЕ

CONTENTS

DOI: https://doi.org/10.17816/DD321971

Методология тестирования и мониторинга программного обеспечения на основе технологий искусственного интеллекта для медицинской диагностики

Ю.А. Васильев, А.В. Владзимирский, О.В. Омелянская, К.М. Арзамасов, С.Ф. Четвериков, Д.А. Румянцев, М.А. Зеленова

Научно-практический клинический центр диагностики и телемедицинских технологий, Москва, Российская Федерация

АННОТАЦИЯ

Обоснование. Мировая сумма инвестиций в компании по разработке программного обеспечения на основе технологий искусственного интеллекта для медицинской диагностики составила 80 млн долларов в 2016 году, 152 млн долларов — в 2017 и, ожидаемо, продолжает расти. Активная деятельность компаний-производителей программного обеспечения должна соответствовать существующим клиническим, биоэтическим, правовым и методологическим основам и стандартам. Как на национальном, так и на международном уровне не существует единых стандартов и протоколов проведения испытаний и мониторинга программного обеспечения на основе технологий искусственного интеллекта для медицинской диагностики.

Цель — разработать универсальную методологию тестирования и мониторинга программного обеспечения на основе технологий искусственного интеллекта для медицинской диагностики, направленную на повышение его качества и внедрение в практическое здравоохранение.

Материалы и методы. В ходе аналитического этапа был проведён обзор литературы по базам данных PubMed и eLIBRARY. Практический этап включал апробацию разработанной методологии в рамках Эксперимента по использованию инновационных технологий в области компьютерного зрения для анализа медицинских изображений и дальнейшего применения в системе здравоохранения города Москвы.

Результаты. Разработана методология тестирования и мониторинга программного обеспечения на основе технологий искусственного интеллекта для медицинской диагностики, направленная на повышение качества данного программного обеспечения и его внедрение в практическое здравоохранение. Методология состоит из 7 этапов: самотестирование, функциональное тестирование, калибровочное тестирование, технологический мониторинг, клинический мониторинг, обратная связь и доработка.

Заключение. Отличительными особенностями методологии являются цикличность этапов тестирования, мониторинга и доработки программного обеспечения, приводящие к постоянному повышению его качества, наличие подробных требований к результатам его работы, участие врачей в его оценке. Методология позволит разработчикам программного обеспечения достичь высоких результатов и продемонстрировать достижения в различных направлениях, а пользователям — сделать осознанный и уверенный выбор среди программ, прошедших независимую и всестороннюю проверку качества.

Ключевые слова: программное обеспечение; искусственный интеллект; рентгенология; диагностическая визуализация; методология; контроль качества.

Как цитировать:
Васильев Ю.А., Владзимирский А.В., Омелянская О.В., Арзамасов К.М., Четвериков С.Ф., Румянцев Д.А., Зеленова М.А. Методология тестирования и мониторинга программного обеспечения на основе технологий искусственного интеллекта для медицинской диагностики // *Digital Diagnostics.* 2023. Т. 4, № 3. С. 252–267. DOI: https://doi.org/10.17816/DD321971

Рукопись получена: 06.04.2023 **Рукопись одобрена:** 15.06.2023 **Опубликована:** 30.08.2023

DOI: https://doi.org/10.17816/DD321971

Methodology for testing and monitoring artificial intelligence-based software for medical diagnostics

Yuriy A. Vasilev, Anton V. Vladzymyrskyy, Olga V. Omelyanskaya, Kirill M. Arzamasov, Sergey F. Chetverikov, Denis A. Rumyantsev, Maria A. Zelenova

Moscow Center for Diagnostics and Telemedicine, Moscow, Russian Federation

ABSTRACT

BACKGROUND: The global amount of investment in companies developing artificial intelligence (AI)-based software technologies for medical diagnostics reached $80 million in 2016, rose to $152 million in 2017, and is expected to continue growing. While software manufacturing companies should comply with existing clinical, bioethical, legal, and methodological frameworks and standards, there is a lack of uniform national and international standards and protocols for testing and monitoring AI-based software.

AIM: This objective of this study is to develop a universal methodology for testing and monitoring AI-based software for medical diagnostics, with the aim of improving its quality and implementing its integration into practical healthcare.

MATERIALS AND METHODS: The research process involved an analytical phase in which a literature review was conducted on the PubMed and eLibrary databases. The practical stage included the approbation of the developed methodology within the framework of an experiment focused on the use of innovative technologies in the field of computer vision to analyze medical images and further application in the health care system of the city of Moscow.

RESULTS: A methodology for testing and monitoring AI-based software for medical diagnostics has been developed, aimed at improving its quality and introducing it into practical healthcare. The methodology consists of seven stages: self-testing, functional testing, calibration testing, technological monitoring, clinical monitoring, feedback, and refinement.

CONCLUSION: Distinctive features of the methodology include its cyclical stages of monitoring and software development, leading to continuous improvement of its quality, the presence of detailed requirements for the results of the software work, and the participation of doctors in software evaluation. The methodology will allow software developers to achieve significant outcomes and demonstrate achievements across various areas. It also empowers users to make informed and confident choices among software options that have passed an independent and comprehensive quality check.

Keywords: software; artificial intelligence; radiology; diagnostic imaging; methodology; quality control.

To cite this article:
Vasilev YuA, Vladzymyrskyy AV, Omelyanskaya OV, Arzamasov KM, Chetverikov SF, Rumyantsev DA, Zelenova MA. Methodology for testing and monitoring artificial intelligence-based software for medical diagnostics. *Digital Diagnostics.* 2023;4(3):252–267. DOI: https://doi.org/10.17816/DD321971

Received: 06.04.2023 **Accepted:** 15.06.2023 **Published:** 30.08.2023

DOI: https://doi.org/10.17816/DD321971

基于人工智能技术的医疗诊断软件测试和监测方法学

Yuriy A. Vasilev, Anton V. Vladzymyrskyy, Olga V. Omelyanskaya, Kirill M. Arzamasov, Sergey F. Chetverikov, Denis A. Rumyantsev, Maria A. Zelenova

Moscow Center for Diagnostics and Telemedicine, Moscow, Russian Federation

简评

论证。2016年，全球对基于人工智能技术开发医疗诊断软件的公司的投资额为8000万美元，2017年为1.52亿美元，并预料还将继续增长。软件公司的积极活动必须符合现有的临床、生物伦理、法律和方法学原理和标准。在国家和国际范围，基于人工智能技术的软件还没有统一的测试和监测标准和协议。

该研究的目的是开发一种通用方法，用于测试和监测基于人工智能技术的医疗诊断软件，以提高其质量和在实际医疗中的应用。

材料和方法。在分析阶段，对PubMed和eLIBRARY数据库进行了文献综述。实用阶段包括在《使用创新计算机视觉技术进行医学图像分析并进一步应用于莫斯科市医疗系统的实验》框架内批准所开发的方法学，并将其进一步应用于莫斯科的医疗保健系统。

结果。我们开发了一套基于人工智能技术的医疗诊断软件测试和监测方法学，旨在提高该软件的质量，并将其应用于实际医疗保健中。该方法学包括7个阶段：自我测试、功能测试、校准测试、技术监测、临床监测、反馈和改进。

结论。该方法学的显著特点是对软件进行周期性的监测和改进，从而不断提高其质量；对软件性能结果并医生参与软件评估提出详细要求。该方法学可使软件开发人员在各个领域取得优异成绩并展示成就，也可使用户在通过独立、全面质量控制的程序中做出明智、自信的选择。

关键词：软件；人工智能；放射学；诊断成像；方法学；质量控制。

引用本文：

Vasilev YuA, Vladzymyrskyy AV, Omelyanskaya OV, Arzamasov KM, Chetverikov SF, Rumyantsev DA, Zelenova MA. 基于人工智能技术的医疗诊断软件测试和监测方法学. *Digital Diagnostics.* 2023;4(3):252–267. DOI: https://doi.org/10.17816/DD321971

收到：06.04.2023 **接受：**15.06.2023 **发布日期：**30.08.2023

BACKGROUND

Global investment in developing software based on artificial intelligence (AI) technologies for medical diagnostics was $80 million in 2016 and $152 million in 2017; it is likely to grow continually [1]. In 2019, the Moscow government decided to conduct a large-scale scientific study (which is still ongoing in 2023) to evaluate the use of innovative computer vision technologies for analyzing medical images and further application in the Moscow healthcare system (hereinafter referred to as the Experiment).[1]

Software manufacturers must comply with current clinical, bioethical, legal, and methodological principles and standards [1]. According to Russian legislation, before using AI-based software in clinical practice, it must be legally approved as a medical device, which requires the software to receive a marketing authorization (MA) from the Federal Service for Surveillance in Healthcare (Roszdravnadzor).[2]

Before submission, the software should be assessed in technical and clinical studies to ensure that the specified functions are met.[3] However, due to particular aspects of AI-based software, such as a lack of user-friendly information regarding its operating process and decision-making principles, there are no uniform standards and test protocols for this purpose at the national and international levels [2]. The Food and Drug Administration (FDA) in the United States also establishes explicit criteria for evaluating and regulating AI-based software [1]. The inability to reliably confirm software compliance has negative consequences, including user distrust in the software, slower implementation in clinical practice, missing positive socioeconomic impacts from software, and slower overall development of the healthcare system [3].

After receiving an MA, post-marketing clinical monitoring should be performed to ensure the safety of using this software in clinical practice.[4] However, the present criteria apply to various medical devices and do not consider special aspects of AI-based software for medical diagnostics [4]. According to the Decision of the Board of the Eurasian Economic Commission, medical devices of the third risk class (including AI-based software) must be monitored annually for 3 year after acquiring an MA.[5] However, more frequent monitoring is required because of the high variability of medical data and the difficulty of predicting changes in environmental conditions, such as the epidemiological situation [5]. Monitoring enables the identification of critical remarks on the results of software operations that require software improvement, and, when the software is finalized, repeated testing and monitoring should be performed.

A retrospective cohort study is the most appropriate for evaluating AI-based medical diagnostics software [1]. This software evaluation method has several disadvantages, the most significant of which is a difference in the actual results of software operation in ideal and practical settings [1]. A common example is the negative experience of introducing the first computer-aided diagnostic system for mammography screening. Large-scale multicenter studies found that using this software increased breast cancer diagnosis by 2%–10% [6]. In 1998, the FDA approved the software for use in clinical practice. However, in real-world settings, this software did not achieve positive results. When interpreting mammography results, it even leads to a decrease in detection rate and an increase in false positive results [6]. The study suggested that radiologists with varying degrees of expertise used the new technology in different ways. More experienced specialists did not pay attention to it, whereas less experienced ones made mistakes due to a false sense of security. The second explanation is that the software was ineffective in detecting certain forms of cancer, which were not found in previous examinations [1].

Therefore, although ethical and legal problems are the most common with AI-based software, there is also an important methodological problem, which can be defined as a lack of universal and comprehensive methodology for testing and monitoring AI-based software for medical diagnostics to improve its quality and further implement it in clinical practice [7]. According to the above, it is important to develop such a methodology. The methodology will not replace the existing legal methods for assessing the safety and effectiveness of software but will exist independently and contribute to the likelihood of successful Roszdravnadzor approval of software. After receiving an MA, this methodology will help further assess and improve software for its effective implementation in clinical practice.

This study aims to develop a universal methodology for testing and monitoring AI-based software for medical diagnostics to improve its quality and implement it in clinical practice.

---

[1] Decree No. 1543-PP of the Moscow Government dated November 21, 2019 on conducting an experiment on the use of innovative technologies in computer vision for analyzing medical images and further application in the Moscow healthcare system. Link: https://docs.cntd.ru/document/563879961.

[2] Decree No. 1906 of the Government of the Russian Federation dated November 24, 2020 on amendments to the Rules for state registration of medical devices. Link: http://publication.pravo.gov.ru/Document/View/0001202011270010.

[3] Federal Law No. 323-FZ dated November 21, 2011. Basics of Health Protection of the Citizens in the Russian Federation. Article 38. Medical devices. Link: https://www.consultant.ru/document/cons_doc_LAW_121895/ddcfddbdbb49e64f085b65473218611b4bb6cd65/.

[4] Order No. 980n of the Ministry of Health of Russia dated September 15, 2020 on approval of the procedure for monitoring the safety of medical devices. Link: https://docs.cntd.ru/document/566006416.

[5] Decision No. 174 of the Board of the Eurasian Economic Commission dated December 22, 2015 on approval of the rules for monitoring the safety, quality, and effectiveness of medical devices. Link: https://www.alta.ru/tamdoc/15kr0174/.

MATERIALS AND METHODS

Study design

The presented methodology was developed by analyzing literature and personal experience.

Development of Methodology

The methodology was developed in two stages: analytical and practical.

To study existing methodologies, literature published in PubMed and eLIBRARY scientific libraries from 2018 to 2023 (the last 5 years) was reviewed using the search terms "methodology for evaluation AI in radiology" and "methodology for assessing AI in radiology." After assessing their relevance, papers were included in the analysis by reading the title and abstract. There were 22 papers [1–22] and five legal acts examined.[6]

Based on the Unified Radiological Information Network (ERIS) of the Unified Medical Information and Analytical System of Moscow (EMIAS), the methodology was tested during the Experiment on using innovative computer vision technologies for analyzing medical images and further application in the Moscow healthcare system. Some testing results are presented in this article as an illustration.

Statistical justification of sample sizes

The number of studies included in the sample was determined at different stages.

1. At the self-testing stage, the size of a data set is not regulated and varies depending on the clinical problem solved by the software.[7] The data sets used at the stages of self-testing, functional, and calibration testing are based on expert consensus data, with histological conclusions used in some cases (e.g., when assessing malignant neoplasms). The process of preparing data sets is described in detail in the corresponding regulations [19].
2. At the functional testing stage, the data set included five studies (based on GOST R 8.736-2011, multiple measurements require at least four measurements).[8] An expert's opinion is considered a true value. An expert is a healthcare professional who has been working as a specialist for more than 5 years and has been trained in AI-based software to describe examinations in the related field (a specific modality and target abnormality). This stage requires at least one technical specialist and one medical expert.
3. At the stage of calibration testing, the data set includes 100 studies with a 50/50 balance (50% of examinations with target abnormality and 50% without it) [20, 21].[9] At this stage, one technical specialist and one medical expert are required.
4. At the stage of technological monitoring, all examinations for the reporting period should be assessed by software for the presence of defects "a" and "b" (based on automated defect detection), with a sample of 80 examinations for defects "c" to "e" [20, 21].[10] At least one technical specialist is required at this stage.
5. At the stage of clinical monitoring, the data set includes 80 examinations, and an expert's opinion is considered the true value [20, 21].[11] At this stage, one expert is required.

Ethical review

This study was conducted as part of another study that had previously been approved by the local ethics committee (No. NCT04489992), "Experiment on the use of innovative technologies in computer vision for analyzing medical images and further application in the Moscow healthcare system" (Moscow experiment).

RESULTS

Based on the literature review, papers were found to describe individual stages of evaluating AI-based software for medical diagnostics, such as validation [1, 5, 8, 9], monitoring [10], implementation [7, 11–13], and regulation [14, 15]. However, there is no unified methodology for testing and monitoring AI-based software for medical diagnostics. There have been papers on the life cycle of AI-based software [16], but they are mainly related to nonmedical software and do not consider special aspects of AI-based software

---

[6] Decree No. 1543-PP of the Moscow Government of the Russian Federation dated November 21, 2019. Link: https://docs.cntd.ru/document/563879961.; Decree No. 1906 of the Government of the Russian Federation dated November 24, 2020. Link: http://publication.pravo.gov.ru/Document/View/0001202011270010.; Article 38 of Federal Law No. 323-FZ dated November 21, 2011. Link: https://www.consultant.ru/document/cons_doc_LAW_121895/); Order No. 980n of the Ministry of Health of Russia dated September 15, 2020. Link: https://docs.cntd.ru/document/566006416.; Order No. 134 of the Moscow Department of Health dated February 16, 2023 Link: https://mosmed.ai/documents/227/order_DZM__134_d_02/16/2023.pdf.

[7] Center for Diagnostics and Telemedicine. Official website. Data sets. Link: https://mosmed.ai/datasets/.

[8] GOST R 8.736-2011. National standard of the Russian Federation. State system for ensuring the uniformity of measurements. Multiple direct measurements. Methods for processing measurement results. Basic provisions. Link: https://docs.cntd.ru/document/1200089016.

[9] Order No. 134 of the Moscow Healthcare Department dated February 16, 2023 on approval of the procedure and conditions for conducting an experiment on the use of innovative technologies in computer vision for analyzing medical images and further Use in the Moscow Healthcare System. Link: https://mosmed.ai/documents/227/order_DZM__134_d_16.02.2023.pdf.

[10] Ibid.

[11] Ibid.

for medical diagnostics. Furthermore, there are guidelines for conducting research and writing scientific publications on AI-based software, but they do not assist with testing and monitoring software [17, 18]. It should be noted that no publications on software modification after testing and monitoring were found. However, software improvement is necessary to improve its quality and effective implementation in clinical practice.

As a result, the authors developed a methodology for testing and monitoring AI-based software for medical diagnostics to improve its quality and use in clinical practice. The methodology consists of seven stages, as shown in Figure 1. The purpose, primary actions, and results are described below for each stage.

Self-testing

The self-testing stage is intended to assess the technical compatibility of software with input data. Software developers (or suppliers) are provided access to an open data set containing files in the Digital Imaging and Communications in Medicine (DICOM) format with anonymized examples of diagnostic examinations.[12] The data set has the following parameters: modality, type of diagnostic procedure, manufacturer, and model of the diagnostic device [19].

Software compatibility with data enables software integration into a healthcare institution's radiology information network and continues with further evaluation, starting with the functional testing stage.[13]

Functional testing

Functional testing is a stage wherein software functions specified by a supplier are checked for availability and functionality. This testing is performed at the technical and clinical levels. On a technical level, the software is assessed based on the following criteria: prioritization of research (triage), availability of an additional series of images from the software, presence of the other series' name, presence of a graphical designation of software on the images of the different series, presence of a warning label "For research purposes only" on images and in DICOM SR, possibility of series synchronization, displaying the probability of abnormality, indication of the category of abnormality, and availability of complete DICOM SR protocol structure (Figures 2 and 3).

This part of functional testing should be performed by technical specialists in accordance with the basic functional requirements developed by the Moscow State Budgetary Institution "Scientific and Practical Clinical Center for Diagnostics and Telemedicine Technologies of the Moscow Department of Health" (Center for Diagnostics and Telemedicine).[14] The medical assessment of software functions should be performed by medical experts in accordance with basic diagnostic requirements developed by the Center for Diagnostics and Telemedicine.[15] Basic diagnostic requirements include criteria, such as mandatory and optional content of software response, format, and form of the submitted response. Basic functional and diagnostic requirements contain common requirements for all software

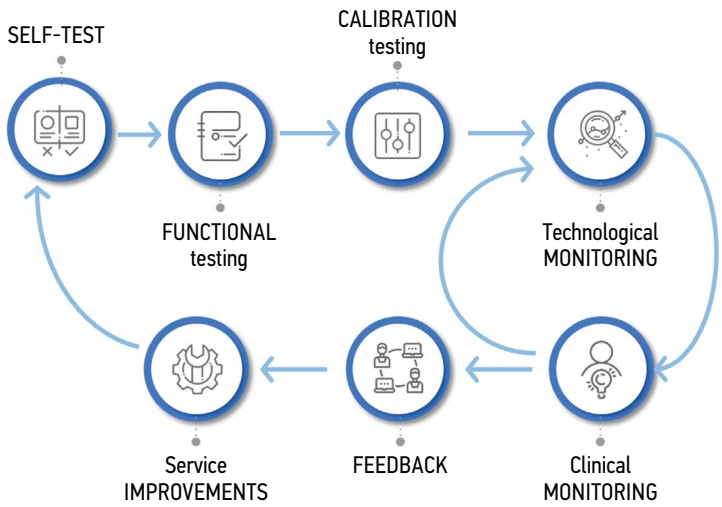

Fig. 1. Methodology for testing and monitoring artificial intelligence–based software for medical diagnostics.

[12] Center for Diagnostics and Telemedicine. Official website. Data sets. Link: https://mosmed.ai/datasets/.

[13] Order No. 134 of the Moscow City Health Department dated February 16, 2023 on approval of the procedure and conditions for conducting an experiment on the use of innovative technologies in computer vision for analyzing medical images and further use in the Moscow healthcare system. Link: https://mosmed.ai/documents/227/order_DZM__134_d_16.02.2023.pdf.

[14] Basic functional requirements for AI service results. Link: https://mosmed.ai/documents/218/Basic_functional_requirements_29.11.2022.pdf.

[15] Basic diagnostic requirements for AI service results. Link: https://mosmed.ai/documents/226/Basic_diagnostic_requirements_22_02_2023.pdf.

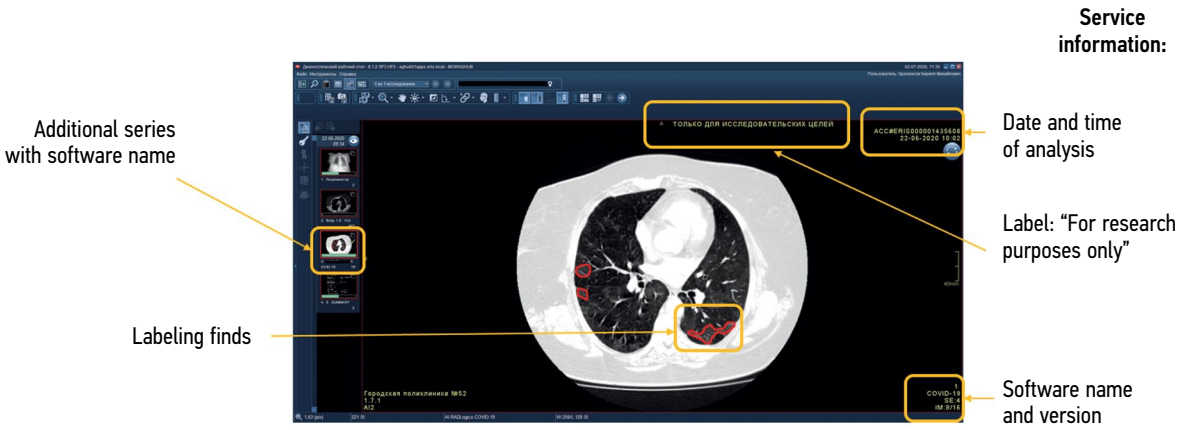

Fig. 2. Main components of the result of using artificial intelligence–based software with images: A reference example.

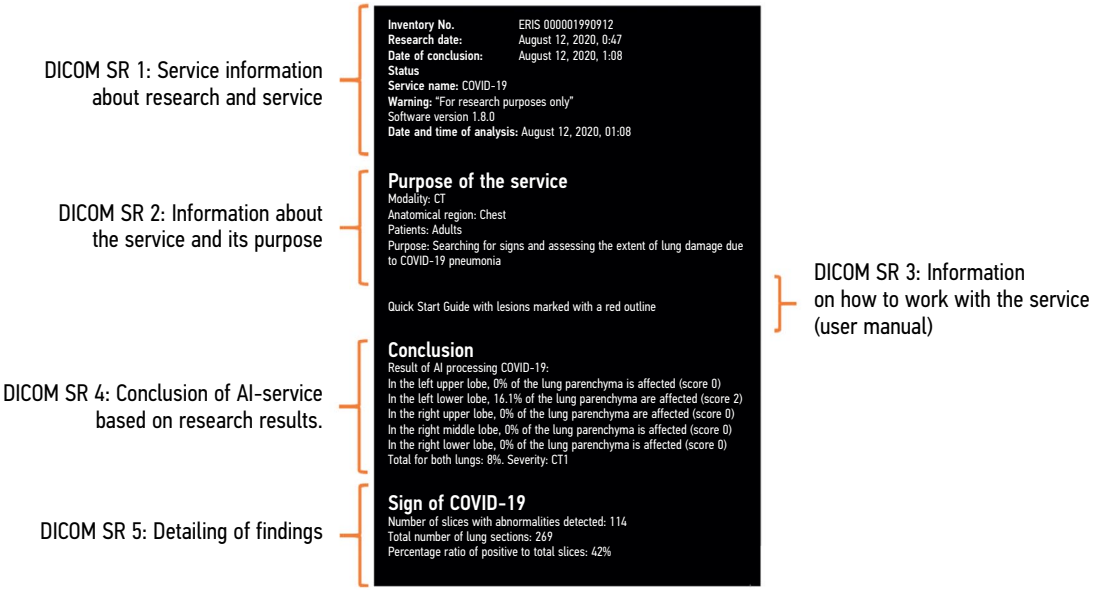

Fig. 3. Main components of the result of using artificial intelligence–based software with DICOM SR: A reference example.

and specific requirements based on the clinical task for which the software is designed.

If critical nonconformities are identified, software testing is stopped until the supplier eliminates their causes. Inconsistencies with basic functional requirements are critical because they negatively affect the HCP work processes and, directly or indirectly, the patient's life and health (Figures 4 and 5).

Functional testing should be repeated after the supplier has eliminated the causes of critical nonconformities. This stage may be repeated no more than twice by the applicant. There are no time limits for the initial retesting after receiving the protocol with unsatisfactory test results. The second retesting should be performed no earlier than 3 months after receiving the last protocol with unsatisfactory test results. If the second retest fails, the applicant may be provided an alternative scientific and practical cooperation option.[16] If no critical inconsistencies are found, the software moves to the calibration testing stage.[17]

Calibration testing

Calibration testing is a stage wherein the diagnostic accuracy of software is determined. The main parameter is the area under the ROC curve (AUC). The optimal value of the activation threshold is determined by examining the ROC curve using Youden's J statistic and maximizing the negative and positive predictive value. Other metrics include sensitivity, specificity, accuracy, and positive and negative

[16] Order No. 134 of the Moscow City Health Department dated February 16, 2023 on approval of the procedure and conditions for conducting an experiment on the use of innovative technologies in computer vision for analyzing medical images and further use in the Moscow healthcare system. Link: https://mosmed.ai/documents/227/order_DZM__134_d_16.02.2023.pdf.

[17] Ibid.

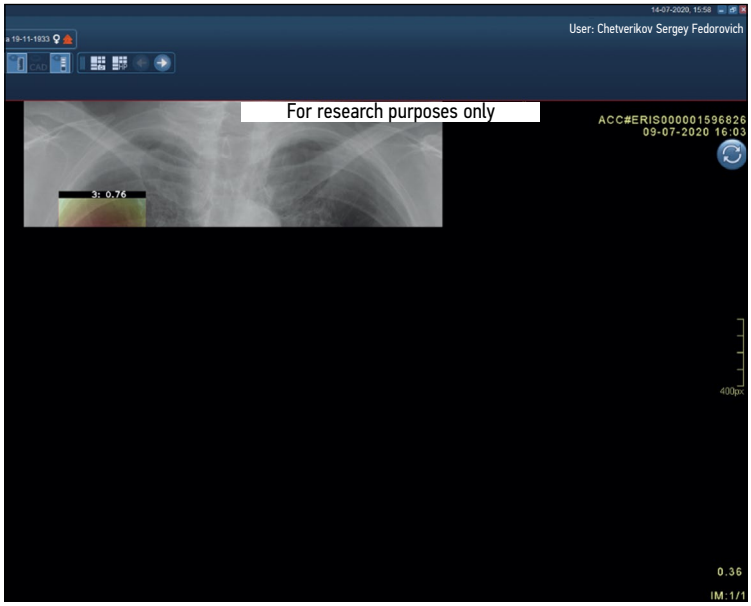

Fig. 4. Image clipping of additional series of artificial intelligence–based software: Critical noncompliance with basic functional requirements.

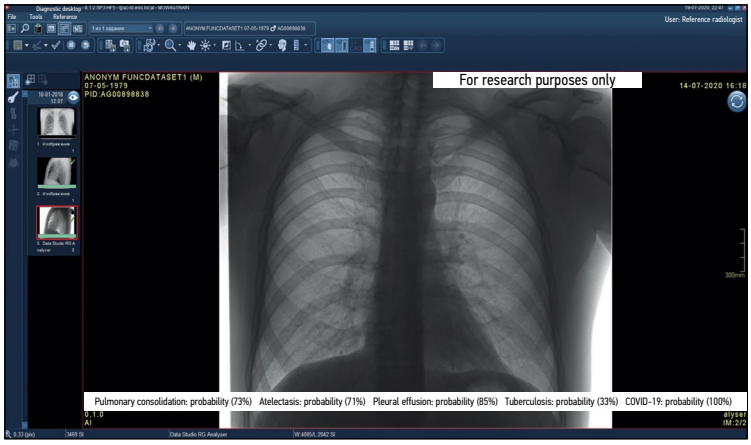

Fig. 5. Overlaying caption texts on images: Critical noncompliance with basic functional requirements.

predictive values. The minimum, average, and maximum time required to analyze one examination are also determined, and numbers of true positive, false negative, false positive, and true negative results are presented as a four-field table. Threshold values for some parameters are as follows: AUC ⩾0.81 or 0.91 (depending on the clinical task); time spent on acceptance, processing of the study, and transmission of analysis results ⩽6.5 min; and percentage of successfully processed examinations ⩾90% [21].[18]

Calibration testing results in a calibration protocol (Figure 6), which may contain critical and noncritical inconsistencies. Noncompliance with the above threshold values and significant deviations from methodological recommendations are considered crucial [21]. If they are identified, software testing is stopped until they are eliminated. In their absence, the software may proceed to a prospective examination analysis as part of the periodic monitoring stage, which includes technological and clinical monitoring.[19]

Technological monitoring

Technological monitoring is a stage involving a periodic technical check of software results. This stage is required for rapid defect identification, timely quality control, and the prevention of functional software errors in radiology practice. Defects that can be identified at this stage are divided into the following groups:

(a) the processing time for one study exceeds 6.5 min,

[18] Order No. 134 of the Moscow City Health Department dated February 16, 2023 on approval of the procedure and conditions for conducting an experiment on the use of innovative technologies in computer vision for analyzing medical images and further use in the Moscow healthcare system. Link: https://mosmed.ai/documents/227/order_DZM__134_d_16.02.2023.pdf.

[19] Ibid.

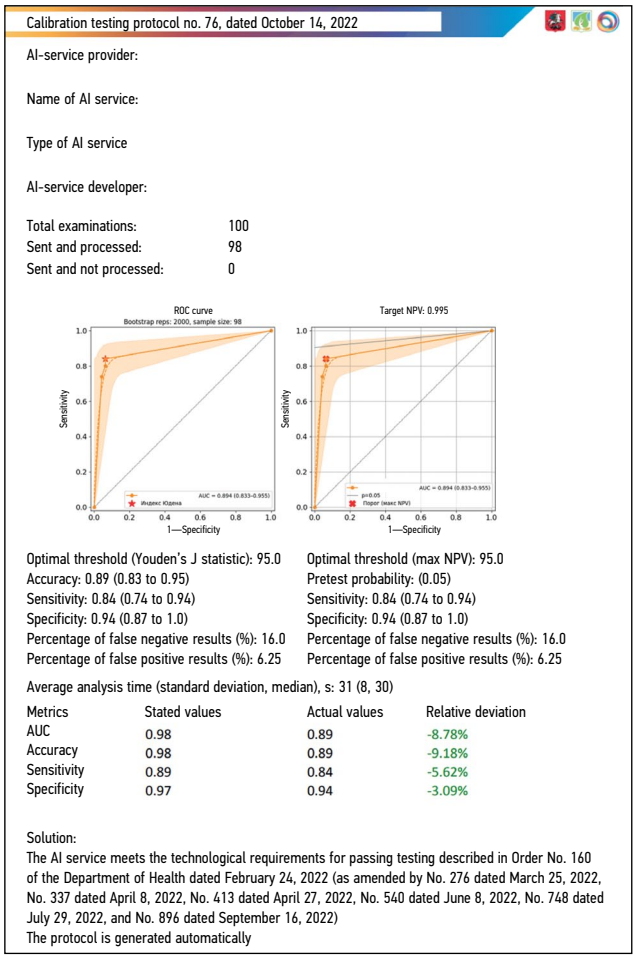

Calibration testing protocol no. 76, dated October 14, 2022

AI-service provider:

Name of AI service:

Type of AI service

AI-service developer:

Total examinations: 100
Sent and processed: 98
Sent and not processed: 0

Optimal threshold (Youden's J statistic): 95.0
Accuracy: 0.89 (0.83 to 0.95)
Sensitivity: 0.84 (0.74 to 0.94)
Specificity: 0.94 (0.87 to 1.0)
Percentage of false negative results (%): 16.0
Percentage of false positive results (%): 6.25

Optimal threshold (max NPV): 95.0
Pretest probability: (0.05)
Sensitivity: 0.84 (0.74 to 0.94)
Specificity: 0.94 (0.87 to 1.0)
Percentage of false negative results (%): 16.0
Percentage of false positive results (%): 6.25

Average analysis time (standard deviation, median), s: 31 (8, 30)

Metrics	Stated values	Actual values	Relative deviation
AUC	0.98	0.89	-8.78%
Accuracy	0.98	0.89	-9.18%
Sensitivity	0.89	0.84	-5.62%
Specificity	0.97	0.94	-3.09%

Solution:
The AI service meets the technological requirements for passing testing described in Order No. 160 of the Department of Health dated February 24, 2022 (as amended by No. 276 dated March 25, 2022, No. 337 dated April 8, 2022, No. 413 dated April 27, 2022, No. 540 dated June 8, 2022, No. 748 dated July 29, 2022, and No. 896 dated September 16, 2022)
The protocol is generated automatically

Fig. 6. Example of a calibration test protocol.

(b) a lack of results from the examinations reviewed,
(c) incorrect operation of the declared software functions, complicating the work of a radiologist or making it impossible to perform it with proper quality,
(d) defects associated with the display of the image area, and
(e) other violations of the integrity and contents of files containing research results, limiting diagnostic interpretation.

Defects "a" and "b" are monitored automatically for all examinations reviewed by software during the reporting period. For defects "c" and "d," semi-automatical monitoring is used with a sample of 80 examinations. An internal report form for monitoring software operation with instructions for monitoring technological defects has been developed for accurate defect assessment (Figure 7). Figure 8 shows graphical information on the average number of technological defects for the "chest radiography" area, with a tendency for the number of defects to decrease.

A technological monitoring report is the deliverable of technological monitoring (Figure 9). If the percentage of detected defects exceeds 10%, then testing this software is suspended until the causes of the defects are eliminated. If the percentage of detected defects does not exceed 10%, then the operation of the software and its periodic monitoring continue.[20]

Clinical monitoring

During periodic monitoring, a clinical assessment of software results is also performed by radiologists. Two

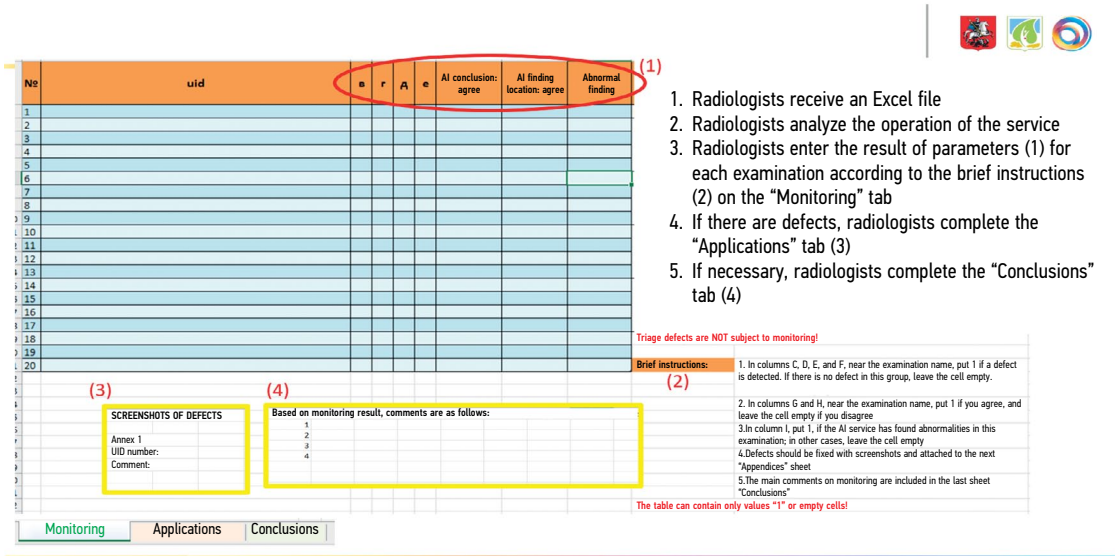

Fig. 7. Form of an internal report on monitoring the operation of artificial intelligence–based software.

[20] Order No. 134 of the Moscow City Health Department dated February 16, 2023 on approval of the procedure and conditions for conducting an experiment on the use of innovative technologies in computer vision for analyzing medical images and further use in the Moscow healthcare system." Link: https://mosmed.ai/documents/227/order_DZM__134_d_16.02.2023.pdf.

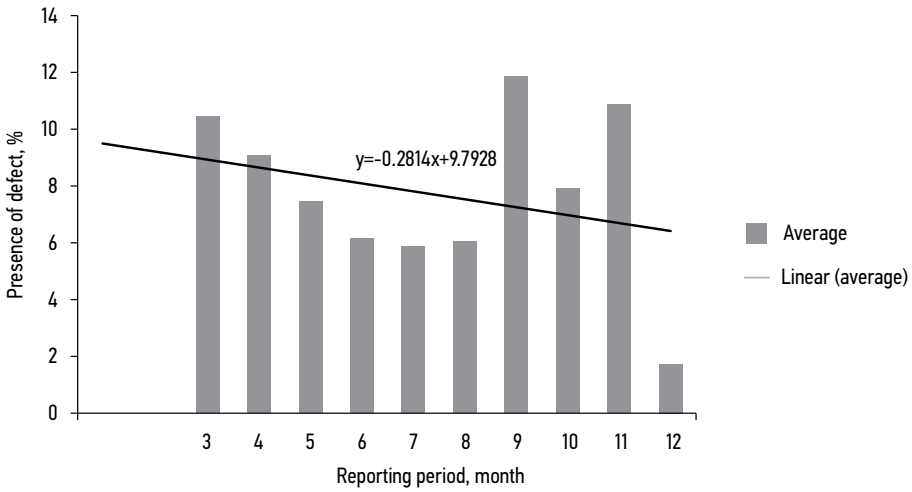

Fig. 8. Changes of technological software defects for "chest radiography" modality.

REPORT ON MONITORING OF TECHNOLOGICAL PARAMETERS OF THE SERVICE OPERATION.

1. AI-service provider:
   Name of AI service:
   AI-service manufacturing company:
   AI-service ID in the experiment:
2. Reporting period:
3. Type of research:
4. Clinical goal:
5. Total number of examinations:
   5.1. Sent for service analysis for the reporting period according to data extracted from ERIS EMIAS, No. 16108
   5.2. Of them, unique according to data extracted from ERIS EMIAS, No.* 16108
6. Number of examinations that passed control, No. 16108
   6.1. Passed manual control, No. 20
7. Number of examinations with defects:
   7.1. With technological defect "a," No., Appendix 1 32
   7.2. With technological defect "b," No., Appendix 2 808
   7.3. With technological defects "c" to "e," No., Appendix 3 1
8. Relative share of examinations:
   8.1. With technological defect "a" for 15,300 examinations, % 0
   8.2. With technological defect "b" for 16,108 examinations, % 5
   8.3. With technological defects "c" to "e" for two examinations, % 5
9. Number of examinations without defects, pc 15267
10. Solution:
Ongoing AI-service participation in the experiment.
11. Notes:

Report date:
Full name of the responsible person: The report is generated automatically.

*0 non-unique examination extracted from ERIS EMIAS for the reporting period.

Fig. 9. Example of a technology monitoring report.

main evaluation criteria include interpretation (conclusion) and localization (labeling) of an abnormal finding. During the assessment, the response options that clinicians can choose from include full compliance, incorrect assessment, false positive result, and false negative result. For example, the wording "Interpretation: Full compliance" is selected when a specialist fully agrees with the software conclusion, and the wording "Interpretation: Incorrect assessment" is selected when the doctor partially agrees with a software conclusion (e.g., the specialist agrees with the presence of abnormal findings but disagrees with its details, or vice versa, they agree with details but disagree with the general conclusion about the possibility or severity of abnormal findings). If the specialist completely disagrees with the software conclusion, the wordings "Interpretation: False positive result" and "Interpretation: False negative result" are used (Figure 10).

The clinical assessment results are entered into the abovementioned internal monitoring report and imported into the monitoring software module, from which a final monitoring report is automatically generated.

Based on periodic monitoring, one of the following conclusions is adopted: "The participation of the software in the Experiment continues," "The participant in the Experiment needs to make changes to the operation of the software," and "The participation of the software in the Experiment is suspended until changes are made to the operation of the software."[21]

Feedback

The stage of radiologist feedback is required to assess the software's practical relevance. The feedback form is in the program window on the radiologist's automated workstation (Figure 11). The software's result may be agreed upon or disagreed upon by a radiologist. In case of disagreement, they select a reason. The primary causes include technological defects and diagnostic inaccuracy. It is necessary to obtain specialist feedback on 5% of all examinations assessed by software. In addition, feedback is collected through a survey of specialists to determine their satisfaction with the software.[22]

[21] Order No. 134 of the Moscow City Health Department dated February 16, 2023 on approval of the procedure and conditions for conducting an experiment on the use of innovative technologies in computer vision for analyzing medical images and further use in the Moscow healthcare system. Link: https://mosmed.ai/documents/227/order_DZM__134_d_16.02.2023.pdf.

[22] Ibid.

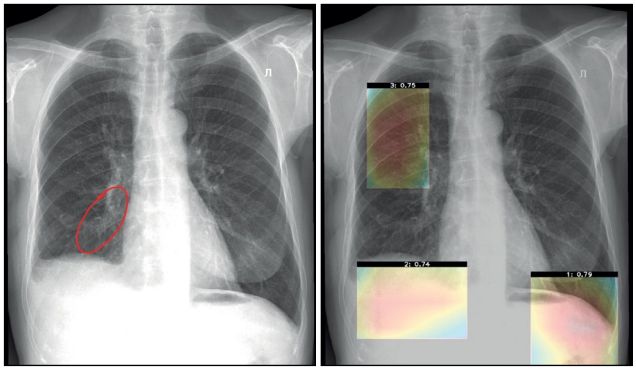

Fig. 10. False negative (the subsegmental atelectasis is not detected in the lower lobe of the right lung): Noncritical noncompliance with basic diagnostic requirements.

Finalization

Suppose a critical comment regarding the software operation is identified at functional, calibration testing, and periodic monitoring stages. In that case, software testing is suspended until the causes of the comment are eliminated. Software finalization is performed by the supplier, which serves as a "secret box" for the healthcare organization. Suppose the modifications required do not involve changes in the initially declared functions or technical architecture and do not affect the diagnostic accuracy of the software. In that case, the applicant can proceed to the next stage of the methodology immediately after making modifications.

If the applicant makes modifications that affect the initially declared functions, technical architecture and diagnostic accuracy of the software, functional and calibration testing should be repeated regardless of what stage of the software methodology it was at.[23]

DISCUSSION

This paper presents a methodology for testing and monitoring the results of AI-based software for medical diagnostics to improve its quality and implement it in clinical practice. The key reasons for its development include the lack of specific requirements for testing and monitoring AI-based software for medical diagnostics in existing regulatory documentation and the lack of regulated principles for software selection by a healthcare organization among various software programs on the market. This methodology does not conflict with legal requirements but considers special characteristics of AI-based software for medical diagnostics. The methodology includes seven unique, clearly organized, scientifically validated stages [1–4, 19–21]; it is supported by legislative documents.[24]

The presence of developed basic functional and diagnostic requirements used at the functional testing stage is a key element of the methodology.[25] The defect and requirement systematization is unique (their detailed descriptions are not provided in the reviewed sources). It is especially worth noting the differentiation between critical and noncritical noncompliance, which is useful for software developers and users. Documents from the Institute of Data Sciences of the American College of Radiologists, which describe the clinical tasks solved using the software and the expected input and output data, are well known on a global scale.[26]

Another important advantage of the methodology is the mandatory software calibration using local data (calibration testing stage) and subsequent validation using real-world data (periodic monitoring stage). According to a foreign systematic review [22], only 6% of AI-based software passed

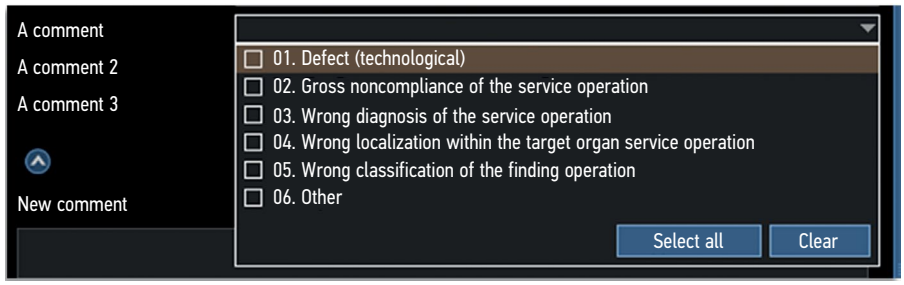

Fig.11. A feedback window in the user interface.

[23] Order No. 134 of the Moscow City Health Department dated February 16, 2023 on approval of the procedure and conditions for conducting an experiment on the use of innovative technologies in computer vision for analyzing medical images and further use in the Moscow healthcare system. Link: https://mosmed.ai/documents/227/order_DZM__134_d_16.02.2023.pdf.

[24] Decree No. 1543-PP of the Moscow Government dated November 21, 2019 Link: https://docs.cntd.ru/document/563879961; Order No. 134 of the Moscow Department of Health dated February 16, 2023. Link:https://mosmed.ai/documents/227/order_DZM__134_d_02/16/2023.pdf.

[25] Basic functional requirements for AI service results Link: https://mosmed.ai/documents/218/Basic_functional_requirements_29.11.2022.pdf; Basic diagnostic requirements for AI service results Link: https://mosmed.ai/documents/226/Basic_diagnostic_requirements_22_02_2023.pdf.

[26] ACR Data Science Institute Releases Landmark Artificial Intelligence Use Cases. 2018. Link: https://www.acr.org/Media-Center/ACR-News-Releases/2018/ACR-Data-Science-Institute-Releases-Landmark-Artificial-Intelligence-Use-Cases.

the external validation stages. Validation can be "broad" and "narrow" [8]. The purpose of "narrow" validation is to determine the "correctness" of the product, that is, to what extent the results of its use correspond to the purposes of its use. This may include clinical validation and usability assessment. "Broad" validation encompasses "narrow" validation and is also associated with quality control, which ensures that software was developed following best practices and methods. This includes algorithm analysis, software testing, and documentation research. In this case, the internal structure of the software is assessed, and it is designated as a "white box" [8].

Moreover, it is important to mention the stage of software finalization after identifying critical inconsistencies. Software finalization provides a gradual decrease in the number of technological defects and an increase in software diagnostic accuracy. Therefore, the methodology will enable developers of AI-based software for medical diagnostics to achieve excellent results in various areas. Users will be able to make an informed and confident choice among software products that have passed an independent quality check, leading to the implementation of software in clinical practice, reducing the workload of radiologists, and increasing the efficiency of diagnostic examination interpretation. As a result, the initial goal of AI-based process automation will be achieved.

This methodology does not replace established medical device registration procedures. Moreover, the entire method or its stages and approaches may be used by regulatory authorities to assess the safety and effectiveness of AI-based software, and it may also be part of a manufacturer's quality management system. The methodology can be used by software developers to prepare a post-registration clinical monitoring plan (which must be submitted as part of a set of documents when registering medical devices) and by healthcare organizations to select the most suitable software for specific conditions and purposes [4]. The methodology is indefinitely applicable, and it complies with the requirements of the Eurasian Economic Commission for 3 year and FDA recommendations for monitoring throughout the entire period of product operation.

Having MA for AI-based software does not eliminate the need to perform all stages of testing in accordance with the presented methodology. Such an approach is justified for at least two reasons. First, a MA may have been obtained by testing specific diagnostic equipment, and the results of the software may change when performed on other equipment. Second, a MA could be obtained to solve a specific clinical task; software developers could add functionalities in the future.

Our paper presented cases from radiologist practice, but the methodology may be adapted to AI-based software used in other areas of clinical medicine. In this case, adjusting certain forms, such as a list of technological defects and a clinical assessment, will be necessary.

Limitations of the study

A limitation of the methodology is the separation of a manufacturer and an assessor. In several methods, software is developed and assessed by one company (concept-to-implementation methodology) [16]. In the case of the presented method, the software is assessed by a third party closer to implementation. Errors a developer makes early in development may still be identified, but correcting them may be more challenging.

The software assesses several examinations at the periodic monitoring stage (>1,000). Due to limited resources, a small number of medical experts, and their high workload, it is impossible to provide quality control for all examinations. Despite the automated generation of a representative pseudo-random sample of examinations, systematic sampling errors may cause errors to be undetected during the periodic monitoring stage.

Research prospects

1. Publication of software evaluation results using the presented methodology (hypothesis: software evaluation based on the presented methodology improves diagnostic accuracy and practical relevance of AI-based software in medical diagnostics).
2. Comparison of software that received and did not receive Roszdravnadzor MAs using the presented methodology.
3. Developing a testing stage as part of the methodology to evaluate software processing results of "unsatisfactory" examinations (with unsuitable anatomical regions, modality, artifacts, improper patient positioning, implants, and other unsuitable medical equipment for this software).

CONCLUSION

A methodology for testing and monitoring AI-based software for medical diagnostics has been developed to improve its quality and implement it in clinical practice. The method consists of seven stages: self-testing, functional testing, calibration testing, process monitoring, clinical monitoring, feedback, and finalization. The methodology is characterized by the presence of cyclical stages of testing, monitoring, and software finalization, which results in continuous improvement in software quality, the availability of explicit requirements for software results, and the involvement of HCPs in software evaluation. The methodology will enable software developers to achieve excellent results and demonstrate achievements in various areas. Users will be able to make an informed and confident decision among software products that have passed an independent and comprehensive quality check.

ADDITIONAL INFORMATION

Funding source. This article was prepared by a group of authors as a part of the research and development effort titled

"Development of a platform for improving the quality of AI services for clinical diagnostics," No. 123031400006-0 in accordance with the Order No. 1196 dated December 21, 2022 "On approval of state assignments funded by means of allocations from the budget of the city of Moscow to the state budgetary (autonomous) institutions subordinate to the Moscow Health Care Department, for 2023 and the planned period of 2024 and 2025" issued by the Moscow Health Care Department.

Competing interests. The authors declare that they have no competing interests.

Authors' contribution. All authors made a substantial contribution to the conception of the work, acquisition, analysis, interpretation of data for the work, drafting and revising the work, final approval of the version to be published and agree to be accountable for all aspects of the work. Yu.A. Vasiliev — development of the concept, approval of the final version of the manuscript; A.V. Vladzimirsky — development of the concept, approval of the final version of the manuscript; O.V. Omelyanskaya — development of methodology, approval of the final version of the manuscript; K.M. Arzamasov — concept development, research, editing and approval of the final version of the manuscript; S.F. Chetverikov — development of methodology, research; D.A. Rumyantsev — literature review, writing and editing the text of the article; M.A. Zelenova — editing the text of the article.

REFERENCES

1. Oakden-Rayner L, Palme LJ. Artificial intelligence in medicine: Validation and study design. In: Ranschart E, Morozov S, Algra P, eds. Artificial intelligence in medical imaging. Cham: Springer; 2019. P. 83–104.

2. Morozov SP, Zinchenko VV, Khoruzhaya AN, et al. Standardization of artificial intelligence in healthcare: Russia is becoming a leader. *Doctor Inform Technol*. 2021;(2):12–19. (In Russ). doi: 10.25881/18110193_2021_2_12

3. Mello AA, Utkin LV, Trofimova TN. Artificial intelligence in medicine: The current state and main directions of development of intellectual diagnostics. *Radiation Diagnost Therapy*. 2020;(1):9–17. (In Russ). doi: 10.22328/2079-5343-2020-11-1-9-17

4. Zinchenko VV, Arzamasov KM, Chetverikov SF, et al. Methodology of post-registration clinical monitoring for software using artificial intelligence technologies. *Modern Technol Med*. 2022;14(5):15–25. (In Russ). doi: 10.17691/stm2022.14.5.02

5. Tanguay W, Acar P, Fine B, et al. Assessment of radiology artificial intelligence software: A validation and evaluation framework. *Can Assoc Radiol J*. 2023;74(2):326–333. doi: 10.1177/08465371221135760

6. Kohli A, Jha S. Why CAD failed in mammography. *J Am Coll Radiol*. 2018;15(3 Pt B):535–537. doi: 10.1016/j.jacr.2017.12.029

7. Recht MP, Dewey M, Dreyer K, et al. Integrating artificial intelligence into the clinical practice of radiology: Challenges and recommendations. *Eur Radiol*. 2020;30(6):3576–3584. doi: 10.1007/s00330-020-06672-5

8. Higgins DC, Johner C. Validation of artificial intelligence containing products across the regulated healthcare industries. *Ther Innov Regul Sci*. 2023;57(4):797–809. doi: 10.1007/s43441-023-00530-4

9. Rudolph J, Schachtner B, Fink N, et al. Clinically focused multi-cohort benchmarking as a tool for external validation of artificial intelligence algorithm performance in basic chest radiography analysis. *Sci Rep*. 2022;12(1):12764. doi: 10.1038/s41598-022-16514-7

10. Allen B, Dreyer K, Stibolt R, et al. Evaluation and real-world performance monitoring of artificial intelligence models in clinical practice: Try it, buy it, check it. *J Am Coll Radiol*. 2021;18(11):1489–1496. doi: 10.1016/j.jacr.2021.08.022

11. Strohm L, Hehakaya C, Ranschaert ER, et al. Implementation of artificial intelligence (AI) applications in radiology: Hindering and facilitating factors. *Eur Radiol*. 2020;30(10):5525–5532. doi: 10.1007/s00330-020-06946-y

12. Sohn JH, Chillakuru YR, Lee S, et al. An open-source, vender agnostic hardware and software pipeline for integration of artificial intelligence in radiology workflow. *J Digit Imaging*. 2020;33(4):1041–1046. doi: 10.1007/s10278-020-00348-8

13. Wichmann JL, Willemink MJ, De Cecco CN. Artificial intelligence and machine learning in radiology: Current state and considerations for routine clinical implementation. *Invest Radiol*. 2020;55(9):619–627. doi: 10.1097/RLI.0000000000000673

14. Larson DB, Harvey H, Rubin DL, et al. Regulatory frameworks for development and evaluation of artificial intelligence-based diagnostic imaging algorithms: Summary and recommendations. *J Am Coll Radiol*. 2021;18(3 Pt A):413–424. doi: 10.1016/j.jacr.2020.09.060

15. Milam ME, Koo CW. The current status and future of FDA-approved artificial intelligence tools in chest radiology in the United States. *Clin Radiol*. 2023;78(2):115–122. doi: 10.1016/j.crad.2022.08.135

16. De Silva D, Alahakoon D. An artificial intelligence life cycle: From conception to production. *Patterns (NY).* 2022;3(6):100489. doi: 10.1016/j.patter.2022.100489

17. Cerdá-Alberich L, Solana J, Mallol P, et al. MAIC-10 brief quality checklist for publications using artificial intelligence and medical images. *Insights Imaging*. 2023;14(1):11. doi: 10.1186/s13244-022-01355-9

18. Vasey B, Novak A, Ather S, et al. DECIDE-AI: A new reporting guideline and its relevance to artificial intelligence studies in radiology. *Clin Radiol*. 2023;78(2):130–136. doi: 10.1016/j.crad.2022.09.131

19. Regulations for the preparation of data sets with a description of approaches to the formation of a representative sample of data. Moscow: Scientific and Practical Clinical Center for Diagnostics and Telemedicine Technologies of the Department of Health of the City of Moscow; 2022. 40 p. (Best practices in radiological and instrumental diagnostics; Part 1). (In Russ).

20. Chetverikov S, Arzamasov KM, Andreichenko AE, et al. Approaches to sampling for quality control of artificial intelligence systems in biomedical research. *Modern Technol Med*. 2023;15(2):19–27. (In Russ). doi: 10.17691/stm2023.15.2.02

21. Morozov SP, Vladzimirsky AV, Klyashtorny VG, et al. Clinical trials of software based on intelligent technologies (radiation diagnostics). Moscow: Scientific and Practical Clinical Center for Diagnostics and Telemedicine Technologies of the Department of Health of the City of Moscow; 2019. 33 p. (In Russ).

22. Kim DW, Jang HY, Kim KW, et al. Design characteristics of studies reporting the performance of artificial intelligence algorithms for diagnostic analysis of medical images: Results from recently published papers. *Korean J Radiol*. 2019;20(3):405–410. doi: 10.3348/kjr.2019.0025

СПИСОК ЛИТЕРАТУРЫ

1. Oakden-Rayner L., Palme L.J. Artificial intelligence in medicine: Validation and study design. In: Ranschart E., Morozov S., Algra P., eds. Artificial intelligence in medical imaging. Cham: Springer, 2019. P. 83–104.

2. Морозов С.П., Зинченко В.В., Хоружая А.Н., и др. Стандартизация искусственного интеллекта в здравоохранении: Россия выходит в лидеры // Врач и информационные технологии. 2021. № 2. С. 12–19. doi: 10.25881/18110193_2021_2_12

3. Мелдо А.А., Уткин Л.В., Трофимова Т.Н. Искусственный интеллект в медицине: современное состояние и основные направления развития интеллектуальной диагностики // Лучевая диагностика и терапия. 2020. № 1. С. 9–17. doi: 10.22328/2079-5343-2020-11-1-9-17

4. Зинченко В.В., Арзамасов К.М., Четвериков С.Ф., и др. Методология проведения пострегистрационного клинического мониторинга для программного обеспечения с применением технологий искусственного интеллекта // Современные технологии в медицине. 2022. Т. 14, № 5. С. 15–25. doi: 10.17691/stm2022.14.5.02

5. Tanguay W., Acar P., Fine B., et al. Assessment of radiology artificial intelligence software: A validation and evaluation framework // Can Assoc Radiol J. 2023. Vol. 74, N 2. P. 326–333. doi: 10.1177/08465371221135760

6. Kohli A., Jha S. Why CAD failed in mammography // J Am Coll Radiol. 2018. Vol. 15, N 3, Pt. B. P. 535–537. doi: 10.1016/j.jacr.2017.12.029

7. Recht M.P., Dewey M., Dreyer K., et al. Integrating artificial intelligence into the clinical practice of radiology: Challenges and recommendations // Eur Radiol. 2020. Vol. 30, N 6. P. 3576–3584. doi: 10.1007/s00330-020-06672-5

8. Higgins D.C., Johner C. Validation of artificial intelligence containing products across the regulated healthcare industries // Ther Innov Regul Sci. 2023. Vol. 57, N 4. P. 797–809. doi: 10.1007/s43441-023-00530-4

9. Rudolph J., Schachtner B., Fink N., et al. Clinically focused multi-cohort benchmarking as a tool for external validation of artificial intelligence algorithm performance in basic chest radiography analysis // Sci Rep. 2022. Vol. 12, N 1. P. 12764. doi: 10.1038/s41598-022-16514-7

10. Allen B., Dreyer K., Stibolt R., et al. Evaluation and real-world performance monitoring of artificial intelligence models in clinical practice: Try it, buy it, check it // J Am Coll Radiol. 2021. Vol. 18, N 11. P. 1489–1496. doi: 10.1016/j.jacr.2021.08.022

11. Strohm L., Hehakaya C., Ranschaert E.R., et al. Implementation of artificial intelligence (AI) applications in radiology: Hindering and facilitating factors // Eur Radiol. 2020. Vol. 30, N 10. P. 5525–5532. doi: 10.1007/s00330-020-06946-y

12. Sohn J.H., Chillakuru Y.R., Lee S., et al. An open-source, vender agnostic hardware and software pipeline for integration of artificial intelligence in radiology workflow // J Digit Imaging. 2020. Vol. 33, N 4. P. 1041–1046. doi: 10.1007/s10278-020-00348-8

13. Wichmann J.L., Willemink M.J., De Cecco C.N. Artificial intelligence and machine learning in radiology: Current state and considerations for routine clinical implementation // Invest Radiol. 2020. Vol. 55, N 9. P. 619–627. doi: 10.1097/RLI.0000000000000673

14. Larson D.B., Harvey H., Rubin D.L., et al. Regulatory frameworks for development and evaluation of artificial intelligence-based diagnostic imaging algorithms: Summary and recommendations // J Am Coll Radiol. 2021. Vol. 18, N 3, Pt. A. P. 413–424. doi: 10.1016/j.jacr.2020.09.060

15. Milam M.E., Koo C.W. The current status and future of FDA-approved artificial intelligence tools in chest radiology in the United States // Clin Radiol. 2023. Vol. 78, N 2. P. 115–122. doi: 10.1016/j.crad.2022.08.135

16. De Silva D., Alahakoon D. An artificial intelligence life cycle: From conception to production // Patterns (NY). 2022. Vol. 3, N 6. P. 100489. doi: 10.1016/j.patter.2022.100489

17. Cerdá-Alberich L., Solana J., Mallol P., et al. MAIC-10 brief quality checklist for publications using artificial intelligence and medical images // Insights Imaging. 2023. Vol. 14, N 1. P. 11. doi: 10.1186/s13244-022-01355-9

18. Vasey B., Novak A., Ather S., et al. DECIDE-AI: A new reporting guideline and its relevance to artificial intelligence studies in radiology // Clin Radiol. 2023. Vol. 78, N 2. P. 130–136. doi: 10.1016/j.crad.2022.09.131

19. Регламент подготовки наборов данных с описанием подходов к формированию репрезентативной выборки данных. Москва: Научно-практический клинический центр диагностики и телемедицинских технологий Департамента здравоохранения города Москвы, 2022. 40 с. (Лучшие практики лучевой и инструментальной диагностики; Часть 1).

20. Четвериков С.Ф., Арзамасов К.М., Андрейченко А.Е., и др. Подходы к формированию выборки для контроля качества работы систем искусственного интеллекта в медико-биологических исследованиях // Современные технологии в медицине. 2023. Т. 15, № 2. С. 19–27. doi: 10.17691/stm2023.15.2.02

21. Морозов С.П., Владзимирский А.В., Кляшторный В.Г., и др. Клинические испытания программного обеспечения на основе интеллектуальных технологий (лучевая диагностика). Москва: Научно-практический клинический центр диагностики и телемедицинских технологий Департамента здравоохранения города Москвы, 2019. 33 с.

22. Kim D.W., Jang H.Y., Kim K.W., et al. Design characteristics of studies reporting the performance of artificial intelligence algorithms for diagnostic analysis of medical images: Results from recently published papers // Korean J Radiol. 2019. Vol. 20, N 3. P. 405–410. doi: 10.3348/kjr.2019.0025

AUTHORS' INFO

*** Denis A. Rumyantsev;**
address: 24/1 Petrovka street, 127051 Moscow, Russia;
ORCID: 0000-0001-7670-7385;
eLibrary SPIN: 8734-2085;
e-mail: RumyantsevDA3@zdrav.mos.ru

Yuriy A. Vasilev, MD, Cand. Sci. (Med.);
ORCID: 0000-0002-0208-5218;
eLibrary SPIN: 4458-5608;
e-mail: npcmr@zdrav.mos.ru

Anton V. Vladzymyrskyy, MD, Dr. Sci. (Med.);
ORCID: 0000-0002-2990-7736;
eLibrary SPIN: 3602-7120;
e-mail: npcmr@zdrav.mos.ru

Olga V. Omelyanskaya;
ORCID: 0000-0002-0245-4431;
eLibrary SPIN: 8948-6152;
e-mail: npcmr@zdrav.mos.ru

Kirill M. Arzamasov, MD, Cand. Sci. (Med.);
ORCID: 0000-0001-7786-0349;
eLibrary SPIN: 3160-8062;
e-mail: ArzamasovKM@zdrav.mos.ru

Sergei F. Chetverikov, Cand. Sci. (Engin.);
ORCID: 0000-0002-3097-8881;
eLibrary SPIN: 3815-8870;
e-mail: ChetverikovSF@zdrav.mos.ru

Maria A. Zelenova;
ORCID: 0000-0001-7458-5396;
eLibrary SPIN: 3823-6872;
e-mail: ZelenovaMA@zdrav.mos.ru

ОБ АВТОРАХ

*** Румянцев Денис Андреевич;**
адрес: Россия, 127051, Москва, ул. Петровка, д. 24, стр. 1;
ORCID: 0000-0001-7670-7385;
eLibrary SPIN: 8734-2085;
e-mail: RumyantsevDA3@zdrav.mos.ru

Васильев Юрий Александрович, канд. мед. наук;
ORCID: 0000-0002-0208-5218;
eLibrary SPIN: 4458-5608;
e-mail: npcmr@zdrav.mos.ru

Владзимирский Антон Вячеславович, д-р мед. наук;
ORCID: 0000-0002-2990-7736;
eLibrary SPIN: 3602-7120;
e-mail: npcmr@zdrav.mos.ru

Омелянская Ольга Васильевна;
ORCID: 0000-0002-0245-4431;
eLibrary SPIN: 8948-6152;
e-mail: npcmr@zdrav.mos.ru

Арзамасов Кирилл Михайлович, канд. мед. наук;
ORCID: 0000-0001-7786-0349;
eLibrary SPIN: 3160-8062;
e-mail: ArzamasovKM@zdrav.mos.ru

Четвериков Сергей Федорович, канд. тех. наук;
ORCID: 0000-0002-3097-8881;
eLibrary SPIN: 3815-8870;
e-mail: ChetverikovSF@zdrav.mos.ru

Зеленова Мария Александровна;
ORCID: 0000-0001-7458-5396;
eLibrary SPIN: 3823-6872;
e-mail: ZelenovaMA@zdrav.mos.ru

* Corresponding author / Автор, ответственный за переписку

DOI: https://doi.org/10.17816/DD375285

Частота сердечных осложнений у детей, выявленных после радикальной коррекции тетрады Фалло с помощью компьютерной томографии

А.М. Кабдуллина[1], В.Е. Синицын[2], Р.И. Рахимжанова[1], Т.Б. Даутов[3], А.Б. Садуакасова[4], Б.Б. Калиев[1], Л.А. Бастарбекова[1], З.А. Молдаханова[1]

[1] Медицинский университет Астана, Астана, Казахстан;
[2] Московский государственный университет имени М.В. Ломоносова, Москва, Российская Федерация;
[3] Национальный научный кардиохирургический центр Республики Казахстан, Астана, Казахстан;
[4] Больница Медицинского центра Управления делами Президента Республики Казахстан, Астана, Казахстан

АННОТАЦИЯ

Обоснование. Частота возникновения тетрады Фалло составляет примерно 0,5/1000 живорождённых, что соответствует 7–10% всех случаев врождённых пороков сердца и является второй по частоте формой сложных врождённых пороков сердца. Достижения в области диагностики, хирургического и послеоперационного лечения тетрады Фалло привели к тому, что всё большее число пациентов этой категории достигает зрелого возраста, при этом наблюдается резкое увеличение выживаемости (почти до 90%) к 30 годам, что требует длительного мониторинга определённых анатомических параметров для своевременного выявления осложнений. Данное исследование направлено на изучение частоты осложнений, выявленных с помощью компьютерной томографии, после радикальной коррекции тетрады Фалло у пациентов детского возраста.

Цель — выявить с помощью компьютерной томографии маркеры наиболее часто встречающихся осложнений после коррекции тетрады Фалло у пациентов детского возраста.

Материалы и методы. Проведён ретроспективный анализ данных 613 пациентов с тетрадой Фалло за период с октября 2011 по июнь 2020 года. В исследование были включены 116 пациентов, из них 69 мужского и 47 женского пола, у которых после коррекции тетрады Фалло возникли осложнения, выявленные с помощью компьютерной томографии. На момент операции средний возраст пациентов составлял от 10 до 36 (в среднем 12) месяцев, средняя масса тела 21 кг, средний рост 105,4 см, средняя площадь поверхности тела 0,74 м^2. Средний возраст пациентов на момент проведения компьютерной томографии составил 17,5 (возрастной диапазон 7–36) лет.

Результаты. Среди 116 пациентов с осложнениями после коррекции тетрады Фалло у 49 был стеноз лёгочной артерии, у 92 — стеноз ветвей лёгочной артерии (из них у 56 — основной ветви левой лёгочной артерии, у 36 — основной ветви правой лёгочной артерии), у 8 — стеноз выходного тракта правого желудочка, у 32 — дефект межжелудочковой перегородки, у 1 — тромбоз шунта, у 12 — послеоперационная деформация лёгочной артерии, у 10 — выраженная дилатация правого желудочка, у 2 — аневризма выходного тракта правого желудочка, в 6 случаях — кальцификация и стеноз кондуита. У пациентов со стенозом ветви левой лёгочной артерии вероятность развития стеноза ветви правой лёгочной артерии была в 6,5 раз выше (p <0,001).

Заключение. Наиболее частыми осложнениями, выявляемыми с помощью компьютерной томографии после коррекции тетрады Фалло, были стеноз лёгочной артерии и её ветвей. Пациенты со стенозом лёгочной артерии и её ветвей не имели существенных различий по возрасту, антропометрическим параметрам (рост, вес, площадь поверхности тела) и гендерному распределению при наличии или отсутствии различных типов стеноза (лёгочной артерии, правой или левой лёгочной артерии), однако стеноз правой лёгочной артерии повышает вероятность развития стеноза левой ветви.

Ключевые слова: мультиспиральная компьютерная томография; тетрада Фалло; осложнения; врождённые пороки сердца; радикальная коррекция.

Как цитировать:
Кабдуллина А.М., Синицын В.Е., Рахимжанова Р.И., Даутов Т.Б., Садуакасова А.Б., Калиев Б.Б., Бастарбекова Л.А., Молдаханова З.А. Частота сердечных осложнений у детей, выявленных после радикальной коррекции тетрады Фалло с помощью компьютерной томографии // *Digital Diagnostics*. 2023. Т. 4, № 3. С. 268–279. DOI: https://doi.org/10.17816/DD375285

Рукопись получена: 02.05.2023 **Рукопись одобрена:** 09.06.2023 **Опубликована:** 04.09.2023

DOI: https://doi.org/10.17816/DD375285

Frequency of various cardiac complications in children with repaired tetralogy of Fallot identified by computer tomography

Azhar M. Kabdullina[1], Valentin E. Sinitsyn[2], Raushan I. Rakhimzhanova[1], Tairkhan B. Dautov[3], Aigul B. Saduakassova[4], Bauyrzhan B. Kaliyev[1], Lyazzat A. Bastarbekova[1], Zhanar A. Moldakhanova[1]

[1] Astana Medical University, Astana, Kazakhstan;
[2] Lomonosov Moscow State University, Moscow, Russian Federation;
[3] Department of the Radiology of National Research Cardiac Surgery Center, Astana, Kazakhstan;
[4] Medical Centre Hospital of President's Affairs Administration of the Republic of Kazakhstan, Astana, Kazakhstan

ABSTRACT

BACKGROUND: Tetralogy of Fallot represents 7–10% of all cases of congenital heart disease, as it occurs in approximately 0.5 per 1,000 live births and is the second most common form of complex congenital heart disease. Advances in diagnosis, surgical techniques, and postoperative treatment have led to an increasing number of patients reaching adulthood, with a dramatic increase in the survival rate to almost 90% at 30 years, thereby creating a need for long-term monitoring of certain anatomic parameters to identify complications in a timely manner. This study aimed to investigate the frequency of computed tomography detected complications after radical correction of Tetralogy of Fallot in pediatric patients.

AIM: to identify markers between the most frequency computed tomography detected complications after repair of Tetralogy of Fallot in pediatric patients.

MATERIALS AND METHODS: A retrospective analysis was conducted on 613 patients with Tetralogy of Fallot from October 2011 to June 2020. The study included a total of 116 patients (69 men and 47 women) who experienced complications after a repair of Tetralogy of Fallot, as identified by computed tomography. At the time of repair of Tetralogy of Fallot, the patient's average age ranged from 10 to 36 months (mean: 12 months), average body weight was 21 kg, average height was 105.4 cm, and average body surface area was 0.74 m^2. The patients' median age at the time of the computed tomography examination was 17.5 years (age range: 7–36 years).

RESULTS: Among the 116 patients who exhibited complications after an repair of Tetralogy of Fallot, 49 had a pulmonary artery stenosis, 92 had a pulmonary artery branch stenosis (56 of them of the left main pulmonary artery branch, and 36 of them of the right main pulmonary artery branch), 8 had a right ventricular outflow tract stenosis, 32 had a ventricular septal defect, 1 had a shunt thrombosis, 12 had a postoperative deformation of the pulmonary artery, 10 exhibited a marked right ventricular dilatation, 2 had an right ventricular outflow tract aneurysm, and 6 suffered from conduit calcification and stenosis. Moreover, patients with left main pulmonary artery branch stenosis had a 6.5 times greater chance of developing an right main pulmonary artery branch stenosis in (p <0.001).

CONCLUSION: The most frequently computed tomography detected complications after a repair of Tetralogy of Fallot were pulmonary artery stenosis and pulmonary artery branch stenosis. Patients with pulmonary artery stenosis and pulmonary artery branch stenosis exhibit no significant differences in terms of age, anthropometric parameters (height, weight, and body surface area), and gender distribution in the presence or absence of different stenosis types (pulmonary artery, right main pulmonary artery branch, or left main pulmonary artery branch). However, an right main pulmonary artery branch stenosis increases the chances of developing an left main pulmonary artery branch stenosis.

Keywords: multidetector computed tomography; tetralogy of Fallot; complications; congenital heart disease; total repair.

To cite this article:
Kabdullina AM, Sinitsyn VE, Rakhimzhanova RI, Dautov TB, Saduakassova AB, Kaliyev BB, Bastarbekova LA, Moldakhanova ZA. Frequency of various cardiac complications in children with repaired Tetralogy of Fallot identified by computer tomography. *Digital Diagnostics.* 2023;4(3):268–279. DOI: https://doi.org/10.17816/DD375285

Received: 02.05.2023 **Accepted:** 09.06.2023 **Published:** 04.09.2023

DOI: https://doi.org/10.17816/DD375285

电子计算机断层扫描确定的法洛四联症修复患儿各种心脏并发症的发生率

Azhar M. Kabdullina[1], Valentin E. Sinitsyn[2], Raushan I. Rakhimzhanova[1], Tairkhan B. Dautov[3], Aigul B. Saduakassova[4], Bauyrzhan B. Kaliyev[1], Lyazzat A. Bastarbekova[1], Zhanar A. Moldakhanova[1]

[1] Astana Medical University, Astana, Kazakhstan;
[2] Lomonosov Moscow State University, Moscow, Russian Federation;
[3] Department of the Radiology of National Research Cardiac Surgery Center, Astana, Kazakhstan;
[4] Medical Centre Hospital of President's Affairs Administration of the Republic of Kazakhstan, Astana, Kazakhstan

简评

论证。法洛四联症（Tetralogy of Fallot，ToF）占所有先天性心脏病（congenital heart disease，CHD）病例的7-10%，每1000例活产中约有0.5例发生，是第二种最常见的复杂先天性心脏病。随着诊断、手术技术和术后治疗的进步，越来越多的患者长大成人，30岁时的存活率急剧上升到近 90%，因此需要对某些解剖参数进行长期监测，以便及时发现并发症。本研究旨在调查儿童患者患儿根治性矫正ToF后计算机断层扫描（computed tomography，CT）发现并发症的发生率。

该研究的目的是确定小儿ToF修复术（repair of ToF，rToF）后CT检测到的最常见并发症之间的标记。

材料和方法。我们对2011年10月至2020年6月期间的613例ToF患者进行了回顾性分析。116名患者（69名男性和47名女性）被纳入该研究，这些患者在接受rToF后出现了通过CT发现的并发症。患者接受rToF时的平均年龄为10至36个月（平均值为12个月），平均体重为21kg，平均身高为105.4cm，平均体表面积（body surface area，BSA）为0.74m^2。患者接受CT检查时的中位年龄为17.5岁（年龄范围：7至36岁）。

结果。在116例rToF后出现并发症的患者中，49例有肺动脉（pulmonary artery，PA）狭窄，92例有PA分支狭窄（其中56例有PA左主分支（left main PA branch，LPA），36例有PA右主分支（right main PA branch，RPA）），8例有右室流出道（right ventricular outflow tract，RVOT）狭窄、32例有室间隔缺损，1例有分流道血栓形成，12例有术后PA变形，10例有明显的右心室扩张，2例有RVOT动脉瘤，6例有导管钙化和狭窄。此外，对于LPA狭窄患者来说，发生RPA狭窄的几率比正常人高出6.5倍（$p<0.001$）。

结论。rToF后最常在CT上发现的并发症是PA狭窄和PA分支狭窄。PA狭窄和PA分支狭窄患者在年龄、人体测量数（身高、体重和BSA）和性别分布方面与是否存在不同狭窄类型（PA、RPA或LPA）无明显差异。然而，RPA狭窄会增加发生LPA狭窄的几率。

关键词：多排计算机断层扫描；法洛四联症；并发症；先天性心脏病；根治性矫正术。

引用本文：
Kabdullina AM, Sinitsyn VE, Rakhimzhanova RI, Dautov TB, Saduakassova AB, Kaliyev BB, Bastarbekova LA, Moldakhanova ZA. 电子计算机断层扫描确定的法洛四联症修复患儿各种心脏并发症的发生率. *Digital Diagnostics.* 2023;4(3):268–279. DOI: https://doi.org/10.17816/DD375285

收到：02.05.2023 **接受：**09.06.2023 **发布日期：**04.09.2023

INTRODUCTION

Tetralogy of Fallot (ToF) represents 7%–10% of all congenital heart disease (CHD) cases, as it occurs in 0.5/1,000 live births and is the second most common form of complex CHD (1). Advances in diagnosis, surgical techniques, and postoperative treatment have led to an increasing number of patients reaching adulthood, with a dramatic increase in the survival rate to almost 90% at 30 years (2), thereby creating a need for long-term monitoring of certain anatomic parameters so that the complications can be identified on time.

After repair of ToF (rToF), imaging tools should be used to assess the right ventricular (RV) volume and any pressure overload due to the tricuspid and pulmonary regurgitation or stenosis, and scan for any RV and left ventricular systolic and diastolic dysfunction, the presence of any postoperative scars, the presence of any RV aneurysms and fibrosis, as well as the presence of any associated anomalies, such as aortic root dilation and aortic insufficiency (1).

Noninvasive imaging plays a critical role in the follow-up of patients after a rToF. Transthoracic echocardiography (TTE) is the primary and routine clinical investigation tool for anatomical and the functional assessment required in these cases. However, it is important to note that the results of the TTE are largely dependent on the operators. Cardiac computed tomography (CT) and magnetic resonance imaging (MRI) have been generally regarded as the complementary tools for this purpose (3)(4).

Multidetector computed tomography (MDCT), with its high spatial, and temporal resolution, plays a crucial role in evaluating complex anatomical findings in both unrepaired and repaired ToF patients (2). A cardiac CT can provide the necessary functional and anatomical information for making informed decision-making in complex CHD cases. Image interpretation is aided by the knowledge of the common approaches to operative repair and the residual hemodynamic abnormalities (5). Technical advances have allowed high-quality images and a marked decrease in the radiation dose of the cardiac CT. For selected indications, cardiac CT may provide better information with a lower risk compared with other diagnostic modalities, proving helpful in the ToF evaluation (1). In contrast, cardiac MRI in small children is mainly limited due to the long examination time requiring conscious sedation or general anesthesia, and the relatively low spatial resolution, which may partly explain the sparse cardiac MRI data in young children with ToF in the literature. Moreover, CT imaging does not interfere with pacemakers and defibrillators, even with the older models that are noncompatible with cardiac magnetic resonance models. The aim of this study was to identify markers between the most frequency CT-detected complications after an rToF in pediatric patients.

MATERIALS AND METHODS

Ethical considerations

The study was approved by the Institutional Review Ethics Committee of the National Research Cardiac Surgery Center (approval #01-92/2021 on 22 April 2021). No anticipated risks to the participants were identified. During data collection, all personal information of the patients was encoded and depersonalized to safeguard patient rights and prevent the disclosure of personal information. Researchers received the electronic database that was limited to the information regarding the demographic and clinical characteristics of the patients, which was analyzed, and reported in an aggregated form only, thereby assuring its confidentiality. This study was conducted according to the principles of the Declaration of Helsinki. Informed consent was obtained from all patients or their legal guardians prior to participation.

Study venue and patients

This is a retrospective study, conducted at a tertiary, highly specialized hospital. CT examinations were performed from December 2011 to June 2020 on patients with a history of rToF who were referred for a cardiac CT examination as part of a clinically necessary standard of care, by the Cardiothoracic Surgery, and the Cardiology Departments. A retrospective analysis of 613 patients with ToF was carried out. Written informed consent was obtained from each participant and the parents of minors before their data was included in the study. We identified 116 patients (69 men, 47 women) with complications of the rToF through their CT results. The patients' average age when the rToF was performed ranged from 10 to 36 months (mean: 12 months), and the patients had an average body weight of 21 kg, an average height of 105.4 cm, and an average body surface area (BSA) of 0.74 m^2. The patients' median age at the time of the CT examination was 17.5 years (age range: 7–36 years) (Table 1).

Patients with the following conditions were excluded from the study population: (i) iodine allergy, (ii) high creatinine levels, and (iii) adults with unrepaired ToF (n = 4). Subsequently, the following inclusion criteria were applied: (i) presence of an informed consent and (ii) prior correction of ToF.

In a total of 613 cardiac CT examinations screened, 138 were performed before any surgical procedures, 20 were performed after a palliative operation (such as shunt, RV outflow tract (RVOT) stent placement, or RVOT widening), 285 were performed after a total surgical rToF (consisting of a closure of the ventricular septal defect (VSD) and of a relief of the RVOT obstruction), and 26 were performed after pulmonary valve replacement (that comprised four treatment stages).

Cardiac CT

Children who had undergone palliative operations and had rTOF underwent scanning using a SOMATOM Definition

Table 1. General characteristics of participants (*N* = 116)

Patient characteristics	Frequency/ mean
Gender, *n* (%)	
Male	69 (59)
Female	47 (41)
Age at initial correction (months)	12 (10–36)
Previous shunt procedure, *n* (%)	25 (21,5)
Initial correction, *n* (%)	
Transannular patch, *n* (%)	67 (57,7)
Myectomy/valvulotomy, *n* (%)	40 (35,5)
Contegra valved conduit, *n* (%)	9 (7,7)
Weight, kg	21,08
Height, cm	105,4
Body surface area, m^2	0,7

Note: cm, centimeter; kg, kilogram; m^2, meter square.

AS 64 CT scanner at the Radiology Department. The scans were conducted with prospective cardiosynchronization and reconstruction, utilizing a slice thickness of 0.6 mm.

All patients were examined in a supine position, head first, with an intravenous bolus administration through an automatic tubeless CT-injector Ohiotandem, and an infusion rate of 1–2 mL/sec.

Infants and young children up to 4 years of age were sedated using oral chloral hydrate (75 mg/kg of body weight) and ketamine (1 mg/kg of body weight), while older children, and adults underwent the examination without sedation.

To optimize the radiation dose during CT, our institution employed standard body-size-adapted protocols. These protocols were based on combinations of body weight and the size of the cardiac shadow observed on scout images, which allowed us to determine the optimal tube current–time product per rotation (6).

Data analysis and interpretation

Descriptive data are presented as percentages (for categorical variables) and as mean ± standard deviation or median (interquartile range), as appropriate. The cohorts were divided into two groups: survivors and deceased patients. Categorical variables were compared using χ^2 tests, while continuous variables were compared using *t*-tests or Mann–Whitney *U* tests.

Comparisons among the three groups were made using a bivariate analysis for normally distributed data. The same analysis was used to assess the association between PA stenosis and other variables. The Pearson's correlation coefficient or the Spearman's rank coefficient was used to assess the correlation between the functional parameters examined in the three different groups. *P*-values were two-sided and were reported as significant at a $p < 0.005$ in all analyses. All statistical analyses were performed using the SPSS software (version 24.0; IBM Corp.).

RESULT

This retrospective study was carried out from October 2011 to June 2020, and 613 patients with ToF were involved. We identified 116 patients with complications after a total rToF through their CT examinations.

In patients post-rToF, 49 had PA stenosis (Table 2), and 92 demonstrated a PA branch stenosis. In 56 of them, the stenosis affected the left main PA branch (Table 3), while in 36 of them; the stenosis affected the right main PA branch (Table 4). Moreover, 8 patients were diagnosed with RVOT stenosis, 32 had developed a VSD, 1 patient had a shunt thrombosis, 12 suffered from a postoperative deformation of the PA, 10 exhibited a marked RV dilatation, 2 had an RVOT aneurysm, and 6 suffered from conduit calcification and stenosis (Figure 1).

A 12-year-old male with repaired tetralogy of Fallot, after implantation of valve-containing conduit Contegra No. 16 and bilateral stents Palmaz Genesis XD 19-10. Cardiac CT image clearly demonstrates thrombosis conduit. All the complications detected by CT were validated with angiography and were operated on.

The most frequent complications observed were PA stenosis and PA branch stenosis. We decided to compare the medical characteristics between the patients with and without PA and PA branch stenosis by conducting a bivariate analysis and by calculating the odds ratios.

Among the three comparison pairs examined, no significant differences were found in terms of patients' age, anthropometric parameters (height, weight, and BSA), and gender distribution in the presence or absence of the different stenosis types (PA, RPA, and LPA). Moreover, there were no significant differences regarding the type of ToF, presence of shunt thrombosis and palliative surgery, or the type of surgery performed ($p > 0.05$). In fact, the data of the comparison groups were comparable according to the aforementioned criteria.

Patients with a VSD exhibited a lower risk for developing LPA stenosis (odds ratio or: 0.039; 95% confidence interval or 95% CI: 0.160.89; $p < 0.005$). At the same time, the presence of VSD was not associated with the risk of developing a stenosis of the PA or of the RPA ($p > 0.005$).

As indicated in Tables 2 and 3, there were no significant associations between the presence of an RVOT stenosis or aneurysm and the development of PA, RPA, or LPA stenosis.

Table 2. Comparison of medical characteristics between patients with and without PA stenosis (*N* = 116)

Variable	No (*n*=67)	Yes (*n*=49)	*p*-value
Age, months	28,5 (29,5)	24,6 (27)	0,48
Height, cm	107,1 (29,4)	103,1 (29,8)	0,47
Weight, kg	22,6 (17,4)	19 (12,9)	0,23
BSA	0,75 (0,29)	0,72 (0,34)	0,5
Gender			0,14
Male	36 (52,2%)	33 (47,8%)	
Female	31 (66%)	16 (34%)	
Palliative operation			0,8
No	52 (57,1%)	39 (42,9%)	
Yes	15 (60%)	10 (40%)	
ToF type			0,08
Pulmonary artery stenosis	56 (55%)	46 (45%)	
Pulmonary atresia	11 (79%)	3 (21%)	
Operation type			0,69
TAP	38 (56,7%)	29 (43,3%)	
No TAP	23 (56,1%)	18 (43,9%)	
Conduit	6 (75%)	2 (25%)	
Shunt thrombosis			0,58
No	66 (57,4%)	49 (42,6%)	
Yes	1 (100%)	0	
VSD			0,84
No	49 (58,3%)	35 (41,7%)	
Yes	18 (56,3%)	14 (43,7%)	
RVOT stenosis			0,26
No	61 (56,5%)	47 (43,5%)	
Yes	6 (75%)	2 (25%)	
RVOT aneurysm			0,33
No	65 (57%)	49 (43%)	
Yes	2 (100%)	0	
PA deformation			0,61
No	60 (58%)	44 (42,3%)	
Yes	7 (58,3%)	5 (41,7%)	
RPA stenosis			0,93
No	46 (57,5%)	34 (42,5%)	
Yes	21 (58,3%)	15 (41,7%)	
LPA stenosis			0,03*
No	29 (48,3%)	31 (51,7%)	
Yes	38 (67,9%)	18 (32,1%)	
RV dilation			0,58
No	61 (57,6%)	45 (42,4%)	
Yes	6 (60%)	4 (40%)	
Conduit calcification and stenosis			0,19
No	62 (56,4%)	48 (43,6%)	
Yes	5 (83,3%)	1 (16,7%)	

Note: *Chi-square test. $OR_{LPAstenosis\ yes}$ = 0.44. Interpretation: The odds ratio of PA stenosis for those who have LPA stenosis is 0.44 times (56% lower) than for those who does to have LPA stenosis.

Table 3. Comparison of medical characteristics between patients with and without LPA stenosis (*N* = 116)

Variable	No (*n*=60)	Yes (*n*=56)	*p*-value
Age, months	29,3 (32,2)	24,3 (24,1%)	0,35
Height, cm	108 (28,3)	102 (30,7)	0,3
Weight, kg	20,3 (12,4)	21,9 (18,7)	0,6
BSA	0,76 (0,33)	0,72 (0,29)	0,46
Gender			0,1
Male	40 (58%)	29 (42%)	
Female	20 (42,6%)	27 (57,4%)	
Palliative operation			0,35
No	45 (49,5%)	46 (50,5%)	
Yes	15 (60%)	10 (40%)	
ToF type			0,06
Pulmonary artery stenosis	56 (55%)	46 (45%)	
Pulmonary atresia	4 (28,6%)	10 (71,4%)	
Operation type			0,96
TAP	34 (50,8%)	33 (49,2%)	
No TAP	22 (53,7%)	19 (46,3%)	
Conduit	4 (50%)	4 (50%)	
Shunt thrombosis			0,52
No	59 (51,3%)	56 (48,7%)	
Yes	1 (100%)	0	
VSD			0,024*
No	38 (45,2%)	46 (54,8%)	
Yes	22 (68,8%)	10 (31,3)	
RVOT stenosis			0,6
No	56 (51,8%)	52 (48,2%)	
Yes	4 (50%)	4 (50%)	
RVOT aneurysm			0,23
No	60 (52,6%)	54 (47,4%)	
Yes	0	2 (100%)	
PA deformation			-
No	56 (53,8%)	48 (46,2%)	0,15
Yes	4 (33,3%)	8 (66,7%)	
RV dilation			0,42
No	54 (51%)	52 (49%)	
Yes	6 (60%)	4 (40%)	
Conduit calcification and stenosis			0,63
No	57 (51,8%)	53 (48,2%)	
Yes	3 (50%)	3 (50%)	

Note: *Chi-square test. $OR_{VSD\ yes}$ = 0.38. Interpretation: The odds of developing LPA stenosis is 0.38 times (62% lower) for those with VSD tan for those without VSD.

Table 4. Comparison of medical characteristics between patients with and without RPA stenosis (*N* = 116)

Variable	No (*n*=80)	Yes (*n*=36)	*p*-value
Age, months	26 (29,5)	28,7 (26,8)	0,64
Height, cm	107,8 (28,2)	100 (31,9)	0,19
Weight, kg	20 (12)	23,6 (22)	0,26
BSA	0,75 (0,32)	0,72 (0,29)	0,61
Gender			0,32
Male	50 (72,5%)	19 (27,5%)	
Female	30 (63,8%)	17 (36,2%)	
Palliative operation			0,35
No	64 (70,3%)	27 (29,7%)	
Yes	16 (64%)	9 (36%)	
ToF type			0,45
Pulmonary artery stenosis	71 (69,6%)	31 (30,4%)	
Pulmonary atresia	9 (64,3%)	5 (35,7%)	
Operation type			0,86
TAP	47 (70,2%)	20 (29,8%)	
No TAP	28 (68,3%)	13 (31,7%)	
Conduit	5 (62,5%)	3 (37,5%)	
Shunt thrombosis			0,69
No	79 (68,7%)	36 (31,3%)	
Yes	1 (100%)	0	
VSD			0,68
No	57 (67,9%)	27 (32,1%)	
Yes	23 (71,9%)	9 (28,1%)	
RVOT stenosis			0,52
No	74 (68,5%)	34 (31,5%)	
Yes	6 (75%)	2 (25%)	
RVOT aneurysm			0,09
No	80 (70,2%)	34 (29,8%)	
Yes	0	2 (100%)	
PA deformation			0,55
No	72 (69,2%)	32 (30,8%)	
Yes	8 (66,7%)	4 (33,3%)	
LPA stenosis			<0,001*
No	52 (86,7%)	8 (13,3%)	
Yes	28 (50%)	28 (50%)	
RV dilation			0,62
No	73 (68,9%)	33 (31,1%)	
Yes	7 (70%)	3 (30%)	
Conduit calcification and stenosis			0,39
No	75 (68,2%)	35 (31,8%)	
Yes	5 (83,3%)	1 (16,7%)	

Note: *Chi-square test. $OR_{LPA\ yes}$ = 6.5. Interpretation: The odds of developing RPA stenosis is 6.5 times (550%) higher for those with LPA stenosis than for those without LPA stenosis.

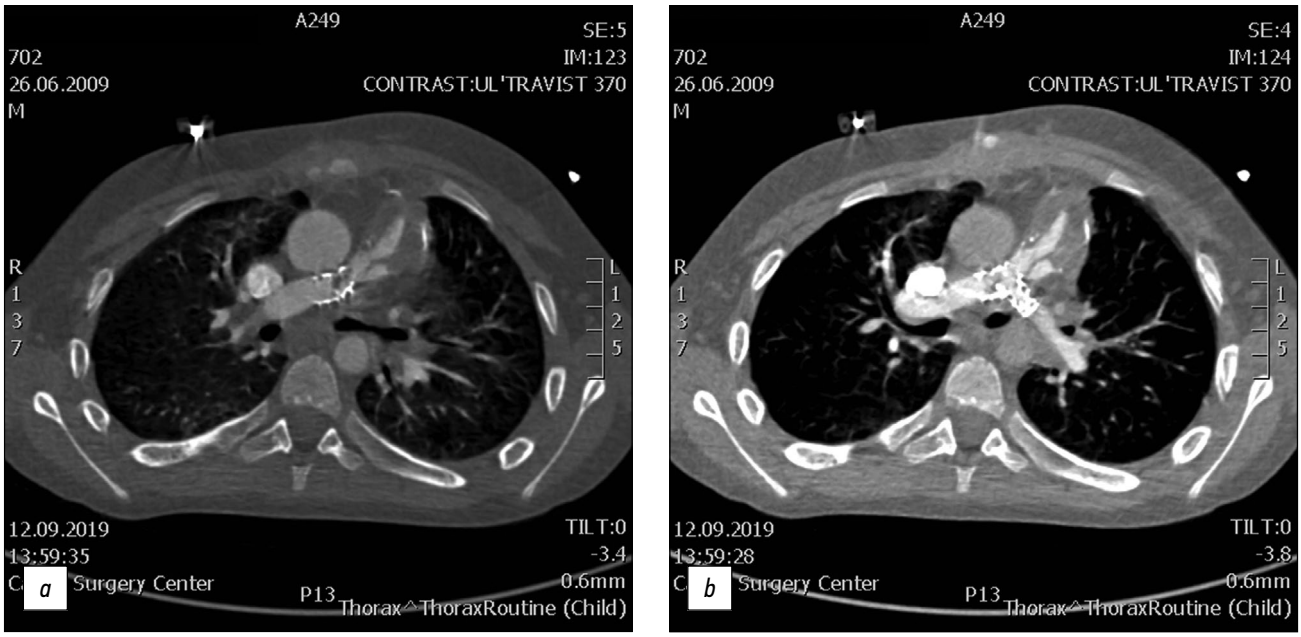

Fig. 1. CT of valve-containing conduit Contegra No. 16 and bilateral stents Palmaz Genesis XD 19-10.

Similar results were obtained for the presence or absence of a PA deformation ($p > 0.005$).

The development of PA stenosis was significantly lower (OR: 0.44; 95% CI 0.21–0.94; $p < 0.005$) among patients with an LPA stenosis, but not with an RPA stenosis ($p > 0.005$). At the same time, patients with an LPA stenosis had a 6.5 times (95% CI: 2.62–16.15; $p < 0.001$) greater chance of developing an RPA stenosis.

No significant associations were found between the RV dilation or the conduit calcification and stenosis and the development of a PA, an RPA, or an LPA stenosis ($p > 0.005$).

DISCUSSION

An increasing number of adult patients with CHD continue to require life-long diagnostic imaging surveillance through cardiac CT and MRI. These patients are characterized by a large spectrum of unique anatomical and functional changes resulting from either single- or multistage palliation and surgical correction. Radiologists involved in the diagnostic task of monitoring treatment effects and detecting potential complications should be familiar with common cardiac CT and MRI findings observed in patients with repaired, complex adult CHD (7).

Due to its high spatial and temporal resolution and the capability of providing high-quality three-dimensional reconstructed images, MDCT has become the primary modality for several patients, predominantly for the evaluation of PA and of the major aortopulmonary collateral arteries (8). In this study, we found that the most frequent complications occurring after a total rToF are PA and PA branch stenosis.

Echocardiography is still considered as the first modality in the evaluation of the postoperative complications following CHD treatment procedures, due to its known advantages of being safe, affordable, and lacking ionizing radiation, along with its superior capabilities in the delineation of the intracardiac anatomy and of the cardiac physiological functions. However, due to its dependency on its operator and the limitation of its narrow acoustic window, echocardiography faces difficulties in the visualization of extracardiac anatomy as well as a number of challenges in the quantitative assessment of the RV size, function, and valve regurgitation (9).

Cardiac CT and cardiac MRI are considered as minimally invasive techniques in the evaluation of the extracardiac postoperative vascular complications. However, in contrast to cardiac MRI, CT is superior in its inherent capability to identify intracardiac anatomical elements, to assess small vessel anatomy (including pulmonary veins, distal PA branches, and aortopulmonary collaterals), and to identify functional, and structural abnormalities or postoperative complications following CHD surgical procedures. Therefore, CT is steadily becoming an invaluable imaging modality capable of filling the gap between echocardiography, cardiac catheterization, and cardiac MRI (10).

Different types of conduits are used in the surgical rToF. The immediate postoperative results are excellent, but with time, progressive conduit obstruction occurs due to patient-prosthesis mismatch, distal anastomotic stenosis, conduit kinking, thrombosis, and the development of calcifications. MDCT can accurately assess the exact mechanism of such conduit obstructions, as well as assess the stenosis level, degree, and extension (2).

Transannular patch repair frequently leads to RVOT dilatation and aneurysms, chronic and severe pulmonary regurgitation, and subsequent RV dilatation, and dysfunction. An RVOT aneurysm is a ventricular wall swelling or its restored outflow, which is considered as an independent predictor of RV dilatation and systolic dysfunction in patients that have been subjected to an rToF. It is also a suitable substrate for the generation of ventricular arrhythmias. MDCT images clearly delineate the RVOT aneurysms as well as any associated dilatation of the main PA and its central branches. MDCT is excellent in depicting the morphology of the RVOT and cardiac abnormalities related to PR, in addition to accurate measurements of the enlarged RV volumes that serve as one of the major criteria for pulmonary valve replacement (2).

The present study had several limitations. First, this study was retrospective, and thereby limited by the small sample size. Additionally, being an observational study, it lacked gold standard for comparison.

CONCLUSION

Our study demonstrated that the most frequent complications observed in pediatric patients with repaired ToF were PA stenosis and PA branch stenosis. Patients with PA and PA branch stenosis exhibit no significant differences in terms of their age, anthropometric parameters (height, weight, and BSA), and gender distribution in the presence or absence of different stenosis types (PA, RPA, LPA). However, the presence of an RPA stenosis provides a greater chance of developing an LPA stenosis.

MDCT is an extremely useful imaging method for evaluating normal and abnormal findings after the surgical rToF due to its wide availability and high spatial and temporal resolution. MDCT is being used with increasing frequency to evaluate patients with ToF, as it provides reliable and accurate assessment of complex anatomy and associated anomalies in unrepaired ToF patients and guides the surgical approach and the necessary type of surgery needed. In addition, MDCT has given us the opportunity to fully understand and assess the late surgical sequelae, surgical complications, and residual lesions. Therefore, it is now essential that corrected ToF patients should have regular follow-ups in order to assess the existence of any residual lesions and surgical complications and to manage them appropriately and in a timely manner.

ADDITIONAL INFORMATION

Funding source. This study was not supported by any external sources of funding.

Competing interests. The authors declare that they have no competing interests.

Authors' contribution. All authors made a substantial contribution to the conception of the work, acquisition, analysis, interpretation of data for the work, drafting and revising the work, final approval of the version to be published and agree to be accountable for all aspects of the work. R.I. Rakhimzhanova, T.B. Dautov — conception and design of the work; A.M. Kabdullina, B.B. Kaliyev, L.A. Bastarbekova, Zh.A. Moldakhanova — acquisition, analysis of data; A.M. Kabdullina, A.B. Saduakassova — interpretation of data; V.E. Sinitsyn — approved the final version of the work.

Acknowledgments. We thank the Chief of the National Research Cardiac Surgery Center MD Ph.D. professor Yuriy V. Pya for the opportunity to carry out this work.

REFERENCES

1. Apostolopoulou SC, Manginas A, Kelekis NL, Noutsias M. Cardiovascular imaging approach in pre and postoperative tetralogy of Fallot. *BMC Cardiovasc Dis*. 2019;19(1):7. doi: 10.1186/s12872-018-0996-9

2. Shaaban M, Tantawy S, Elkafrawy F, et al. Multi-detector computed tomography in the assessment of tetralogy of Fallot patients: Is it a must? *Egyptian Heart J*. 2020;72(1):17. doi: 10.1186/s43044-020-00047-3

3. Goo HW. Changes in right ventricular volume, volume load, and function measured with cardiac computed tomography over the entire time course of tetralogy of Fallot. *Korean J Radiol*. 2019;20(6):956–966. doi: 10.3348/kjr.2018.0891

4. Stout KK, Daniels CJ, Aboulhosn JA, et al. 2018 AHA/ACC Guideline for the management of adults with congenital heart disease: Executive summary: A report of the American College of Cardiology / American Heart Association Task Force on Clinical Practice Guidelines. *J Am College Cardiol*. 2019;73(12):1494–1563. doi: 10.1016/j.jacc.2018.08.1028

5. Chelliah A, Shah AM, Farooqi KM, Einstein AJ. Cardiovascular CT in cyanotic congenital heart disease. *Curr Cardiovasc Imaging Rep*. 2019;12(7):30. doi: 10.1007/s12410-019-9507-3

6. Goo HW. Comparison of chest pain protocols for electrocardiography-gated dual-source cardiothoracic CT in children and adults: The effect of tube current saturation on radiation dose reduction. *Korean J Radiol*. 2018;19(1):23–31. doi: 10.3348/kjr.2018.19.1.23

7. Siripornpitak S, Goo HW. CT and MRI for repaired complex adult congenital heart diseases. *Korean J Radiol*. 2021;22(3):308–323. doi: 10.3348/kjr.2020.0895

8. Singh R, Jain N, Kumar S, Garg N. Multi-detector computed tomography angiographic evaluation of right ventricular outflow tract obstruction and other associated cardiovascular anomalies in tetralogy of Fallot patients. *Polish J Radiol*. 2019;84:511–516. doi: 10.5114/pjr.2019.91203

9. Kossaify A. Echocardiographic assessment of the right ventricle, from the conventional approach to speckle tracking and three-

dimensional imaging, and insights into the "Right Way" to explore the forgotten chamber. *Clin Med Insights Cardiol*. 2015;9:65–75. doi: 10.4137/CMC.S27462

10. Pushparajah K, Duong P, Mathur S, Babu-Narayan SV. Cardiovascular MRI and CT in congenital heart disease. *Echo Res Pract*. 2019;6(4):R121–138. doi: 10.1530/ERP-19-0048

СПИСОК ЛИТЕРАТУРЫ

1. Apostolopoulou S.C., Manginas A., Kelekis N.L., Noutsias M. Cardiovascular imaging approach in pre and postoperative tetralogy of Fallot // BMC Cardiovasc Dis. 2019. Vol. 19, N 1. P. 7. doi: 10.1186/s12872-018-0996-9

2. Shaaban M., Tantawy S., Elkafrawy F., et al. Multi-detector computed tomography in the assessment of tetralogy of Fallot patients: Is it a must? // Egyptian Heart J. 2020. Vol. 72, N 1. P. 17. doi: 10.1186/s43044-020-00047-3

3. Goo H.W. Changes in right ventricular volume, volume load, and function measured with cardiac computed tomography over the entire time course of tetralogy of Fallot // Korean J Radiol. 2019. Vol. 20, N 6. P. 956–966. doi: 10.3348/kjr.2018.0891

4. Stout K.K., Daniels C.J., Aboulhosn J.A., et al. 2018 AHA/ACC Guideline for the management of adults with congenital heart disease: Executive summary: A report of the American College of Cardiology / American Heart Association Task Force on Clinical Practice Guidelines // J Am College Cardiol. 2019. Vol. 73, N 12. P. 1494–1563. doi: 10.1016/j.jacc.2018.08.1028

5. Chelliah A., Shah A.M., Farooqi K.M., Einstein A.J. Cardiovascular CT in cyanotic congenital heart disease // Curr Cardiovasc Imaging Rep. 2019. Vol. 12, N 7. P. 30. doi: 10.1007/s12410-019-9507-3

6. Goo H.W. Comparison of chest pain protocols for electrocardiography-gated dual-source cardiothoracic CT in children and adults: The effect of tube current saturation on radiation dose reduction // Korean J Radiol. 2018. Vol. 19, N 1. P. 23–31. doi: 10.3348/kjr.2018.19.1.23

7. Siripornpitak S., Goo H.W. CT and MRI for repaired complex adult congenital heart diseases // Korean J Radiol. 2021. Vol. 22, N 3. P. 308–323. doi: 10.3348/kjr.2020.0895

8. Singh R., Jain N., Kumar S., Garg N. Multi-detector computed tomography angiographic evaluation of right ventricular outflow tract obstruction and other associated cardiovascular anomalies in tetralogy of Fallot patients // Polish J Radiol. 2019. Vol. 84. P. 511–516. doi: 10.5114/pjr.2019.91203

9. Kossaify A. Echocardiographic assessment of the right ventricle, from the conventional approach to speckle tracking and three-dimensional imaging, and insights into the «Right Way» to explore the forgotten chamber // Clin Med Insights Cardiol. 2015. Vol. 9. P. 65–75. doi: 10.4137/CMC.S27462

10. Pushparajah K., Duong P., Mathur S., Babu-Narayan S.V. Cardiovascular MRI and CT in congenital heart disease // Echo Res Pract. 2019. Vol. 6, N 4. P. R121–138. doi: 10.1530/ERP-19-0048

AUTHORS' INFO

*** Azhar M. Kabdullina;**
address: 49A Beybitshilik street, 01000 Astana, Kazakhstan;
ORCID: 0000-0003-0521-5484;
eLibrary SPIN: 4169-1761;
e-mail: azharazh@mail.ru

Valentin E. Sinitsyn, MD, Dr. Sci. (Med.), Professor;
ORCID: 0000-0002-5649-2193;
eLibrary SPIN: 8449-6590;
e-mail: vsini@mail.ru

Raushan I. Rakhimzhanova, MD, Dr. Sci. (Med.), Professor;
ORCID: 0000-0002-3490-6324;
e-mail: rakhimzhanova01@rambler.ru

Tairkhan B. Dautov, MD, Dr. Sci. (Med.), Professor;
ORCID: 0000-0002-5267-0108;
e-mail: tairkhan.dautov@mail.ru

Aigul B. Saduakassova, MD, Dr. Sci. (Med.);
ORCID: 0000-0001-7089-5696;
e-mail: sadik.a@mail.ru

Bauyrzhan B. Kaliyev;
ORCID: 0000-0003-4825-749X;
e-mail: Baur233113@mail.ru

ОБ АВТОРАХ

*** Кабдуллина Ажар Муслюмкановна;**
адрес: Казахстан, 01000, Астана, ул. Бейбитшилик, д. 49А;
ORCID: 0000-0003-0521-5484;
eLibrary SPIN: 4169-1761;
e-mail: azharazh@mail.ru

Синицын Валентин Евгеньевич, д-р мед. наук, профессор;
ORCID: 0000-0002-5649-2193;
eLibrary SPIN: 8449-6590;
e-mail: vsini@mail.ru

Рахимжанова Раушан Ибжановна, д-р мед. наук, профессор;
ORCID: 0000-0002-3490-6324;
e-mail: rakhimzhanova01@rambler.ru

Даутов Таирхан Бекполатович, д-р мед. наук, профессор;
ORCID: 0000-0002-5267-0108;
e-mail: tairkhan.dautov@mail.ru

Садуакасова Айгуль Болатовна, д-р мед. наук;
ORCID: 0000-0001-7089-5696;
e-mail: sadik.a@mail.ru

Калиев Бауржан Бахытович;
ORCID: 0000-0003-4825-749X;
e-mail: Baur233113@mail.ru

* Corresponding author / Автор, ответственный за переписку

Lyazzat A. Bastarbekova;
ORCID: 0000-0001-8246-4754;
eLibrary SPIN: 8634-6601;
e-mail: lbastarbekova@mail.ru

Zhanar A. Moldakhanova;
ORCID: 0000-0002-5980-9563;
e-mail: moldahanova1991@mail.ru

Бастарбекова Лаззат Абылхановна;
ORCID: 0000-0001-8246-4754;
eLibrary SPIN: 8634-6601;
e-mail: lbastarbekova@mail.ru

Молдаханова Жанар Акбергенова;
ORCID: 0000-0002-5980-9563;
e-mail: moldahanova1991@mail.ru

DOI: https://doi.org/10.17816/DD494103

Магнитно-резонансная томография сердца у пациентов, переболевших коронавирусной инфекцией (COVID-19)

А.С. Максимова, Н.И. Рюмшина, Т.А. Шелковникова, О.В. Мочула, Н.Д. Анфиногенова, В.Ю. Усов

Томский национальный исследовательский медицинский центр, Научно-исследовательский институт кардиологии, Томск, Российская Федерация

АННОТАЦИЯ

Обоснование. Нередким осложнением коронавирусной инфекции (COVID-19) является миокардит.

Цель — сравнить различные паттерны повреждения миокарда у пациентов, перенёсших COVID-19, и пациентов допандемийного периода по данным магнитно-резонансной томографии сердца с парамагнитным контрастным усилением.

Материалы и методы. В ретроспективное исследование включено 47 пациентов, которым выполняли магнитно-резонансную томографию сердца с парамагнитным контрастным усилением для исключения острого миокардита. В группу 1 вошли 34 пациента с перенесённой коронавирусной инфекцией, подтверждённой результатами исследования мазка со слизистой носо- и/или ротоглотки методом полимеразной цепной реакции, в группу 2 — 13 человек, магнитно-резонансную томографию сердца которым проводили до начала пандемии коронавирусной инфекции (2017 г).

Результаты. Средняя продолжительность от появления жалоб до проведения магнитно-резонансной томографии составила 166 дней. Снижение толерантности к физическим нагрузкам обнаружено у 77% пациентов, боль в области сердца, одышка и сердцебиение — у 14 (42%), 30 (88%) и 28 (85%) пациентов группы 1 соответственно. В группе 2 отмечены одышка у 4 (30%) пациентов, боли в области сердца — у 9 (69%), сердцебиение и/или ощущение ритма сердца — у 6 (46%). У пациентов группы 1 поражение миокарда носило более распространённый характер, из них у 1/3 сохранялись усиление лёгочного рисунка и выпот в плевральную полость. В группе 1 мужчины имели более низкую фракцию выброса левого желудочка, меньшие показатели глобальной продольной деформации и более высокие функциональные показатели левого предсердия (p <0,05). У женщин статистические различия отмечались только по количеству поражённых сегментов миокарда левого желудочка.

Заключение. Вирус SARS-CoV-2 вызывает распространённое поражение сердца с вовлечением значительного количества сегментов миокарда. Среди мужчин достоверно чаще развиваются поствоспалительные осложнения в виде нарушения сократительной функции левого желудочка и левого предсердия. Полученные результаты указывают на необходимость дальнейшей оценки долгосрочных последствий перенесённого COVID-19 на сердечно-сосудистую систему. Магнитно-резонансная томография сердца с контрастированием в данном случае может быть чувствительным инструментом визуализации для выявления тяжести поражения сердца.

Ключевые слова: магнитно-резонансная томография; сердце; коронавирусная инфекция; COVID-19; миокардит; левое предсердие.

Как цитировать:

Максимова А.С., Рюмшина Н.И., Шелковникова Т.А., Мочула О.В., Анфиногенова Н.Д., Усов В.Ю. Магнитно-резонансная томография сердца у пациентов, переболевших коронавирусной инфекцией (COVID-19) // *Digital Diagnostics.* 2023. Т. 4, № 3. С. 280–291. DOI: https://doi.org/10.17816/DD494103

Рукопись получена: 16.06.2023 **Рукопись одобрена:** 10.07.2023 **Опубликована:** 23.08.2023

DOI: https://doi.org/10.17816/DD494103

Cardiac magnetic resonance imaging in patients with history of COVID-19

Aleksandra S. Maksimova, Nadezhda I. Ryumshina, Tatiana A. Shelkovnikova, Olga V. Mochula, Nina D. Anfinogenova, Wladimir Yu. Ussov

Tomsk National Research Medical Center, Cardiology Research Institute, Tomsk, Russian Federation

ABSTRACT

BACKGROUND: Myocarditis is among the most common complications arising from coronavirus infection (COVID-19).

AIM: This study aims to find the differences in the patterns of myocardial injury between patients who had COVID-19 and those from the pre-pandemic period, as determined by contrast-enhanced cardiac magnetic resonance imaging.

MATERIALS AND METHODS: The study encompassed a retrospective analysis of 47 patients who underwent contrast-enhanced cardiac magnetic resonance imaging to rule out acute myocarditis. Group 1 comprised 34 patients with a confirmed history of COVID-19 through PCR testing (nasal and/or throat swabs), while Group 2 comprised 13 individuals who underwent contrast-enhanced cardiac magnetic resonance imaging in 2017 prior to the onset of the COVID-19 pandemic. All patients enrolled in the study had clinical manifestation of cardiac injury without signs of coronary artery disease as an underlying cause of condition.

RESULTS: The mean time from the onset of heart symptoms to the administration of contrast-enhanced cardiac magnetic resonance imaging was 166 days. In group 1, a decrease in exercise tolerance was observed in 77% of patients, and 14 (42%), 30 (88%), and 28 (85%) of patients complained of chest pain, shortness of breath, and heart palpitations, respectively. In group 2, four patients (30%) had dyspnea, nine patients (69%) complained of chest pain, and six patients (46%) had heart palpitations and/or feeling of arrhythmia. Myocardial injury in group 1 was more generalized. The third of them had displayed preserved increased pulmonary vascularity and pleural effusion. Within group 1, men had significantly lower left ventricular ejection fraction, lower values of global longitudinal deformation, and higher values of left atrial function compared with the corresponding parameters in women. Differences in women were found only in the number of the affected segments in the left ventricular myocardium.

CONCLUSION: SARS-CoV-2 virus caused extended myocardial injury, affecting a significant number of myocardial segments. Men had more frequent postinflammatory complications, characterized by abnormal function of the left ventricle and left atrium. Obtained results require continuous efforts for further assessment of long-term consequences of previous COVID-19 to the cardiovascular system. In this regard, contrast-enhanced cardiac magnetic resonance imaging may represent a sensitive imaging tool for the assessment of cardiac injury severity.

Keywords: magnetic resonance imaging; heart; coronavirus infection; COVID-19; myocarditis; left atrium.

To cite this article:
Maksimova AS, Ryumshina NI, Shelkovnikova TA, Mochula OV, Anfinogenova ND, Ussov WYu. Cardiac magnetic resonance imaging in patients with history of COVID-19. *Digital Diagnostics.* 2023;4(3):280–291. DOI: https://doi.org/10.17816/DD494103

Received: 16.06.2023 **Accepted:** 10.07.2023 **Published:** 23.08.2023

DOI: https://doi.org/10.17816/DD494103

患过冠状病毒感染（COVID-19）患者的心脏磁共振成像

Aleksandra S. Maksimova, Nadezhda I. Ryumshina, Tatiana A. Shelkovnikova, Olga V. Mochula, Nina D. Anfinogenova, Wladimir Yu. Ussov

Tomsk National Research Medical Center, Cardiology Research Institute, Tomsk, Russian Federation

简评

论证。心肌炎是冠状病毒感染（COVID-19）的一种不罕见并发症。

该研究的目的是通过顺磁对比剂增强的心脏磁共振成像，比较患过COVID-19和大流行前患者心肌损伤的不同模式。

材料和方法。一项回顾性研究纳入了47名接受顺磁对比剂增强心脏磁共振成像检查来排除急性心肌炎的患者。第1组包括34名通过鼻咽和/或口咽粘膜涂片聚合酶链反应分析证实曾患过冠状病毒感染的患者，第2组包括13名在冠状病毒大流行（2017年）前接受心脏磁共振成像检查的患者。

结果。从发病到磁共振成像的平均时间为166天。在第一组中，77%的患者运动耐量降低了，分别有14（42%）、30（88%）和28（85%）名患者出现了心脏疼痛、呼吸困难和心悸。在第2组中，有4名患者（30%）出现了呼吸困难，有9名患者（69%）出现了心脏疼痛，有6名患者（46%）出现了心悸和/或心律不齐。心肌损伤在第1组患者中更为普遍，其中1/3患者有持续性肺强化和胸腔积液。在第1组中，男性的左心室射血分数较低，整体纵向应变较低，左心房功能较高（p<0,05）。对于女性病人来说，仅在左心室心肌受影响节段的数量上存在统计上的差异。

结论。SARS-CoV-2病毒导致广泛的心脏损伤，累及大量心肌节段。对于男性病人来说，更容易出现左心室和左心房收缩功能障碍等炎症后并发症。结果表明，有必要进一步评估COVID-19对心血管系统的长期影响。在这种情况下，带有对比剂的心脏磁共振成像可能是检测心脏损伤严重程度的灵敏成像工具。

关键词：磁共振成像；心脏；冠状病毒感染；COVID-19；心肌炎；左心房。

引用本文：

Maksimova AS, Ryumshina NI, Shelkovnikova TA, Mochula OV, Anfinogenova ND, Ussov WYu. 患过冠状病毒感染（COVID-19）患者的心脏磁共振成像. *Digital Diagnostics.* 2023;4(3):280–291. DOI: https://doi.org/10.17816/DD494103

收到：16.06.2023 **接受：**10.07.2023 **发布日期：**23.08.2023

Abbreviations

BSA body surface area
EDV end-diastolic volume
EF ejection fraction
ESV end-systolic volume
ESVi end-systolic volume index
LA left atrium
LAV left atrial volume
LAVi left atrium volume index
LGE late gadolinium enhancement
LV left ventricle
MRI magnetic resonance imaging

BACKGROUND

Since March 2020, COVID-19, caused by SARS-CoV-2 infection, has been declared a global pandemic. COVID-19 primarily affects the respiratory system [1], and treatment is aimed mainly at respiratory complications. On the other hand, the new coronavirus infection has a major influence on the cardiovascular system, particularly in patients with pre-existing cardiovascular diseases [2]. COVID-19 can cause myocardial injury at any stage of the infection, including the viral, pulmonary, inflammatory, and recovery phases and later stages after symptoms appear [3]. COVID-19 patients have been linked to arrhythmia, cardiac failure, and myocarditis [4]. The mechanisms of cardiac damage caused by SARS-CoV-2 infection are not entirely known.

The most common complication of coronavirus infection is myocarditis. Myocarditis manifests clinically as modest symptoms, such as fatigue and dyspnea, to rapid disease progression with heart failure and cardiogenic shock [5]. Imaging is critical for assessing many elements of myocardial damage, allowing for a precise diagnosis and early treatment. Contrast-enhanced cardiac magnetic resonance imaging (MRI) is recommended by the Russian and European Societies of Cardiology as an insightful, non-invasive method of imaging diagnosis in myocarditis, ensuring detailed visualization of anatomical structures and assessment of functional heart disorders [6, 7].

According to the World Health Organization, COVID-19 is no longer classified as a global pandemic. However, the pandemic's long-term negative, harmful ramifications, including major cardiovascular issues, are only beginning to emerge. Thus, cardiac viability testing in post-COVID-19 patients is still important and warrants further research [8]. Furthermore, differences in study designs and inclusion/exclusion criteria, as well as imaging methodologies and data analysis, interpretation, and reporting in terms of changes in cardiac MRI findings, all contribute to high degree of variability in published study results.

The study compared different patterns of myocardial injury in post-COVID-19 patients to prepandemic patients using contrast-enhanced cardiac MRI data.

MATERIALS AND METHODS

Study design

This retrospective study was conducted in accordance with Good Clinical Practice and the principles described in the Helsinki Declaration.

Study conditions

The study was performed in the Department of X-ray and Imaging Diagnosis, Cardiology Research Institute, Tomsk National Research Medical Center of the Russian Academy of Sciences. All patients provided informed consent to paramagnetic contrast-enhanced cardiac MRI.

Eligibility criteria

Inclusion criteria for Group 1: a history of SARS-CoV-2 infection confirmed by polymerase chain reaction testing, no symptoms of acute respiratory infection at the time of cardiac MRI, a negative polymerase chain reaction test for COVID-19, objective evidence of symptomatic cardiac injury, without signs of ischemic heart disease (chest pain/discomfort, palpitations, and dyspnea), and a mean time from the onset of complaints to MRI 166 ± 17.

Inclusion criteria for Group 2: objective evidence of symptomatic cardiac damage without indicators of ischemic heart disease (chest pain/discomfort, palpitations, and dyspnea) and cardiac MRI performed before the COVID-19 pandemic (2017).

Exclusion criteria for both groups included a history of myocardial infarction and low-quality cardiac MRI scans, which made analysis challenging.

Cardiac MRI protocol

The Vantage Titan MRI Scanner (Toshiba, Japan) was used to perform paramagnetic contrast-enhanced cardiac MRI and ECG- and respiratory-gated 1.5T MRI. Short- and long-axis MRI images of the myocardium were acquired before and after contrast enhancement. As a paramagnetic contrast agent, 0.5 M Gadobutrol was administered intravenously at a 0.1-mL/kg body weight dose. The slice thickness was 10 mm, with no gaps, and the data were recorded to a 256 × 256 matrix. T1- and T2-weighted sequences and a fat suppression sequence were used to assess the myocardium;

dynamic SSFP sequences were used to determine the left ventricular (LV) volume and function; and gradient inversion-recovery sequences (GR-IR) were used to identify abnormal contrast uptake areas. The time of inversion (TI) was selected individually (mean TI = 300 ± 10 ms). The approved 17-segment model of localization diagnosis for LV myocardium was used to analyze areas of defective myocardium.

Cardiac MRI scans were examined in the Medical Genomics Resource Sharing Center using the cvi42 program (Circle Cardiovascular Imaging, Calgary, Canada). The Lake–Louise criteria were used for the diagnosis of myocarditis. Major criteria included edema, hyperemia, and regional fibrosis, and minor criteria included pericardial effusion or hyperintensive signal from the pericardium and LV wall motion abnormality [9]. On T2-weighted images (T2WI), the edema ratio (ER) was calculated as the myocardial-to-skeletal muscle signal intensity ratio. ER >2.0 was considered a symptom of edema. On T1WI, the relative paramagnetic contrast uptake (hyperemia) was assessed in inferolateral LV segments, which are most commonly affected by inflammatory changes. A relative paramagnetic contrast uptake of more than >4.0 was considered a symptom of hyperemia.

The presence and nature (subendocardial, subepicardial, or intramural) of late gadolinium enhancement (LGE) and the number of involved segments were assessed. The outlines of the endocardium and epicardium were used to automatically identify the functional characteristics of the left and right ventricles. End-diastolic volume (EDV), end-systolic volume (ESV), ejection fraction (EF), left ventricular global radial and longitudinal strain, and minimum and maximum left atrial volume were among the functional parameters measured. The following parameters were calculated based on these measurements:

- left atrium volume index (LAVi, mL/m^2) = LA volume/BSA, where LA = left atrium; BSA = body surface area;
- end-diastolic volume index (EDVi): EDVi = EDV/BSA;
- end-systolic volume index (ESVi): ESVi = ESV/BSA.

LA functional parameters were calculated as follows:

- LA ejection fraction (LAEF) = ([LAVmax – LAVmin]/LAVmax) × 100%;
- LA strain = ([LAVmax – LAVmin)/LAVmin) × 100% [10].

Furthermore, pericardial effusion, pleural effusion, and enhanced pulmonary vascularity were also evaluated.

Statistical processing

Statistical analysis was performed using STATISTICA 10 software. Absolute (*n*) and relative (%) frequencies are used to represent categorical variables. The mean (m) and standard deviation (*SD*) or median (Me) and interquartile range [Q1; Q3] are used to represent continuous variables. The Shapiro–Wilk test was used to determine the normality of distribution. For categorical variables, the unpaired *t* test (for normal distribution) or Mann–Whitney *U* test (for nonnormal distribution) was used, and for continuous variables, the chi-squared test was used. $P < 0.05$ was considered significant.

RESULTS

Study subjects

A contrast-enhanced cardiac MRI was done on 47 patients to rule out acute myocarditis. The first group consisted of 34 individuals with a coronavirus infection history verified by polymerase chain reaction testing of a nasopharyngeal and/or oropharyngeal swab. Before the COVID-19 pandemic (2017), a cardiologist referred 13 patients for cardiac MRI. Table 1 shows the clinical characteristics of patients and cardiac MRI parameters in the study group. The study and control groups were balanced by sex, age, and body mass index. In Group 1, 77% of patients reported lower exercise tolerance, whereas 14 (42%), 30 (88%), and 28 (85%) felt chest discomfort, dyspnea, and palpitations, respectively. In Group 2, four (30%) patients complained of dyspnea, nine (69%) reported chest pain, and six (46%) reported palpitations.

In the early phase of contrast enhancement (1–2 min), there was no difference between the groups in LV and LA functional metrics or contrast uptake. Group 1 patients demonstrated more severe myocardial injury, with more segments showing a nonischemic pattern of LGE. Furthermore, pulmonary changes (i.e., increased pulmonary vascularity and pleural effusion) remained in one-third of Group 1 patients during cardiac MRI (Figure 1).

Male patients in Group 1 exhibited considerably lower LVEF, lower global longitudinal strain, and higher LA functional characteristics, according to an intragroup comparison by sex. Only the number of affected LV myocardium segments differed significantly in female patients (Table 2). Male and female groups had no age differences ($p = 0.78$ and $p = 0.18$, respectively).

Key study findings

Our study found that post-COVID-19 patients had a higher number of affected LV myocardium segments based on delayed paramagnetic contrast uptake (a sign of fibrotic changes) than prepandemic patients with suspected myocarditis; however, the myocardial injury was nonspecific. Male patients showed lower LVEF, lower LV global longitudinal strain, and higher LV volume with reduced LV contractility. Because the SARS-CoV-2 virus primarily affects the respiratory system, the heterogeneous lung tissue thickening, and pleural effusion observed in post-COVID-19 patients were believed to represent evidence of long-term recovery from a respiratory infection. The control group did not show any of these changes.

DISCUSSION

Previous research [11] shows that the most prevalent COVID-19 symptoms are dyspnea and chest discomfort.

Table 1. Clinical characteristics and cardiac MRI parameters in post-COVID-19 patients and control individuals

Parameter	Group 1 COVID-19(+) *n* = 34	Group 2 COVID-19(–) *n* = 13	*p*
Age, year	62.5 [55; 66]	52 [45; 65]	0.07
Male, *n* (%)	12 (35.3)	6 (46.1)	0.49
Body mass index, kg/m^2	30.69±5.22	27.75±4.05	0.08
Body surface area, m^2	1.95±0.27	1.97±0.17	0.15
Heart rate, bpm	72.73±8.75	78±21.6	0.23
Concomitant diseases, *n* (%):			
• Hypertension	17 (50)	7 (53)	0.81
• Diabetes mellitus	2 (5)	0	0.37
• Ischemic heart disease	8 (23)	4 (30)	0.61
• Chronic obstructive pulmonary disease	9 (26)	1 (7)	0.16
Cardiac symptoms, *n* (%):			
• Chest pain	14 (42)	4 (30)	0.51
• Palpitations	30 (88)	9 (69)	0.12
• Dyspnea	28 (85)	6 (46)	0.01*
• Decreased exercise tolerance	26 (77)	5 (39)	0.01*
LVEF, %	55.07±19.34	63.31±4.9	0.14
EDV LV, mL	113 [94.7; 153.8]	135.6 [116.72; 167.79]	0.98
ESV LV, mL	41 [28.9; 83]	50.87 [46.85; 63.04]	0.31
EDVi LV, mL/m^2	61.5 [48.2; 72.6]	69.5 [62.1; 79.9]	0.13
ESVi LV, mL/m^2	22.7 [16.4; 45.7]	26.1 [23.1;30.6]	0.39
ER	1.5±0.36	1.58±0.39	0.54
Edema (visual), *n* (%)	5 (14.7)	0 (0)	0.14
LGE, *n* (%)	33 (97)	12 (92.3)	0.47
Number of LGE segments	6.79±2.36	3.25±1.48	0.000*
Pericardial effusion, *n* (%)	22 (64.7)	5 (38)	0.10
Pleural effusion, *n* (%)	10 (29.4)	0 (0)	0.03*
Increased pulmonary vascularity, *n* (%)	12 (35.3)	0 (0)	0.01*
GRS LV, %	17.52±9.61	16.86±5.54	0.82
GLS LV, %	-10.51±5.49	-10.96±2.66	0.78
Contrast enhancement index on T1-WI of the basal inferolateral segment	1.54±0.29	1.71±0.53	0.17
Contrast enhancement index on T1-WI of the medial inferolateral segment	1.53±0.29	1.51±0.5	0.89
Contrast enhancement index on T1-WI of the apical lateral segment	1.55±0.34	1.38±0.33	0.13
LAV max, mL	72.39 [56.3; 110.15]	57.80 [51.84; 96.6]	0.32
LAV min, mL	35.44 [18.47; 62.09]	21.35 [19.0; 42.07]	0.49
RAV max, mL	35.205 [31.08;53.11]	40.2 [31.8; 51.095]	0.68
RAV min, mL	66.47 [55.96; 96.75]	84.945 [66.14; 93.305]	0.30
LAVi, mL/m^2	39.13 [32.09; 51.09]	27.8 [27.2; 43.89]	0.17
LAEF, %	53.55 [37.26; 163.32]	61.22 [55.35; 64.51]	0.13
LA strain, %	115.28 [59.39; 163.32]	149.7 [121.74; 173.93]	0.30

Note. The data are presented as the median (Me) and interquartile range [Q1; Q3].

Abbreviations: EDV, end-diastolic volume; ESV, end-systolic volume; EDVi, end-diastolic volume index; ER, edema ratio; ESVi, end-systolic volume index; GRS LV, global radial strain left ventricular; LA strain, left atrial strain; LAEF, left atrial ejection fraction; LAV, left atrial volume; LAVi, left atrium volume index; LGE, late gadolinium enhancement; LVEF, left ventricular ejection fraction; RAV, right atrium volume; T1-WI, T1-weighted images.

*$p < 0.05$.

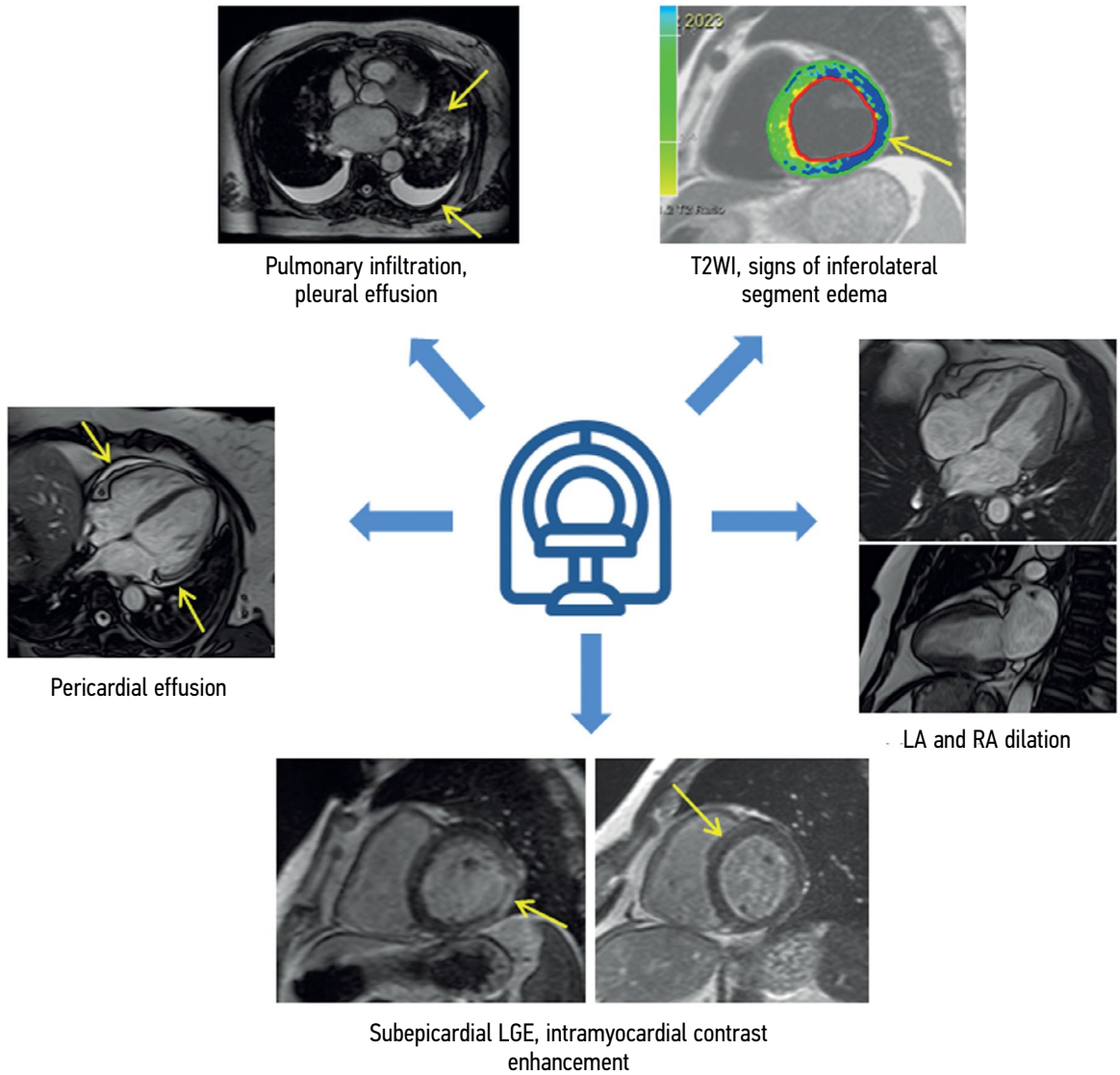

Fig. 1. Characteristic symptoms detected on contrast-enhanced cardiac MRI in the group of post-COVID-19 patients. LA, left atrium; LGE, late gadolinium enhancement; RA, right atrium; T2WI, T2-weighted image.

Table 2. Comparative analysis of the left ventricular and left atrial function based on MRI findings

Parameter	Men			Women		
	COVID-19(+)	COVID-19(–)	*p*	COVID-19(+)	COVID-19(–)	*p*
LVEF, %	38 [26.2; 54.5]	63 [62.5; 63.9]	0.04*	65 [59; 70]	64.5 [60.5; 67.7]	0.78
Number of LGE segments	7.5 [6.5; 9.5]	4 [3; 4]	0.03*	6.5 [5; 8]	3 [2; 4]	0.00*
Longitudinal strain	-7.0 [-9.3; -3.1]	-10.2 [-11.1; -8.2]	0.04*	-14.6 [-15.8; -10.2]	-10.9 [-15; -9.3]	0.62
LA volume, min., mL	83.8 [37.3; 127.8]	25.6 [18; 35.3]	0.02*	25 [16.1; 35.9]	21.4 [20; 48.9]	0.59
LA ejection fraction, %	30.1 [12.1; 47.8]	63.5 [54.9; 68.5]	0.01*	59.9 [53.4; 72.2]	59.9 [55.3; 64.5]	0.94
LA strain, %	43.1 [13.9; 91.9]	173.8 [121.7; 217.9]	0.01*	149.9 [114.7; 259.7]	143.7 [101; 157.9]	0.43

Note. The data are presented as the median (Me) and interquartile range [Q1; Q3].

Abbreviations: LA, left atrium; LGE, late gadolinium enhancement; LVEF, left ventricular ejection fraction.
*$p < 0.05$.

Unfortunately, these symptoms remain even in patients with a negative SARS-CoV-2 test, resulting in a chronic COVID-19 syndrome. The long-term risks and clinical significance of these symptoms are not fully understood. The clinical indications found in this group of patients were considered to be the outcome of continuous myocardial injury caused by inflammation. However, most of our patients did not have myocardial edema, and the myocardium-to-muscle tissue signal intensity ratio on T2WI was within normal limits. Furthermore, there were no statistically significant differences in the increase in myocardium signal intensity within the first few minutes after the contrast injection. Thus, our sample lacked two of the three major MRI criteria for myocarditis (edema and hyperemia), preventing a definite diagnosis of myocarditis based on current guidelines [12].

In the study by Feofanova, evaluating the cardiovascular system in 36 patients with a history of acute COVID-19, there was a significant increase in LA volume with preserved LVEF. Only 8.4% of patients had a decline in LA systolic function, whereas 83.3% had a rise in LV volume [13]. Furthermore, the majority of study participants had LV myocardial hypertrophy (94.4%), pulmonary hypertension (72.2%), and atrial and ventricular ectopic activity manifested by supraventricular arrhythmia (94.4%), ventricular arrhythmia (63.9%), and paroxysmal supraventricular tachycardia (36.1%). The decreased heart function observed in our study was not statistically significant. The mean LVEF was 55%, with a median EDV of 61.5 mL/m^2. LAVi in Group 1 exceeded 39.13 mL/m^2, whereas LAVi in Group 2 was 27.8 mL/m^2. The LV wall thickness in our sample was within normal limits, and pulmonary alterations remained in one-third of post-COVID-19 patients. There were no cases of rhythm disturbance (a common post-COVID-19 complication) in our sample.

According to some studies, the earlier indicator of LV myocardium remodeling is a decrease in LV longitudinal and/or global strain [14]. The LV longitudinal strain was reduced in both groups, although there were no significant differences between them. In our study, 21% of the patients (mainly men) had decreased LV contractility.

Our data indicating gender inequalities between groups are significant. As previously stated, Group 1 patients, both male and female, showed more severe LV myocardial injury in terms of the number of segments with fibrotic changes ($p < 0.0000$). A comparison of LAVi, LAEF, and LA strains revealed no significant differences. However, when adjusted for sex, the LA strain and LAEF were significantly lower in male post-COVID-19 patients.

LA volume reflects LV filling pressure and, consequently, the degree of LV diastolic dysfunction [2, 3]. According to some studies, an increase in LA volume is related to an increased risk of atrial fibrillation [15–17] and thromboembolism if it is accompanied by dysfunction in atrial fibrillation patients [18]. Changes in LA volume index and LAEF in patients with heart failure with intact ejection fraction and sinus rhythm are independently related to poor cardiovascular outcomes, comparable with those in persistent atrial fibrillation when LA measures have no predictive value [19].

The evidence on gender differences in LA remodeling, particularly in post-COVID-19 patients, is limited. Chistyakova et al. [20] found an increase in LAVi in all study groups compared with the control group in their cardiac function and endothelial dysfunction research in post-COVID-19 patients. According to some authors, LA remodeling is more prevalent in women. In the group of patients with recurrent atrial fibrillation with hypotension, for example, women exhibited a substantially lower LAEF than men (39% [28; 50] vs. 50% [42; 55], $p = 0.02$) [10]. In women with atrial fibrillation, LA diameter has been shown to be an independent predictor of cardiovascular death ($p = 0.003$) [21, 22]. According to EchoCG performed in post-COVID-19 patients 1 year after discharge, LAEF was significantly lower in the group with a decrease in LV global longitudinal strain (1.3 ± 0.3 vs. 1.4 ± 0.3 mL/m^2; $p = 0.052$) [23]. Men have a higher incidence of atrial fibrillation regardless of COVID-19, whereas women have more evident atrial remodeling on high-density electroanatomic mapping and a higher incidence of arrhythmia recurrences after atrial fibrillation ablation. These modifications could explain why women have a higher incidence of recurrence and contribute to gender differences in the clinical course of atrial fibrillation [24]. Gender differences in atrial changes in post-COVID-19 patients require further research because they may be clinically significant for preventing atrial fibrillation and arrhythmia recurrences after atrial fibrillation ablation.

LA remodeling may be caused by a strong immune response, persistent inflammation, [25] endothelial damage, and microvascular thrombogenicity [26]. The possibility of virus retention in cardiomyocytes, resulting in fibrotic changes, cannot be completely ruled out.

The absence of a uniform approach to study design, which results in variability of study groups and makes study findings difficult to compare, can explain contradictory findings by different authors. However, it is clear that post-COVID-19 pneumonia patients with increased LAVi, LAEF, and LA strain with preserved LVEF require close monitoring to prevent or timely detection of complications, such as heart failure, LV dysfunction, and arrhythmia.

Limitations of the study

Each patient in our study had one cardiac MRI after the onset of symptoms. As a result, we cannot be certain that the observed findings did not exist prior to SARS-CoV-2 infection. Notably, the nonischemic LGEs found could be nonspecific and caused by undetected myocarditis before SARS-CoV-2 infection.

CONCLUSION

The SARS-CoV-2 virus unquestionably causes a more severe cardiac injury involving a greater number of myocardial segments. Residual effects of COVID-19

pneumonia, such as heterogeneous lung tissue thickening and pleural effusion, persist for longer. Male patients had a much higher prevalence of postinflammatory sequelae, manifesting as decreased LV and LA contractility.

Our findings highlight the need for further research into the long-term cardiovascular complications of COVID-19. In this case, contrast-enhanced cardiac MRI can be a sensitive imaging tool for evaluating the severity of cardiac injury.

ADDITIONAL INFORMATION

Funding source. This research was supported by the Russian Science Foundation (project #22-15-00313).

Competing interests. The authors declare that they have no competing interests.

Authors' contribution. All authors made a substantial contribution to the conception of the work, acquisition, analysis, interpretation of data for the work, drafting and revising the work, final approval of the version to be published and agree to be accountable for all aspects of the work. A.S. Maksimova, N.I. Ryumshina, T.A. Shelkovnikova — concept and design of the study, performance and analysis of cardiac MRI, drafting of the clinical conclusion, drafting of the text; O.V. Mochula, V.Y. Usov — performance and analysis of cardiac MRI, drafting of the clinical conclusion; N.D. Anfinogenova — concept and design of the study, drafting of the English version of the manuscript, general guidance.

REFERENCES

1. Ussov WY, Nudnov NV, Ignatenko GA, et al. Primary and prospective imaging of the chest using magnetic resonance imaging in patients with viral lung damage in COVID-19. *Medical Imaging*. 2020;24(4):11–26. (In Russ). doi: 10.24835/1607-0763-2020-4-11-26

2. Srinivasan A, Wong F, Couch LS, Wang BX. Cardiac complications of COVID-19 in low-risk patients. *Viruses.* 2022;14(6):1322. doi: 10.3390/v14061322

3. Cosyns B, Lochy S, Luchian ML, et al. The role of cardiovascular imaging for myocardial injury in hospitalized COVID-19 patients. *Eur Heart J Cardiovasc Imaging.* 2020;21(7):709–714. doi: 10.1093/ehjci/jeaa136

4. Huang L, Zhao P, Tang D, et al. Cardiac involvement in patients recovered from COVID-2019 identified using magnetic resonance imaging. *JACC Cardiovasc Imaging.* 2020;13(11):2330–2339. doi: 10.1016/j.jcmg.2020.05.004

5. Luetkens JA, Isaak A, Öztürk C, et al. Cardiac MRI in suspected acute COVID-19 myocarditis. *Radiol Cardiothorac Imaging*. 2021;3(2):e200628. doi: 10.1148/ryct.2021200628

6. Puntmann VO, Carerj ML, Wieters I, et al. Outcomes of cardiovascular magnetic resonance imaging in patients recently recovered from coronavirus disease 2019 (COVID-19). *JAMA Cardiol.* 2020;5(11):1265–1273. doi: 10.1001/jamacardio.2020.3557

7. Ferreira VM, Plein S, Wong TC, et al. Cardiovascular magnetic resonance for evaluation of cardiac involvement in COVID-19: Recommendations by the society for cardiovascular magnetic resonance. *J Cardiovasc Magn Reson.* 2023;25(1):21. doi: 10.1186/s12968-023-00933-0

8. Yong SJ. Long COVID or post-COVID-19 syndrome: Putative pathophysiology, risk factors, and treatments. *Infect Dis (Lond).* 2021;53(10):737–754. doi: 10.1080/23744235.2021.1924397

9. Lewis AJ, Burrage MK, Ferreira VM. Cardiovascular magnetic resonance imaging for inflammatory heart diseases. *Cardiovascular Diagnosis Therapy*. 2020;10(3):598–609. doi: 10.21037/cdt.2019.12.09

10. Kokhan EV, Ozova M., Romanova VA, et al. Left atrial phasic function in patients with hypertension and recurrent atrial fibrillation: Gender differences of the relationship with diastolic dysfunction and central aortic pressure. *Rational Pharmacotherapy Cardiology*. 2019;15(5):622–633. (In Russ). doi: 10.20996/1819-6446-2019-15-5-622-633

11. Kravchenko D, Isaak A, Zimmer S, et al. Cardiac MRI in patients with prolonged cardiorespiratory symptoms after mild to moderate COVID-19. *Radiology.* 2021;301(3):E419–E425. doi: 10.1148/radiol.2021211162

12. Arutyunov GP, Paleev FN, Moiseeva OM, et al. 2020 Clinical practice guidelines for myocarditis in adults. *Russ J Cardiol.* 2021;26(11):4790. (In Russ). doi: 10.15829/1560-4071-2021-4790

13. Feofanova TB, Zaletova TS, Abakarov RM, Zainudinov ZM. Assessment of the state of the cardiovascular system in patients with COVID-19. *Int J Med Psychol.* 2021;4(7):84–87. (In Russ).

14. Shirokov NE, Yaroslavskaya EI, Krinochkin DV, et al. Relationship between latent left ventricular contractile dysfunction and signs of immune inflammation in patients with COVID-19 pneumonia. *Cardiovascular Therapy Prevention.* 2023;22(3):3434. (In Russ). doi: 10.15829/1728-8800-2023-3434

15. Pozios I, Vouliotis AI, Dilaveris P, Tsioufis C. Electro-mechanical alterations in atrial fibrillation: Structural, electrical, and functional correlates. *J Cardiovasc Dev Dis.* 2023;10(4):149. doi: 10.3390/jcdd10040149

16. Raisi-Estabragh Z, McCracken C, Condurache D, et al. Left atrial structure and function are associated with cardiovascular outcomes independent of left ventricular measures: A UK Biobank CMR study. *Eur Heart J Cardiovasc Imaging*. 2022;23(9):1191–1200. doi: 10.1093/ehjci/jeab266

17. Floria M, Radu S, Gosav EM, et al. Left atrial structural remodelling in non-valvular atrial fibrillation: What have we learnt from CMR? *Diagnostics (Basel).* 2020;10(3):137. doi: 10.3390/diagnostics10030137

18. Kim HD, Cho DH, Kim MN, et al. Left atrial dysfunction, fibrosis and the risk of thromboembolism in patients with paroxysmal and persistent atrial fibrillation. *Int J Heart Fail.* 2022;4(1):42–53. doi: 10.36628/ijhf.2021.0043

19. Schönbauer R, Kammerlander AA, Duca F, et al. Prognostic impact of left atrial function in heart failure with preserved ejection fraction in sinus rhythm vs persistent atrial fibrillation. *ESC Heart Fail.* 2022;9(1):465–475. doi: 10.1002/ehf2.13723

20. Chistyakova MV, Govorin AV, Mudrov VA, et al. Heart damage and endothelial dysfunction in patients with coronavirus infection. *Therapists Bulletin*. 2023;(1):1–7. (In Russ).

21. Rienstra M, van Veldhuisen DJ, Hagens VE, et al. Gender-related differences in rhythm control treatment in persistent atrial fibrillation. *J Am Coll Cardiol.* 2005;46(7):1298–306. doi: 10.1016/j.jacc.2005.05.078

22. Proietti M, Raparelli V, Basili S, et al. Relation of female sex to left atrial diameter and cardiovascular death in atrial fibrillation: The AFFIRM Trial. *Int J Cardiol.* 2016;(207):258–263. doi: 10.1016/j.ijcard.2016.01.169
23. Yaroslavskaya EI, Krinochkin DV, Shirokov NE, et al. Clinical and echocardiographic profile of patients one year after COVID-19 pneumonia depending on the left ventricular global longitudinal strain. *Siberian J Clin Experimental Med*. 2022;37(4):52–62. (In Russ). doi: 10.29001/2073-8552-2022-37-4-52-62
24. Wong GR, Nalliah CJ, Lee G, et al. Sex-Related differences in atrial remodeling in patients with atrial fibrillation: Relationship to ablation outcomes. *Circ Arrhythm Electrophysiol*. 2022;15(1):e009925. doi: 10.1161/CIRCEP.121.009925
25. Bräuninger H, Stoffers B, Fitzek AD, et al. Cardiac SARS-CoV-2 infection is associated with pro-inflammatory transcriptomic alterations within the heart. *Cardiovasc Res.* 2022;118(2):542–555. doi: 10.1093/cvr/cvab322
26. Wu L, Jiang Z, Meulendijks ER, et al. Atrial inflammation and microvascular thrombogenicity are increased in deceased COVID-19 patients. *Cardiovasc Pathol.* 2023;(64):107524. doi: 10.1016/j.carpath.2023.107524

СПИСОК ЛИТЕРАТУРЫ

1. Усов В.Ю., Нуднов Н.В., Игнатенко Г.А., и др. Первичная и проспективная визуализация грудной клетки при магнитно-резонансной томографии у пациентов с вирусным поражением легких при COVID-19 // Медицинская визуализация. 2020. Т. 24, № 4. С. 11–26. doi: 10.24835/1607-0763-2020-4-11-26
2. Srinivasan A., Wong F., Couch L.S., Wang B.X. Cardiac complications of COVID-19 in low-risk patients // Viruses. 2022. Vol. 14, N 6. P. 1322. doi: 10.3390/v14061322
3. Cosyns B., Lochy S., Luchian M.L., et al. The role of cardiovascular imaging for myocardial injury in hospitalized COVID-19 patients // Eur Heart J Cardiovasc Imaging. 2020. Vol. 21, N 7. P. 709–714. doi: 10.1093/ehjci/jeaa136
4. Huang L., Zhao P., Tang D., et al. Cardiac involvement in patients recovered from COVID-2019 identified using magnetic resonance imaging // JACC Cardiovasc Imaging. 2020. Vol. 13, N 11. P. 2330–2339. doi: 10.1016/j.jcmg.2020.05.004
5. Luetkens J.A., Isaak A., Öztürk C., et al. Cardiac MRI in suspected acute COVID-19 myocarditis // Radiol Cardiothorac Imaging. 2021. Vol. 3, N 2. e200628. doi: 10.1148/ryct.2021200628
6. Puntmann V.O., Carerj M.L., Wieters I., et al. Outcomes of cardiovascular magnetic resonance imaging in patients recently recovered from coronavirus disease 2019 (COVID-19) // JAMA Cardiol. 2020. Vol. 5, N 11. P. 1265–1273. doi: 10.1001/jamacardio.2020.3557
7. Ferreira V.M., Plein S., Wong T.C. et al. Cardiovascular magnetic resonance for evaluation of cardiac involvement in COVID-19: Recommendations by the Society for cardiovascular magnetic resonance // J Cardiovasc Magn Reson. 2023. Vol. 25, N 1. P. 21. doi: 10.1186/s12968-023-00933-0
8. Yong S.J. Long COVID or post-COVID-19 syndrome: Putative pathophysiology, risk factors, and treatments // Infect Dis (Lond). 2021. Vol. 53, N 10. P. 737–754. doi: 10.1080/23744235.2021.1924397
9. Lewis A.J., Burrage M.K., Ferreira V.M. Cardiovascular magnetic resonance imaging for inflammatory heart diseases // Cardiovascular Diagnosis and Therapy. 2020. Vol. 10, N 3. P. 598–609. doi: 10.21037/cdt.2019.12.09
10. Кохан Е.В., Озова Е.М., Романова В.А., и др. Фазовый анализ функции левого предсердия у пациентов с артериальной гипертонией и фибрилляцией предсердий: гендерные особенности связи с диастолической дисфункцией и параметрами центрального давления // Рациональная фармакотерапия в кардиологии. 2019. Т. 15, № 5. С. 622–633. doi: 10.20996/1819-6446-2019-15-5-622-633
11. Kravchenko D., Isaak A., Zimmer S., et al. Cardiac MRI in patients with prolonged cardiorespiratory symptoms after mild to moderate COVID-19 // Radiology. 2021. Vol. 301, N 3. P. E419–E425. doi: 10.1148/radiol.2021211162
12. Арутюнов Г.П., Палеев Ф.Н., Моисеева О.М., и др. Миокардиты у взрослых. Клинические рекомендации-2020 // Российский кардиологический журнал. 2021. Т. 266, № 11. С. 4790. doi: 10.15829/1560-4071-2021-4790
13. Феофанова Т.Б., Залетова Т.С., Абакаров Р.М., Зайнудинов З.М. Оценка состояния сердечно-сосудистой системы у пациентов, перенесших COVID-19 // Int J Med Psychol. 2021. Т. 4, № 7. С. 84–87.
14. Широков Н.Е., Ярославская Е.И., Криночкин Д.В., и др. Связь вариантов скрытой контрактильной дисфункции левого желудочка и признаков иммунного воспаления у пациентов, перенесших COVID-19-пневмонию // Кардиоваскулярная терапия и профилактика. 2023. Т. 22, № 3. С. 3434. doi: 10.15829/1728-8800-2023-3434
15. Pozios I., Vouliotis A.I., Dilaveris P., Tsioufis C. Electro-mechanical alterations in atrial fibrillation: Structural, electrical, and functional correlates // J Cardiovasc Dev Dis. 2023. Vol. 10, N 4. P. 149. doi: 10.3390/jcdd10040149
16. Raisi-Estabragh Z., McCracken C., Condurache D., et al. Left atrial structure and function are associated with cardiovascular outcomes independent of left ventricular measures: A UK Biobank CMR study // Eur Heart J Cardiovasc Imaging. 2022. Vol. 23, N 9. P. 1191–1200. doi: 10.1093/ehjci/jeab266
17. Floria M., Radu S., Gosav E.M., et al. Left atrial structural remodelling in non-valvular atrial fibrillation: What have we learnt from CMR? // Diagnostics (Basel). 2020. Vol. 10, N 3. P. 137. doi: 10.3390/diagnostics10030137
18. Kim H.D., Cho D.H., Kim M.N., et al. Left atrial dysfunction, fibrosis and the risk of thromboembolism in patients with paroxysmal and persistent atrial fibrillation // Int J Heart Fail. 2022. Vol. 4, N 1. P. 42–53. doi: 10.36628/ijhf.2021.0043
19. Schönbauer R., Kammerlander A.A., Duca F., et al. Prognostic impact of left atrial function in heart failure with preserved ejection fraction in sinus rhythm vs persistent atrial fibrillation // ESC Heart Fail. 2022. Vol. 9, N 1. P. 465–475. doi: 10.1002/ehf2.13723
20. Чистякова М.В., Говорин А.В., Мудров В.А., и др. Поражение сердца и эндотелиальная дисфункция у больных, перенесших коронавирусную инфекцию // Вестник терапевта. 2023. № 1. С. 1–7.
21. Rienstra M., Van Veldhuisen D.J., Hagens V.E., et al. Gender-Related differences in rhythm control treatment in persistent atrial fibrillation // J Am Coll Cardiol. 2005. Vol. 46, N 7. P. 1298–306. doi: 10.1016/j.jacc.2005.05.078

22. Proietti M., Raparelli V., Basili S., et al. Relation of female sex to left atrial diameter and cardiovascular death in atrial fibrillation: The AFFIRM Trial // Int J Cardiol. 2016. N 207. P. 258–263. doi: 10.1016/j.ijcard.2016.01.169
23. Ярославская Е.И., Криночкин Д.В., Широков Н.Е., и др. Клинико-эхокардиографический профиль пациентов, перенесших пневмонию COVID-19, через год после выписки в зависимости от глобальной продольной деформации левого желудочка // Сибирский журнал клинической и экспериментальной медицины. 2022. Т. 37, № 4. С. 52–62. doi: 10.29001/2073-8552-2022-37-4-52-62
24. Wong G.R., Nalliah C.J., Lee G., et al. Sex-Related differences in atrial remodeling in patients with atrial fibrillation: Relationship to ablation outcomes // Circ Arrhythm Electrophysiol. 2022. Vol. 15, N 1. P. e009925. doi: 10.1161/CIRCEP.121.009925
25. Bräuninger H., Stoffers B., Fitzek A.D., et al. Cardiac SARS-CoV-2 infection is associated with pro-inflammatory transcriptomic alterations within the heart // Cardiovasc Res. 2022. Vol. 118, N 2. P. 542–555. doi: 10.1093/cvr/cvab322
26. Wu L., Jiang Z., Meulendijks E.R., et al. Atrial inflammation and microvascular thrombogenicity are increased in deceased COVID-19 patients // Cardiovasc Pathol. 2023. N 64. P. 107524. doi: 10.1016/j.carpath.2023.107524

AUTHORS' INFO

*** Nadezhda I. Ryumshina,** MD, Cand. Sci. (Med.);
address: 111a Kievskaya street, 634012 Tomsk, Russia;
ORCID: 0000-0002-6158-026X;
eLibrary SPIN: 6555-8937;
e-mail: n.rumshina@list.ru

Aleksandra S. Maksimova, MD, Cand. Sci. (Med.);
ORCID: 0000-0002-4871-3283;
eLibrary SPIN: 2879-9550;
e-mail: asmaximova@yandex.ru

Tatiana A. Shelkovnikova, MD, Cand. Sci. (Med.);
ORCID: 0000-0001-8089-2851;
eLibrary SPIN: 1826-7850;
e-mail: fflly@mail.ru

Olga V. Mochula, MD, Cand. Sci. (Med.);
ORCID: 0000-0002-7502-7502;
eLibrary SPIN: 3712-8492;
e-mail: mochula.olga@gmail.com

Nina D. Anfinogenova, MD, Dr. Sci. (Med.);
ORCID: 0000-0003-1106-0730;
eLibrary SPIN: 6784-5440;
e-mail: cardio.intl@gmail.com

Wladimir Yu. Ussov, MD, Dr. Sci. (Med.), Professor;
ORCID: 0000-0002-7352-6068;
eLibrary SPIN: 1299-2074;
e-mail: ussov1962@yandex.ru

ОБ АВТОРАХ

*** Рюмшина Надежда Игоревна,** канд. мед. наук;
адрес: Россия, 634012, Томск, ул. Киевская, д. 111а;
ORCID: 0000-0002-6158-026X;
eLibrary SPIN: 6555-8937;
e-mail: n.rumshina@list.ru

Максимова Александра Сергеевна, канд. мед. наук;
ORCID: 0000-0002-4871-3283;
eLibrary SPIN: 2879-9550;
e-mail: asmaximova@yandex.ru

Шелковникова Татьяна Александровна, канд. мед. наук;
ORCID: 0000-0001-8089-2851;
eLibrary SPIN: 1826-7850;
e-mail: fflly@mail.ru

Мочула Ольга Витальевна, канд. мед. наук;
ORCID: 0000-0002-7502-7502;
eLibrary SPIN: 3712-8492;
e-mail: mochula.olga@gmail.com

Анфиногенова Нина Джоновна, д-р мед. наук;
ORCID: 0000-0003-1106-0730;
eLibrary SPIN: 6784-5440;
e-mail: cardio.intl@gmail.com

Усов Владимир Юрьевич, д-р мед. наук, профессор;
ORCID: 0000-0002-7352-6068;
eLibrary SPIN: 1299-2074;
e-mail: ussov1962@yandex.ru

* Corresponding author / Автор, ответственный за переписку

DOI: https://doi.org/10.17816/DD501771

Рентгеноконтрастные шаблоны для определения минеральной плотности кости по данным конусно-лучевой и мультиспиральной компьютерной томографии

Ш.Д. Хоссаин[1], А.В. Петряйкин[2], А.А. Мураев[1], А.Б. Данаев[3], Д.В. Буренчев[2], А.А. Долгалев[3], Ю.А. Васильев[2], Д.Е. Шарова[2], С.Ю. Иванов[1, 4]

[1] Российский университет дружбы народов имени Патриса Лумумбы, Москва, Российская Федерация;
[2] Научно-практический клинический центр диагностики и телемедицинских технологий, Москва, Российская Федерация;
[3] Ставропольский государственный медицинский университет, Ставрополь, Российская Федерация;
[4] Первый Московский государственный медицинский университет имени И.М. Сеченова (Сеченовский Университет), Москва, Российская Федерация

АННОТАЦИЯ

Обоснование. Конусно-лучевая компьютерная томография позволяет проводить диагностику на этапе планирования различных манипуляций в челюстно-лицевой области, в частности при дентальной имплантации. Преимущества данного метода: высокое пространственное разрешение, низкая лучевая нагрузка, доступность исследований, однако имеется существенный недостаток — отсутствие возможности определения плотности кости челюстей в единицах Хаунсфилда (HU).

Цели — разработать набор рентгеноконтрастных шаблонов с заданной рентгеновской плотностью на основе гидрофосфата калия и β-трикальцийфосфата; изучить результаты сканирования шаблона на конусно-лучевом и мультисрезовом компьютерных томографах; определить алгоритм кросс-калибровки для оценки минеральной плотности кости челюстей в HU и по классификации C. Misch.

Материалы и методы. В качестве рентгеноконтрастного шаблона использованы раствор гидрофосфата калия, суспензия β-трикальцийфосфата. В микропробирках шаблона объёмом 0,25 мл заданы следующие концентрации гидрофосфата калия: 49,96; 99,98; 174,99; 349,99; 549,98 мг/мл; суспензия β-трикальцийфосфата с эквивалентной концентрацией гидрофосфата калия 1506 мг/мл. Шаблоны моделируют типы плотности костной ткани по C. Misch. Исследование шаблонов проводилось на 2 мультисрезовых и 4 конусно-лучевых компьютерных томографах.

Результаты. В ходе работы проанализированы зависимости Gray Value (GV) для конусно-лучевых и HU для мультисрезовых компьютерных томографов от заданных значений минеральной плотности кости. Отмечается существенный разброс измеренных величин. Различаются углы наклона зависимостей и формы кривых. После кросс-калибровки показана хорошая сопоставимость пересчитанных значений относительно режима исследуемого мультисрезового компьютерного томографа.

Заключение. Разработанный рентеноконтрастный шаблон позволяет стандартизировать денситометрические показатели для конусно-лучевых и различных мультисрезовых компьютерных томографов: в среднем разброс после кросс-калибровки снижается в 10 раз, что обеспечивает возможность классификации костной ткани в HU по C. Misch.

Ключевые слова: конусно-лучевая компьютерная томография; мультиспиральная компьютерная томография; кросс-калибровка; минеральная плотность кости; рентгеновская плотность; денситометрия; имплантация зубов.

Как цитировать:
Хоссаин Ш.Д., Петряйкин А.В., Мураев А.А., Данаев А.Б., Буренчев Д.В., Долгалев А.А., Васильев Ю.А., Шарова Д.Е., Иванов С.Ю. Рентгеноконтрастные шаблоны для определения минеральной плотности кости по данным конусно-лучевой и мультиспиральной компьютерной томографии // *Digital Diagnostics.* 2023. Т. 4, № 3. С. 292–305. DOI: https://doi.org/10.17816/DD501771

Рукопись получена: 21.06.2023 **Рукопись одобрена:** 22.08.2023 **Опубликована:** 30.08.2023

DOI: https://doi.org/10.17816/DD501771

Bone mineral density radiopaque templates for cone beam computed tomography and multidetector computed tomography

Shazmim D. Hossain[1], Alexey V. Petraikin[2], Alexandr A. Muraev[1], Aslan B. Danaev[3], Dmitry V. Burenchev[2], Alexander A. Dolgalev[3], Yuriy A. Vasilev[2], Dariya E. Sharova[2], Sergey Yu. Ivanov[1, 4]

[1] Peoples Friendship University of Russia, Moscow, Russian Federation;
[2] Research and Practical Clinical Center for Diagnostics and Telemedicine Technologies, Moscow, Russian Federation;
[3] Stavropol State Medical University, Moscow, Russian Federation;
[4] The First Sechenov Moscow State Medical University (Sechenov University), Moscow, Russian Federation

ABSTRACT

BACKGROUND: Cone beam computed tomography is widely applied for diagnostics and planning various manipulations in the maxillofacial region, for example, dental implantation. Its advantages include high spatial resolution, low radiation exposure, and cost-effectiveness. However, it has a significant drawback: the inability to determine the density of the jaw bone in Hounsfield Units (HU).

AIMS: This study aimed to develop radiopaque templates with sets of X-ray density based on potassium hydrophosphate and beta-tricalcium phosphate, to study templates on various cone beam computed tomography and multidetector computed tomography devices, and to determine a cross-calibration algorithm for assessing the bone mineral density of the jaw in HU.

MATERIALS AND METHODS: The bone mineral density template comprised microtubes (0.25 ml) with potassium hydrophosphate concentrations of 49.96, 99.98, 174.99, 349.99, and 549.98 mg/ml, and a suspension of beta-tricalcium phosphate with an equivalent concentration of potassium hydrophosphate 1,506 mg/ml, designed to simulate the types of bone density according to C. Mish. The study was carried out on two multidetector computed tomography and four cone beam computed tomography machines. Cross-calibration was referred on the "standard" multidetector computed tomography 1 mode 120 kV, 200 mA.

RESULTS: There was a significant scatter of the X-ray values (HU for multidetector computed tomography and GV for cone beam computed tomography) vs. bone mineral density, with varying slopes, bias, and curve shapes. After cross-calibration, good comparability corresponding to the multidetector computed tomography 1 mode was shown. The median of the differences before cross-calibration was 160 relative units (HU, GV), after decreased by 10 times and amounted to 16 rel. units (p=0.000). The mean difference for cone beam computed tomography was significantly higher (30 rel. units) than for multidetector computed tomography (8 rel. units) (p=0.024, Mann–Whitney U test).

CONCLUSION: The developed radiopaque template enables the standardization of densitometric indicators for cone beam computed tomography and various multidetector computed tomography modes. On average, the spread after cross-calibration is reduced by 10 times, which makes it possible to classify bone tissue in HU according to C. Mish.

Keywords: cone beam computed tomography; multidetector computed tomography; cross-calibration; bone mineral density; X-ray density; densitometry; dental implantation.

To cite this article:
Hossain ShD, Petraikin AV, Muraev AA, Danaev AB, Burenchev DV, Dolgalev AA, Vasilev YuA, Sharova DE, Ivanov SYu. Bone mineral density radiopaque templates for cone beam computed tomography and multidetector computed tomography. *Digital Diagnostics*. 2023;4(3):292–305. DOI: https://doi.org/10.17816/DD501771

Received: 21.06.2023 **Accepted:** 22.08.2023 **Published:** 30.08.2023

DOI: https://doi.org/10.17816/DD501771

利用锥形束和多层螺旋计算机断层扫描数据测定骨矿物质密度的X射线对比模板

Shazmim D. Hossain[1], Alexey V. Petraikin[2], Alexandr A. Muraev[1], Aslan B. Danaev[3], Dmitry V. Burenchev[2], Alexander A. Dolgalev[3], Yuriy A. Vasilev[2], Dariya E. Sharova[2], Sergey Yu. Ivanov[1, 4]

[1] Peoples Friendship University of Russia, Moscow, Russian Federation;
[2] Research and Practical Clinical Center for Diagnostics and Telemedicine Technologies, Moscow, Russian Federation;
[3] Stavropol State Medical University, Moscow, Russian Federation;
[4] The First Sechenov Moscow State Medical University (Sechenov University), Moscow, Russian Federation

简评

论证。锥形束计算机断层扫描（cone beam computed tomography，CBCT）允许在颌面部各种操作的规划阶段进行诊断，特别是在牙种植入方面。这种方法的优点是空间分辨率高、辐射量低、便于研究。然而，它也有一个明显的缺点：无法确定以亨氏（Hounsfield Unit，HU）单位的颌骨密度。CBCT中的X射线密度是以Gray Value（GV）单位确定的。

该研究的目的是根据磷酸氢二钾（DHP）和β-磷酸三钙（β-TCP）开发一套具有特定X射线密度的X射线对比模板，研究在CBCT和多层螺旋计算机断层扫描（MSCT）上扫描模板的结果，确定用于估算HU下颌骨矿物质密度的交叉校验算法，并根据C.Mish进行分类。

材料和方法。使用DHP溶液、β-TCP悬浮液作为X射线对比模板。模板的0.25ml微量试管中DHP的浓度分别为：49.96、99.98、174.99、349.99、549.98mg/ml，β-TCP悬浮液中DHP的等效浓度为1506mg/ml。这些模板根据C.Mish分类模拟了骨密度类型。这些模板检验是在2个MSCT和4个CBCT上进行的。在“标准”MSCT1模式120kV、200mA上进行了交叉校验；对所获得的依赖关系进行了线性和二次近似。

结果。在工作过程中，我们分析了CBCT的GV和MSCT的HU与IPC给定值的关系。我们发现了测量值存在显著差异。相关斜率角度和曲线形状各不相同。交叉校验后，与MSCT1模式相比，重新计算的数值具有良好的可比性。交叉校验前测量值的中位数差异为160个相对单位（HU、GV），重新计算后显著减少了10倍，为16个相对单位（p=0,000），可靠显示了CBCT的平均差异（30个相对单位）大于MSCT的平均差异（8个相对单位），p=0,024；采用曼-惠特尼U检验进行了比较。

结论。我们开发的X射线对比模板允许使CBCT和不同MSCT模式的密度测定指数标准化，交叉校验后的分散平均减少了10倍，这提供根据C.Mish对HU中的骨组织进行分类的可能性。.

关键词：锥形束计算机断层扫描；多层螺旋计算机断层扫描；交叉校验；骨矿物质密度；X射线密度；密度测定；牙种植入。

引用本文：
Hossain ShD, Petraikin AV, Muraev AA, Danaev AB, Burenchev DV, Dolgalev AA, Vasilev YuA, Sharova DE, Ivanov SYu. 利用锥形束和多层螺旋计算机断层扫描数据测定骨矿物质密度的X射线对比模板. *Digital Diagnostics.* 2023;4(3):292–305. DOI: https://doi.org/10.17816/DD501771

收到： 21.06.2023 **接受：** 22.08.2023 **发布日期：** 30.08.2023

Abbreviations

CBCT: cone beam computed tomography
CT: computed tomography
BMD: bone mineral density
MDCT: multidetector computed tomography

BACKGROUND

The discovery of computed tomography (CT) in 1972 enabled the visualization of various areas of the human body using three-dimensional (3D) images [1]. Computed tomography is used in many therapeutic areas, and with the development of dental implantation, it has been the most often used modality in dentistry [2]. One of the key standards for determining radiological densitometric parameters of bone tissue is the Hounsfield unit (HU), a relative quantitative measurement of radio density [3]. Misch [4] uses this scale as a basis for a dental bone density classification.

Because of the high ionizing radiation dose and high financial costs associated with multidetector computed tomography (MDCT), a safer and less expensive cone beam computed tomography (CBCT) was developed. However, this technology has some limitations, the most significant of which is the presence of specific artifacts and poor accuracy in determining the radiographic density [5–7]. Radiographic density in CBCT is defined as a relative mean gray value (GV) compared with Hounsfield units (HUs), which are stable radiographic density units used in MDCT. This makes it impossible to adequately identify individual anatomical and density characteristics of the patient's bone structures, which are necessary for planning dental implantation. These limitations are determined by tissue X-ray absorption patterns, scanning parameters, and the CBCT reconstruction algorithm [8]. As a result, a universal calibration method is required to reduce CBCT errors, improve bone density measurement accuracy, and lower the risk of intraoperative and postoperative complications.

Radiopaque templates should be developed to complete this task. It is possible to use potassium hydrogen phosphate, which has X-ray absorption properties similar to calcium hydroxyapatite, the main mineral complex of normal bone. Previously, the use of potassium hydrogen phosphate to simulate phantom bone mineral density (BMD) was justified [9]. This approach enables the simulation of a wide range of BMD values in bone samples using a scan process as close as possible, using identical examination modes and simulating X-ray absorption by the patient's tissues. This approach is used in quantitative CT [9].

Our experimental study aims to evaluate the effectiveness of BMD radiopaque templates and cross-calibration algorithms for a more accurate assessment of densitometric parameters of six computer tomographs (four CBCTs [CBCT 1, CBCT 2, CBCT 3, and CBCT 4] and two MDCTs [MDCT 1 and MDCT 2]), with abbreviations followed by serial numbers of test scanners).

The study aims to develop a set of radiopaque templates with a given radiographic density using potassium hydrogen phosphate and β-tricalcium phosphate and evaluate the results of scanning templates using various CBCTs and MDCTs to develop a cross-calibration algorithm for assessing mineral density of the jawbone using the Misch classification.

MATERIALS AND METHODS

General characteristics of a mineral density template

A specific mass concentration of potassium hydrogen phosphate was used for manufacturing the model BMD sample. Due to its high solubility, the exact concentration range to simulate the spongy substance and the low-density cortical layer (50–550 mg/mL) can be determined. The high-density cortical layer was modeled using a suspension of water-insoluble β-tricalcium phosphate, equivalent to bone hydroxyapatite. Concentrations were adjusted to obtain substances from all bone density classes (D1–D5) according to the Misch classification (Table 1) [4].

The calibration template consisted of two sets of 0.25-mL plastic tubes positioned around 50-mL tubes (Figure 1). Calibration tubes included (a) distilled water, (b–f) 50–550-mg/mL potassium hydrogen phosphate solutions, (g) 846-mg/mL β-tricalcium phosphate solution with a potassium hydrogen phosphate equivalent content of 1,500 mg/mL (see Table 1). Three 50-mL tubes with fixed templates were filled with 65.97- and 58.64-mg/mL potassium hydrogen phosphate solutions and water. These tubes were not used for calibration (see Figure 1).

A crystalline hydrate of potassium hydrogen phosphate with a content of the primary substance $K_2HPO_4 \times 3H_2O$ >99% according to GOST 2493-75 (Pan Reac Applichem ITV Reagents) was used to prepare a solution of this substance. β-tricalcium phosphate was also used, with a $Ca_3 \times (PO_4)2$ content of >98% (Sigma-Aldrich). OHAUS Pioneer analytical balances with accuracy class according to GOST OIML R 76-1-2011 I (special) were used for weighing. Potassium hydrogen phosphate samples were dissolved in degassed distilled water in a volumetric flask (49.89 mL; relative error for volume 0.06%).

Table 1. Characteristics of the created bone mineral density template compared with Carl E. Misch's classification

Tube number in the template (0.25 mL)	Values obtained in the study			Misch scale	
	Specified BMD concentration (mg/mL)	Actual BMD concentration	Measured HU for MDCT 1 (line 5, Table 2)	Bone type	HU
1	0	0	1.5	—	—
2	50	49.96	78	D5	<150
3	100	99.98	161	D4	150–350
4	175	174.99	281	D4	150–350
5	350	349.99	540	D3	350–850
6	550	549.98	816[a]	D2	850–1,250
7	1,500	1,506	2,165	D1	>1,250

Note. BMD, bone mineral density; MDCT, tested multidetector computed tomography scanner 1.
[a]Sample below the appropriate Misch density range.

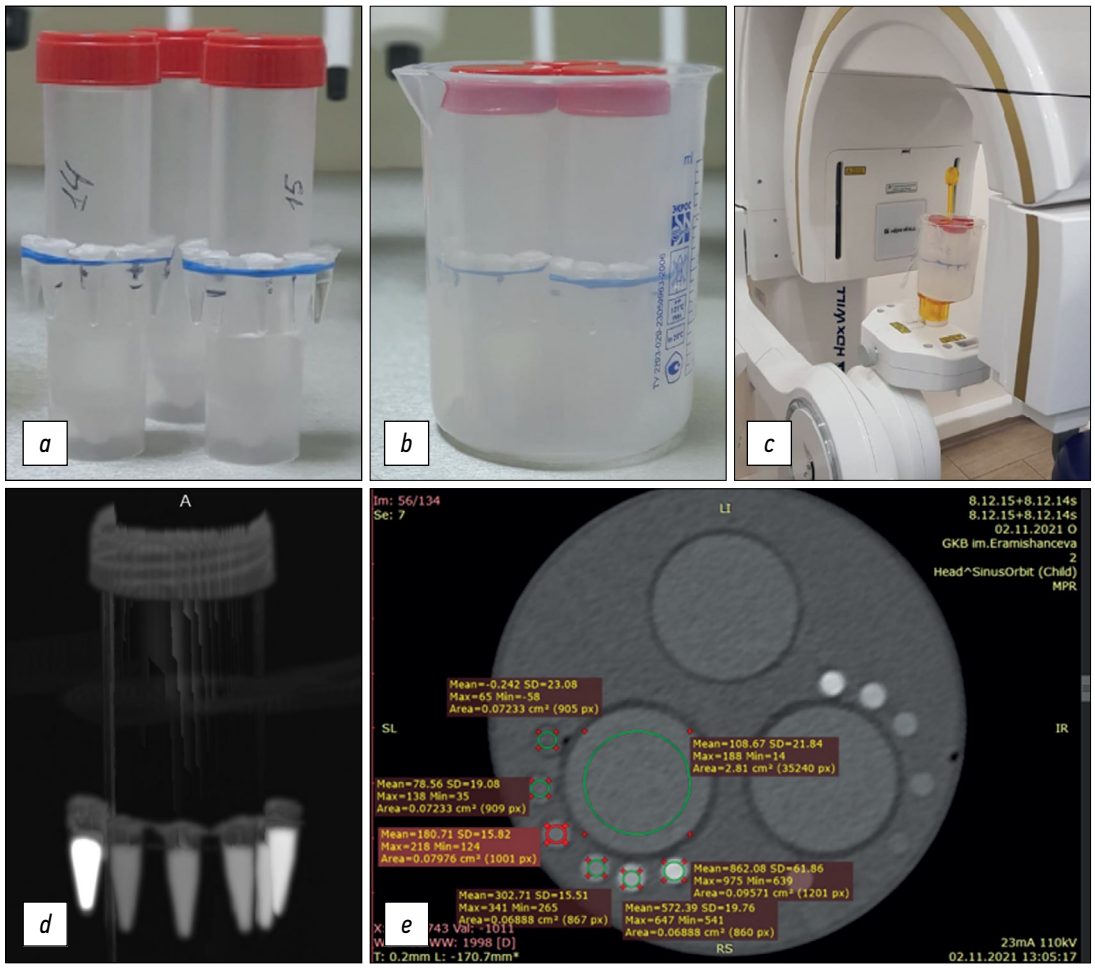

Fig. 1. General sequence of the study steps: (*a*) original tubes with a radiopaque substance (radiopaque mineral density templates) in air; (*b*) original tubes with radiopaque substance in water; (*c*) example of fixing and examining templates using a cone-beam computed tomography scanner; (*d*) MIP reconstruction using multidetector computed tomography scanner; (*e*) example of viewing and processing original tube sections in DICOM format (Radiant) and evaluating their characteristics using the tested multidetector computed tomography scanner 3 (see Table 2, line 7).

Characteristics of the study

The templates were scanned using standard clinical maxillofacial imaging modes. Scanner characteristics and examination modes are summarized in Table 2. Results were analyzed for four CBCTs from three manufacturers (see Table 2, lines 1–4), two MDCTs from two manufacturers (see Table 2, lines 5–7), and two modes for one MDCT (line 5: normal [120 kV, 200 mA] and low dose [80 kV, 10 mA]). Two sets of BMD templates with identical potassium hydrogen phosphate dilutions (one with an added high-density sample

Table 2. Scanner types and scanning modes evaluated in the study

No.	Scanner (company and country of origin); abbreviation used	Tube voltage (kV)	Tube current (mA)
1	Orthopantomograph OP 3D (Kavo, USA); CBCT 1	95	4
2	HDX WILL (HDX Will Corp., Korea); CBCT 2	85	8
3	Orthopantomograph OP300 (Kavo, USA); CBCT 3	90	3, 2
4	Vatech PaX-Uni3D (Vatech Global, South Korea); CBCT 4	90	5
5	GE Discovery NM/CT 670 (GE Healthcare, USA); MDCT 1[a]	120	200
6	GE Discovery LOW/CT 670 (GE Healthcare, USA); MDCT 2	80	10
7	Siemens Somatom Perspective (Siemens, USA); MDCT 3	110	23

Note. MDCT 1, tested multidetector computed tomography scanner 1.
[a]MDCT 1 (line 5) is used as the standard for cross-calibration in further study steps.

of β-tricalcium phosphate) were fixed around 25-mm tubes (see Figure 1a and 1d), which were then placed in an 85-mm cylinder filled with distilled water (see Figure 1b and 1e), which was established in a scanner (see Figure 1c). The water environment is necessary to simulate the effect of beam hardening [10], making phantom study conditions closer to clinical settings.

Results

The results of a CT study of "in water" and "in air" patterns are expected to be compared to assess the influence of absorbing properties of the liquid medium, the oral cavity. Images were obtained in DICOM format (see Figures 1e and 2).

Statistical analysis

Mean values and standard deviations were calculated for BMD samples in templates. Radiographic density values were averaged for BMD samples of corresponding templates. The obtained data were processed in Excel and Statistica 10, and HU (for MDCT), GV (for CBCT), and BMD parameters were compared. Linear and quadratic lines of approximation were used. The MDCT mode of 120 kV and 200 mA was used as the internal standard for cross-calibration (see Table 1, column 4; Table 2, line 5). Considering the small sample size and heterogeneous conditions, nonparametric statistics (Mann–Whitney *U* test) were used to compare groups.

RESULTS

Radiographic density measurements of BMD templates are presented in HUs for MDCT and GVs for CBCT in Figures 1 and 2. There is a significant scatter for measured values, although for individual scanners, the measured radiographic density of water (negative GV values are reported for CBCT 2 and CBCT 4). Figure 2 compares the phantom obtained for

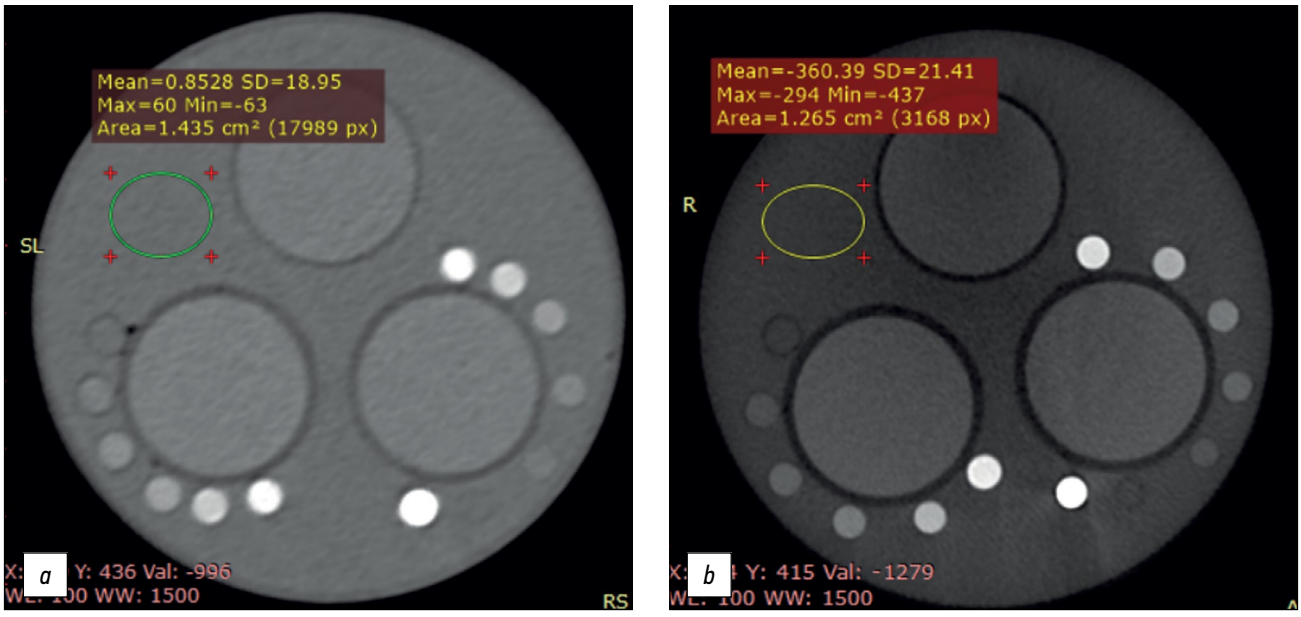

Fig. 2. Radiopaque phantom with bone mineral density templates using the same visualization parameters of the "window" (window level 100/window width 1,500 for bone tissue) for (*a*) tested multidetector computed tomography scanner 3 and (*b*) cone-beam computed tomography scanner 2: different contrast intensity is visible, measured values of water density: 0.85 HU for multidetector scanner and 360 GV for cone beam scanner.

MDCT using the same "window" visualization parameters for bone tissue (window level 100/window width). MDCT 3 (a) and CBCT 2 (b) have different contrasts. The measured values of the radiographic density of water are –0.85 HUs for MDCT and –360 GVs for CBCT.

Slopes and shapes of radiographic density to BMD curves differ significantly (Figure 3).

Cross-calibration was proposed to unify the measurements performed, which is to determine formulas for recalculating each specific measurement for different scanners using a universal internal standard, that is, MDCT 1 (120 kV, 200 mA; see Table 2, line 5). For this purpose, dependences were initially constructed in reverse coordinates (Figure 4).

Figure 4 shows BMD dependences on HU or GV, inverse coordinates to Figure 3. Approximation lines were created using Excel, including linear lines for CBCT 1 and 3 and MDCT 1–3 and quadratic for CBCT 2 and 4 (the corresponding formulas are shown in Figure 4). The decision to apply the approximation law was based on a visual analysis of the dependence pattern. For CBCT 1, the dependence was divided into two ranges, and its dependent patterns were determined. This is related to artifacts identified during image analysis.

The resulting dependency formulas (see Figure 4) enable us to calculate cross-calibration formulas after simple transformations related to the "standard" MDCT mode of 120 kV and 200 mA (see Table 2, line 5). These formulas are presented in Table 3 (column 2). These formulas should be used according to the following algorithm: measured values of radiographic density of bone samples or templates, expressed in HU for MDCT and GV for CBCT, are substituted as a factor (x) on the right side of formulas; in this case, the calculated value (y) corresponds to the radiographic density of a given sample, expressed in HU, if scanned in MDCT 1 mode. These densities can be assessed using the Misch scale (see Table 1) to determine the appropriate type of bone tissue D1–5.

All radiographic densities for the corresponding scanning modes were recalculated using this cross-calibration algorithm. These data are presented in Figure 5. Compared with Figure 3, good data consistency is reported.

DISCUSSION

During the study, CT scanners revealed varying densitometric parameters for the same BMD values (see Figure 3). Radiographic densities of MDCT scanners for water were closest to 0, expressed in HUs: MDCT 1 (1.5), MDCT 2 (–9), and MSKT 3 (14). CBCT has more significant scatters than GVs: CBCT 1 (210), CBCT 2 (–305), CBCT 3 (171), and CBCT 4 (–400). The most reliable radiographic density of distilled water was achieved with MDCT 1 with a scanning mode of 120 kV and 200 mA, selected as an internal standard for cross-calibration. The subsequent dependency pattern in Figure 3 was also heterogeneous regarding curve slope and shapes (significant nonlinearity was reported for CBCT 2 and 3). Rearranging the results in reverse coordinates using approximation lines (see Figure 4) enabled us to determine

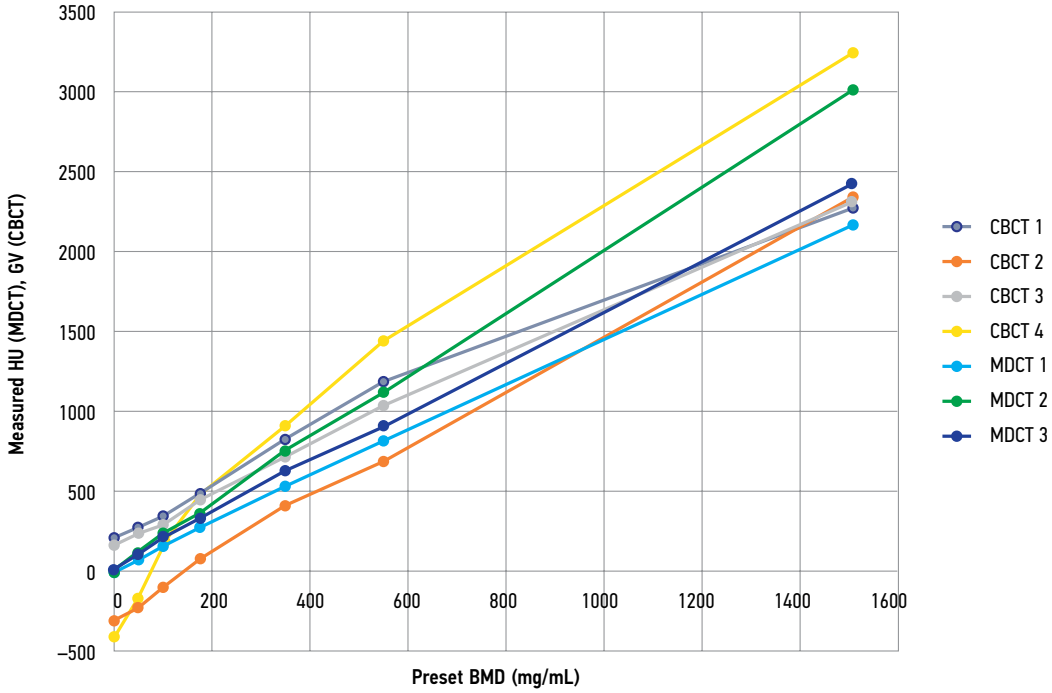

Fig. 3. Dependence of measured radiographic densities (HU for MDCT and GV for CBCT) on preset bone mineral densities before cross-calibration: there is a significant scatter of HU values when using different modes and MDCT scanners and GV values when using other CBCT scanners. CBCT, cone beam computed tomography scanner; MDCT, multidetector computed tomography scanner.

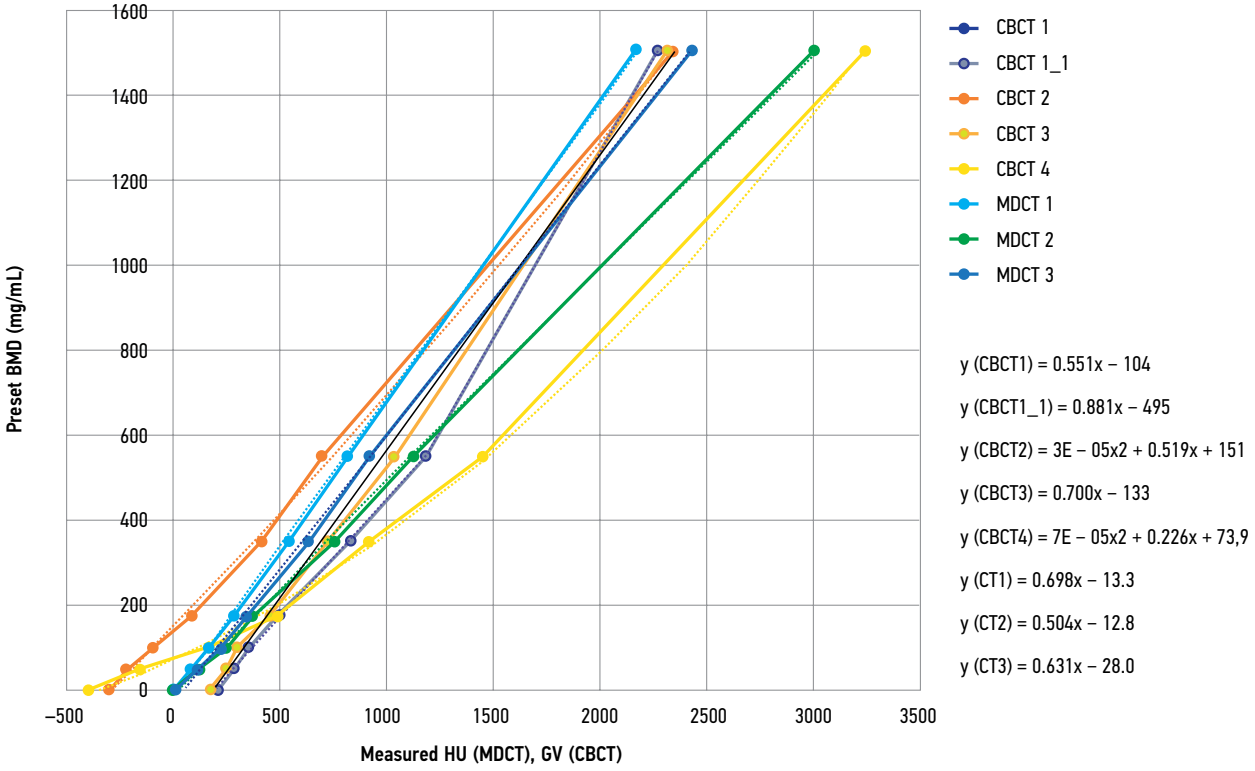

Fig. 4. Inverse dependencies compared with Figure 2: Mineral density versus radiographic density in GV and HU. The resulting lines of approximation were used to determine formulas for cross-calibration.

Table 3. Formulas for cross-calibration for each tested scanner

Abbreviated name of scanners (as in Table 1)	Formulas for cross-calibration relative to MDCT 1
CBCT 1 (0–350 mg/mL) CBCT 1_1 (350–1,506 mg/mL)	$y = 0.819 \times (x) - 164$ $y = 1.31 \times (x) - 164$
CBCT 2	$y = 4.4 \times 10^{-5} \times (x)^2 + 0.771 \times (x) + 234$
CBCT 3	$y = 1.04 \times (x) - 188$
CBCT 4	$y = 1.04 \times (x)^2 + 0.335 \times (x) + 120$
MDCT 2	$y = 0.748 \times (x) - 9.14$
MDCT 3	$y = 0.937 \times (x) - 51.5$

Note. In formulas, *x* means the measured values of HU or GV using the corresponding CT scanner; *y* represents the calculated value for cross-calibration relative to CT 1 (i.e., bone tissue density in HU when using CT 1 from Table 1). CBCT 1–4 mean serial numbers of the tested cone-beam computed tomography scanners; MDCT 2 and 3 mean serial numbers of the tested multidetector computed tomography.

algorithms for cross-calibration relative to MDCT 1 mode of 120 kV and 200 mA (see Table 2, line 5). These formulas are provided in Table 3. After cross-calibration, recalculated data showed good comparability with MDCT 1. The median difference between measured values and MDCT 1 value before cross-calibration was 160 relative units (HU and GV), and after recalculation, it was decreased by 10 times to 16 relative units ($p = 0.000$). Despite the cross-calibration, the average difference for CBCT was significantly higher (30 relative units) than for MDCT (eight relative units; $p = 0.024$). Values were compared using a Mann–Whitney *U* test. Moreover, the average relative difference in density units between the two templates was 17.69% for CBCT and 4.7% for MDCT.

Due to a significant scatter in relative differences between two templates with different spatial locations (see Figure 2) and a larger scatter relative to the average values of the standard mode of 120 kV and 200 mA after cross-calibration in CBCT, synchronous templates are required, that is, templates located in the oral cavity near the proposed implantation zone of the patient examined. An asynchronous technique effectively used in quantitative CT may be ineffective in CBCT due to several artifacts that cause signal heterogeneity [11]. Calibration is required for specific equipment, modes, and patients.

At present, relative units HU are used in the radiological classification by Misch (see Table 1, columns 5 and 6), which is the main stage of planning dental implantation

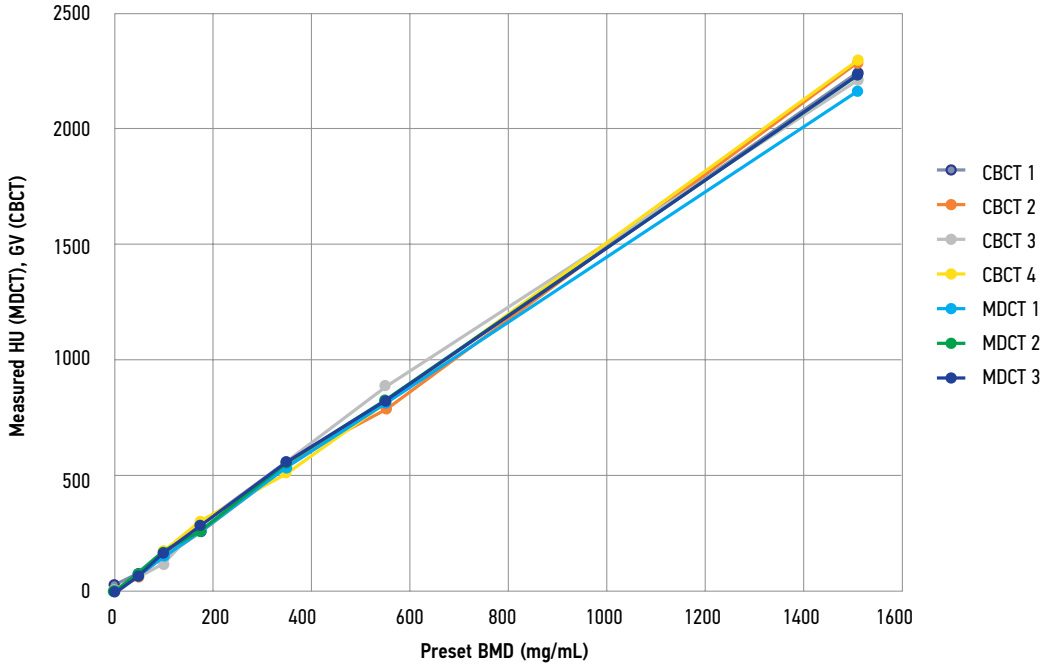

Fig. 5. Dependence of the recalculated radiographic densities (HU for MDCT and GV for CBCT) on preset bone mineral densities after cross-calibration. Good agreement is noted between the adjusted data. Cross-calibration was performed relative to the MDCT 1 scanner with 120 kV, 200-mA mode. CBCT, cone beam computed tomography scanner; MDCT 1, tested multidetector computed tomography scanner 1.

and selecting a subsequent surgery protocol. In this experimental study, conditions were simulated when the densities of the radiopaque template correspond to the main types of bone tissue, according to Misch (see Table 1), which are D1–5. After cross-calibration, it was shown that it is possible to reliably estimate the HU of various MDCT modes and CBCT methods. This method is inexpensive and easy to use.

A radiopaque template saturated with potassium hydrogen phosphate has long been used in dosimetry as a cortical bone equivalent material [12]. This material was previously used for reference radiopaque phantoms in various dilutions [11, 13]. Moreover, composite materials based on water-insoluble hydroxyapatite or tricalcium phosphate can be considered radiopaque. As in bone tissue, the radiographic density of potassium hydrogen phosphate and tricalcium phosphate changes in concordance with radiographic energy changes [14, 15]. In this experimental study, several voltages were used. We selected scanning modes recommended by manufacturers ranging from 80 to 120 kV, depending on the type of equipment. Densitometric parameters of water correspond to 0 on the HU scale, which is set when calibrating MDCT [1]. MDCT scanners were the most similar to this value parameter.

Phantoms (radioopaque templates) based on potassium hydrogen phosphate were previously used to develop unified measurements and further classify calcifications of vessel walls and bone tissue [16, 17]. Lower accuracy was reported for scanners with low voltage and spatial resolution [18]. Errors in measuring BMD were associated with CT scanner voltage, the reconstruction algorithm used, characteristic scattering artifacts, and a lack of photons at detectors; the radiation power (mA) has a lesser effect [11]. All CT scans of radiopaque templates were performed in the water-immersed state, with dimensions comparable to the sizes of the oral cavity and surrounding soft tissues, making the model conditions closer to scanning real patients [19].

Our quantitative study using radiopaque templates yielded more comprehensive results than previous studies that assessed one type of CT scanner and one type of radiopaque template [20–23]. Because we used original templates with seven specified BMD values and compared six scanners, our study is more unique and evidential. Our study found that using radiopaque templates standardizes and compensates for shortcomings in densitometric classification using CBCT, significantly affecting planning and performing dental procedures [24, 25].

In the future, synchronous radiopaque templates will be used for various types of maxillofacial surgeries, including dental implantation. Using radiopaque templates for planning dental implantation will allow for the development a highly personalized surgery protocol [26–30]. A similar pattern of bone density dependences is observed when comparing CBCT and MDCT; however, individual measurements differ significantly [26]. Our cross-calibration algorithm significantly reduces these differences.

In addition to errors in determining BMD using CBCT, geometric distortions should be assessed [31–34]. Medelnik et al. [35] evaluated the reproducibility of anatomical landmarks and the accuracy of various CBCT and MDCT. Elshenawy et al. [36] reported that an increased area of interest parallel to voxel size may reduce the accuracy of

linear CBCT measurements, particularly when assessing small distances. The authors stressed the need to appropriately evaluate object density in addition to determining geometric distortions.

CONCLUSION

When four CBCTs and two MDCTs are used to assess the same bone mineral density samples, the created radiopaque template shows a large scatter of radiographic densities. According to Misch, cross-calibration standardizes densitometric parameters for CBCT and various MDCT modes while reducing scatter by 10 times, allowing bone tissue to be classified. The most promising strategy is to use individual synchronous templates located directly near the area of the proposed dental intervention.

ADDITIONAL INFORMATION

Funding source. This article was prepared by the authors as part of the research and development work (EGISU number: 123031400007-7) in accordance with the Program of the Moscow Department of Health for 2023-2025.

Competing interests. The authors declare that they have no competing interests.

Authors' contribution. All authors made a substantial contribution to the conception of the work, acquisition, analysis, interpretation of data for the work, drafting and revising the work, final approval of the version to be published and agree to be accountable for all aspects of the work. Sh.D. Hossain, A.B. Danaev, A.A. Dolgalev — writing the text of the article, performing the experimental part of the research; A.A. Muraev, D.V. Burenchev, S.Yu. Ivanov — study concept and design; A.V. Petraikin, Yu.A. Vasilev, D.E. Sharova — data analysis.

REFERENCES

1. Hounsfield GN. Computerized transverse axial scanning (tomography). Description of system. *Br J Radiol.* 1973;46(552): 1016–1022. doi: 10.1259/0007-1285-46-552-1016

2. Bornstein MM, Scarfe WC, Vaughn VM, Jacobs R. Cone beam computed tomography in implant dentistry: A systematic review focusing on guidelines, indications, and radiation dose risks. *Int J Oral Maxillofac Implants.* 2014;29(Suppl):55–77. doi: 10.11607/jomi.2014suppl.g1.4

3. DenOtter TD, Schubert J. Hounsfield Unit. In: StatPearls. Treasure Island (FL): StatPearls Publishing; 2022.

4. Kim Y, Oh TJ, Misch CE, Wang HL. Occlusal considerations in implant therapy: Clinical guidelines with biomechanical rationale. *Clin Oral Implants Res.* 2005;16(1):26–35. doi: 10.1111/j.1600-0501.2004.01067.x

5. Woelber JP, Fleiner J, Rau J, et al. Accuracy and usefulness of CBCT in periodontology: A systematic review of the literature. *Int J Periodontics Restorative Dent.* 2018;38(2):289–297. doi: 10.11607/prd.2751

6. Song D, Shujaat S, de Faria Vasconcelos K, et al. Diagnostic accuracy of CBCT versus intraoral imaging for assessment of peri-implant bone defects. *BMC Med Imaging.* 2021;21(1):23. doi: 10.1186/s12880-021-00557-9

7. Savoldi F, Yon MJ, Kwok VM, et al. Accuracy of CBCT in the identification of mental, lingual, and retromolar foramina: A comparison with visual inspection of human dry mandibles. *Int J Periodontics Restorative Dent.* 2021;41(6):e277–e286. doi: 10.11607/prd.4770

8. Levi C, Gray JE, McCullough EC, Hattery RR. The unreliability of CT numbers as absolute values. *AJR Am J Roentgenol.* 1982;139(3): 443–447. doi: 10.2214/ajr.139.3.443

9. Petraikin AV, Skripnikova IA. Quantitative computed tomography, modern data. Review. *Medical Imaging.* 2021;25(4):134–146. (In Russ). doi: 10.24835/1607-0763-1049

10. Ivanov DV, Kirillova IV, Kossovich LY, et al. Influence of convolution kernel and beam-hardening effect on the assessment of trabecular bonemineral density using quantitative computed tomography. *News Saratov University.* 2020;20(2):205–219. (In Russ). doi: 10.18500/1816-9791-2020-20-2-205-219

11. Petraikin AV, Smorchkova AK, Kudryavtsev ND, et al. Comparison of two asynchronous QCT methods. *Medical Imaging.* 2020;24(4): 108–118. (In Russ). doi: 10.24835/1607-0763-2020-4-108-118

12. Witt RM, Cameron JR. Bone Standards. USAEC Progress Report No. COO-1422-42 US Atomic Energy Comission, Madison, Wisconsin; 1969.

13. Cann CE, Genant HK. Precise measurement of vertebral mineral content using computed tomography. *J Comput Assist Tomogr.* 1980;4(4):493–500. doi: 10.1097/00004728-198008000-00018

14. Hubbell JH. Photon cross sections, attenuation coefficients, and energy absorption coefficients from 10 keV to 100 GeV. National Institute of Standards and Technology, Gaithersburg, MD; 1969. doi: 10.6028/NBS.NSRDS.29

15. International Commission on Radiation Units and Measurements (ICRU). Tissue Substitutes in Radiation Dosimetry and Measurement. *ICRU Report*.1989;(44):1–189.

16. Nikolaev AE, Korkunova OA, Blokhin IA, et al. Calcification density oncomputed tomography depending on scanning parameters: Phantom study. (In Russ). *Med Imaging.* 2020;24(4):119–132. doi: 10.24835/1607-0763-2020-4-119-132

17. Gaur A, Dhillon M, Puri N, et al. Questionable accuracy of CBCT in determining bone density: A comparative CBCT-CT in vitro study. *Dent Med Probl.* 2022;59(3):413–419. doi: 10.17219/dmp/143504

18. Martinez C, de Molina C, Desco M, Abella M. Optimization of a calibration phantom for quantitative radiography. *Med Phys.* 2021;48(3):1039–1053. doi: 10.1002/mp.14638

19. Hu Z, Wang T, Pan X, et al. Comparison of diagnosis of cracked tooth using contrast-enhanced CBCT and micro-CT. *Dentomaxillofac Radiol.* 2021;50(7):20210003. doi: 10.1259/dmfr.20210003

20. Lehmann L, Alvarez R, Macovski A, et al. Generalized image combinations in dual KVP digital radiography. *Med Phys.* 1981;8(5):659–667. doi: 10.1118/1.595025

21. Chuang KS, Huang H. Comparison of four dual energy image decomposition methods. *Physics Med Biol.* 1988;33(4):455. doi: 10.1088/0031-9155/33/4/005

22. Gingold EL, Hasegawa BH. Systematic bias in basis material decomposition applied to quantitative dual-energy X-ray imaging. *Med Phys.* 1992;19(1):25–33. doi: 10.1088/0031-9155/33/4/005

23. Cardinal HN, Fenster A. An accurate method for direct dual-energy calibration and decomposition. *Med Phys*. 1990;17(3):327–341. doi: 10.1118/1.596512
24. Jacobs R, Salmon B, Codari M, et al. Cone beam computed tomography in implant dentistry: recommendations for clinical use. *BMC Oral Health.* 2018;18(1):88. doi: 10.1186/s12903-018-0523-5
25. Dolgalev AA, Danaev AB, Yusupov RD, et al. Objective assessment of measurement error in significant cone-beam computed tomography in dental practice. *Med Alphabet.* 2022;(7):65–68. (In Russ). doi: 10.33667/2078-5631-2022-7-65-68
26. Cassetta M, Stefanelli LV, Di Carlo S, et al. The accuracy of CBCT in measuring jaws bone density. *Eur Rev Med Pharmacol Sci*. 2012;16(10):1425–1429.
27. Harvey S, Patel S. Guidelines and template for reporting on CBCT scans. *Br Dent J.* 2020;228(1):15–18. doi: 10.1038/s41415-019-1115-8
28. Cassetta M, Stefanelli LV, Pacifici A, et al. How accurate is CBCT in measuring bone density? A comparative CBCT-CT in vitro study. *Clin Implant Dent Relat Res.* 2014;16(4):471–478. doi: 10.1111/cid.12027
29. Parsa A, Ibrahim N, Hassan B, et al. Bone quality evaluation at dental implant site using multislice CT, micro-CT, and cone beam CT. *Clin Oral Implants Res.* 2015;26(1):e1–7. doi: 10.1111/clr.12315
30. Van Dessel J, Nicolielo LF, Huang Y, et al. Accuracy and reliability of different cone beam computed tomography (CBCT) devices for structural analysis of alveolar bone in comparison with multislice CT and micro-CT. *Eur J Oral Implantol.* 2017;10(1):95–105.
31. Dillenseger JP, Matern JF, Gros CI, et al. MSCT versus CBCT: Evaluation of high-resolution acquisition modes for dento-maxillary and skull-base imaging. *Eur Radiol.* 2015;25(2):505–515. doi: 10.1007/s00330-014-3439-8
32. Schegerer AA, Lechel U, Ritter M, et al. Dose and image quality of cone-beam computed tomography as compared with conventional multislice computed tomography in abdominal imaging. *Invest Radiol.* 2014;49(10):675–684. doi: 10.1097/RLI.0000000000000069
33. Veldhoen S, Schöllchen M, Hanken H, et al. Performance of cone-beam computed tomography and multidetector computed tomography in diagnostic imaging of the midface: A comparative study on Phantom and cadaver head scans. *Eur Radiol.* 2017;27(2):790–800. doi: 10.1007/s00330-016-4387-2
34. Grunz JP, Weng AM, Gietzen CH, et al. Evaluation of ultra-high-resolution cone-beam CT prototype of twin robotic radiography system for cadaveric wrist imaging. *Acad Radiol.* 202;28(10):e314–e322. doi: 10.1016/j.acra.2020.06.018
35. Medelnik J, Hertrich K, Steinhäuser-Andresen S, et al. Accuracy of anatomical landmark identification using different CBCT- and MSCT-based 3D images: An in vitro study. *J Orofac Orthop.* 2011;72(4):261–278. doi: 10.1007/s00056-011-0032-5
36. Elshenawy H, Aly W, Salah N, et al. Influence of small, midi, medium and large fields of view on accuracy of linear measurements in CBCT imaging: Diagnostic accuracy study. *Open Access Maced J Med Sci.* 2019;7(6):1037–1041. doi: 10.3889/oamjms.2019.232

СПИСОК ЛИТЕРАТУРЫ

1. Hounsfield G.N. Computerized transverse axial scanning (tomography). Description of system // Br J Radiol. 1973. Vol. 46, N 552. P. 1016–1022. doi: 10.1259/0007-1285-46-552-1016
2. Bornstein M.M., Scarfe W.C., Vaughn V.M., Jacobs R. Cone beam computed tomography in implant dentistry: A systematic review focusing on guidelines, indications, and radiation dose risks // Int J Oral Maxillofac Implants. 2014. Vol. 2014, N 29, Suppl. P. 55–77. doi: 10.11607/jomi.2014suppl.g1.4
3. DenOtter T.D., Schubert J. Hounsfield Unit. In: StatPearls. Treasure Island (FL): StatPearls Publishing; March 9, 2022.
4. Kim Y., Oh T.J., Misch C.E., Wang H.L. Occlusal considerations in implant therapy: Clinical guidelines with biomechanical rationale // Clin Oral Implants Res. 2005. Vol. 16, N 1. P. 26–35. doi: 10.1111/j.1600-0501.2004.01067.x
5. Woelber J.P., Fleiner J., Rau J., et al. Accuracy and usefulness of CBCT in periodontology: A systematic review of the literature // Int J Periodontics Restorative Dent. 2018. Vol. 38, N 2. P. 289–297. doi: 10.11607/prd.2751
6. Song D., Shujaat S., de Faria Vasconcelos K., et al. Diagnostic accuracy of CBCT versus intraoral imaging for assessment of peri-implant bone defects // BMC Med Imaging. 2021. Vol. 21, N 1. P. 23. doi: 10.1186/s12880-021-00557-9
7. Savoldi F., Yon M.J., Kwok V.M., et al. Accuracy of CBCT in the identification of mental, lingual, and retromolar foramina: A comparison with visual inspection of human dry mandibles // Int J Periodontics Restorative Dent. 2021. Vol. 4, N 6. P. e277–e286. doi: 10.11607/prd.4770
8. Levi C., Gray J.E., McCullough E.C., Hattery R.R. The unreliability of CT numbers as absolute values // AJR Am J Roentgenol. 1982. Vol. 139, N 3. P. 443–447. doi: 10.2214/ajr.139.3.443
9. Петряйкин А.В., Скрипникова И.А. Количественная компьютерная томография, современные данные. Обзор // Медицинская визуализация. 2021. Т. 25, № 4. С. 134–146. doi: 10.24835/1607-0763-1049
10. Иванов Д.В., Кириллова И.В., Коссович Л.Ю., и др. Влияние конволюционных ядер и эффекта «упрочнения луча» на оценку минеральной плотности губчатой костной ткани с использованием количественной компьютерной томографии // Известия Саратовского университета. 2020. Т. 20, № 2. С. 205–219. doi: 10.18500/1816-9791-2020-20-2-205-219
11. Петряйкин А.В., Сморчкова А.К., Кудрявцев Н.Д., и др. Сравнение двух методик асинхронной КТ-денситометрии // Медицинская визуализация. 2020. Т. 24, № 4. С. 108–118. doi: 10.24835/1607-0763-2020-4-108-118
12. Witt R.M., Cameron J.R. Bone Standards. USAEC Progress Report COO-1422-42, US Atomic Energy Comission, Madison, Wisconsin, 1969.
13. Cann C.E., Genant H.K. Precise measurement of vertebral mineral content using computed tomography // J Comput Assist Tomogr. 1980. Vol. 4, N 4. P. 493–500. doi: 10.1097/00004728-198008000-00018
14. Hubbell J.H. Photon cross sections, attenuation coefficients, and energy absorption coefficients from 10 keV to 100 GeV. National Institute of Standards and Technology, Gaithersburg, MD, 1969. doi: 10.6028/NBS.NSRDS.29
15. International Commission on Radiation Units and Measurements (ICRU). Tissue Substitutes in Radiation Dosimetry and Measurement // ICRU Report. 1989. N 44. P. 1–189.
16. Николаев А.Е., Коркунова О.А., Блохин И.А., и др. Плотность кальцификации при компьютерной томографии в зависимости от параметров сканирования: фантомное исследова-

ние // Медицинская визуализация. 2020. Т. 24, № 4. С. 119–132. doi: 10.24835/1607-0763-2020-4-119-132
17. Gaur A., Dhillon M., Puri N., et al. Questionable accuracy of CBCT in determining bone density: A comparative CBCT-CT in vitro study // Dent Med Probl. 2022. Vol. 59, N 3. P. 413–419. doi: 10.17219/dmp/143504
18. Martinez C., de Molina C., Desco M., Abella M. Optimization of a calibration phantom for quantitative radiography // Med Phys. 2021. Vol. 48, N 3. P. 1039–1053. doi: 10.1002/mp.14638
19. Hu Z., Wang T., Pan X., et al. Comparison of diagnosis of cracked tooth using contrast-enhanced CBCT and micro-CT // Dentomaxillofac Radiol. 2021. Vol. 50, N 7. P. 20210003. doi: 10.1259/dmfr.20210003
20. Lehmann L., Alvarez R., Macovski A., et al. Generalized image combinations in dual KVP digital radiography // Med Phys. 1981. Vol. 8, N 5. P. 659–667. doi: 10.1118/1.595025
21. Chuang K.S., Huang H. Comparison of four dual energy image decomposition methods // Physics Med Biol. 1988. Vol. 33, N 4. P. 455. doi: 10.1088/0031-9155/33/4/005
22. Gingold E.L., Hasegawa B.H. Systematic bias in basis material decomposition applied to quantitative dual-energy X-ray imaging // Med Phys. 1992. Vol. 9, N 1. P. 25–33. doi: 10.1118/1.596889
23. Cardinal H.N., Fenster A. An accurate method for direct dual-energy calibration and decomposition // Med Phys. 1990. Vol. 17, N 3. P. 327–341. doi: 10.1118/1.596512
24. Jacobs R., Salmon B., Codari M., et al. Cone beam computed tomography in implant dentistry: Recommendations for clinical use // BMC Oral Health. 2018. Vol. 18, N 1. P. 88. doi: 10.1186/s12903-018-0523-5
25. Долгалев А.А., Данаев А.Б., Юсупов Р.Д., и др. Объективная оценка погрешности показателей плотности при проведении конусно-лучевой компьютерной томографии в стоматологической практике // Медицинский алфавит. 2022. № 7. С. 65–68. doi: 10.33667/2078-5631-2022-7-65-68
26. Cassetta M., Stefanelli L.V., Di Carlo S., et al. The accuracy of CBCT in measuring jaws bone density // Eur Rev Med Pharmacol Sci. 2012. Vol. 16, N 10. P. 1425–1429.
27. Harvey S., Patel S. Guidelines and template for reporting on CBCT scans // Br Dent J. 2020. Vol. 228, N 1. P. 15–18. doi: 10.1038/s41415-019-1115-8
28. Cassetta M., Stefanelli L.V., Pacifici A., et al. How accurate is CBCT in measuring bone density? A comparative CBCT-CT in vitro study // Clin Implant Dent Relat Res. 2014. Vol. 16, N 4. P. 471–478. doi: 10.1111/cid.12027
29. Parsa A., Ibrahim N., Hassan B., et al. Bone quality evaluation at dental implant site using multislice CT, micro-CT, and cone beam CT // Clin Oral Implants Res. 2015. Vol. 26, N 1. P. e1–7. doi: 10.1111/clr.12315
30. Van Dessel J., Nicolielo L.F., Huang Y., et al. Accuracy and reliability of different cone beam computed tomography (CBCT) devices for structural analysis of alveolar bone in comparison with multislice CT and micro-CT // Eur J Oral Implantol. 2017. Vol. 10, N 1. P. 95–105.
31. Dillenseger J.P., Matern J.F., Gros C.I., et al. MSCT versus CBCT: Evaluation of high-resolution acquisition modes for dento-maxillary and skull-base imaging // Eur Radiol. 2015. Vol. 25, N 2. P. 505–515. doi: 10.1007/s00330-014-3439-8
32. Schegerer A.A., Lechel U., Ritter M., et al. Dose and image quality of cone-beam computed tomography as compared with conventional multislice computed tomography in abdominal imaging // Invest Radiol. 2014. Vol. 49, N 10. P. 675–684. doi: 10.1097/RLI.0000000000000069
33. Veldhoen S., Schöllchen M., Hanken H., et al. Performance of cone-beam computed tomography and multidetector computed tomography in diagnostic imaging of the midface: A comparative study on Phantom and cadaver head scans // Eur Radiol. 2017. Vol. 27, N 2. P. 790–800. doi: 10.1007/s00330-016-4387-2
34. Grunz J.P., Weng A.M., Gietzen C.H., et al. Evaluation of ultra-high-resolution cone-beam CT prototype of twin robotic radiography system for cadaveric wrist imaging // Acad Radiol. 2021. Vol. 28, N 10. P. e314–e322. doi: 10.1016/j.acra.2020.06.018
35. Medelnik J., Hertrich K., Steinhäuser-Andresen S., et al. Accuracy of anatomical landmark identification using different CBCT- and MSCT-based 3D images: An in vitro study // J Orofac Orthop. 2011. Vol. 72, N 4. P. 261–278. doi: 10.1007/s00056-011-0032-5
36. Elshenawy H., Aly W., Salah N., et al. Influence of small, midi, medium and large fields of view on accuracy of linear measurements in CBCT imaging: Diagnostic accuracy study // Open Access Maced J Med Sci. 2019. Vol. 7, N 6. P. 1037–1041. doi: 10.3889/oamjms.2019.232

AUTHORS' INFO

*** Alexey V. Petraikin,** MD, Dr. Sci. (Med.), Assistant Professor;
address: 24/1 Petrovka street, 127051 Moscow, Russia;
ORCID: 0000-0003-1694-4682;
eLibrary SPIN: 6193-1656;
e-mail: alexeypetraikin@gmail.com

Shazmim D. Hossain;
ORCID: 0000-0002-5410-1849;
eLibrary SPIN: 3760-3723;
e-mail: shazmim@mail.ru

Alexandr A. Muraev, MD, Dr. Sci. (Med.), Professor;
ORCID: 0000-0003-3982-5512;
eLibrary SPIN: 1431-5936;
e-mail: muraev_aa@pfur.ru

ОБ АВТОРАХ

*** Петряйкин Алексей Владимирович,** д-р мед. наук, доцент;
адрес: Россия, 127051, Москва, ул. Петровка, д. 24, стр. 1;
ORCID: 0000-0003-1694-4682;
eLibrary SPIN: 6193-1656;
e-mail: alexeypetraikin@gmail.com

Хоссаин Шазмим Джахан;
ORCID: 0000-0002-5410-1849;
eLibrary SPIN: 3760-3723;
e-mail: shazmim@mail.ru

Мураев Александр Александрович, д-р мед. наук, профессор;
ORCID: 0000-0003-3982-5512;
eLibrary SPIN: 1431-5936;
e-mail: muraev_aa@pfur.ru

* Corresponding author / Автор, ответственный за переписку

Aslan B. Danaev;
ORCID: 0000-0003-4754-3101;
eLibrary SPIN: 7266-7722;
e-mail: aslandanaev111@mail.ru

Dmitry V. Burenchev, MD, Dr. Sci. (Med.);
ORCID: 0000-0003-2894-6255;
eLibrary SPIN: 2411-3959;
e-mail: BurenchevDV@zdrav.mos.ru

Alexander A. Dolgalev, MD, Dr. Sci. (Med.), Assistant Professor;
ORCID: 0000-0002-6352-6750;
eLibrary SPIN: 5941-5771;
e-mail: dolgalev@dolgalev.pro

Yuriy A. Vasilev, MD, Cand. Sci. (Med.);
ORCID: 0000-0002-0208-5218;
eLibrary SPIN: 4458-5608;
e-mail: VasilevYA1@zdrav.mos.ru

Dariya E. Sharova;
ORCID: 0000-0001-5792-3912;
eLibrary SPIN: 1811-7595;
e-mail: SharovaDE@zdrav.mos.ru

Sergey Yu. Ivanov, MD, Dr. Sci. (Med.), Professor, Corresponding Member of the Russian Academy of Sciences;
ORCID: 0000-0001-5458-0192;
eLibrary SPIN: 2607-2679;
e-mail: syivanov@yandex.ru

Данаев Аслан Барадинович;
ORCID: 0000-0003-4754-3101;
eLibrary SPIN: 7266-7722;
e-mail: aslandanaev111@mail.ru

Буренчев Дмитрий Владимирович, д-р мед. наук;
ORCID: 0000-0003-2894-6255;
eLibrary SPIN: 2411-3959;
e-mail: BurenchevDV@zdrav.mos.ru

Долгалев Александр Александрович, д-р мед. наук, доцент;
ORCID: 0000-0002-6352-6750;
eLibrary SPIN: 5941-5771;
e-mail: dolgalev@dolgalev.pro

Васильев Юрий Александрович, канд. мед. наук;
ORCID: 0000-0002-0208-5218;
eLibrary SPIN: 4458-5608;
e-mail: VasilevYA1@zdrav.mos.ru

Шарова Дарья Евгеньевна;
ORCID: 0000-0001-5792-3912;
eLibrary SPIN: 1811-7595;
e-mail: SharovaDE@zdrav.mos.ru

Иванов Сергей Юрьевич, д-р мед. наук, профессор, чл.-корр. РАН;
ORCID: 0000-0001-5458-0192;
eLibrary SPIN: 2607-2679;
e-mail: syivanov@yandex.ru

DOI: https://doi.org/10.17816/DD529668

Терминология рака прямой кишки: консенсусное соглашение Рабочей группы экспертов POPP, AOP и PATPO

Т.П. Березовская[1], Н.А. Рубцова[2], В.Е. Синицын[3], И.В. Зароднюк[4], Н.В. Нуднов[5], А.В. Мищенко[6], Ю.Л. Трубачева[4], Т.А. Берген[7], П.Ю. Гришко[6], С.С. Балясникова[8], Я.А. Дайнеко[1], Д.В. Рыжкова[9], М.М. Ходжибекова[2], Н.А. Ручьева[10], И.Е. Тюрин[8], С.И. Ачкасов[4], А.А. Невольских[1], С.С. Гордеев[8], И.В. Дрошнева[2]

[1] Медицинский радиологический научный центр имени А.Ф. Цыба — филиал ФГБУ «Национальный медицинский исследовательский центр радиологии», Обнинск, Российская Федерация;
[2] Московский научно-исследовательский онкологический институт имени П.А. Герцена — филиал ФГБУ «Национальный медицинский исследовательский центр радиологии», Москва, Российская Федерация;
[3] Московский государственный университет имени М.В. Ломоносова, факультет фундаментальной медицины, Москва, Российская Федерация;
[4] Национальный медицинский исследовательский центр колопроктологии имени А.Н. Рыжих, Москва, Российская Федерация;
[5] Российский научный центр рентгенорадиологии, Москва, Российская Федерация;
[6] Национальный медицинский исследовательский центр онкологии имени Н.Н. Петрова, Москва, Российская Федерация;
[7] Национальный медицинский исследовательский центр имени академика Е.Н. Мешалкина, Москва, Российская Федерация;
[8] Национальный медицинский исследовательский центр онкологии имени Н.Н. Блохина, Москва, Российская Федерация;
[9] Национальный медицинский исследовательский центр имени В.А. Алмазова, Москва, Российская Федерация;
[10] Национальный медицинский исследовательский центр трансплантологии и искусственных органов имени академика В.И. Шумакова, Москва, Российская Федерация

АННОТАЦИЯ

Унифицированная терминология — необходимое условие успешной междисциплинарной коммуникации в онкологии. Многообразие анатомических, патоморфологических и клинических терминов, используемых при раке прямой кишки, нередко сопровождается неоднозначной их трактовкой как в отечественной, так и зарубежной научной литературе. Это не только усложняет взаимодействие между специалистами, но и затрудняет сравнение результатов лечения рака прямой кишки, полученных в разных лечебных учреждениях.

На основе анализа современной отечественной и международной научно-методической литературы по раку прямой кишки были отобраны ключевые термины, используемые при диагностике и планировании лечения злокачественного новообразования, с последующим двукратным онлайн-обсуждением их трактовок экспертами Российского общества рентгенологов и радиологов, Ассоциации онкологов России и Российской ассоциации терапевтических радиационных онкологов до достижения консенсуса (≥80%) экспертов по всем пунктам. Термины, по которым консенсус не был достигнут, не включены в итоговый список.

В результате работы составлен список анатомических, патоморфологических и клинических терминов, используемых при диагностике, стадировании и планировании лечения рака прямой кишки, и на основе консенсуса экспертов определена их трактовка.

Предложен словарь терминов, рекомендуемых при описании и формулировке заключения диагностических исследований у пациентов с раком прямой кишки.

Ключевые слова: рак прямой кишки; стадирование; неоадъювантное лечение; хирургическое лечение; магнитно-резонансная томография; МРТ; лучевая диагностика.

Как цитировать:

Березовская Т.П., Рубцова Н.А., Синицын В.Е., Зароднюк И.В., Нуднов Н.В., Мищенко А.В., Трубачева Ю.Л., Берген Т.А., Гришко П.Ю., Балясникова С.С., Дайнеко Я.А., Рыжкова Д.В., Ходжибекова М.М., Ручьева Н.А., Тюрин И.Е., Ачкасов С.И., Невольских А.А., Гордеев С.С., Дрошнева И.В. Терминология рака прямой кишки: консенсусное соглашение Рабочей группы экспертов POPP, AOP и PATPO // *Digital Diagnostics.* 2023. Т. 4, № 3. С. 306–321. DOI: https://doi.org/10.17816/DD529668

Рукопись получена: 03.07.2023 **Рукопись одобрена:** 10.07.2023 **Опубликована:** 04.09.2023

DOI: https://doi.org/10.17816/DD529668

Terminology of rectal cancer: consensus agreement of the expert working group

Tatiana P. Berezovskaya[1], Natalia A. Rubtsova[2], Valentin E. Sinitsyn[3], Irina V. Zarodnyuk[4], Nicolai V. Nudnov[5], Andrei V. Mishchenko[6], Yuliya L. Trubacheva[4], Tatiana A. Bergen[7], Pavel Yu. Grishko[6], Svetlana S. Balyasnikova[8], Yana A. Dayneko[1], Darya V. Ryjkova[9], Malika M. Hodzhibekova[2], Nataliya A. Rucheva[10], Igor E. Turin[8], Sergey I. Achkasov[4], Alexey A. Nevolskikh[1], Sergey S. Gordeev[8], Inna V. Droshneva[2]

[1] A.F. Tsyba Medical Radiological Research Center — branch National Medical Research Radiological Center, Obninsk, Russian Federation;
[2] P.A. Herzen Moscow Research Oncological Institute — branch National Medical Research Radiological Center, Moscow, Russian Federation;
[3] Lomonosov Moscow State University, Moscow, Russian Federation;
[4] State Scientific Centre of Coloproctology, Moscow, Russian Federation;
[5] Russian Scientific Center of Roentgenoradiology, Moscow, Russian Federation;
[6] N.N. Petrov National Medical Research Centre of Oncology, Moscow, Russian Federation;
[7] E. Meshalkin National Medical Research Center, Moscow, Russian Federation;
[8] N.N. Blokhin National Medical Research Center of Oncology, Moscow, Russian Federation;
[9] Almazov National Medical Research Centre, Moscow, Russian Federation;
[10] V.I. Shumakov National Medical Research Center of Transplantology and Artificial Organs, Moscow, Russian Federation

ABSTRACT

Unified terminology is a necessary condition for successful interdisciplinary communication within the field of oncology. The variety of anatomical, pathomorphological, and clinical terms used in rectal cancer is often accompanied by their ambiguous interpretation both in domestic and foreign scientific literature. This not only complicates the interaction between specialists, but also complicates the comparison of the results of rectal cancer treatment obtained in different medical institutions.

Based on the analysis of recent domestic and international scientific and methodological literature on rectal cancer, the key terms used in the diagnosis and treatment planning of rectal cancer were selected, followed by a two-time online discussion of their interpretations by experts from the Russian Society of Radiologists and Therapeutic Radiation Oncologists, the Association of Oncologists of Russia, and the Russian Association of Therapeutic Radiation Oncologists until reaching consensus (≥80%) of experts on all items. Terms that fail to attain consensus were excluded in the final list.

A list of anatomical, pathomorphological, and clinical terms used in the diagnosis, staging, and treatment planning of rectal cancer has been compiled and, based on expert consensus, their interpretation has been determined.

A lexicon recommended in the description and formulation of the conclusion of diagnostic studies in patients with rectal cancer is proposed.

Keywords: rectal cancer; staging; neoadjuvant treatment; surgical treatment; magnetic resonance imaging; radiology.

To cite this article:
Berezovskaya TP, Rubtsova NA, Sinitsyn VE, Zarodnyuk IV, Nudnov NV, Mishchenko AV, Trubacheva YuL, Bergen TA, Grishko PYu, Balyasnikova SS, Dayneko YaA, Ryjkova DV, Hodzhibekova MM, Rucheva NA, Turin IE, Achkasov SI, Nevolskikh AA, Gordeev SS, Droshneva IV. Terminology of rectal cancer: consensus agreement of the expert working group. *Digital Diagnostics.* 2023;4(3):306–321. DOI: https://doi.org/10.17816/DD529668

Received: 03.07.2023 **Accepted:** 10.07.2023 **Published:** 04.09.2023

DOI: https://doi.org/10.17816/DD529668

直肠癌术语：RSR、AOR和RATRO专家工作组达成的一致意见

Tatiana P. Berezovskaya[1], Natalia A. Rubtsova[2], Valentin E. Sinitsyn[3], Irina V. Zarodnyuk[4], Nicolai V. Nudnov[5], Andrei V. Mishchenko[6], Yuliya L. Trubacheva[4], Tatiana A. Bergen[7], Pavel Yu. Grishko[6], Svetlana S. Balyasnikova[8], Yana A. Dayneko[1], Darya V. Ryjkova[9], Malika M. Hodzhibekova[2], Nataliya A. Rucheva[10], Igor E. Turin[8], Sergey I. Achkasov[4], Alexey A. Nevolskikh[1], Sergey S. Gordeev[8], Inna V. Droshneva[2]

[1] A.F. Tsyba Medical Radiological Research Center — branch National Medical Research Radiological Center, Obninsk, Russian Federation;
[2] P.A. Herzen Moscow Research Oncological Institute — branch National Medical Research Radiological Center, Moscow, Russian Federation;
[3] Lomonosov Moscow State University, Moscow, Russian Federation;
[4] State Scientific Centre of Coloproctology, Moscow, Russian Federation;
[5] Russian Scientific Center of Roentgenoradiology, Moscow, Russian Federation;
[6] N.N. Petrov National Medical Research Centre of Oncology, Moscow, Russian Federation;
[7] E. Meshalkin National Medical Research Center, Moscow, Russian Federation;
[8] N.N. Blokhin National Medical Research Center of Oncology, Moscow, Russian Federation;
[9] Almazov National Medical Research Centre, Moscow, Russian Federation;
[10] V.I. Shumakov National Medical Research Center of Transplantology and Artificial Organs, Moscow, Russian Federation

简评

统一术语是肿瘤学跨学科交流取得成功的必要条件。直肠癌的解剖学、病理形态学和临床术语多种多样，国内外科学文献对这些术语的解释往往模棱两可。这不仅使专科医生之间的交流变得复杂，而且难以比较不同医疗机构的直肠癌治疗效果。

根据对国内外关于直肠癌的现代科学和方法学文献的分析，选出了恶性肿瘤诊断和治疗计划中使用的关键术语，然后由俄罗斯放射科医师协会（Russian Society of Radiology，RSR）、俄罗斯肿瘤科医生协会（Associations of Oncologists of Russia，AOR）和俄罗斯医疗放射肿瘤科医生协会（Russian Association of Therapeutic Radiation Oncologists，RATRO）的专家对这些术语的解释进行了两次在线讨论，直到专家们就所有项目达成共识（≥80%）。未达成共识的术语没有被纳入最终清单。

这项研究产生了一份用于直肠癌诊断、分期和治疗计划的解剖学、病理形态学和临床术语清单，并通过专家共识确定了这些术语的释义。

建议一份术语表，用于描述和制定直肠癌患者诊断检查的结论。

关键词：直肠癌；分期；肿瘤辅助治疗；手术治疗；磁共振成像；MRI；放射诊断。

引用本文：

Berezovskaya TP, Rubtsova NA, Sinitsyn VE, Zarodnyuk IV, Nudnov NV, Mishchenko AV, Trubacheva YuL, Bergen TA, Grishko PYu, Balyasnikova SS, Dayneko YaA, Ryjkova DV, Hodzhibekova MM, Rucheva NA, Turin IE, Achkasov SI, Nevolskikh AA, Gordeev SS, Droshneva IV. 直肠癌术语：RSR、AOR和RATRO专家工作组达成的一致意见. *Digital Diagnostics.* 2023;4(3):306–321. DOI: https://doi.org/10.17816/DD529668

收到：03.07.2023 **接受：**10.07.2023 **发布日期：**04.09.2023

List of abbreviations

AOR — Association of Oncologists of Russia
ICD-10 — International Statistical Classification of Diseases and Related Health Problems, Tenth Revision
MRI — Magnetic resonance imaging
RATRO — Russian Association of Therapeutic Radiation Oncologists
RORR — Russian Society of Radiologists and Radiologists
T2-WI — T2-weighted image (image acquisition mode in magnetic resonance imaging)
CRM — Circumferential resection margin
AJCC-TNM8 — National Validation of the 8th American Joint Committee on Cancer Staging System
TNM — International classification of stages of malignant neoplasms (tumor, nodus, and metastasis)
TRG — Tumor regression grading

INTRODUCTION

Uniform terminology in describing radiological examinations and formulating conclusions for patients with rectal cancer is crucial for ensuring adequate understanding among the treating physician and all members of the multidisciplinary medical team. Currently, magnetic resonance imaging (MRI) plays a crucial role in staging, supplemented by transrectal ultrasound in the early stages of rectal cancer. Staging involves assessing various anatomical and pathological factors that influence rectal cancer treatment planning. It is essential for all specialists to be aware of relevant terms and their clear interpretation for effective communication for the benefit of patients and comparison of rectal cancer treatment outcomes across different healthcare institutions.

CONSENSUS GUIDELINES ON TERMINOLOGY AND INTERPRETATION OF RECTAL CANCER IMAGING RESULTS

Procedure for a working group to create national recommendations on a unified terminology for rectal cancer diagnostics

To accomplish this goal, a working group (WG) comprising experts from the Russian Society of Radiologists and Radiologists (RORR) was established. The group represented 10 leading healthcare institutions in the Russian Federation providing specialized care to patients with rectal cancer. Additionally, experts from the Association of Oncologists of Russia (AOR) and the Russian Association of Therapeutic Radiation Oncologists (RATRO) were involved in developing the current clinical guidelines for rectal cancer. The group included 15 diagnostic radiology specialists, 3 surgical oncologists, and a radiology oncologist.

Three WG members, who are authors of this paper (BTP, MAV, and GPJ) searched the PubMed, Medline, and eLibrary databases for literature about staging, prevalence assessment, treatment planning in rectal cancer, and evaluation of effectiveness of neoadjuvant therapy from 2007 to 2023, with extraction of the main terms and their interpretations. The list of terms was sent to all WG members for review, followed by two online discussions until an expert consensus (≥80%) was reached regarding the interpretation of each term. Terms that did not reach a consensus opinion (low-grade rectal cancer, early rectal cancer, and tumor regrowth) were excluded from this paper. The final version of the manuscript was sent to all WG members and received their approval.

A consensus list of recommended terms of staging, extent assessment, and treatment planning in rectal cancer and their definitions for use in medical diagnostic reports (primarily for MRI) is given below.

List of terms and their definitions agreed by expert consensus

Terms to assess prevalence and location of rectal cancer

Rectal cancer is a malignant tumor that develops from rectal epithelial cells, typically exhibiting adenocarcinoma structure and localized within 15 cm from the anus (ICD-10 code: C20) [1]. Tumors with a lower pole located above this level are classified as malignant neoplasms of the rectosigmoid junction (ICD-10 code: C19). Tumors with the histological structure of squamous cell carcinoma, localized in the anal canal, are classified as malignant neoplasms of the anus and anal canal (ICD-10 code: C21). Squamous cell carcinoma of the anal canal can spread above the anorectal junction and involve the rectal ampulla, while rectal cancer with the structure of adenocarcinoma can spread into the anal canal or have a predominant localization there. In such cases, the histological type of malignant neoplasms determines not only the approach to TNM classification (rectal cancer/anal cancer) but also the choice of treatment method.

Some anatomical structures of the pelvis, rectum, and anal canal play an important role in the primary staging of rectal cancer. Awareness of these structures and the ability to recognize them on images is critical for accurate characterization of the primary tumor [2–5].

Surgical anal canal: For transrectal ultrasound and MRI, the lower border of the anal canal is considered to be the distal edge of the internal sphincter. For transrectal ultrasound, the upper border of the internal sphincter is considered to be the upper border. For MRI, the anorectal junction is considered.

The anal margin refers to the anocutaneous line, the junction of the anoderm with the perianal skin, corresponding to the distal edge of the internal sphincter of the anal canal/ intersphincteric groove on sagittal MRI (Fig. 1). From this level, the distance to the lower edge of the tumor is measured on sagittal T2-weighted images along the center of the lumen of the anal canal and rectum [6].

The anorectal junction is the connection between the anal canal and the rectum, corresponding to the upper edge of the puborectalis muscle, clearly defined on T2-WI in the coronal plane, or the anorectal angle, defined on T2-WI in the sagittal plane (Fig. 1). The distance from the anorectal junction to the inferior margin of the tumor is important for surgery planning and should be indicated in the diagnostic report [6].

The dentate line is the upper limit of the anatomical anal canal, which is shorter than the surgical one. The location of the dentate line approximately corresponds to the middle of the internal sphincter. It is not visualized by MRI.

The anal sphincter complex includes the internal and external anal sphincters and the puborectalis muscle (Fig. 1).

The internal anal sphincter is a continuation of the internal circular muscle layer of the rectum, comprising smooth muscle tissue. On MRI, it is determined by a significant thickening of the intrinsic muscle layer of the wall at the level of the anal canal (Fig. 1). The signal from the internal sphincter on T2-weighted images is slightly higher than that of the external sphincter, and with contrast enhancement, it appears more intense.

The external anal sphincter is a striated muscle, which is a continuation of the puborectal muscle, divided into three layers, such as the subcutaneous circular layer, superficial ellipsoidal layer, connected to the coccyx, and deep layer, closely connected with the puborectalis muscle (Fig. 1).

The intersphincteric space is a connective-cellular tissue space that separates internal and external anal sphincters and is characterized by a high signal on T2-WI (Fig. 1).

Mesorectal fascia is a thin fascial sheath that limits the rectum and the surrounding fatty tissue. On T2-WI, it appears as a hypointense circular line (Fig. 1). In men, the mesorectal fascia in front merges with the Denonvilliers' fascia, while in women, it merges with the rectovaginal fascia (septum). At the back, it connects with the presacral fascia; it completely surrounds the rectum only to the level of the transitional fold of the peritoneum with its lateral and posterior parts above and only the posterior rectum at the level of the upper ampullary. Caudally, the mesorectal fascia passes into the intersphincteric space.

The muscular layer of the rectum consists of an inner circular and outer longitudinal layer, which are defined as a single hypointense layer on T2-weighted MRI images, limited internally by a hyperintense submucosal layer and externally by hyperintense mesorectal tissue (Fig. 1).

The elevator muscle of the anus (m. levator ani) is a muscle complex (Fig. 1), consisting of the puborectalis, pubococcygeus, iliococcygeus, and anal-coccygeal fibrous muscles and anococcygeal ligament. Tumors infiltrating the elevator muscle of anus are classified as T4b.

The transitional fold of peritoneum is formed at the point of transition of the peritoneum from the pelvic organs to the rectal wall, with the lower point of attachment along the anterior wall of the intestine and obliquely going up the side walls. It separates the peritonized and non-peritonized parts of the rectum. On T2-WI, it appears as a hypointense line, displaying a V-shape in the axial plane, and passes from

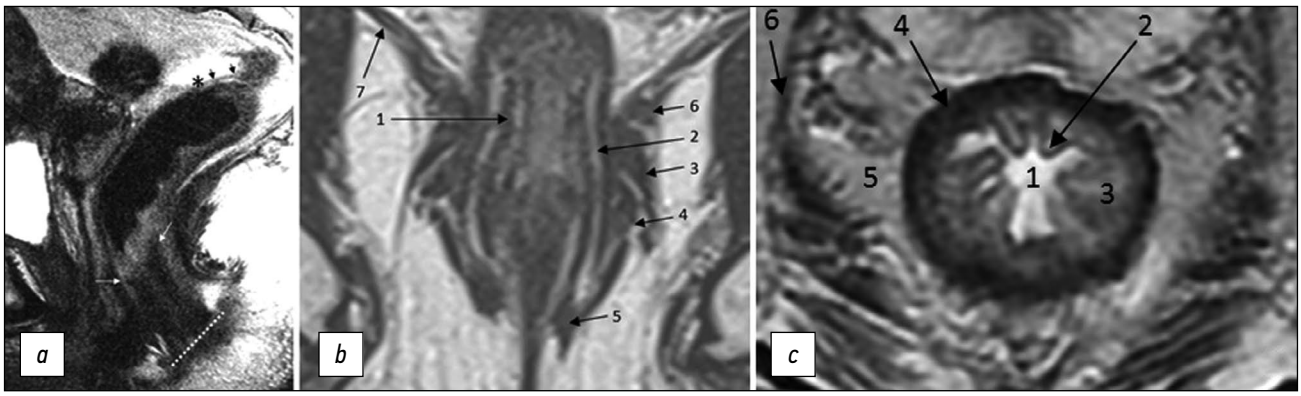

Fig. 1. MRI anatomy of the rectum on T2-WI. (*a*) Sagittal plane: anal edge (intersphincteric groove; dotted line); anorectal junction (angle) at the level of the upper border of the internal sphincter of the anal canal (white arrows); transitional fold of the peritoneum at the lower point of attachment of the pelvic visceral peritoneum to the rectal wall (asterisk); peritonealized part of the rectum (black arrows). (*b*) Coronal plane: 1, internal sphincter of the anal canal; 2, intersphincteric space; 3, deep portion of the external sphincter; 4, superficial portion of the external sphincter; 5, subcutaneous portion of the external sphincter; 6, puborectalis muscle; 7, elevator muscle of anus (levator ani). (*c*) Axial plane: 1, intestinal lumen; 2, mucous membrane; 3, submucosal layer; 4, muscle layer; 5, mesorectal tissue; 6, mesorectal fascia.

the apex of the seminal vesicles (in men) or from the body of the uterus (in women) in the sagittal plane (Fig. 1). Lymphatic drainage from tumors located above the transitional fold of the peritoneum mainly occurs through the upper rectal and lower mesenteric lymph nodes. Tumors below the transitional fold of the peritoneum can drain through the internal iliac and obturator lymph nodes. When describing MRI findings, it is recommended to indicate the position of the tumor relative to the transitional fold of the peritoneum (completely below/crosses/completely above) [6].

The presacral space is a fibrous space delimited in front by the presacral fascia (the posterior part of the parietal layer of the fascia of the pelvis). It contains presacral veins and plexuses.

The rectal mucosa is the innermost, thin layer of the rectal wall. When visualized, it has a hypointense signal on T2-weighted images due to the lamina propria (Fig. 1).

Terms related to primary staging of rectal cancer

For primary staging of rectal cancer, MRI is the preferred diagnostic method. For the initial stages of rectal cancer, transrectal ultrasound is recommended [1, 3, 7–9]. Currently, staging is carried out according to the TNM classification of the Union for International Cancer Control (UICC; 8th ed., 2017) [10].

Below are some terms that, along with the "T" category, are important for characterizing the primary tumor [2, 4, 5].

The depth of extramural invasion is the maximum distance from the outer edge of the muscular layer of the wall at the base of the extramural component of the primary tumor to its outer edge, as observed on high-resolution T2-WI oriented perpendicular to the intestinal wall at the level of the tumor (Fig. 2). The depth of extramural invasion is used to determine the substage of T3 tumors.

Category T according to the TNM system. Category T, established based on the examinations of a primary patient with rectal cancer, is called clinical and is denoted by the prefix "c" (cT). If radiological examination methods were used for staging, then the prefix "i" (iT) is used.

T1: Tumor has grown into the submucosa. Subclassification of T1 tumors according to Kikuchi [11]: T1sm1: depth of submucosa invasion up to 1/3; T1sm2: depth of submucosa invasion er up to 2/3; T1sm3: complete tumor invasion of the entire submucosal layer. Transrectal ultrasound is preferred to evaluate T1 tumors.

T2: Tumor has grown into the muscle layer. Transrectal ultrasound is reported to be more accurate in diagnosing T1/T2 tumors (sensitivity 94%, specificity 86%) compared with MRI (sensitivity 94%, specificity 70%) but less accurate in determining lymph node status [12].

T3: Tumor has grown through the muscularis propria and into the subserosa or non-peritoneal peri-intestinal tissue (T3 tumors are divided into the following substages: T3a <1mm; T3b 1–5mm; T3c 5–15mm; T4d >15mm). To assess extramural tumor growth, it is recommended to use high-resolution T2-WI perpendicular to the bowel wall at the level of the tumor.

T4: Tumor invades the serosa/peritoneum of the pelvis (T4a) or surrounding organs and tissues (T4b), including pelvic organs (uterus, ovaries, vagina, prostate, seminal vesicles, bladder, ureters, urethra, and bones), skeletal muscles (obturator, piriformis, elevator muscle of anus,

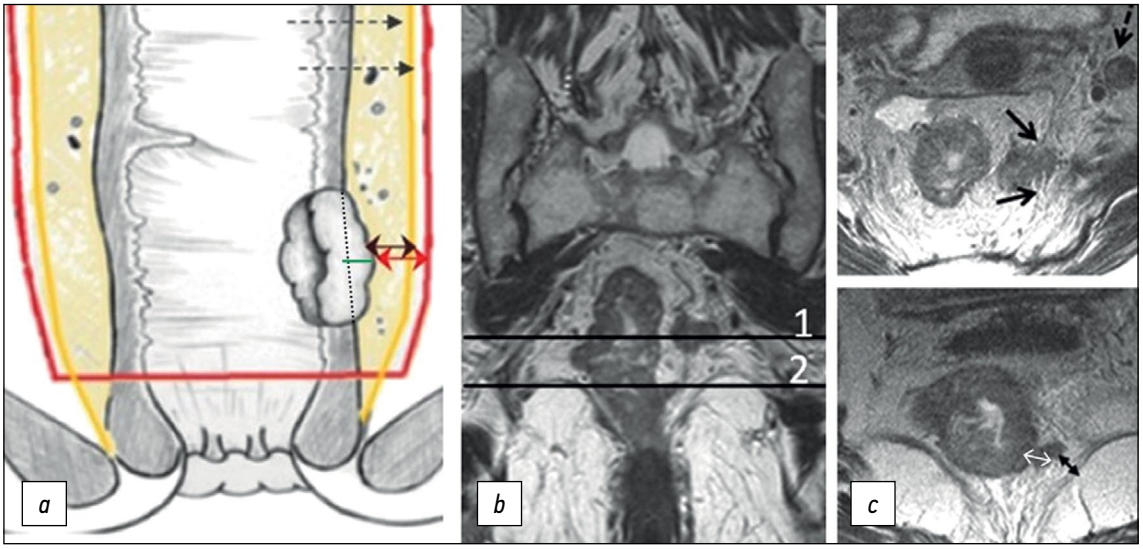

Fig. 2. Circular border (edge) of rectal resection during total mesorectumectomy. (*a*) Diagram showing extramural growth of the tumor (green line); mesorectal fascia (yellow line); circular border (edge) of resection (red line); distance from the tumor to the mesorectal fascia (double black arrow); distance from the tumor to the circular border (edge) of resection (double red arrow). (*b*) T2-weighted images in the coronal plane of the tumor of the lower ampullary part of the rectum with extramural vascular invasion and deposit at the level of axial T2-weighted images. (*c*) Upper axial section corresponds to the level of the deposit involving the mesorectal fascia (black arrows), extramesorectal lymph node (dotted arrow). The lower axial section corresponds to the level of extramural vascular invasion. The depth of extramural invasion (a double white arrow). The distance from the tumor to the elevator muscle of anus (a double black arrow).

ischiococcygeus, puborectalis, and external anal sphincter), sciatic or sacral nerves, sacrospinous/sacrotuberous ligaments, any extramesorectal vessel, any loop of colon or small intestine outside the primary lesion, and extramesorectal fiber [13].

Staging of rectal cancer extending into the anal canal requires detailed assessment of the anal canal and sphincter complex using high-resolution T2-WI in the coronal plane parallel to the anal canal. The "cT" category is recommended to be determined primarily based on the extent of the tumor at the rectal level. Involvement of the external sphincter, puborectalis, and elevator muscle of anus should be classified as cT4b. Extension into the anal canal should be described separately, detailing the affected structures (internal sphincter, intersphincteric space, and/or pelvic floor). The report should additionally indicate whether the is positive (+) or negative (–) [13]. For tumors that have grown into the anal canal below the dentate line, the inguinal lymph nodes may be considered regional (as defined in AJCC-TNM8).

Locally advanced rectal cancer is a primary tumor that has grown beyond the muscular layer (T3/T4) and/or affects regional lymph nodes (N1/2) but has no signs of distant metastases (M0).

Circumferential resection margin (CRM) is a surgery and pathology term defined as the surface of surgical excision of the non-peritoneal part of the rectum, which should pass along the mesorectal fascia when performing a total mesorectumectomy.

The status of CRM is determined by histological examination of the surgically removed rectum specimens. It can be predicted based on MRI by the shortest distance between the extramural component of the tumor/deposit/affected lymph node and the mesorectal fascia. Involvement of the CRM is indicated as CRM(+) if this distance is ⩽1 mm. For low-lying rectal cancer, the shortest distance is determined to the elevator muscle of anus. The distance from enlarged lymph nodes without signs of extracapsular spread (with smooth contours) is not considered and should be regarded as CRM(–) [13].

Extramural vascular/venous invasion in histological examination represents intravascular growth of the tumor beyond the rectal wall, serving as a predictor of poor prognosis, lymphatic and distant metastases, and tumor recurrence [14–17]. On T2-WI, extramural vascular/venous invasion is characterized by the spread of a tumor signal into the vascular structures of the mesorectal tissue [6, 18, 19], which can be combined with the increased diameter of the affected vessel or with the tumor extending beyond its walls with the formation of a node, beaded, or worm-like structure. It is important to note that the MRI assessment of extramural venous invasion in vessels less than 3 mm in diameter is unreliable. When determining the category "T" (T3 and T4 tumors) in cases of fusion of the primary tumor and an extramural venous invasion lesion, their total size should be considered.

Tumor adhesion is considered in imaging when it is challenging to clearly trace the fatty tissue between the tumor and the neighboring organ. In this situation, there is no MR signal from the tumor tissue within the structure of the adjacent neighboring organ. This option is recommended to be regarded as "possible invasion" [20]. According to the AJCC-TNM8, it should be classified as "mrT4b," with subsequent clarification of the stage after surgery. If microscopic examination does not reveal tumor elements at the adhesion site, then such a case is classified as "pT1-3," depending on the depth of invasion.

Terms related to describing colorectal cancer

The description of a tumor does not affect staging, but it is important for characterizing the tumor. Here are terms used to describe tumors.

Desmoplastic reaction is a fibrous reaction of the tumor stroma that occurs at the border with normal tissue in the form of connective tissue spicules without tumor cells. It can be observed both in the primary tumor, making it difficult to differentiate T2 and T3a-b tumors on MRI and after neoadjuvant chemoradiotherapy.

Mucinous cancer is a prognostically unfavorable histological variant of rectal cancer with tumor content of extracellular mucin >50% of the tumor volume. On MRI, mucin accumulations have a hyperintense signal on T2-WI (Fig. 3).

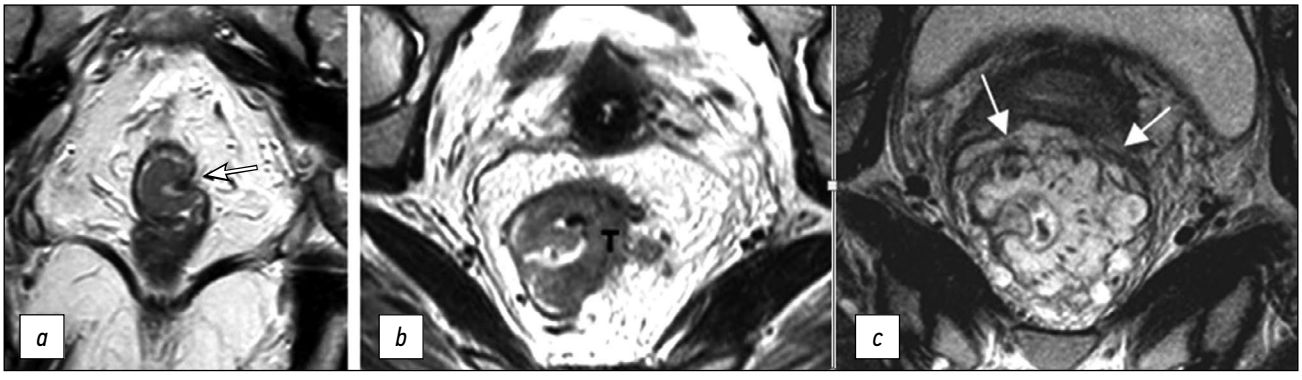

Fig. 3. Variants of tumor image on T2-WI. (*a*) Polypoid/exophytic tumor (arrow). (*b*) Semicircular tumor (T), extramural vascular invasion (arrows). (*c*) Mucinous tumor (arrows).

The tumor lesion is usually represented by ulceration/erosion in the center of the tumor, where the maximum depth of tumor invasion is determined.

Polypoid tumor is a tumor with an exophytic type of growth (Fig. 3). It may have a pedicle with clearly visible feeding vessels. The location of such a tumor can be indicated using a conventional dial (12 o'clock for the center of the anterior wall, 6 o'clock for the center of the posterior wall, 3 o'clock for the center of the left wall, and 9 o'clock for the center of the right wall).

A semicircular tumor occupies only part of the circumference of the rectum.

Circular/subcircular tumor spreads over the entire or almost entire circumference of the rectal lumen (Fig. 3).

Terms related to localization, staging, and criteria for lymph node involvement in rectal cancer

Lymph node assessment is an important aspect of rectal cancer staging, although it is less precise than for T category [21]. According to a meta-analysis [22], the sensitivity and specificity of MRI in the assessment of lymph node involvement are 73% (95% CI 68–77) and 74% (95% CI 68–80), respectively. Computed tomography and transrectal ultrasound demonstrate diagnostic effectiveness comparable with MRI [23].

Not all lymph nodes located in the pelvis are regional for rectal cancer and are classified as "N." When assessing pelvic lymph nodes as regional, it is important to consider their location (Fig. 4) and, if possible, indicate it in the examination report. Here are terms related to location, staging, and criteria for lymph node involvement.

Category "N" according to the TNM system: N0: absence of abnormal locoregional lymph nodes; N1: 1 to 3 abnormal regional lymph nodes (N1a: 1 lymph node; N1b: 2-3 lymph nodes; N1c: tumor deposit); N2: >3 abnormal regional lymph nodes (N2a: 4 to 6 lymph nodes; N2b: ≥7 lymph nodes). When describing, it is acceptable to use "N(+)" in the presence of abnormal regional lymph nodes, regardless of their number, and "N(–)" in the absence of abnormal regional lymph nodes.

Regional lymph nodes (N). According to the latest AJCC-TNM8, regional lymph nodes include mesorectal/pararectal, superior rectal, inferior mesenteric, and internal iliac lymph nodes, without specific mention of the obturator lymph nodes. However, the obturator lymph nodes are usually classified as regional lymph nodes [21]. All other pelvic lymph nodes, including inguinal, external iliac, common iliac, and para-aortic lymph nodes, are not regional in rectal cancer and should be regarded as distant metastases (M).

Mesorectal lymph nodes are located in the mesorectum and are regional ones.

The lower mesenteric and upper rectal lymph nodes are classified as regional and are removed during a total mesorectumectomy. It is recommended to mark the most suspicious upper lymph node of these chains, as it may change the site of vessel ligation during total mesorectumectomy.

Morphological criteria for involvement of mesorectal, superior rectal, and inferior mesenteric lymph nodes include (a) uneven boarders, (b) heterogeneous structure, and (c) rounded shape. Suspicious lymph nodes are (a) <5 mm in size if three morphological criteria are met; (b) 5 to 9 mm in size if two criteria are met; and (c) >9 mm in all cases. After neoadjuvant chemoradiotherapy, all lymph nodes larger than 5 mm should be considered suspicious [8].

A deposit is defined in pathology as a single tumor nodule in the mesorectal tissue without evidence of identifiable lymph node tissue or vascular/nervous structures. It is designated as "N1c," regardless of the number of deposits. The number of tumor deposits is not added to the number of positive lymph nodes [24]. To date, there is insufficient evidence regarding MRI's ability to reliably differentiate between lymph nodes and tumor deposits [13]. Deposits may form due to intermittent tumor spread, lymphatic spread, venous or perineural invasion, or complete lymph node replacement [25]. On MRI, distinguishing between positive lymph nodes with extracapsular extension, extranodal tumor deposits, and intermittent extramural vascular invasion is challenging. Available evidence suggests that all these conditions have a worse prognosis than lymph node involvement [26]. Tumor deposits in the mesorectum or along the large rectal vessels, combined with signs of extramural vascular/venous invasion, are regarded as "N1c," EMVI(+). Deposits without signs of extramural vascular/venous invasion are regarded as "N1c," EMVI(–).

The lateral pelvic lymph nodes, situated at the side pelvic walls, are lymph nodes external to the mesorectal fascia, including the external, internal iliac, and obturator lymph nodes. When describing them, it is better, whenever possible, to indicate a more specific location. During primary staging, it is recommended to consider regional lateral pelvic lymph nodes (internal iliac and obturator) with a short axis (≥7 mm) as suspicious [12, 27]. Morphological criteria for lateral pelvic lymph nodes are not recommended [13].

The internal iliac lymph nodes are regional and, in the case of rectal cancer, are included in the scope of dissection of the lateral pelvic lymph nodes. They are located along the internal iliac vessels. At the level of the obturator muscle, they are localized medially to the internal iliac artery; lymph nodes lateral to the internal iliac artery are considered obturator lymph nodes (Fig. 4).

The obturator lymph nodes are regional. They are located between the external and internal iliac arteries, medially to the internal obturator muscle and laterally to the internal iliac artery (Fig. 4).

The external iliac lymph nodes are not regional. They are located along the external iliac vessels (Fig. 4) and are divided into lateral, middle/median, and medial chains. The lateral subgroup is located laterally to the external iliac artery. The middle/median group is between the artery and the vein. The medial group is posterior to the external iliac vein. The lymph nodes in the medial subgroup are located

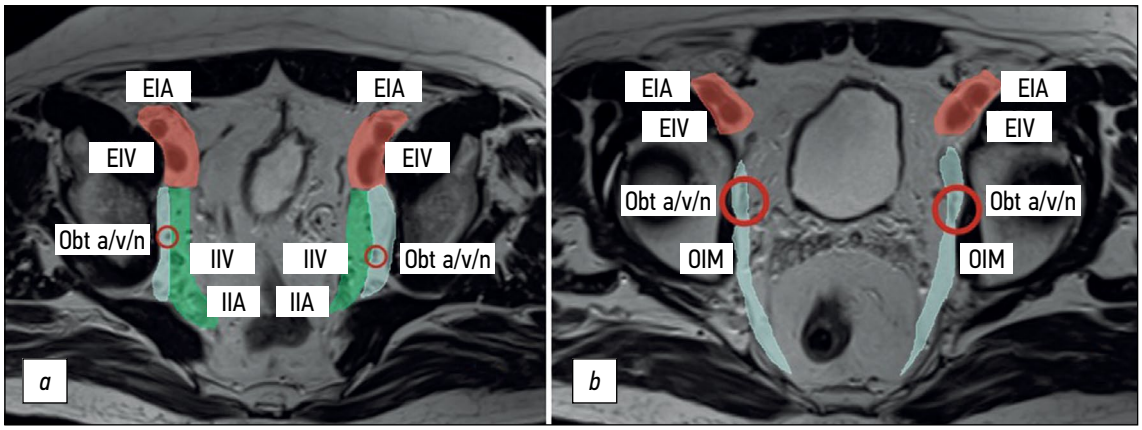

Fig. 4. Localization of the lateral pelvic lymph nodes (colored): external iliac lymph nodes are red; obturator lymph nodes are blue; and internal iliac lymph nodes are green. Shown in levels (*a*) proximal and (*b*) distal. EIA: external iliac artery; EIV: external iliac vein; IIV: internal iliac vein; IIA: internal iliac artery; Obt a/v/n: obturator artery/vein/nerve; OIM: obturator internus muscle.

near the obturator vessels and obturator lymph nodes. This can cause diagnostic difficulties because they are often indistinguishable from the obturator lymph nodes localized along the obturator artery at the point of its origin from the internal iliac (hypogastric) artery at the level of the internal obturator muscles [3]. Involvement of the external iliac lymph nodes in rectal cancer is extremely rare. Non-regional lymph nodes are considered suspicious if they measure >10 mm in short axis.

Inguinal lymph nodes are not regional in rectal cancer, but are regional in squamous cell carcinoma of the anal canal. They are located in the groin area below the inguinal ligament. They can be classified as regional for tumors extending below the dentate line [13]. They are divided into superficial (anterior to the saphenous vein and superficial femoral vessels) and deep (medial to the femoral vessels).

Terms to describe response to neoadjuvant chemoradiation therapy

Currently, a combination neoadjuvant chemoradiation therapy is widely used to treat patients with rectal cancer, significantly affecting the planning of further treatment. MRI is currently considered the optimal imaging modality for assessing effectiveness of neoadjuvant chemoradiation therapy. Here are terms recommended to describe response to neoadjuvant chemoradiation therapy.

Pathologic complete response (pCR) is a response to neoadjuvant chemoradiation therapy, characterized by the complete absence of viable tumor cells during pathological examination of the surgical specimen.

Clinical complete response (cCR) is a response to neoadjuvant chemoradiotherapy, characterized by the absence of a clinically detectable tumor during digital rectal examination, MRI, and endoscopy. It is used as a surrogate for pCR. On MRI, it represents either subtle fibrosis of the rectal wall in the tumor bed without residual areas of tumor signal or recovery of a normal rectal wall without any evidence of tumor [28].

Near-complete response was introduced because some patients, initially showing a good but incomplete response during the follow-up examination, may be re-evaluated after a longer interval after neoadjuvant chemoradiation therapy and may achieve a cCR.

Downstaging is a term describing downstaging of the T or N category after neoadjuvant chemoradiation therapy. The post-treatment category is indicated by the prefix "y," for example, yT0 means no visible primary tumor.

Downsizing refers to the decrease in size of a tumor or its regional metastases after neoadjuvant therapy without changing T or N categories.

Tumor regression grading (TRG) is a system for assessing the response to neoadjuvant chemoradiotherapy, derived from a modification of the Mandard pathological staging (MRI TRG). It involves a qualitative assessment of the ratio of a low MR signal from fibrous tissue and a medium-intensity signal from a residual tumor on T2-WI.

- **mrTRG1 (complete response)** means no macroscopic signs of residual tumor tissue/a minimal area of fibrosis is visualized (thin scar).
- **mrTRG2 (significant/almost complete response)** means the presence of dense fibrous scar, with no signs of tumor tissue visualized (according to pathological data, tumor cells are absent/single in settings of dense fibrosis).
- **mrTRG3 (moderate response)** means fibrosis predominates (>50%), while an MR signal of medium intensity is visualized, which is characteristic for tumor tissue.
- **mrTRG4 (minimal response)** means the MR signal from the tumor tissue predominates, combined with a small/minimal structural fibrosis.
- **mrTRG5 (no response/progression)** means only an MR signal of medium intensity, characteristic of tumor tissue, without signs of fibrosis (Fig. 5).

Current clinical experience shows that this system has poor correlation with pathological TRG, limited positive predictive value of pCR and poor reproducibility with low

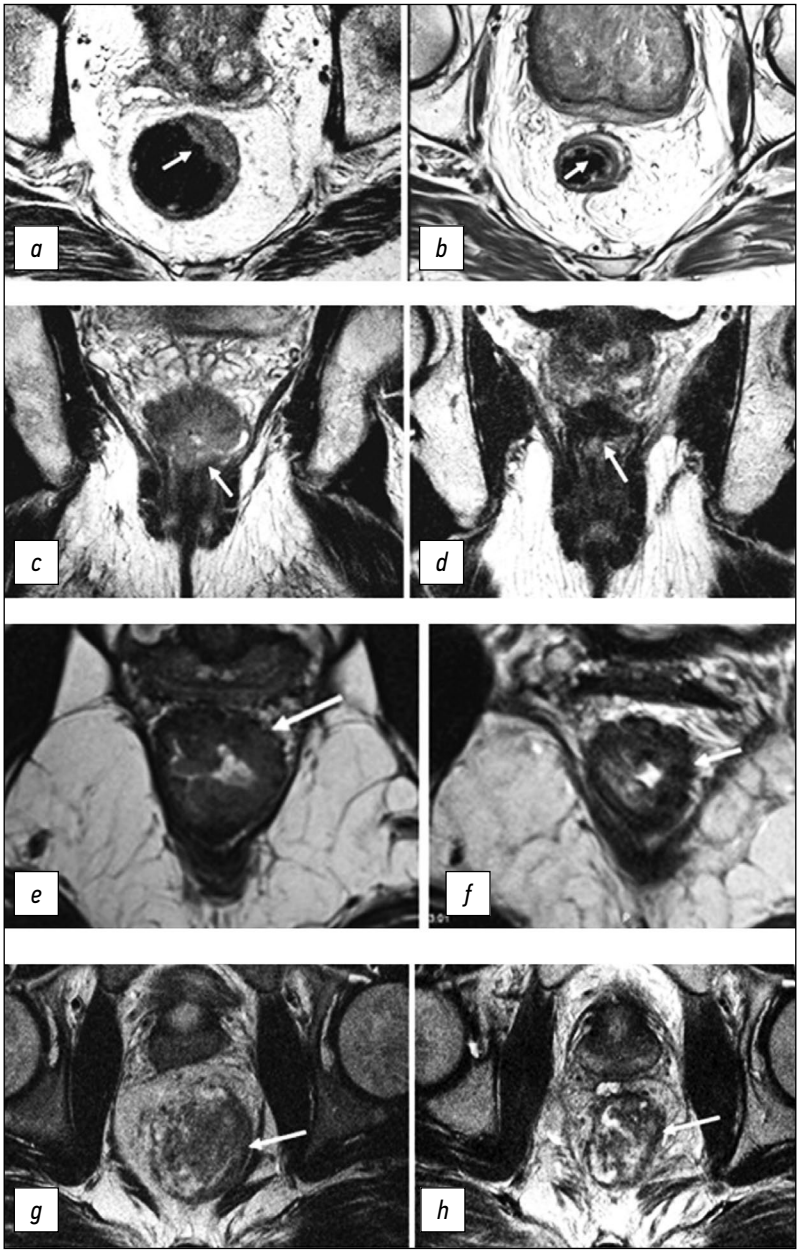

Fig. 5. Assessment of tumor regression on high-resolution T2-WI using TRG. TRG1: (*a*) Tumor located at the 12–2 o'clock position before neoadjuvant chemoradiation therapy (arrow); (*b*) after treatment, the tumor is replaced by a linear area of submucosal fibrosis. TRG2: (*c*) Tumor in the lower ampullary rectum before chemoradiation therapy (arrow); (*d*) after treatment, the tumor is determined as an area of thick fibrosis (arrow), without macroscopic MR signs of tumor. TRG3: (*e*) Semicircular tumor in the lower ampullary rectum before chemoradiation therapy (arrow); (*f*) after treatment, the tumor has a mixed MR signal with a predominance of a low-intensity signal, characteristic of fibrosis, and preservation of macroscopic areas of a tumor MR signal of medium intensity (arrow). TRG4: (*g*) Tumor before chemoradiation therapy (arrow); (*h*) after treatment (arrow), there are no signs of response to treatment; the MR signal of the tumor tissue persists.

kappa values [29, 30]. Therefore, further research is required to find ways of improving its diagnostic efficiency.

The scar in the irradiated tumor bed is characterized by a hypointense T2-WI signal without signs of diffusion limitation on diffusion-weighted images.

Submucosal edema is identified after neoadjuvant chemoradiation therapy as an area of high signal intensity on T2-WI in the rectal wall adjacent to the treated tumor and should not be misinterpreted as a tumor.

Mucinous/colloid degeneration (mucinous response) is characterized by high T2-WI signal of acellular mucin accumulations that lack viable tumor cells. It may be observed in non-mucinous tumors after neoadjuvant chemoradiation therapy. In the case of a mucinous tumor, remaining post-treatment mucin may also not contain tumor cells. However, it is difficult to distinguish between acellular and cellular mucin using MRI.

Terms to describe treatment options for colorectal cancer

Surgery is the main treatment option for rectal cancer. In the case of locally advanced tumor, it is used after

neoadjuvant treatment. Here are terms used to describe treatment options for colorectal cancer.

A total mesorectumectomy involves excision of the rectum along the mesorectal fascia en bloc with mesorectal fat, vessels, and lymph nodes. It is considered to be the gold standard for radical treatment of colorectal cancer [31].

Partial mesorectumectomy involves partial removal of mesorectal tissue, followed by its intersection and preservation of part of the mesorectal tissue of the anastomosed area of the rectum.

Anterior resection/low anterior resection is the most common type of surgery in rectal cancer, accompanied by a total or partial mesorectumectomy and formation of a colorectal anastomosis.

Intersphincteric resection is a sphincter-sparing operation for low-grade rectal cancer, with only part of the internal anal sphincter removed and with the external anal sphincter preserved. This is followed by a coloanal anastomosis. It can be used in some cases when the intersphincteric space is not infiltrated by a tumor.

Abdominoperineal excision involves resection of the entire sphincter complex with formation of a permanent colostomy.

Abdominal-anal resection of the rectum is a treatment method involving a total mesorectumectomy but with formation of a coloanal anastomosis.

Extralevator abdominoperineal excision is a variant of the standard abdominoperineal excision with a wider excision of the sphincter complex and the elevator muscle of anus.

Pelvic exenteration involves radical resection en bloc of all pelvic organs affected by the tumor, often followed by visceral reconstruction, including restoration of the passage for intestinal contents and using one of the urine diversion methods [32]. The 5-year overall survival rate after pelvic exenteration for primary locally advanced rectal cancer is 30–55%; for recurrent tumors, it usually does not exceed 20–25% [33].

Transanal excision is local excision of the tumor through its entire thickness to the mesorectal tissue. Lymph nodes are not removed.

Transanal endoscopic microsurgery is excision of the tumor to the full thickness of the mesorectal tissue using video endoscopic technologies. This technique provides a higher visibility of the rectal wall and higher possibility of its full-thickness excision with subsequent suturing of the defect.

R0/R1/R2 surgeries are categorized in accordance with the accepted criteria for the radicality of operations. R0 is radical removal of the tumor without microscopic and macroscopic residual tumor. R1 is marginal resection, microscopic residual tumor. R2 is incomplete tumor removal, macroscopic residual tumor. Residual tumor should be determined after a subjective assessment by a surgeon and an objective morphological examination.

Preoperative radiation therapy is conducted as a prolonged course (5–6 weeks) in combination with radiosensitizing chemotherapy or as a short, concentrated course (1 week) without concomitant chemotherapy.

Neoadjuvant chemoradiation therapy is a combination of chemotherapy and radiation therapy, which is conducted before surgery. Chemotherapy here is considered radiosensitizing and not "systemic" (for the treatment of distant metastases).

Neoadjuvant chemotherapy is a type of chemotherapy administered immediately before surgical removal of the primary tumor to improve outcomes of surgery/radiation therapy and prevent metastases.

CONCLUSION

Based on expert consensus, a vocabulary has been prepared to provide diagnostic radiology specialists with terms for describing and interpreting results of rectal cancer imaging.

ADDITIONAL INFORMATION

Funding source. This article was not supported by any external sources of funding.

Competing interests. The authors declare that they have no competing interests.

Authors' contribution. All authors made a substantial contribution to the conception of the work, acquisition, analysis, interpretation of data for the work, drafting and revising the work, final approval of the version to be published and agree to be accountable for all aspects of the work

REFERENCES

1. Rectal cancer. Clinical recommendations. Approved at the meeting of the Scientific and Practical Council of the Ministry of Health of the Russian Federation. Moscow; 2022.(In Russ). Available from: https://cr.minzdrav.gov.ru/recomend/554_3. Accessed: 15.08.2023.

2. Bogveradze N, Snaebjornsson P, Grotenhuis BA, et al. MRI anatomy of the rectum: Key concepts important for rectal cancer staging and treatment planning. *Insights Imaging.* 2023;14(1):13. doi: 10.1186/s13244-022-01348-8

3. Gollub MJ, Arya S, Beets-Tan RG, et al. Use of magnetic resonance imaging in rectal cancer patients: Society of Abdominal Radiology (SAR) rectal cancer disease-focused panel (DFP) recommendations 2017. *Abdom Radiol.* 2018;43(11):2893–2902. doi: 10.1007/s00261-018-1642-9

4. Nougaret S, Rousset P, Gormly K, et al. Structured and shared MRI staging lexicon and report of rectal cancer: A consensus proposal by the French Radiology Group (GRERCAR) and Surgical Group (GRECCAR) for rectal cancer. *Diagn Interv Imaging.* 2022;103(3):127–141. doi: 10.1016/j.diii.2021.08.003

5. Grishko PY, Balyasnikova SS, Samsonov DV, et al. A modern view on the principles of diagnosis and treatment of rectal cancer according to MRI data (literature review). *Medical Visualization.* 2019;23(2):7–26.(In Russ). doi: 10.24835/1607-0763-2019-2-7-26
6. Fernandes MC, Gollub MJ, Brown G. The importance of MRI for rectal cancer evaluation. *Surg Oncol*. 2022;(43):101739. doi: 10.1016/j.suronc.2022.101739
7. Glynne-Jones R, Wyrwicz L, Tiret E, et al. Rectal cancer: ESMO clinical practice guidelines for diagnosis, treatment and follow-up. *Ann Oncol*. 2017;28(Suppl 4):22–40. doi: 10.1093/anonc/mdx22 4
8. Beets-Tan R, Lambregts D, Maas M, et al. Magnetic resonance imaging for clinical management of rectal cancer: Updated recommendations from the 2016 European Society of Gastrointestinal and Abdominal Radiology (ESGAR) consensus meeting. *Eur Radiol*. 2018;28(4):1465–1475. doi: 10.1007/s0033 0-017-5026-2
9. Oien K, Forsmo HM, Rösler C, et al. Endorectal ultrasound and magnetic resonance imaging for staging of early rectal cancers: How well does it work in practice? *Acta Oncol*. 2019;58(Sup1):49–54. doi: 10.1080/0284186X.2019.1569259
10. Brierley JD, Gospodarowicz MK, Wittekind C. TNM Classification of Malignant Tumours. 8th ed. Wiley-Blackwell; 2017. 272 p.
11. Kikuchi R, Takano M, Takagi K, et al. Management of early invasive colorectal cancer. Risk of recurrence and clinical guidelines. *Dis Colon Rectum*. 1995;38(12):1286–1295. doi: 10.1007/BF02049154
12. Boot J, Gomez-Munoz F, Beets-Tan R. Imaging of rectal cancer. *Radiologe*. 2019;59(Suppl 1):46–50. doi: 10.1007/s00117-019-0579-5
13. Lambregts D, Bogveradze N, Blomqvist L, et al. Current controversies in TNM for the radiological staging of rectal cancer and how to deal with them: Results of a global online survey and multidisciplinary expert consensus. *Eur Radiol*. 2022;32(7):4991–5003. doi: 10.1007/s00330-022-08591-z
14. Mainovskaya OA, Rybakov EG, Chernyshov SV, et al. New morphological risk factors for metastasis to regional lymph nodes in rectal cancer with invasion of the submucosal base. *Coloproctology*. 2021;20(4):22–33. (In Russ). doi: 10.33878/2073-7556-2021-20-4-22-33
15. Volkova SN, Stashuk GA, Chermensky GV, Naumov EK. The role of MRI in the detection of extramural vascular invasion as an indicator of the presence of regional and distant metastases of cancer of the lower ampullary rectum. *Experimental Clin Gastroenterol*. 2019;164(4):66–71. (In Russ). doi: 10.31146/1682-8658-ecg-164-4-66-71
16. Lord AC, D'Souza N, Shaw A, et al. MRI-diagnosed tumor deposits and EMVI status have superior prognostic accuracy to current clinical TNM staging in rectal cancer. *Ann Surg*. 2022;276(2):334–344. doi: 10.1097/SLA.0000000000004499
17. Rokan Z, Simillis C, Kontovounisios C, et al. Locally recurrent rectal cancer according to a standardized MRI classification system: A systematic review of the literature. *J Clin Med*. 2022;11(12):3511. doi: 10.3390/jcm11123511
18. Grishko PY, Mishchenko AV, Ivko OV, et al. The possibilities of multiparametric magnetic resonance imaging in assessing the effectiveness of neoadjuvant treatment of rectal cancer. *Radiation Diagnostics Therapy*. 2019;10(4):49–56.(In Russ).
19. Inoue A, Sheedy SP, Heiken JP, et al. MRI-detected extramural venous invasion of rectal cancer: Multimodality performance and implications at baseline imaging and after neoadjuvant therapy. *Insights Imaging*. 2021;(2):110. doi: 10.1186/s13244-021-01023-4
20. Al-Sukhni E, Milot L, Fruitman M, et al. Diagnostic Accuracy of MRI for assessment of t category, lymph node metastases, and circumferential resection margin involvement in patients with rectal cancer: A systematic review and meta-analysis. *Ann Sur Oncol*. 2012;19(7):2212–2222. doi: 10.1245/s10434-011-2210-5
21. Borgheresi A, De Muzio F, Agostini A, et al. Lymph nodes evaluation in rectal cancer: Where do we stand and future perspective. *J Clin Med*. 2022;11(9):2599. doi: 10.3390/jcm11092599
22. Zhuang Z, Zhang Y, Wei M, et al. Magnetic resonance imaging evaluation of the accuracy of various lymph node staging criteria in rectal cancer: A systematic review and meta-analysis. *Front Oncol*. 2021;(11):709070. doi: 10.3389/fonc.2021.709070
23. Li X, Sun Y, Tang L, et al. Evaluating local lymph node metastasis with magnetic resonance imaging, endoluminal ultrasound and computed tomography in rectal cancer: A meta-analysis. *Color Dis*. 2015;17(6):129–135. doi: 10.1111/codi.12909
24. Weiser MR. AJCC 8th ed. Colorectal cancer. *Ann Surg Oncol*. 2018;25(6):1454–1455. doi: 10.1245/s10434-018-6462-1
25. Ueno H, Nagtegaal ID, Quirke P, et al. Tumor deposits in colorectal cancer: Refining their definition in the TNM system. *A G Surg*. 2023;7(2):225–235. doi: 10.1002/ags3.12652
26. Santiago I, Figueiredo N, Parés O, et al. MRI of rectal cancer: Relevant anatomy and staging key points. *Insights Imaging*. 2020;11(1):100. doi: 10.1186/s13244-020-00890-7
27. Ogura A, Konishi T, Cunningham C, et al. Neoadjuvant (chemo) radiotherapy with total mesorectal excision only is not sufficient to prevent lateral local recurrence in enlarged nodes: Results of the multicenter lateral node study of patients with low cT3/4 rectal cancer. *J Clin Oncol*. 2019;37(1):33–43. doi: 10.1200/JCO.18.00032
28. Gollub MJ, Costello JR, Ernst RD, et al. A primer on rectal MRI in patients on watch-and-wait treatment for rectal cancer. *Abdom Radiol*. 2023. doi: 10.1007/s00261-023-03900-6
29. Berezovskaya TP, Daineko YA, Nevolskikh AA, et al. Prospective evaluation of the use of the MRTG system in determining the effectiveness of neoadjuvant chemoradiotherapy in patients with rectal cancer. *Bulletin Radiol Radiol*. 2021;102(1):6–17. (In Russ). doi: 10.20862/0042-4676-2021-102-1-6-17
30. Almeida RR, Souza D, Matalon SA, et al. Rectal MRI after neoadjuvant chemoradiation therapy: A pictorial guide to interpretation. *Abdom Radiol*. 2021;46(7):3044–3057. doi: 10.1007/s00261-021-03007-w
31. Shelygin YA, Chernyshov SV, Kazieva LY, et al. Comparative analysis of open and transanal total mesorectumectomy in rectal cancer. *Coloproctology*. 2018;(4):67–73. (In Russ).
32. Maistrenko NA, Khvatov AA, Sazonov AA. Pelvic exenterations in the treatment of locally advanced tumors. *Bulletin Surnamed after Grekov*. 2014;173(6):37–43. (In Russ).
33. Sidorov DV, Alekseev BY, Grishin NA, et al. Variants of pelvic exenteration in locally advanced primary and recurrent rectal cancer. *Oncology J named after P.A. Herzen*. 2013;(6):7–13. (In Russ).

СПИСОК ЛИТЕРАТУРЫ

1. Рак прямой кишки. Клинические рекомендации. Одобрены на заседании научно-практического совета Министерства здравоохранения Российской Федерации. Москва, 2022. Режим доступа: https://cr.minzdrav.gov.ru/recomend/554_3. Дата обращения: 15.08.2023.

2. Bogveradze N., Snaebjornsson P., Grotenhuis B.A., et al. MRI anatomy of the rectum: Key concepts important for rectal cancer staging and treatment planning // Insights Imaging. 2023. Vol. 14, N 1.P. 13. doi: 10.1186/s13244-022-01348-8

3. Gollub M.J., Arya S., Beets-Tan R.G., et al. Use of magnetic resonance imaging in rectal cancer patients: Society of Abdominal Radiology (SAR) rectal cancer disease-focused panel (DFP) recommendations 2017 // AbdomRadiol. 2018. Vol. 43, N 11. P. 2893–2902. doi: 10.1007/s00261-018-1642-9

4. Nougaret S., Rousset P., Gormly K., et al. Structured and shared MRI staging lexicon and report of rectal cancer: A consensus proposal by the French Radiology Group (GRERCAR) and Surgical Group (GRECCAR) for rectal cancer // DiagnInterv Imaging. 2022. Vol. 103, N 3. P. 127–141. doi: 10.1016/j.diii.2021.08.003

5. Гришко П.Ю., Балясникова С.С., Самсонов Д.В., и др. Современный взгляд на принципы диагностики и лечения рака прямой кишки по данным МРТ (обзор литературы) // Медицинская визуализация. 2019. Т. 23, № 2. С. 7–26. doi: 10.24835/1607-0763-2019-2-7-26

6. Fernandes M.C., Gollub M.J., Brown G. The importance of MRI for rectal cancer evaluation // Surg Oncol. 2022. N 43. P. 101739. doi: 10.1016/j.suronc.2022.101739

7. Glynne-Jones R., Wyrwicz L., Tiret E., et al. Rectal cancer: ESMO clinical practice guidelines for diagnosis, treatment and follow-up // Ann Oncol. 2017. Vol. 28, Suppl. 4. P. 22–40. doi: 10.1093/anonc/mdx22 4

8. Beets-Tan R., Lambregts D., Maas M., et al. Magnetic resonance imaging for clinical management of rectal cancer: Updated recommendations from the 2016 European Society of Gastrointestinal and Abdominal Radiology (ESGAR) consensus meeting // EurRadiol. 2018. Vol. 28, N 4. P. 1465–1475. doi: 10.1007/s0033 0-017-5026-2

9. Oien K., Forsmo H.M., Rösler C., et al. Endorectal ultrasound and magnetic resonance imaging for staging of early rectal cancers: how well does it work in practice? // Acta Oncol. 2019. Vol. 58, Sup1. P. 49–54.doi: 10.1080/0284186X.2019.1569259

10. Brierley J.D., Gospodarowicz M. K., Wittekind C. TNM Classification of Malignant Tumours. 8th ed. Wiley-Blackwell, 2017. 272 p.

11. Kikuchi R., Takano M., Takagi K., et al. Management of early invasive colorectal cancer. Risk of recurrence and clinical guidelines // Dis Colon Rectum. 1995. Vol. 38, N 12. P. 1286–1295. doi: 10.1007/BF02049154

12. Boot J., Gomez-Munoz F., Beets-Tan R. Imaging of rectal cancer // Radiologe. 2019. Vol. 59, Suppl. 1. P. 46–50. doi: 10.1007/s00117-019-0579-5

13. Lambregts D., Bogveradze N., Blomqvist L., et al. Current controversies in TNM for the radiological staging of rectal cancer and how to deal with them: Results of a global online survey and multidisciplinary expert consensus // EurRadiol. 2022. Vol. 32, N 7. P. 4991–5003. doi: 10.1007/s00330-022-08591-z

14. Майновская О.А., Рыбаков Е.Г., Чернышов С.В., и др. Новые морфологические факторы риска метастазирования в регионарные лимфоузлы при раке прямой кишки с инвазией в подслизистую основу // Колопроктология. 2021. Т. 20, № 4. С. 22–33. doi: 10.33878/2073-7556-2021-20-4-22-33

15. Волкова С.Н., Сташук Г.А., Черменский Г.В., Наумов Е.К. Роль МРТ в выявлении экстрамуральной сосудистой инвазии как индикатора наличия регионарных и отдаленных метастазов рака нижнеампулярного отдела прямой кишки // Экспериментальная и клиническая гастроэнтерология. 2019. Т. 164, № 4. С. 66–71. doi: 10.31146/1682-8658-ecg-164-4-66-71

16. Lord A.C., D'Souza N., Shaw A., et al. MRI-diagnosed tumor deposits and EMVI status have superior prognostic accuracy to current clinical TNM staging in rectal cancer // Ann Surg. 2022. Vol. 276, N 2. P. 334–344. doi: 10.1097/SLA.0000000000004499

17. Rokan Z., Simillis C., Kontovounisios C., et al. Locally recurrent rectal cancer according to a standardized MRI classification system: A systematic review of the literature // J Clin Med. 2022. Vol. 11, N 12. P. 3511.doi: 10.3390/jcm11123511

18. Гришко П.Ю., Мищенко А.В., Ивко О.В., и др. Возможности мультипараметрической магнитно-резонансной томографии в оценке эффективности неоадъювантного лечения рака прямой кишки // Лучевая диагностика и терапия. 2019. Т. 10, № 4. С. 49–56.

19. Inoue A., Sheedy S.P., Heiken J.P., et al. MRI-detected extramural venous invasion of rectal cancer: Multimodality performance and implications at baseline imaging and after neoadjuvant therapy // Insights Imaging. 2021. N 12. P. 110. doi: 10.1186/s13244-021-01023-4

20. Al-Sukhni E., Milot L., Fruitman M., et al. Diagnostic Accuracy of MRI for assessment of t category, lymph node metastases, and circumferential resection margin involvement in patients with rectal cancer: A systematic review and meta-analysis // Annals Surgical Oncology. 2012. Vol. 19, N 7. P. 2212–2222. doi: 10.1245/s10434-011-2210-5

21. Borgheresi A., De Muzio F., Agostini A., et al. Lymph nodes evaluation in rectal cancer: Where do we stand and future perspective // J Clin Med. 2022. Vol. 11, N 9. P. 2599. doi: 10.3390/jcm11092599

22. Zhuang Z., Zhang Y., Wei M., et al. Magnetic resonance imaging evaluation of the accuracy of various lymph node staging criteria in rectal cancer: A systematic review and meta-analysis // Front Oncol. 2021. N 11. P. 709070. doi: 10.3389/fonc.2021.709070

23. Li X., Sun Y., Tang L., et al. Evaluating local lymph node metastasis with magnetic resonance imaging, endoluminal ultrasound and computed tomography in rectal cancer: A meta-analysis // Color Dis. 2015. Vol. 17, N 6. P. 129–135.doi: 10.1111/codi.12909

24. Weiser M.R. AJCC 8th edition: Colorectal cancer // Ann Surg Oncol. 2018.Vol. 25, N 6.P. 1454–1455. doi: 10.1245/s10434-018-6462-1

25. Ueno H.,Nagtegaal I.D., Quirke P., et al. Tumor deposits in colorectal cancer: Refining their definition in the TNM system // A G Surg. 2023. Vol. 7, N 2. P. 225–235. doi: 10.1002/ags3.12652

26. Santiago I., Figueiredo N., Parés O., et al. MRI of rectal cancer: Relevant anatomy and staging key points // Insights Imaging. 2020. Vol. 11, N 1. P. 100. doi: 10.1186/s13244-020-00890-7

27. Ogura A., Konishi T., Cunningham C., et al. Neoadjuvant (chemo)radiotherapy with total mesorectal excision only is not sufficient to prevent lateral local recurrence in enlarged nodes: Results of the multicenter lateral node study of patients with low cT3/4 rectal cancer // J Clin Oncol. 2019. Vol. 37, N 1. P. 33–43. doi: 10.1200/JCO.18.00032

28. Gollub M.J., Costello J.R., Ernst R.D., et al. A primer on rectal MRI in patients on watch-and-wait treatment for rectal cancer // Abdom Radiol. 2023. doi: 10.1007/s00261-023-03900-6
29. Березовская Т.П., Дайнеко Я.А., Невольских А.А., и др. Проспективная оценка использования системы mrTRG в определении эффективности неоадъювантной химиолучевой терапии у больных раком прямой кишки // Вестник рентгенологии и радиологии. 2021. Т. 102, № 1. С. 6–17. doi: 10.20862/0042-4676-2021-102-1-6-17
30. Almeida R.R., Souza D., Matalon S.A., et al. Rectal MRI after neoadjuvant chemoradiation therapy: A pictorial guide to interpretation // AbdomRadiol. 2021. Vol. 46, N 7. P. 3044–3057. doi: 10.1007/s00261-021-03007-w
31. Шелыгин Ю.А., Чернышов С.В., Казиева Л.Ю., и др. Сравнительный анализ открытой и трансанальной тотальной мезоректумэктомии при раке прямой кишки // Колопроктология. 2018. № 4. С. 67–73.
32. Майстренко Н.А., Хватов А.А, Сазонов А.А. Экзентерации малого таза в лечении местнораспространенных опухолей // Вестник хирургии им. Грекова. 2014. Т. 173, № 6. С. 37–43.
33. Сидоров Д.В., Алексеев Б.Я., Гришин Н.А., и др. Варианты экзентерации малого таза при местнораспространенном первичном и рецидивном раке прямой кишки // Онкология. Журнал им. П.А. Герцена. 2013. № 6. С. 7–13.

AUTHORS' INFO

*** Tatiana P. Berezovskaya,** MD, Dr. Sci. (Med.), Professor;
address: 4 Korolev street, 249036 Obninsk, Russia;
ORCID: 0000-0002-3549-4499;
eLibrary SPIN: 5837-3465;
e-mail berez@mrrc.obninsk.ru

Natalia A. Rubtsova, MD, Dr. Sci. (Med.);
ORCID: 0000-0001-8378-4338;
eLibrary SPIN: 9712-9091;
e-mail rna17@ya.ru

Valentin E. Sinitsyn, MD, Dr. Sci. (Med.), Professor;
ORCID: 0000-0002-5649-2193;
eLibrary SPIN: 8449-6590;
e-mail vsin@mail.ru

Irina V. Zarodnyuk, MD, Dr. Sci. (Med.);
ORCID: 0000-0002-9442-7480;
eLibrary SPIN: 8310-8989;
e-mail zarodnyuk_iv@gnck.ru

Nicolai V. Nudnov, MD, Dr. Sci. (Med.), Professor;
ORCID: 0000-0001-5994-0468;
eLibrary SPIN: 3018-2527;
e-mail nudnov@rncrr.ru

Andrei V. Mishchenko, MD, Dr. Sci. (Med.);
ORCID: 0000-0001-7921-3487;
eLibrary SPIN: 8825-4704;
e-mail dr.mishchenko@mail.ru

Yuliya L. Trubacheva, MD, Dr. Sci. (Med.);
ORCID: 0000-0002-8403-195X;
eLibrary SPIN: 3427-9074;
e-mail trubacheva_ul@gnck.ru

Tatiana A. Bergen, MD, Dr. Sci. (Med.);
ORCID: 0000-0003-1530-1327;
eLibrary SPIN: 5467-7347;
e-mail tbergenl@yandex.ru

Pavel Yu. Grishko, MD, Cand. Sci. (Med.);
ORCID: 0000-0003-4665-6999;
eLibrary SPIN: 3109-1583;
e-mail: dr.grishko@mail.ru

ОБ АВТОРАХ

*** Березовская Татьяна Павловна,** д-р мед. наук, профессор;
адрес: Россия, 249036, Обнинск, ул. Королева, д. 4;
ORCID: 0000-0002-3549-4499;
eLibrary SPIN: 5837-3465;
e-mail berez@mrrc.obninsk.ru

Рубцова Наталья Алефтиновна, д-р мед. наук;
ORCID: 0000-0001-8378-4338;
eLibrary SPIN: 9712-9091;
e-mail rna17@ya.ru

Синицын Валентин Евгеньевич, д-р мед. наук, профессор;
ORCID: 0000-0002-5649-2193;
eLibrary SPIN: 8449-6590;
e-mail vsin@mail.ru

Зароднюк Ирина Владимировна, д-р мед. наук;
ORCID: 0000-0002-9442-7480;
eLibrary SPIN: 8310-8989;
e-mail zarodnyuk_iv@gnck.ru

Нуднов Николай Васильевич, д-р мед. наук, профессор;
ORCID: 0000-0001-5994-0468;
eLibrary SPIN: 3018-2527;
e-mail nudnov@rncrr.ru

Мищенко Андрей Владимирович, д-р мед. наук;
ORCID: 0000-0001-7921-3487;
eLibrary SPIN: 8825-4704;
e-mail dr.mishchenko@mail.ru

Трубачева Юлия Леонидовна, д-р мед. наук;
ORCID: 0000-0002-8403-195X;
eLibrary SPIN: 3427-9074;
e-mail trubacheva_ul@gnck.ru

Берген Татьяна Андреевна, д-р мед. наук;
ORCID: 0000-0003-1530-1327;
eLibrary SPIN: 5467-7347;
e-mail tbergenl@yandex.ru

Гришко Павел Юрьевич, канд. мед. наук;
ORCID: 0000-0003-4665-6999;
eLibrary SPIN: 3109-1583;
e-mail: dr.grishko@mail.ru

* Corresponding author / Автор, ответственный за переписку

Svetlana S. Balyasnikova, MD, Cand. Sci. (Med.);
ORCID: 0000-0002-9666-9301;
eLibrary SPIN: 3987-2336;
e-mail: Balasnikova.Svetlana@gmail.com

Yana A. Dayneko, MD, Cand. Sci. (Med.);
ORCID: 0000-0002-4524-0839;
e-mail vorobeyana@gmail.com

Darya V. Ryjkova, MD, Dr. Sci. (Med.), Professor;
ORCID: 0000-0002-7086-9153;
e-mail d_ryjkova@mail.ru

Malika M. Hodzhibekova, MD, Dr. Sci. (Med.);
ORCID: 0000-0002-2172-5778;
eLibrary SPIN: 3999-7304;
e-mail malika_25@mail.ru

Nataliya A. Rucheva, MD, Cand. Sci. (Med.);
ORCID: 0000-0002-8063-4462;
eLibrary SPIN: 2196-8300;
e-mail: rna1969@yandex.ru

Igor E. Turin, MD, Dr. Sci. (Med.), Professor;
ORCID: 0000-0002-8587-4422;
eLibrary SPIN: 6499-2398;
e-mail: igortyurin@gmail.com

Sergey I. Achkasov, MD, Dr. Sci. (Med.), Professor, Corresponding Member of the Academy of Sciences;
ORCID: 0000-0001-9294-5447;
eLibrary SPIN: 5467-1062;
e-mail achkasovy@mail.ru

Alexey A. Nevolskikh, MD, Dr. Sci. (Med.);
ORCID: 0000-0001-5961-2958;
eLibrary SPIN: 3787-6139;
e-mail alexey.nevol@gmail.com

Sergey S. Gordeyev, MD, Dr. Sci. (Med.);
ORCID: 0000-0002-9303-8379;
eLibrary SPIN: 6577-5540;
e-mail ss.netoncology@gmail.com

Inna V. Droshneva, MD, Cand. Sci. (Med.);
eLibrary SPIN: 1908-2624;
e-mail droshnevainna@mail.ru

Балясникова Светлана Сергеевна, канд. мед. наук;
ORCID: 0000-0002-9666-9301;
eLibrary SPIN: 3987-2336;
e-mail: Balasnikova.Svetlana@gmail.com

Дайнеко Яна Александровна, канд. мед. наук;
ORCID: 0000-0002-4524-0839;
e-mail vorobeyana@gmail.com

Рыжкова Дарья Викторовна, д-р мед. наук, профессор;
ORCID: 0000-0002-7086-9153;
e-mail d_ryjkova@mail.ru

Ходжибекова Малика Маратовна, д-р мед. наук;
ORCID: 0000-0002-2172-5778;
eLibrary SPIN: 3999-7304;
e-mail malika_25@mail.ru

Ручьева Наталья Александровна, канд. мед. наук;
ORCID: 0000-0002-8063-4462;
eLibrary SPIN: 2196-8300;
e-mail: rna1969@yandex.ru

Тюрин Игорь Евгеньевич, д-р мед. наук, профессор;
ORCID: 0000-0002-8587-4422;
eLibrary SPIN: 6499-2398;
e-mail: igortyurin@gmail.com

Ачкасов Сергей Иванович, д-р мед. наук, профессор, чл.-корр. РАН;
ORCID: 0000-0001-9294-5447;
eLibrary SPIN: 5467-1062;
e-mail achkasovy@mail.ru

Невольских Алексей Алексеевич, д-р мед. наук;
ORCID: 0000-0001-5961-2958;
eLibrary SPIN: 3787-6139;
e-mail: alexey.nevol@gmail.com

Гордеев Сергей Сергеевич, д-р мед. наук;
ORCID: 0000-0002-9303-8379;
eLibrary SPIN: 6577-5540;
e-mail ss.netoncology@gmail.com

Дрошнева Инна Викторовна, канд. мед. наук;
eLibrary SPIN: 1908-2624;
e-mail droshnevainna@mail.ru

DOI: https://doi.org/10.17816/DD530656

Актуализация формы федерального государственного статистического наблюдения № 3-ДОЗ «Сведения о дозах облучения пациентов при проведении медицинских рентгенорадиологических исследований»: часть 2 (рекомендации по заполнению формы)

А.В. Водоватов[1, 2], Л.А. Чипига[1, 3, 4], П.С. Дружинина[1], И.Г. Шацкий[1], А.В. Петрякова[1, 5], С.С. Сарычева[1], А.М. Библин[1], Рустам Р. Ахматдинов[1], Руслан Р. Ахматдинов[1], Ю.Н. Капырина[2], А.А. Братилова[1], И.В. Солдатов[6], З.А. Лантух[6], В.Г. Пузырев[2], С.А. Рыжов[6, 7, 8]

[1] Санкт-Петербургский научно-исследовательский институт радиационной гигиены имени профессора П.В. Рамзаева, Санкт-Петербург, Российская Федерация;
[2] Санкт-Петербургский государственный педиатрический медицинский университет, Санкт-Петербург, Российская Федерация;
[3] Российский научный центр радиологии и хирургических технологий имени академика А.М. Гранова, Санкт-Петербург, Российская Федерация;
[4] Национальный медицинский исследовательский центр имени В.А. Алмазова, Санкт-Петербург, Российская Федерация;
[5] Городская больница № 40 Курортного административного района, Санкт-Петербург, Российская Федерация;
[6] Научно-практический клинический центр диагностики и телемедицинских технологий, Москва, Российская Федерация;
[7] Ассоциация медицинских физиков России, Москва, Российская Федерация;
[8] Национальный медицинский исследовательский центр детской гематологии, онкологии и иммунологии имени Дмитрия Рогачева, Москва, Российская Федерация

АННОТАЦИЯ

Приказом Росстата № 880 от 30 ноября 2022 года утверждена новая редакция формы федерального статистического наблюдения № 3-ДОЗ «Сведения о дозах облучения пациентов при проведении медицинских рентгенорадиологических исследований», которая существенно отличается от предыдущей редакции. В частности, скорректирована и изменена структура таблиц формы № 3-ДОЗ с выделением в отдельные графоклетки высокодозовых исследований; переработан раздел по радионуклидной диагностике с переходом на предоставление информации по уровням облучения пациентов при использовании отдельных радионуклидов с выделением гибридных исследований; внедрены отдельные таблицы с информацией о числе рентгенорадиологических исследований и коллективных дозах для детских пациентов; сокращено количество исследований, для которых представлены типичные (средние) эффективные дозы пациентов.

В рамках настоящей работы представлена структура актуализированной формы № 3-ДОЗ, а также даны рекомендации по её заполнению, направленные на повышение достоверности предоставляемых данных и снижение количества процедурных ошибок.

Данная работа является продолжением статьи Водоватова А.В., Чипиги Л.А., Братиловой А.А., Дружининой П.С., Шацкого И.Г., Петряковой А.В., Сарычевой С.С., Библина А.М., Ахматдинова Р.Р., Капыриной Ю.В., Солдатова И.В., Пузырева В.Г., Рыжова С.А. «Актуализация формы федерального государственного статистического наблюдения № 3-ДОЗ «Сведения о дозах облучения пациентов при проведении медицинских рентгенорадиологических исследований». Предпосылки к переработке», опубликованной в журнале «Радиационная гигиена» (2023. Т. 16, № 2. С. 126–136. DOI: https://doi.org/10.21514/1998-426X-2023-16-2-126-136).

Ключевые слова: единая система контроля и учёта индивидуальных доз облучения граждан; ЕСКИД; дозы облучения; форма № 3-ДОЗ; пациенты; медицинское облучение.

Как цитировать:

Водоватов А.В., Чипига Л.А., Дружинина П.С., Шацкий И.Г., Петрякова А.В., Сарычева С.С., Библин А.М., Ахматдинов Р.Р., Ахматдинов Р.Р., Капырина Ю.Н., Братилова А.А., Солдатов И.В., Лантух З.А., Пузырев В.Г., Рыжов С.А. Актуализация формы федерального государственного статистического наблюдения № 3-ДОЗ «Сведения о дозах облучения пациентов при проведении медицинских рентгенорадиологических исследований»: часть 2 (рекомендации по заполнению формы) // *Digital Diagnostics.* 2023. Т. 4, № 3. С. 322–339. DOI: https://doi.org/10.17816/DD530656

Рукопись получена: 07.07.2023 **Рукопись одобрена:** 01.08.2023 **Опубликована:** 24.08.2023

DOI: https://doi.org/10.17816/DD530656

Update of the federal governmental statistical surveillance form № 3-DOZ: "Data on patient doses from medical X-ray examinations"— Part 2 (FORM completion Recommendations)

Aleksandr V. Vodovatov[1, 2], Larisa A. Chipiga[1, 3, 4], Polina S. Druzhinina[1], Ilya G. Shatskiy[1], Anastasiya V. Petryakova[1, 5], Svetlana S. Sarycheva[1], Artem M. Biblin[1], Rustam R. Akhmatdinov[1], Ruslan R. Akhmatdinov[1], Yulia N. Kapyrina[2], Anzhelika A. Bratilova[1], Ilya V. Soldatov[6], Zoya A. Lantukh[6], Victor G. Puzyrev[2], Sergey A. Ryzhov[6, 7, 8]

[1] Saint-Petersburg Research Institute of Radiation Hygiene after Professor P.V. Ramzaev, Saint Petersburg, Russian Federation;
[2] Saint-Petersburg State Pediatric Medical University, Saint Petersburg, Russian Federation;
[3] Granov Russian Research Center of Radiology and Surgical Technologies, Saint Petersburg, Russian Federation;
[4] Almazov National Medical Research Centre, Saint Petersburg, Russian Federation;
[5] City Hospital No. 40 of the Kurortny administrative district, Saint Petersburg, Russian Federation;
[6] Research and Practical Clinical Center for Diagnostics and Telemedicine Technologies, Moscow, Russian Federation;
[7] Association of Medical Physicists in Russia, Moscow, Russian Federation;
[8] Dmitry Rogachev National Medical Research Center of Pediatric Hematology, Oncology and Immunology, Moscow, Russian Federation

ABSTRACT

The form of federal governmental statistical surveillance № 3-DOZ, titled "Data on patient doses from medical X-ray examinations," has changed significantly by the order of Rosstat N 880. In particular, the structure of the form's has been revised: studies involving high doses were dedicated from the rest; the section on radionuclide diagnostics has been redesigned; the information on the levels of patient exposure when using individual radionuclides and in hybrid studies have been displayed; information on the number of radiological studies and collective doses for pediatric patients have been introduced; and the number of studies for which typical (average) effective doses of patients are presented has been reduced. The structure of the updated form № 3-DOZ is presented within the framework of this work.

In this article, recommendations for filling out № 3-DOZ have been developed in order to increase the reliability of the data provided and reduce the number of procedural errors.

This work is a continuation of the article Vodovatov A.V., Chipiga L.A., Bratilova A.A., Druzhinina P.S., Shatskiy I.G., Petryakova A.V., Sarycheva S.S., Biblin A.M., Akhmatdinov R.R., Kapyrina Yu.N., Soldatov I.V., Puzyrev V.G., and Ryzhov S.A. "Update of the federal governmental statistical surveillance form № 3-DOZ "Data on patient doses from medical X-ray examinations". Perquisites for the update, published in the journal Radiatsionnaya Gygiena (2023. Vol. 16, N 2. P. 126–136. DOI: https://doi.org/10.21514/1998-426X-2023-16-2-126-136).

Keywords: unified system of individual dose control of the Russian federation citizens; effective dose; form № 3-DOZ; patients; medical exposure.

To cite this article:
Vodovatov AV, Chipiga LA, Druzhinina PS, Shatskiy IG, Petryakova AV, Sarycheva SS, Biblin AM, Akhmatdinov RR, Akhmatdinov RR, Kapyrina YuN, Bratilova AA, Soldatov IV, Lantukh ZA, Puzyrev VG, Ryzhov SA. Update of the federal governmental statistical surveillance form № 3-DOZ: "Data on patient doses from medical X-ray examinations"— Part 2 (FORM completion Recommendations). *Digital Diagnostics.* 2023;4(3):322–339. DOI: https://doi.org/10.17816/DD530656

Received: 07.07.2023 **Accepted:** 01.08.2023 **Published:** 24.08.2023

DOI: https://doi.org/10.17816/DD530656

更新第3-DOZ号联邦国家统计观察表《医疗X射线放射检查期间患者所受辐射剂量的信息》：第2部分（填表建议）

Aleksandr V. Vodovatov[1, 2], Larisa A. Chipiga[1, 3, 4], Polina S. Druzhinina[1], Ilya G. Shatskiy[1], Anastasiya V. Petryakova[1, 5], Svetlana S. Sarycheva[1], Artem M. Biblin[1], Rustam R. Akhmatdinov[1], Ruslan R. Akhmatdinov[1], Yulia N. Kapyrina[2], Anzhelika A. Bratilova[1], Ilya V. Soldatov[6], Zoya A. Lantukh[6], Victor G. Puzyrev[2], Sergey A. Ryzhov[6, 7, 8]

[1] Saint-Petersburg Research Institute of Radiation Hygiene after Professor P.V. Ramzaev, Saint Petersburg, Russian Federation;
[2] Saint-Petersburg State Pediatric Medical University, Saint Petersburg, Russian Federation;
[3] Granov Russian Research Center of Radiology and Surgical Technologies, Saint Petersburg, Russian Federation;
[4] Almazov National Medical Research Centre, Saint Petersburg, Russian Federation;
[5] City Hospital No. 40 of the Kurortny administrative district, Saint Petersburg, Russian Federation;
[6] Research and Practical Clinical Center for Diagnostics and Telemedicine Technologies, Moscow, Russian Federation;
[7] Association of Medical Physicists in Russia, Moscow, Russian Federation;
[8] Dmitry Rogachev National Medical Research Center of Pediatric Hematology, Oncology and Immunology, Moscow, Russian Federation

简评

俄罗斯国家统计局2022年11月30日第880号命令批准了新版第3-DOZ号联邦统计观察表《医疗X射线放射检查期间患者所受辐射剂量的信息》，该表与旧版有很大不同。特别是对第3-DOZ号表中的表格结构进行了调整和更改，将高剂量检查分配到单独的栏目中；重新设计了放射性核素诊断部分，过渡到提供使用单个放射性核素时患者受照射水平的信息以及混合检查的分配；引入了单独的表格，其中包含儿科患者的X射线放射检查数量和集体剂量信息；减少了提供患者典型（平均）有效剂量的检查数量。

本文介绍更新后的第3-DOZ号表的结构，并对其填写提出了建议，旨在提高所提供数据的可靠性并减少程序性错误的数量。

本文是Vodovatov A.V.、Chipiga L.A.、Bratilova A.A.、Druzhinina P.S.、Shatsky I.G.、Petryakova A.V.、Sarycheva S.S.、Biblin A.M.、Akhmatdinov R.R.、Kapyrina Y.V.、Soldatov I.V.、Puzyrev V.G.和Ryzhov S.A.、Ryzhov S.A.《更新第3-DOZ号联邦国家统计观察表《医疗X射线放射检查期间患者辐射剂量的信息》。修订的前提条件》文章的续篇，发表于《辐射卫生》杂志（2023。Vol.16，№2。P.126-136。DOI：https://doi.org/10.21514/1998-426X-2023-16-2-126-136）。

关键词：公民个人辐射剂量统一控制和核算系统；USMID；辐射剂量；第3-DOZ号表；患者；医疗照射。

引用本文：
Vodovatov AV, Chipiga LA, Druzhinina PS, Shatskiy IG, Petryakova AV, Sarycheva SS, Biblin AM, Akhmatdinov RR, Akhmatdinov RR, Kapyrina YuN, Bratilova AA, Soldatov IV, Lantukh ZA, Puzyrev VG, Ryzhov SA. 更新第3-DOZ号联邦国家统计观察表《医疗X射线放射检查期间患者所受辐射剂量的信息》：第2部分（填表建议）. *Digital Diagnostics*. 2023;4(3):322–339. DOI: https://doi.org/10.17816/DD530656

收到：07.07.2023 **接受：**01.08.2023 **发布日期：**24.08.2023

INTRODUCTION

The Form No. 3-DOZ (hereinafter "the Form") is designed to assess changes in diagnostic radiology structure and collective doses caused by medical exposure of the Russian Federation population [1–3]. Data obtained using this Form are used for radiation-hygienic certification of the Russian Federation territories and for preparing a state report on the population's sanitary and epidemiological condition [4, 5]. The 3-DOZ study results are used in the annual report "Radiation Doses Received by the Population of the Russian Federation" [6].

Order No. 880 of Federal State Statistics Service (Rosstat),[1] dated November 30, 2022, approved a new version of Federal Statistical Monitoring Form No. 3-DOZ, "Data on Radiation Doses Received by Patients from Medical Radiological Examinations," which differs significantly from the standard version approved sequentially by Rosstat Resolution No. 51 dated September 21, 2006[2], and Rosstat Order No. 411 dated October 16, 2013[3]. Since 2006, no changes have been made, except for the correction of Form completion instructions and the content of the title page. The following significant changes were made to the revised version of Form No. 3-DOZ:

- the structure of the Form tables has been updated and changed, with special space added for high-dose examinations, such as computed tomography (CT) with contrast media; CT scan of several anatomical areas (chest + abdomen, abdomen + pelvis, and whole body), and interventional radiology;
- the section on radionuclide diagnostics has been revised to include information on patient exposure levels when using individual radionuclides, as well as hybrid examinations, such as positron emission tomography combined with computed tomography (PET/CT) and single photon emission computed tomography combined with computed tomography (SPECT/CT);
- the classification of CT and interventional (special) examinations has been aligned with Form No. 30 of the Ministry of Healthcare of the Russian Federation;
- separate tables have been prepared for information on the number of radiological examinations and collective doses for pediatric patients; and
- the number of examinations, including data on typical (average) effective patient doses, has reduced.

The reasons for implementing these provisions were detailed in a previous authors' paper [7].

Many changes may be associated with various challenges when completing the updated Form. Therefore, the authors aimed to prepare recommendations and clarifications for the updated Form's complete instructions.

During the first years after the implementation of the updated Form, specialists responsible for completing it may encounter some difficulties. Therefore, this paper provides recommendations for completing the Form. Moreover, some regions, in collaboration with the Saint Petersburg Research Institute of Radiation Hygiene, named after Professor P.V. Ramzaev of the Federal Service for the Oversight of Consumer Protection and Welfare (hereinafter referred to as the Institute of Radiation Hygiene), published training materials and automated the process of submitting reports through web resources [8, 9].

It is appropriate to describe the structure of the updated Form in detail, highlight the key features of completing it, and provide recommendations to reduce completion errors associated with the transition to the new Form.

STRUCTURE OF UPDATED FORM NO. 3-DOZ AND RECOMMENDATIONS FOR ITS COMPLETION AIMED AT INCREASING THE RELIABILITY OF DATA PROVIDED AND REDUCING THE NUMBER OF PROCEDURE ERRORS

General provisions

The first key difference between the updated Form and the old one is the change in the title page in accordance with current legislation.[4] In the previous version, the executive authorities of the Russian Federation's constituent entities were identified as subjects of official statistical accounting, such as the Main Directorate of Special Programs of the President of the Russian Federation, Presidential Administration of Russia, Federal Budgetary Institution of Healthcare "Center for Hygiene and Epidemiology," Federal

[1] Order of Rosstat No. 880 dated November 30, 2022 on approval of the federal statistical monitoring form with the Form completion instructions for the Federal Service for the Oversight of Consumer Protection and Welfare to organize federal statistical monitoring of the sanitary condition of a constituent entity of the Russian Federation. Link: https://normativ.kontur.ru/document?moduleId=1&documentId=437635.

[2] Resolution of Rosstat No. 51 dated September 21, 2006 on approval of statistical tools for Rospotrebnadzor to organize statistical monitoring of population incidence of infectious and parasitic diseases, preventive vaccinations, sanitary condition of territories, summer health institutions for children and adolescents, disinfection activities, and radiation doses. Link: https://normativ.kontur.ru/document?moduleId=1&documentId=223414.

[3] Order of Rosstat No. 411 dated October 16, 2013 on approval of statistical tools for the Federal Service for the Oversight of Consumer Protection and Welfare to organize federal statistical monitoring of the sanitary condition of territories, occupational diseases (poisonings), and radiation doses. Link: https://normativ.kontur.ru/document?moduleId=1&documentId=443740.

[4] Order of Rosstat No. 880 dated November 30, 2022 on approval of the federal statistical monitoring form with the Form completion instructions for the Federal Service for the Oversight of Consumer Protection and Welfare to organize federal statistical monitoring of the sanitary condition of a constituent entity of the Russian Federation. Link: https://normativ.kontur.ru/document?moduleId=1&documentId=437635.

Budgetary Institution "Research Institute of Radiation Hygiene named after Professor P.V. Ramzaev." According to Part 1 of Article 5 of Federal Law No. 282-FZ of November 29, 2007[5] (hereinafter referred to as the Law on Statistical Accounting), official statistical accounting in the Russian Federation is carried out by subjects of official statistical accounting. Article 2 of the Law on Statistical Accounting, paragraph 4, contains a comprehensive list of official statistical accounting topics that exclude the bodies and organizations indicated above. Only respondents and subjects of official statistical accounting may be shown in the Form, and the same bodies cannot be deemed independent subjects of official statistical accounting and Form respondents simultaneously. A compromise approach was established when developing the latest version of the Form: only respondents (legal entities and individual entrepreneurs using sources of ionizing radiation for medical purposes) and subjects (Rospotrebnadzor) of statistical registration are left on the title page.

Simultaneously, the entire procedure for completing and submitting the Form remained unchanged. A healthcare organization submits forms for the reporting year by April 1 to an executive healthcare authority of a constituent entity of the Russian Federation, including institutions and structural divisions of federal executive authorities listed in paragraph 4 of Regulations on the implementation of federal state sanitary and epidemiological supervision in the Russian Federation, approved by Decree No. 476 of the Government of the Russian Federation dated June 15, 2013 (as applicable).[6] Before May 1, the executive healthcare authorities of a constituent entity of the Russian Federation provided data to the Federal Budgetary Institution "Center for Hygiene and Epidemiology" in that constituent entity. Before May 15, the Center for Hygiene and Epidemiology in the constituent entity of the Russian Federation provided data to the Office of Rospotrebnadzor of the constituent entity of the Russian Federation. Rospotrebnadzor departments of the constituent entities of the Russian Federation provide data to the Research Institute of Radiation Hygiene.

Summary reporting data from the Research Institute of Radiation Hygiene, Federal Medical-Biological Agency, structural divisions of the Ministry of Defense of the Russian Federation, the Ministry of Internal Affairs of the Russian Federation, the Federal Security Service of the Russian Federation, the Federal Service of the Troops of the National Guard of the Russian Federation, the Federal Security Service of the Russian Federation, the Federal Penitentiary Service, the Main Directorate of Special Programs of the President of the Russian Federation and the Presidential Administration of Russia, respectively, in the Armed Forces of the Russian Federation, other troops, military formations and organizations, at defense and defense manufacturing facilities, security, internal affairs, and other special services in accordance with Decree No. 476 of the Government of the Russian Federation dated June 5, 2013[7] (according to affiliation) should also be provided to Rospotrebnadzor before May 15.

The updated Form is divided into three sections (10 tables): the first and second sections are radiological examinations, and the third is radionuclide examinations. The first section (Tables 1100, 1200, 1300, and 1400) presents procedure data without monitoring or considering patient radiation doses.[8] The lack of dosage control and recording violates Article 18 of the Federal Law on Population Radiation Protection[9] and SanPiN 2.6.1.1192-03[10]. As an exception, temporary completion of Section 1 tables of the Form is allowed. All healthcare institutions should monitor and record individual patient radiation doses when conducting radiological examinations.

The second section (Tables 2100, 2200, 2300, and 2400) contains information on procedures with estimated patient doses based on measured parameters. The first two sections consist of four tables that detail the total patient radiation doses and the number of radiological procedures performed on children (0–17 yr) and adults (over 18 yr). All data are presented in absolute terms.

Tables 1100, 1300, 2100, and 2300 present information on doses received by patients during radiological examinations for diagnostics and treatment purposes. Tables 1100 (adults) and 1300 (children) should include collective doses based on statistical data on the number of various radiological procedures performed during the reporting year and average individual doses for each type of procedure (for procedures

---

[5] Federal Law No. 282-FZ dated November 29, 2007 on official statistical accounting and the system of state statistics in the Russian Federation. Link: https://www.consultant.ru/document/cons_doc_LAW_72844/.

[6] Decree No. 476 of the Government of the Russian Federation dated June 05, 2013 on issues of state control (supervision) and invalidation of certain acts of the Government of the Russian Federation (with amendments and additions). Link: https://base.garant.ru/70394016/.

[7] Decree No. 476 of the Government of the Russian Federation dated June 05, 2013, on issues of state control (supervision) and invalidation of certain acts of the Russian Federation (with amendments and additions). Link: https://www.consultant.ru/document/cons_doc_LAW_147378/.

[8] Guidelines Completing federal state statistical monitoring form No. 3-DOZ. Project. Link: http://niirg.ru/PDF/MR_3-DOS_2013.pdf.

[9] Federal Law No. 3-FZ dated January 09, 1996 (as amended on March 18, 2023) "On Radiation Protection of the Population." Article 18. Control and recording of individual radiation doses. Access mode: https://www.consultant.ru/document/cons_doc_LAW_8797/2d546164990e9137dc5b194a17843d8762e08451.

[10] Resolution of the Chief State Sanitary Doctor of the Russian Federation dated 02/18/2003 No. 8 "On the implementation of SanPiN 2.6.1.1192-03" (together with "SanPiN 2.6.1.1192-03. 2.6.1. Ionizing radiation, radiation safety. Hygienic requirements for the device and operation of X-ray rooms, devices and conducting X-ray examinations. Sanitary rules and regulations"). Access mode: https://www.consultant.ru/document/cons_doc_LAW_41439/.

with no control and accounting for patient radiation doses). Tables 1100, 1300, 2100, and 2300 should not include duplicate data.

When performing radiological procedures (procedures with patient radiation doses monitored and recorded), Tables 2100 (adults) and 2300 (children) should present collective doses based on standard patient radiation doses.[11]

Columns 3–12 of Tables 1100, 1300, 2100, and 2300 present data based on various types of diagnostic radiological and therapeutic procedures specified in the column headers.

The structural differences between the previous and updated versions of Form No. 3-DOZ are presented in Table 1.

Recommendations for completing tables in Form No. 3-DOZ

Healthcare organizations must provide a completed Form for all medical diagnostic radiation sources, including endovascular and interventional procedures. Data on radiation, radionuclide therapy, and radionuclide diagnostics *in vitro* are not included in Form No. 3-DOZ. Form No. 3-DOZ is completed in radiation therapy departments for all diagnostic examinations to prepare the patient for a course of radiation therapy (dosimetry planning). Magnetic resonance imaging and ultrasound examinations are also not listed in the Form because they do not expose the patient to ionizing radiation.

The Form considers the number of radiological procedures and examinations performed. A radiological procedure is defined as a single patient exposure while examining a specific anatomical area (one image); a radiological examination is a complete cycle of examination of a patient's certain organ (anatomical area), which may include several procedures using different projections and/or different types (Figure 1). Form No. 3-DOZ is completed only for the number

Table 1. Structural changes in the updated Form No. 3-DOZ

Section	Previous version	Updated version	Method of effective dose determination
Radiological examinations, dose estimation method	Collective dose — 1000 Number of procedures — 1100	Collective dose, adults — 1000 Number of procedures, adults — 1100	Average effective doses based on reference literature [10, 11]
		Collective dose, children — 1300 Number of procedures, children — 1400	
Radiological examinations, dose control	Collective dose — 2000 Number of procedures — 2100	Collective dose, adults — 2100 Number of procedures, adults — 2200	Standard effective doses based on current regulatory and methodological documents[12]
		Collective dose, children — 2300 Number of procedures, children — 2400	
The number of radionuclide examinations performed and the resulting effective patient radiation doses	3000	Adults—3100	Standard effective based on current regulatory and methodological documents[13]
		Children—3200	

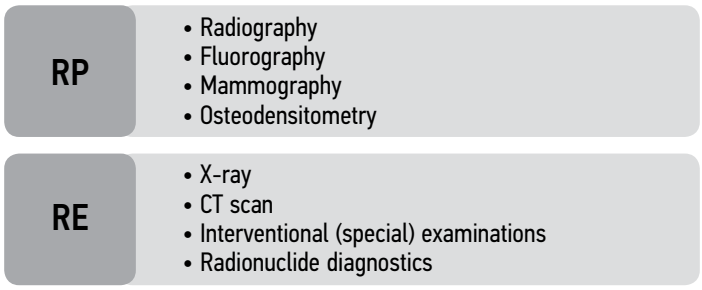

Fig. 1. Classification of radiological diagnostic methods using ionizing radiation. RE, radiological examination; RP, radiological procedure.

[11] Guidelines MUK 2.6.1.1797-03 Control of effective radiation doses for patients when conducting medical radiological examinations" (https://docs.cntd.ru/document/1200035983); Guidelines MU 2.6.1.3151-13 Evaluation and accounting of effective doses for patients when conducting radionuclide diagnostic examinations (https://base.garant.ru/70747326/).

[12] Guidelines 2.6.1.3584-19. 2.6.1. Ionizing radiation, radiation protection. Changes in MU 2.6.1.2944-11 Control of effective radiation doses for patients when conducting medical radiological examinations (https://www.consultant.ru/document/cons_doc_LAW_368034/); Guidelines MR 2.6.1.0296-22 Optimization of radiation protection of patients in diagnostic radiology by using reference diagnostic levels (https://base.garant.ru/405781973/).

[13] Guidelines MU 2.6.1.3151-13 Evaluation and accounting of effective doses for patients when conducting radionuclide diagnostic examinations (https://base.garant.ru/70747326/); Guidelines MR 2.6.1.0296-22 Optimization of radiation protection for patients in diagnostic radiology by using reference diagnostic levels (https://base.garant.ru/405781973/).

of examinations for all combined examinations (fluoroscopic, interventional, radionuclide examinations combined with CT); individual structural elements of radiological examinations (e.g., CT in SPECT/CT or PET/CT; X-rays as part of fluoroscopy or interventional examinations) are not highlighted (see Figure 1).

The total number of radiological examinations may be smaller than the total number of radiological procedures for a particular organ or anatomical area.

It is recommended to use the Federal Directory Diagnostic Investigations classification when assigning radiological examinations/procedures of a particular anatomical area [12].

Radiography

The column "Radiography" (columns 3 and 4) should include information about effective doses obtained by patients during radiographic examinations (two-dimensional projection X-ray images), fluorographic examinations of the chest, and screening examinations of mammary glands.

Information on radiological examinations performed using analog and digital X-ray machines should be presented in columns 3 and 4, respectively.

The absence of a special segment for fluorographic examinations (screening chest radiography) is worth noting. Data on fluorographic examinations performed using photography and X-ray film are presented in column 3 (film radiographs), line 2 (including preventive procedures). Data on fluorographic examinations performed using digital X-ray machines (U-arc type and scanning fluorographs) are presented in column 4 (digital radiographs), line 2 (including preventive procedures). All examinations performed using fluorography machines are shown in lines for the corresponding anatomical areas and columns 3 and 4 for analog and digital devices, respectively.

Data on mammary gland screening examinations performed on analog and digital machines are presented in column 3, line 22, and column 4, line 22, respectively.

General information about table changes in Form No. 3-DOZ for radiographic examinations is presented in Table 2.

Table 2. Structural changes in radiography information in the updated Form No. 3-DOZ

Field of interest in the previous Form	Line of the previous Form	Field of interest in the updated Form	Line of the updated Form	Comment
Chest	Line 01 (2000)	Chest	Adults — Line 01 (2100) Children — Line 01 (2300)	Including both preventive and diagnostic examinations
Chest, including preventive procedures	Line 02 (2000)	Chest, including preventive procedures	Adults — Line 02 (2100) Children — Line 02 (2300)	In the new Form, all fluorographic (screening) chest examinations (film and digital) are presented in this line.
Extremities	Line 03 (2000)	Upper extremities	Adults — Line 07 (2100) Children — Line 07 (2300)	—
		Lower extremities	Adults — Line 08 (2100) Children — Line 08 (2300)	
Cervical vertebrae	Line 04 (2000)	Cervical spine	Adults — Line 09 (2100) Children — Line 09 (2300)	—
Thoracic vertebrae	Line 05 (2000)	Thoracic spine	Adults — Line 10 (2100) Children — Line 10 (2300)	—
Lumbar vertebrae	Line 06 (2000)	Lumbar spine	Adults — Line 11 (2100) Children — Line 11 (2300)	—

Table 2. Ending

Field of interest in the previous Form	Line of the previous Form	Field of interest in the updated Form	Line of the updated Form	Comment
Pelvis and thigh	Line 07 (2000)	Pelvic organs	Adults — Line 12 (2100) Children — Line 12 (2300)	—
		Hip joint	Adults — Line 13 (2100) Children — Line 13 (2300)	
Ribs and sternum	Line 08 (2000)	Ribs and sternum	Adults — Line 14 (2100) Children — Line 14 (2300)	—
Abdominal organs	Line 09 (2000)	Abdomen	Adults — Line 15 (2100) Children — Line 15 (2300)	—
Upper gastrointestinal tract	Line 10 (2000)	Upper gastrointestinal tract	Not to be completed	Not to be filled out
Lower gastrointestinal tract	Line 11 (2000)	Lower gastrointestinal tract	Not to be completed	Not to be filled out
Skull, maxillofacial region	Line 12 (2000)	Skull, brain, maxillofacial region	Adults — Line 18 (2100) Children — Line 18 (2300)	—
Teeth	Line 13 (2000)	Teeth	Adults — Line 19 (2100) Children — Line 19 (2300)	Targeted images — Line 19, column 03/04 Orthopantomograms — Line 19, column 04
Kidneys, urinary system	Line 14 (2000)	Kidneys, urinary system	Adults — Line 20 (2100) Children — Line 20 (2300)	Including irrigoscopy
Breast	Line 15 (2000)	Breast	Adults — Line 21 (2100) Children — Line 21 (2300)	—
including preventive procedures	Line 16 (2000)	including preventive procedures (line 21)	Adults — Line 22 (2100) Children — Line 22 (2300)	—
Others	Line 17 (2000)	Others	Adults — Line 26 (2100) Children — Line 26 (2300)	—
Total	Line 18 (2000)	Total	Adults — Line 27 (2100) Children — Line 27 (2300)	—

DOI: https://doi.org/10.17816/DD530656

Fluoroscopy

Fluoroscopy includes examinations that involve the administration of a contrast agent orally, rectally, or through a urological catheter. Examples of completing the "Fluoroscopy" column in updated Form No. 3-DOZ are presented in Table 3.

Computed tomography

The updated Form adds a section for contrast-enhanced and unenhanced CT scans. Data on contrast-enhanced and unenhanced CT examinations of pediatric and adult patients should be presented in columns 7 and 6, respectively.

The updated Form provides detailed information about CT examinations of the circulatory system, including the heart, coronary vessels, and thoracic and abdominal aorta.

Please remember that individual CT scans will not be counted. A single CT scan may consist of one or more scans of the same anatomical area. For example, one CT examination of the liver or kidneys and urinary tract using intravenous contrast may consist of one to five scans yet is counted as one examination. The total dose for all phases should be considered for multiphase CT scans with contrast administration.

Information on lung cancer screening using low-dose CT and breast tomosynthesis is presented in lines 2 of column 6 and 22 of column 6, respectively.

The updated Form has separate lines for examining two or more anatomical regions or an anatomical region and a particular organ. Information on such examinations is presented in lines 23–25. Information on whole body CT examinations is shown in line 25, "Other."

General information on changes in CT examination tables of Form No. 3-DOZ is presented in Table 4.

Interventional examinations

In the updated Form of 3-DOZ, the section on interventional (special) examinations has been significantly revised. In accordance with Form No. 30, "Information about a healthcare organization" of the Ministry of Health

Table 3. Examples of filling out the "X-ray" column in the updated Form No. 3-DOZ

Fluoroscopy	Localization	Line of the updated Form	Type of effective dose determination procedure[14]
Chest X-ray	Rib cage	Line 01 — Chest organs	Lungs
X-ray of the thoracic region and the spinal cerebrospinal fluid pathways with contrast	Thoracic spine, cerebrospinal fluid tracts of the spinal cord	Line 10 — Thoracic spine	Thoracic spine
X-ray of the stomach and duodenum with contrast X-ray of the stomach and duodenum with double contrast	Stomach, duodenum	Line 15 — Abdominal organs	Stomach
X-ray of the pharynx and esophagus with contrast X-ray of the esophagus with contrast	Pharynx, esophagus	Line 16 — Upper gastrointestinal tract	Esophagus
X-ray of the passage of contrast material through the intestine	Gastrointestinal tract	Line 17 — Lower gastrointestinal tract	Intestines
X-ray of the small intestine through an ileostomy	Small intestine	Line 17 — Lower gastrointestinal tract	Intestines
X-ray of the colon with contrast X-ray of the colon with double contrast	Colon	Line 17 — Lower gastrointestinal tract	Intestines
X-ray of the rectum with functional tests X-ray of the rectum during defecation	Rectum	Line 17 — Lower gastrointestinal tract	Intestines
X-ray of paranasal sinus fistula	Paranasal sinuses	Line 18 — Skull, brain, maxillofacial area	Scull

[14] Guidelines MU 2.6.1.3584-19 Changes to MU 2.6.1.2944-19 Control of effective radiation doses for patients when conducting medical radiological examinations. Link: https://base.garant.ru/73515396/.

Table 4. Computed tomography

Field of interest in the previous Form	Line of the previous Form	Field of interest in the updated Form	Line of the updated Form	Comment
Chest	Line 01 (2000)	Chest organs	Adults — Line 01 (2100) Children — Line 01 (2300)	—
Chest, including preventive procedures	Line 02 (2000)	Chest organs, of which due to preventive procedures	Adults — Line 02 (2100) Children — Line 02 (2300)	Information on lung cancer screening using low-dose computed tomography Information on periodic medical examinations of decreed groups using computed tomography
Absent	Absent	Heart	Adults — Line 03 (2100) Children — Line 03 (2300)	—
Absent	Absent	Heart, of which on the coronary vessels	Adults — Line 0 4 (2100) Children — Line 0 4 (2300)	—
Absent	Absent	Thoracic aorta	Adults — Line 0 5 (2100) Children — Line 0 5 (2300)	—
Absent	Absent	Abdominal aorta	Adults — Line 06 (2100) Children — Line 06 (2300)	—
Limbs	Line 03 (2000)	Upper limbs	Adults — Line 07 (2100) Children — Line 07 (2300)	—
		Lower limbs	Adults — Line 08 (2100) Children — Line 08 (2300)	
Cervical vertebrae	Line 04 (2000)	Cervical spine	Adults — Line 09 (2100) Children — Line 09 (2300)	—
Thoracic vertebrae	Line 05 (2000)	Thoracic spine	Adults — Line 10 (2100) Children — Line 10 (2300)	—
Lumbar vertebrae	Line 06 (2000)	Lumbar spine	Adults — Line 11 (2100) Children — Line 11 (2300)	—
Pelvis and thigh	Line 07 (2000)	Pelvic organs	Adults — Line 12 (2100) Children — Line 12 (2300)	—
		Hip joint	Adults — Line 13 (2100) Children — Line 13 (2300)	
Ribs and sternum	Line 08 (2000)	Ribs and sternum	Adults — Line 14 (2100) Children — Line 14 (2300)	—
Abdomen	Line 09 (2000)	Abdomen	Adults — Line 15 (2100) Children — Line 15 (2300)	—
Upper gastrointestinal tract	Line 10 (2000)	Upper gastrointestinal tract	Adults — Line 16 (2100) Children — Line 16 (2300)	—
Lower gastrointestinal tract	Line 11 (2000)	Lower gastrointestinal tract	Adults — Line 17 (2100) Children — Line 17 (2300)	—
Skull, maxillofacial region	Line 12 (2000)	Skull, brain, maxillofacial region	Adults — Line 18 (2100) Children — Line 18 (2300)	—
Teeth	Line 13 (2000)	Teeth	Adults — Line 19 (2100) Children — Line 19 (2300)	—

DOI: https://doi.org/10.17816/DD530656

Table 4. Ending

Field of interest in the previous Form	Line of the previous Form	Field of interest in the updated Form	Line of the updated Form	Comment
Kidneys, urinary system	Line 14 (2000)	Kidneys, urinary system	Adults — Line 20 (2100) Children — Line 20 (2300)	—
Breast	Line 15 (2000)	Breast	Adults — Line 21 (2100) Children — Line 21 (2300)	—
Of these, due to preventive procedures	Line 16 (2000)	Including through preventive procedures (from line 21)	Adults — Line 22 (2100) Children — Line 22 (2300)	Column 7, "Contrast-enhanced computer tomography," for this line cannot be completed
Absent	Absent	Thorax + abdomen	Adults — Line 23 (2100) Children — Line 23 (2300)	—
Absent	Absent	Thorax + abdomen + pelvis	Adults — Line 24 (2100) Children — Line 24 (2300)	—
Absent	Absent	Abdomen + pelvis	Adults — Line 24 (2100) Children — Line 24 (2300)	—
Others	Line 17 (2000)	Others	Adults — Line 26 (2100) Children — Line 26 (1300)	Computed tomography of the whole body is performed as part of fluoroscopic diagnostics
Total	Line 18 (2000)	Total	Adults — Line 27 (2100) Children — Line 27 (2300)	-

of the Russian Federation,[15] all interventional examinations are divided into four subgroups: intravascular (angiography and endovascular procedures) and extravascular (surgical procedures guided by medical imaging), diagnostic (imaging only), and therapeutic (X-ray-guided surgery).

Columns 8–11 present all interventional procedures performed using mobile interventional machines in X-ray operating rooms, X-ray rooms, and outside specially equipped rooms (e.g., operating rooms, treatment rooms, and emergency departments).

Criteria for imaging classification are provided in Federal Statistical Monitoring Form No. 30, "Data on a healthcare organization," approved by Rosstat Order No. 985 on December 27, 2022.[16]

Columns 8–11 present information on radiology-guided interventional (extravascular) and endovascular interventions performed for diagnostic (columns 8 and 9) and treatment (columns 10 and 11) purposes. This section also includes information on intravenous contrast examinations.

Intravascular examinations (columns 8 and 10) are radiology-guided examinations of blood vessels using minimally invasive instruments. These include examinations, such as aortography, cavagraphy, phlebography, arteriography, angiocardiography, coronary angiography, lymphography, angioplasty, endovascular techniques, embolization, recanalization, bypass surgery, and vascular dilatation.

Extravascular examinations (columns 9 and 11) include any radiology-guided examinations of internal organs using minimally invasive instruments. These include procedures such as cystography, cholangiodrainage, nephrostomy, lithotripsy, urography, stenting of the kidneys and ureter, hysterosalpingography, arthroscopy, osteosynthesis, vertebroplasty, kyphoplasty, and installation of an intramedullary pin.

Other

Column 12 presents information on examinations not included in columns 3–11.

In line with the anatomical area of interest, information on osteodensitometry is presented in the "Other" column. Lines 23–25 present information on combined examinations

[15] Order of Rosstat No. 863 dated December 30, 2020 (as amended on December 20, 2021) on approval of federal statistical monitoring forms with the Form completion instructions for the Ministry of Health of the Russian Federation to organize federal statistical monitoring in healthcare. Federal statistical monitoring form No. 30 Data on a medical organization. Link: https://www.consultant.ru/document/cons_doc_LAW_373430/d752954a35641c33df844c2e2d910dcb3154d0a2/.

[16] Order of Rosstat No. 985 dated December 27, 2022 on approval of federal statistical monitoring forms with the Form completion instructions for the Ministry of Health of the Russian Federation to organize federal statistical monitoring in healthcare. Link: https://normativ.kontur.ru/document?moduleId=1&documentId=439986.

of two or more anatomical areas. In this case, these types of examinations should be considered only in lines 23–25 without being duplicated in lines 01–22.

Radionuclide diagnostics

Significant changes have been made in Section 3, "Information on radionuclide examinations." The number of examinations has increased significantly from 10 in the previous Form to 20 in the updated one.

Tables 3100 and 3200 should provide data on the number of radionuclide examinations performed during the reporting year and collective doses received by pediatric and adult patients. The number of radionuclide examinations in columns 3–6 of Tables 3100 and 3200 should be interpreted as the number of patients who have received radiopharmaceutical agents. Regardless of the number of consecutive scans (measurements), they are all treated as a single examination.

The following recommendations for completing the Form (listing types of examinations) will help in assigning an examination to the appropriate group:

- The "Skeleton" line includes bone scintigraphy.
- The "Three-phase examination" line includes three-phase examinations of soft tissues and bones.
- The "Liver/spleen" line includes dynamic and static examinations of the liver and spleen.
- The "Thyroid (Tc)" line includes thyroid examinations using ^{99m}Tc-labeled radiopharmaceuticals.
- The "Thyroid gland (I)" line includes thyroid gland examinations using ^{123}I-labeled radiopharmaceuticals.
- The "Parathyroid gland" line contains examinations of the parathyroid gland (if an additional examination of the thyroid gland is performed, it is included in the corresponding line "Thyroid gland," i.e., line 04 or 05).
- The "Neuroendocrine system (I)" line includes examinations with ^{123}I-MIBG.
- The "Brain" line includes brain examinations and brain perfusion examinations.
- The "Lungs" line includes lung perfusion examinations and lung ventilation examinations.
- The "Heart" line includes examinations of the myocardium, including those with functional tests, examinations of the sympathetic nervous system of the myocardium, and radionuclide ventriculography.
- The "Lymphatic system" line includes examinations of the lymphatic system, excluding examination of sentinel nodes.
- The "Lymphatic sentinel nodes" line includes examinations of lymphatic sentinel nodes.
- The "Kidneys (Tc)" line includes renography and dynamic and static examinations of kidneys using ^{99m}Tc-labeled radiopharmaceuticals.
- The "Kidneys (I)" line includes dynamic and static examinations of kidneys using ^{123}I-labeled radiopharmaceuticals.
- The "Whole body" line includes examinations of the whole body to detect inflammatory or oncological lesions, including PET/CT studies.
- The "Examinations using tumorotropic radiopharmaceuticals" line includes examinations with tumorotropic radiopharmaceuticals, excluding PET/CT scans.
- The "Angiography and phlebography" line includes radionuclide angiography and phlebography.
- The "Gastrointestinal tract" line includes stomach, esophagus, and intestines examinations.
- The "Other" line includes examinations not included in lines 01–18.

For hybrid PET/CT and SPECT/CT examinations, the number of examinations should be recorded in column 3, the collective radiopharmaceutical dose should be recorded in column 7, and the CT scanning dose should be recorded in column 8. Patient radiation doses for each examination are assessed by a healthcare organization in accordance with MU 2.6.1.3700-21.[17] The instructions for most radiopharmaceuticals used in the Russian Federation include dose coefficient values based on a patient's age.

RADIATION-HYGIENIC CERTIFICATION

Form 3-DOZ is the information basis for an organization's radiation-hygienic certification. The procedure for transferring data from the Form to the organization's radiation-hygienic passport is provided in Table 5.

CONCLUSION

In 2022, many years of updating Form No. 3-DOS were completed. The updated version of this Form contributes significantly to the information collected on the structure of diagnostic radiology activities and collective doses associated with medical exposure. This Form allows us to collect information about high-dose radiological examinations, such as multiphase CT with intravenous contrast, CT scans of several anatomical areas, hybrid examinations (PET/CT and SPECT/CT), and the entire range of interventional and radionuclide procedures. Because these examinations are associated with high individual patient doses (>20 mSv per procedure), this helps distinguish these examinations from the general nomenclature.

For the first time in Russian (and foreign) practice, obtaining information on radiation doses and the structure of diagnostic procedures for pediatric patients is possible. Requirements

[17] Guidelines MU 2.6.1.3700-21 "Evaluation and accounting of effective doses for patients when conducting radionuclide diagnostic examinations." Link: https://base.garant.ru/403589750/.

Table 5. The procedure for completing the radiation-hygienic passport of an organization based on the data from updated Form 3-DOZ

Types of procedures	Number of procedures for the reporting year, no. per year (sum of values from Tables 1200 + 1400 + 2200 + 2400, except for radionuclide examinations)	Average individual dose, mSv/procedure	Collective dose, person-Sv/year (sum of values from Tables 1100 + 1300 + 2100 + 2300, except for radionuclide research)	Measured doses, %
Fluorographic	Line 02, column 3 + Line 02, column 4	Collective dose/ number of procedures × 1,000	Line 02, column 3 + Line 02, column 4	Sum of values from Tables 2200 + 2400/sum of values from Tables 1200 + 1400 + 2200 + 2400
Radiographic	Line 27, column 3 + Line 27, column 4 — (Line 02, column 3 + Line 02, column 4)	Collective dose/ number of procedures × 1,000	Line 27, column 3 + Line 27, column 4 — (Line 02, column 3 + Line 02, column 4)	Sum of values from Tables 2200 + 2400/sum of values from Tables 1200 + 1400 + 2200 + 2400
Fluoroscopic	Line 27, column 5	Collective dose/ number of procedures × 1,000	Line 27, column 5	Sum of values from Tables 2200 + 2400/sum of values from Tables 1200 + 1400 + 2200 + 2400
CT scan	Line 27, column 6 + Line 27, column 7	Collective dose/ number of procedures × 1,000	Line 27, column 6 + Line 27, column 7	Sum of values from Tables 2200 + 2400/sum of values from Tables 1200 + 1400 + 2200 + 2400
Special examinations	Sum of rows 27, columns 8–11	Collective dose/ number of procedures × 1,000	Sum of rows 27, columns 8–11	Sum of values from Tables 2200 + 2400/sum of values from Tables 1200 + 1400 + 2200 + 2400
Radionuclide examinations	Tables 3100 + 3200 Line 20, column 6	Collective dose/ number of procedures × 1000 or Line 20, column 11	Tables 3100 + 3200 Line 20, column 10	—
Others	Line 27, column 12	Collective dose/ number of procedures × 1,000	Line 27, column 12	Sum of values from Tables 2200 + 2400/sum of values from Tables 1200 + 1400 + 2200 + 2400

for submitting 3-DOZ forms at the organizational and subject levels remained unchanged. The implemented changes will significantly increase the potential of Form No. 3-DOZ to analyze medical exposure levels in the Russian Federation population and make management decisions.

Due to the significant changes, specialists from the Research Institute of Radiation Hygiene are developing new software for completing Form No. 3-DOZ. Detailed instructions for using new software will be presented by the authors in the next paper.

ADDITIONAL INFORMATION

Funding source. The article was performed within framework of project "Development and improvement of dose data collection methods for patients undergoing X-ray examinations in the Russian Federation considering the approvement of new version of form № 3-DOZ" and part of the research and development effort titled "Scientific advances in medical, technological and organizational aspects of radiation safety in health care" (USIS No. №123031500006-9) in accordance with the Order No. 1196 dated December 21, 2022 "On approval of state assignments funded by means of allocations from the budget of the city of Moscow to the state budgetary (autonomous) institutions subordinate to the Moscow Health Care Department, for 2023 and the planned period of 2024 and 2025" issued by the Moscow Health Care Department.

Competing interests. The authors declare that they have no competing interests.

Authors' contribution. All authors made a substantial contribution to the conception of the work, acquisition, analysis, interpretation of data for the work, drafting and revising the work, final approval of the version to be published and agree to be accountable for all aspects of the work. A.V. Vodovatov developed design of the study, determined aims and objectives, prepared draft of the manuscript and presented the final version of manuscript for submission; L.A. Chipiga developed the changes in the structure of data on diagnostic nuclear medicine in form № 3-DOZ, prepared sections of manuscript on nuclear

medicine; A.A. Bratilova performed analysis of the currant state of form № 3-DOZ, edited the draft versions of the manuscript; P.S. Druzhinina developed the changes in the structure of data on computed tomography in form № 3-DOZ, prepared sections of manuscript on computed tomography; I.G. Shatskiy developed the changes in the structure of data on pediatric patients in form № 3-DOZ, prepared sections of manuscript on pediatric exposure; A.V. Petryakova developed the changes in the structure of data on diagnostic nuclear medicine in form № 3-DOZ, prepared sections of manuscript on nuclear medicine; S.S. Sarycheva developed the changes in the structure of data on interventional examinations in form №3-DOZ, prepared sections of manuscript on interventional examinations; A.M. Biblin was responsible for the management of the study, edited draft versions of the manuscript; Rustam R. Akhmatdinov, Ruslan R. Akhmatdinov prepared section on the changes in software; Yu.V. Kapyrina developed the changes in the structure of data on interventional examinations in form №3-DOZ, prepared sections of manuscript on interventional examinations; I.V. Soldatov developed approaches for harmonization of form №3-DOZ with statistical form of the Ministry of Healthcare; Z.A. Lantukh developed approaches for harmonization of form №3-DOZ with statistical form of the Ministry of Healthcare, edited draft version of manuscript; V.G. Puzyrev developed approaches for harmonization of form №3-DOZ with statistical form of the Ministry of Healthcare; S.A. Ryzhov performed literature review, edited draft version of manuscript.

REFERENCES

1. Onischenko GG, Popova AYu, Romanovich IK, et al. Modern principles of the radiation protection from sources of ionizing radiation in medicine. Part 2: radiation risks and development of the system of radiation protection. *Radiatsionnaya Gygiena*. 2017;10(3):7–17. (In Russ). doi: 10.21514/1998-426X-2017-10-3-7-17

2. Ryzhov SA, Vodovatov AV, Soldatov IV, et al. Proposals for Improving the System of Radiation Safety in Medical Exposure. Part 1. Analysis of information contained in state reporting forms and information databases in Moscow. *Radiatsionnaya Gygiena*. 2022;15(3):92–109. (In Russ). doi: 10.21514/1998-426X-2022-15-3-92-109

3. Simonova VG. Analysis of the radiation levels of the population of the Orel region during X-ray radiological studies. *Sanitarniy Vrach*. 2023;(3):186–192. doi: 10.33920/med-08-2303-07

4. Barkovsky AN, Kormanovskaya TA, Vodovatov AV, et al. Management of data on the exposure of the Russian population for the State report on evaluation of sanitary-epidemiological well-being of the public in the Russian Federation. *Radiatsionnaya Gygiena*. 2022;15(4):134–141. (In Russ). doi: 10.21514/1998-426X-2022-15-4-134-141

5. Rospotrebnadzor. On the state of sanitary-epidemiological wellbeing of public in the Russian Federation in 2020: State report. Moscow: Federal Service for Surveillance on Consumer Rights Protection and Human Wellbeing; 2021. 256 p. (In Russ).

6. Barlovsky AN, Akhmatdinov RR, Akhmatdinov RR, et al. Radiation situation on the territory of the Russian Federation in 2021: Reference book. Saint Petersburg; 2022. 76 p. (In Russ).

7. Vodovatov AV, Chipiga LA, Bratilova AA, et al. Update of the federal governmental statistical surveillance form № 3-DOZ "Data on patient doses from medical X-ray examinations". Perquisites for the update. *Radiatsionnaya Gygiena*. 2023;16(2):126–136. (In Russ). doi: 10.21514/1998-426X-2023-16-2-126-136

8. Center for Diagnostics and Telemedicine [Internet]. 3-DOZ report. (In Russ). Available from: https://3doz.telemedai.ru/. Accessed: 04.05.2023.

9. Druzhinina YuV, Tolkachev KV, Ryzhov SA, et al. Certificate of state registration of the database No. 2021622191. Data of Dicom files of X-ray examinations conducted on computed tomographs: No. 2021622060: application 06.10.2021: publ. 19.10.2021; applicant State Budgetary Institution of Healthcare of the city of Moscow "Scientific and Practical Clinical Center for Diagnostics and Telemedicine Technologies of the Department of Healthcare of the City of Moscow". (In Russ).

10. Vodovatov AV, Golikov VYu, Kalnitsky SA, et al. Evaluation of levels of exposure of adult patients from common radiographic examinations in the Russian Federation in 2009–2014. *Radiatsionnaya Gygiena*. 2017;10(3):66–75. (In Russ). doi: 10.21514/1998-426X-2017-10-3-66-75

11. Balonov MI, Golikov VYu, Vodovatov AV, et al. Scientific foundations of radiation protection in modern medicine. Vol. 1. Radiation diagnostics. Ed. by M.I. Balonov. Saint Petersburg; 2019. 320 p. (In Russ).

12. Federal Handbook of Instrumental Diagnostic Studies. (In Russ). Available from: https://fnsi2.rt-eu.ru/dictionaries/1.2.643.5.1.13.13.11.1471/passport/2.17. Accessed: 04.05.2023.

СПИСОК ЛИТЕРАТУРЫ

1. Онищенко Г.Г., Попова А.Ю., Романович И.К., и др. Радиационно-гигиеническая паспортизация и ЕСКИД — информационная основа принятия управленческих решений по обеспечению радиационной безопасности населения Российской Федерации. Сообщение 1. Основные достижения и задачи по совершенствованию // Радиационная гигиена. 2017. Т. 10, № 3. С. 7–17. doi: 10.21514/1998-426X-2017-10-3-7-17

2. Рыжов С.А., Водоватов А.В., Солдатов И.В., и др. Предложения по совершенствованию системы радиационной безопасности при медицинском облучении. Часть 1. Анализ информации, содержащейся в государственных отчетных формах и информационных базах данных, на примере города Москвы // Радиационная гигиена. 2022. Т. 15, № 3. С. 92–109. doi: 10.21514/1998-426X-2022-15-3-92-109

3. Симонова В.Г. Анализ уровней облучения населения Орловской области при рентгенорадиологических исследованиях // Санитарный врач. 2023. № 3. С. 186–192. doi: 10.33920/med-08-2303-07

4. Барковский А.Н., Кормановская Т.А., Водоватов А.В., и др. Формирование блока данных об уровнях облучения населения России для включения в Государственный доклад о состоянии санитарно-эпидемиологического благополучия населения в Российской Федерации // Радиационная гигиена. 2022. Т. 15, № 4. С. 134–141. doi: 10.21514/1998-426X-2022-15-4-134-141
5. Роспотребнадзор. О состоянии санитарно-эпидемиологического благополучия населения в Российской Федерации в 2020 году: Государственный доклад. Москва: Федеральная служба по надзору в сфере защиты прав потребителей и благополучия человека, 2021. 256 с.
6. Барковский А.Н., Ахматдинов Р.Р., Ахматдинов Р.Р., и др. Дозы облучения населения Российской Федерации в 2020 году: информационный сборник. Санкт-Петербург, 2021. 80 с.
7. Водоватов А.В., Чипига Л.А., Братилова А.А., и др. Актуализация формы федерального государственного статистического наблюдения № 3-ДОЗ «Сведения о дозах облучения пациентов при проведении медицинских рентгенорадиологических исследований». Предпосылки к переработке // Радиационная гигиена. 2023. Т. 16, № 2. С. 126–136. doi: 10.21514/1998-426X-2023-16-2-126-136
8. Центр диагностики и телемедицины [интернет]. Отчет 3-ДОЗ. Режим доступа: https://3doz.telemedai.ru/. Дата обращения: 04.05.2023.
9. Дружинина Ю.В., Толкачев К.В., Рыжов С.А., и др. Свидетельство о государственной регистрации базы данных № 2021622191. Данные Dicom-файлов рентгенологических исследований, проведенных на компьютерных томографах: № 2021622060: заявл. 06.10.2021: опубл. 19.10.2021; заявитель Государственное бюджетное учреждение здравоохранения города Москвы «Научно-практический клинический центр диагностики и телемедицинских технологий Департамента здравоохранения города Москвы».
10. Водоватов А.В., Голиков В.Ю., Кальницкий С.А., и др. Анализ уровней облучения взрослых пациентов при проведении наиболее распространенных рентгенографических исследований в Российской Федерации в 2009–2014 гг. // Радиационная гигиена. 2017. Т. 10, № 3. С. 66–75. doi: 10.21514/1998-426X-2017-10-3-66-75
11. Балонов М.И., Голиков В.Ю., Водоватов А.В., и др. Научные основы радиационной защиты в современной медицине. Т. 1. Лучевая диагностика / под ред. профессора М.И. Балонова. Санкт-Петербург, 2019. 320 с.
12. Федеральный справочник инструментальных диагностических исследований. Режим доступа: https://fnsi2.rt-eu.ru/dictionaries/1.2.643.5.1.13.13.11.1471/passport/2.17. Дата обращения: 04.05.2023.

AUTHORS' INFO

*** Aleksandr V. Vodovatov,** Cand. Sci. (Biol.),
Assistant Professor;
address: 8 Mira street, 197101 Saint Petersburg, Russia;
ORCID: 0000-0002-5191-7535;
eLibrary SPIN: 4560-8978;
e-mail: vodovatoff@gmail.com

Larisa A. Chipiga, Cand. Sci. (Tech),
Assistant Professor;
ORCID: 0000-0001-9153-3061;
eLibrary SPIN: 3920-7798;
e-mail: larisa.chipiga@gmail.com

Polina S. Druzhinina;
ORCID: 0000-0003-2921-067X;
eLibrary SPIN: 9003-3234;
e-mail: druzhininapauline@gmail.com

Ilya G. Shatskiy;
ORCID: 0000-0003-2809-0223;
eLibrary SPIN: 4905-3329;
e-mail: i.Shatskiy@niirg.ru

Anastasiya V. Petryakova;
ORCID: 0000-0003-2663-9091;
eLibrary SPIN: 1683-4733;
e-mail: nastya.petryakova@gmail.com

Svetlana S. Sarycheva;
ORCID: 0000-0002-4493-0280;
eLibrary SPIN: 5132-1416;
e-mail: svetlana2003@mail.ru

ОБ АВТОРАХ

*** Водоватов Александр Валерьевич,** канд. биол. наук,
доцент;
адрес: Россия, 197101, Санкт-Петербург, ул. Мира, д. 8;
ORCID: 0000-0002-5191-7535;
eLibrary SPIN: 4560-8978;
e-mail: vodovatoff@gmail.com

Чипига Лариса Александровна, канд. тех. наук,
доцент;
ORCID: 0000-0001-9153-3061;
eLibrary SPIN: 3920-7798;
e-mail: larisa.chipiga@gmail.com

Дружинина Полина Сергеевна;
ORCID: 0000-0003-2921-067X;
eLibrary SPIN: 9003-3234;
e-mail: druzhininapauline@gmail.com

Шацкий Илья Геннадьевич;
ORCID: 0000-0003-2809-0223;
eLibrary SPIN: 4905-3329;
e-mail: i.Shatskiy@niirg.ru

Петрякова Анастасия Валерьевна;
ORCID: 0000-0003-2663-9091;
eLibrary SPIN: 1683-4733;
e-mail: nastya.petryakova@gmail.com

Сарычева Светлана Сергеевна;
ORCID: 0000-0002-4493-0280;
eLibrary SPIN: 5132-1416;
e-mail: svetlana2003@mail.ru

* Corresponding author / Автор, ответственный за переписку

Artem M. Biblin;
ORCID: 0000-0002-3139-2479;
eLibrary SPIN: 7840-0144;
e-mail: a.biblin@niirg.ru

Rustam R. Akhmatdinov;
ORCID: 0000-0002-4151-5380;
eLibrary SPIN: 7379-4951;
e-mail: rust.akh@niirg.ru

Ruslan R. Akhmatdinov;
ORCID: 0009-0000-2300-6788;
eLibrary SPIN: 7255-4107;
e-mail: rusl.akh@niirg.ru

Yuliya N. Kapyrina;
ORCID: 0000-0002-1018-5200;
eLibrary SPIN: 4969-0394;
e-mail: kapirina-yuliya@yandex.ru

Anzhelika A. Bratilova;
ORCID: 0000-0002-6489-3974;
eLibrary SPIN: 3156-7214;
e-mail: bratilova@gmail.com

Ilya V. Soldatov;
ORCID: 0000-0002-4867-0746;
eLibrary SPIN: 4065-6048;
e-mail: SoldatovIV2@zdrav.mos.ru

Zoya A. Lantukh;
ORCID: 0000-0001-6623-9610;
eLibrary SPIN: 5486-6496;
e-mail: LantukhZA@zdrav.mos.ru

Viktor G. Puzyrev, MD, Cand. Sci. (Med.), Assistant Professor;
ORCID: 0000-0002-0185-3545;
eLibrary SPIN: 2727-0049;
e-mail: vgpuzyrev@mail.ru

Sergey A. Ryzhov;
ORCID: 0000-0002-0640-7368;
eLibrary SPIN: 6595-4011;
e-mail: mosrg@mail.ru

Библин Артем Михайлович;
ORCID: 0000-0002-3139-2479;
eLibrary SPIN: 7840-0144;
e-mail: a.biblin@niirg.ru

Ахматдинов Рустам Расимович;
ORCID: 0000-0002-4151-5380;
eLibrary SPIN: 7379-4951;
e-mail: rust.akh@niirg.ru

Ахматдинов Руслан Расимович;
ORCID: 0009-0000-2300-6788;
eLibrary SPIN: 7255-4107;
e-mail: rusl.akh@niirg.ru

Капырина Юлия Николаевна;
ORCID: 0000-0002-1018-5200;
eLibrary SPIN: 4969-0394;
e-mail: kapirina-yuliya@yandex.ru

Братилова Анжелика Анатольевна;
ORCID: 0000-0002-6489-3974;
eLibrary SPIN: 3156-7214;
e-mail: bratilova@gmail.com

Солдатов Илья Владимирович;
ORCID: 0000-0002-4867-0746;
eLibrary SPIN: 4065-6048;
e-mail: SoldatovIV2@zdrav.mos.ru

Лантух Зоя Александровна;
ORCID: 0000-0001-6623-9610;
eLibrary SPIN: 5486-6496;
e-mail: LantukhZA@zdrav.mos.ru

Пузырев Виктор Геннадьевич, канд. мед. наук, доцент;
ORCID: 0000-0002-0185-3545;
eLibrary SPIN: 2727-0049;
e-mail: vgpuzyrev@mail.ru

Рыжов Сергей Анатольевич;
ORCID: 0000-0002-0640-7368;
eLibrary SPIN: 6595-4011;
e-mail: mosrg@mail.ru

DOI: https://doi.org/10.17816/DD420053

Дозиомика в анализе медицинских изображений и перспективы её использования в клинической практике

В.А. Солодкий, Н.В. Нуднов, М.Е. Иванников, Э.С-А. Шахвалиева, В.М. Сотников, А.Ю. Смыслов

Российский научный центр рентгенорадиологии, Москва, Российская Федерация

АННОТАЦИЯ

Обоснование. В последние годы увеличивается количество статей с использованием термина «дозиомика», однако литературные обзоры на русском языке по данной теме отсутствуют.

Цель настоящего обзора — описать основные принципы дозиомики как направления радиомики и проанализировать исследования по оценке возможностей применения их в клинической практике.

Материалы и методы. Систематический поиск литературы был произведён в базе данных PubMed с поисковым запросом «dosiomics OR dosiomic», а также в базе данных eLibrary с поисковым запросом «дозиомика». По состоянию на апрель 2023 года были опубликованы 43 зарубежных исследования на тему использования дозиомики в клинической практике и одна отечественная работа с определением термина «дозиомика».

Результаты. Проанализированы 43 зарубежных исследования на тему использования дозиомики в клинической практике и 1 отечественная статья с определением термина «дозиомика». Проанализированные работы разделены на три группы согласно их тематике и составлены таблицы, описывающие результаты 27 исследований по прогнозированию клинических исходов.

Заключение. В настоящее время дозиомика является новым и перспективным направлением радиомики, применяемым в текстурном анализе медицинских изображений, связанных с лучевым лечением онкологических больных. Дозиомика может способствовать развитию более персонализированного подхода к планированию лучевой терапии, прогнозированию лучевых повреждений нормальных тканей и диагностике рецидивов.

Ключевые слова: дозиомика; радиомика; лучевая терапия; машинное обучение; искусственный интеллект; текстурный анализ; постлучевой пневмонит.

Как цитировать:

Солодкий В.А., Нуднов Н.В., Иванников М.Е., Шахвалиева Э.С-А., Сотников В.М., Смыслов А.Ю. Дозиомика в анализе медицинских изображений и перспективы её использования в клинической практике // *Digital Diagnostics.* 2023. Т. 4, № 3. С. 340–355. DOI: https://doi.org/10.17816/DD420053

Рукопись получена: 15.05.2023 **Рукопись одобрена:** 15.06.2023 **Опубликована:** 30.08.2023

DOI: https://doi.org/10.17816/DD420053

Dosiomics in the analysis of medical images and prospects for its use in clinical practice

Vladimir A. Solodkiy, Nikolay V. Nudnov, Mikhail E. Ivannikov, Elina S-A. Shakhvalieva, Vladimir M. Sotnikov, Aleksei Yu. Smyslov

Russian Scientific Center of Roentgenoradiology, Moscow, Russian Federation

ABSTRACT

BACKGROUND: In recent years, there has been a notable increase in the number of articles using the term “dosiomics”. However, there are no literature reviews on this topic in the Russian language.

AIM: This study aims to describe the basic principles of dosiomics as a derivative of radiomics and to analyze studies devoted to assessing the possibilities of its application in clinical practice.

MATERIALS AND METHODS: A systematic literature search was performed in the PubMed database using the search query “dosiomics OR dosiomic”, and in the eLibrary database using the search query “dosiomics”. By April 2023, 43 foreign articles and 1 Russian article had been published.

RESULTS: The analysis encompassed 43 foreign studies investigating the use of dosiomics in clinical practice, alongside one Russian article that provided a definition of the term “dosiomics”. The analyzed papers were divided into three groups according to their subject matter, and two tables describing the results of 27 studies on the prediction of clinical outcomes were created.

CONCLUSION: Currently, dosiomics is a new and promising derivative of radiomics used in the textural analysis of medical images associated with radiation treatment of cancer patients. Dosiomics can contribute to the development of a more personalized approach to the planning of radiotherapy, the prediction of radiation damage of normal tissues, and the diagnosis of recurrence.

Keywords: dosiomics; radiomics; radiation therapy; machine learning; artificial intelligence; texture analysis; radiation pneumonitis.

To cite this article:
Solodkiy VA, Nudnov NV, Ivannikov ME, Shakhvalieva ES-A, Sotnikov VM, Smyslov AYu. Dosiomics in the analysis of medical images and prospects for its use in clinical practice. *Digital Diagnostics.* 2023;4(3):340–355. DOI: https://doi.org/10.17816/DD420053

Received: 15.05.2023 **Accepted:** 15.06.2023 **Published:** 30.08.2023

DOI: https://doi.org/10.17816/DD420053

医学图像分析中的Dosiomics及其在临床实践中的应用前景

Vladimir A. Solodkiy, Nikolay V. Nudnov, Mikhail E. Ivannikov,
Elina S-A. Shakhvalieva, Vladimir M. Sotnikov, Aleksei Yu. Smyslov

Russian Scientific Center of Roentgenoradiology, Moscow, Russian Federation

简评

论证。近年来，使用“dosiomics”一词的文章数量不断增加，但却没有关于这一主题的俄文文献综述。

本综述的目的是描述dosiomics作为放射组学分支的基本原理，并分析相关研究，以评估其在临床实践中的潜在应用。

材料和方法。在PubMed数据库中以“dosiomics OR dosiomic”为检索词进行了系统文献检索，在eLibrary数据库中以“дозиомика”（“dosiomics”）为检索词进行了系统文献检索。截至2023年4月，共发表了43项关于在临床实践中使用dosiomics的国外研究和1篇定义“dosiomics”一词的国内文章。

结果。我们分析了43篇关于在临床实践中使用dosiomics的国外研究和1篇定义“dosiomics”一词的国内文章。我们将所分析的文章按主题分为三组，并将27项关于预测临床结果的研究结果编制成表格。

结论。目前，dosiomics是放射组学的一个新的有前途的分支，应用于与癌症患者放射治疗有关的医学图像的纹理分析。Dosiomics可能有助于开发更个性化的放疗计划、预测对正常组织的辐射损伤和诊断复发。

关键词：dosiomics；放射组学；放射治疗；机器学习；人工智能；纹理分析；放疗后肺炎。

引用本文：
Solodkiy VA, Nudnov NV, Ivannikov ME, Shakhvalieva ES-A, Sotnikov VM, Smyslov AYu. 医学图像分析中的Dosiomics及其在临床实践中的应用前景. *Digital Diagnostics.* 2023;4(3):340–355. DOI: https://doi.org/10.17816/DD420053

收到：15.05.2023 **接受：**15.06.2023 **发布日期：**30.08.2023

INTRODUCTION

Radiation therapy is one of the most widely used treatments in cancer patients. Radiation therapy can be performed alone or in conjunction with surgery or chemotherapy, although there is a substantial risk of developing post-radiation problems [1]. As a result, toxicity assessment is an important aspect of radiation therapy planning and delivery [2].

Personalized dose selection is one approach to addressing this problem (e.g., increasing the dose for low-risk patients or optimizing treatment for patients with a high risk of complications [2]). At the planning stage of radiation therapy, prediction models are built to assess the risk of radiation damage to healthy organs and tissues based on various parameters.

Radiomics has recently gained popularity as a means of analyzing radiological data. This machine learning–based method for extracting quantitative characteristics from medical images (typically describing shape, intensity, and texture) may be used to develop prediction models [3].

Radiomics is commonly used to diagnose chest disorders such as nodules and cancer, obstructive and restrictive diseases, and infiltrative lung diseases [4–7]. Furthermore, radiomics has been successfully used to predict treatment side effects, such as pneumonitis associated with radiation therapy and immunotherapy, and distinguish between iatrogenic lung injury and tumor recurrence [7]. Radiomics has gained popularity in predicting the COVID-19 course [8–10]. Radiomics can help in diagnosis, prognosis, treatment, follow-up, and monitoring treatment response [11].

In addition to radiomics, the concept of "dosiomics" is becoming more popular. This radiomics area is used for the 3D distribution of radiation therapy doses to extract useful data for forecasting radiation therapy [12–14]. An integrated approach is becoming more popular for predicting post-radiation damage based on dosiomics, radiomics, and clinical data [13].

This study aims to describe the fundamental principles of dosiomics as a subfield of radiomics and examine a study that evaluates the potential for its use in clinical practice.

Search and inclusion criteria for literature sources

A systematic literature search was performed using a PubMed database with the search term "dosiomics OR dosiomic" and an eLibrary database with the search term "dosiomics." By April 2023, 43 global papers have been published.

Therefore, 43 global studies evaluating the use of dosiomics in clinical practice and one Russian study defining the term "dosiomics" were analyzed [15]. The papers were divided into three groups based on their topics, and a summary table was compiled describing 27 studies according to their value for clinical outcome prediction.

BASICS OF RADIOMICS AND DOSIOMICS: METHODS FOR EXTRACTING TEXTURE CHARACTERISTICS FROM COMPUTED TOMOGRAPHIC IMAGES

Radiomics is a technology to establish a relationship between multiple quantitative characteristics extracted from medical images of organs and tissues and the clinical picture of the disease using multivariate statistical analysis [16].

Radiomics features define tissue pictures' textural characteristics to identify image biomarkers and develop predictive rules [17].

Figure 1 presents steps to extract and analyze radiomics features using lung computed tomography (CT) as an example. The area of interest is divided after a radiological assessment to isolate the lesion from the surrounding healthy tissue. For large and spatially heterogeneous lesions, 3D segmentation can provide more information. Segmentation can be done manually, semi-automatically, or automatically. The inaccessible radiomics features for visual assessment are

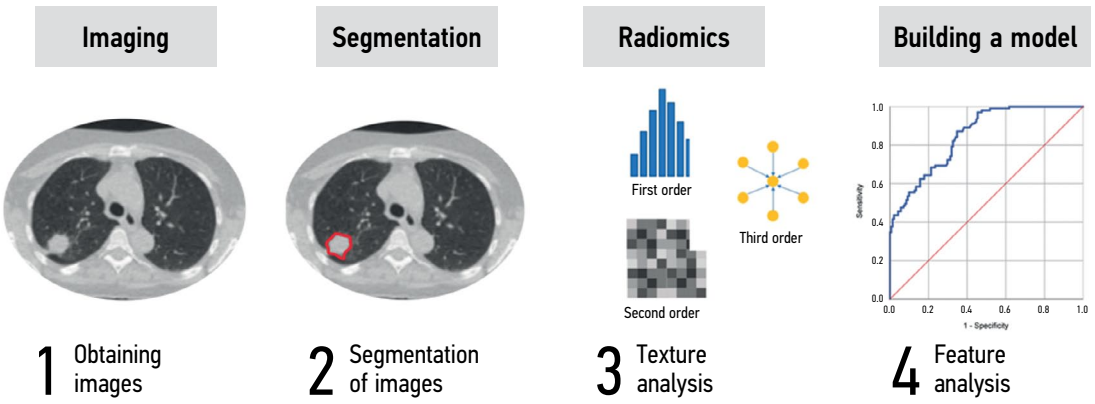

Fig. 1. Stages of extraction and analysis of radiomics features.

then calculated using mathematical techniques. First-order statistics, gray-level adjacency, and homogeneity matrices are common parameters. The final stage involves reducing the sample size, statistical analysis, and selecting the most significant features while removing associated values to construct a decision rule using machine learning methods [18].

Key radiomics features

Radiomics features are extracted from medical images using the open-source PyRadiomics package. Radiomics uses two main groups of parameters: first-order statistics and texture matrices of adjacency and uniformity. These include the following matrices [16–18]:

- Gray-Level Co-occurrence Matrix (GLCM)
- Gray-Level Run-Length Matrix (GLRLM)
- Gray-Level Size Zone Matrix (GLSZM)
- Neighboring Gray Tone Difference Matrix (NGTDM)
- Gray-Level Dependence Matrix (GLDM)

First-order statistics use a pixel intensity histogram in a region of interest to characterize gray frequency distribution without considering spatial relationships between pixels [19]. These features are known as first-order statistics because they are based on examining a single pixel or voxel without considering the surrounding areas' intensity.

Higher-order statistical measures consider the relative spatial location of voxels, allowing them to define texture characteristics. The most common are halftone adjacency and uniformity matrices (GLCM, GLRLM, and GLSZM). NGTDM and GLDM are less common.

GLCM is a second-order histogram of gray levels [19]. It captures spatial relationships between pixels or voxels with predefined gray-level intensities in different directions (horizontal, vertical, or diagonal for 2D analysis and 13 directions for 3D analysis) and a predefined distance between pixels or voxels (Figure 2; hereafter, the principle of calculating matrix parameters in 2D space will be presented) [20].

GLRLM is a matrix described by Galloway. It represents the spatial distribution of vectors of successive pixels with the same gray-level in one or more directions in two or three dimensions (Figure 3).

GLSZM quantitatively describes image areas with the same gray-level, consisting of adjacent voxels. According to Thibault et al. [23], GLSZM is similar to GLRLM, but the first matrix is based on the calculated number of groups (so-called zones) of interconnected neighboring pixels or voxels with the same gray-level (Figure 4). A more uniform texture will result in a wider, flatter matrix. GLSZM cannot be calculated for different directions but can be calculated for varied distances between pixels or voxels in the neighborhood. GLSZM parameters can be determined in two (eight nearby pixels) or three (26 neighboring voxels) dimensions [19].

For NGTDM, the texture characteristics of a given matrix represent the intensity difference between adjacent voxels [24].

GLDM quantifies gray-level dependencies in an image [19, 25].

Dosiomics

Dosiomics is a relatively new area of radiomics. It is a textural study of radiation dose distribution used in radiation therapy planning.

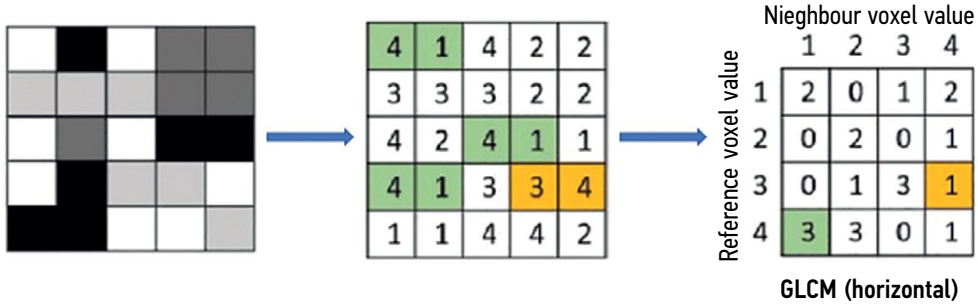

Fig. 2. Example of calculating GLCM parameters: three pairs of neighboring pixels with intensity levels 4 and 1 (highlighted in green).

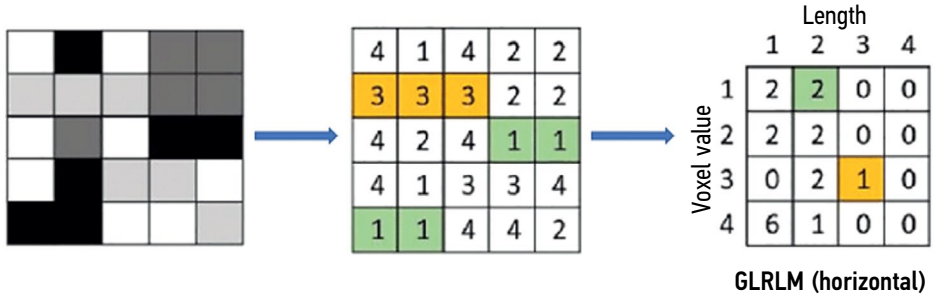

Fig. 3. An example of calculating GLRLM parameters: there is one group of three pixels with the same gray-level (3), located sequentially (highlighted in orange).

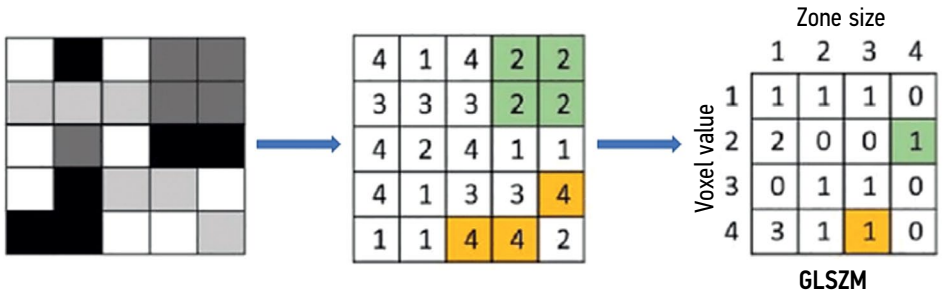

Fig. 4. Example of calculating GLSZM parameters: there is one zone consisting of four pixels with a gray-level of 2 (highlighted in green).

The first scientific articles originate from 2018 when Gabry et al. [26] used this approach to predict xerostomia after radiation therapy in 15 head and neck cancer patients.

The process of obtaining dosiomics features includes two steps.

1. Radiation therapy 3D planning uses a sequence of parallel X-ray CT images, with the anatomical structures and target volume defined manually or using an automatic mathematical contouring program in the planning system [27, 28].
2. After acquiring 3D dose distribution models, they are processed using radiomics masks with open code implemented in Python, and quantitative textural parameters of an area of interest are generated. These parameters, which include the textural qualities outlined above (first-order statistics with adjacency and uniformity matrices), are retrieved from dose distribution models, and are referred to as dosiomics features.

Rossi et al. [29] reported a textural analysis of a 3D radiation dose distribution model in the rectal area. After mapping the radiation dose distribution, the area of interest is treated with radiomics masks, and textural characteristics are extracted. Figure 5 shows dosiomics features extracted from the area of interest.

Because the studied data array often has a disproportionately large number of input variables, there is the problem of reducing the dimensions of the attribute space. One of the most prominent guidelines for the relationship between the number of features and observations is the 20 EPV rule. EPV (events per independent variable) is defined as the number of occurrences per independent variable, calculated by adding the number of patients in a smaller subgroup to the number of input characteristics used when creating a prediction model [30].

The next step is to reduce the attribute space's dimensions using one of several methods, such as the

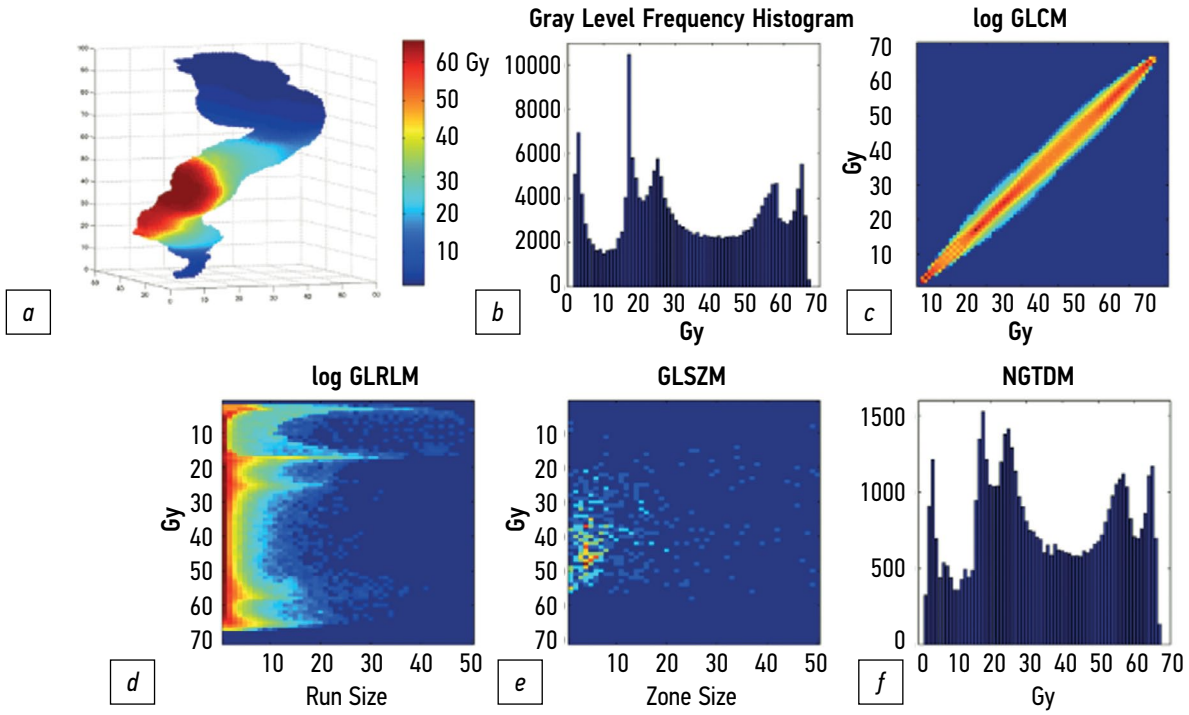

Fig. 5. Texture analysis of a 3D model of radiation dose distribution to the rectal area: (*a*) 3D dose distribution in the rectum, (*b*) gray-level frequency histogram, (*c*) GLCM, (*d*) GLRLM, (*e*) GLSZM, and (f) NGTDM.

principal component method, linear discriminant analysis, and random forest method (importance function) [31, 32]. Then, using machine learning approaches, eliminate linked values to construct a decision rule [18]. At the final stage, multivariate statistical analysis is undertaken using a forecasting model chosen based on the purpose of the examination. The accuracy of binary classification models is often assessed using a receiver operating characteristic (ROC) and denoted as the area under the curve (AUC) in studies. The curve uses sensitivity (the fraction of genuine positives) and specificity (the proportion of true negatives). The concordance index (C-index) is the most commonly used metric for evaluating the performance of survival models. Based on the Kendall correlation coefficient, this measures the rank correlation between predicted risk scores and observed scores at individual points in time.

USE OF DOSIOMICS IN CLINICAL PRACTICE

According to reviewed foreign literature, three main areas of research can be distinguished: the use of dosiomics features to predict radiation damage to healthy tissues, prediction of tumor relapses, and evaluation of the stability as well as reproducibility of dosiomic signs. Some literature reviews were also prepared; for example, groups of authors led by Sun [33] and Zhang [34] described dosiomics as a new direction in texture analysis of medical images.

Use of dosiomics features in predicting radiation damage to healthy tissues

All of these studies try to develop models (rules) for predicting cases of radiation damage in cancer patients. Most papers compared the efficacy of prognostic rules based on various types of data such as clinical factors, dose-volume histograms (DVH), indicators of radiobiological models of tumor control probability (TCP) and normal tissue complication probability (NTCP), dosiomics, radiomics, and dosimetry features.

The parameters researchers use, their combinations, and the statistical methods vary significantly from study to study. Most studies examined the ability to predict post-radiation pneumonitis in cancer patients after radiation therapy. According to the literature, the incidence of post-radiation pneumonitis ranges widely (from 5% to 58%) and it is one of the most prevalent consequences after lung cancer radiation therapy [1]. The most extensive research in this area was conducted by Zhang et al. in 2023 [35], using data from 314 retrospectively collected and 35 prospectively enrolled patients with lung cancer. The models used radiomics, dosiomics, DVHs, and clinical factors. In the external testing sample, a decision rule constructed by integrating radiomics, dosiomics, and clinical data showed the best predictive ability with an AUC of 0.855 (95% confidence interval, 0.719–0.990) [35]. According to the findings of this study, models based on integrating various parameters are more accurate.

Other researchers confirmed that a model based on a combination of dosiomics and radiomics features has the best predictive ability. Similar results were obtained by Li et al. [36, 37], who extracted metrics from specifically segmented functional areas of the lung, and Huang et al. [2]. Hence, a model by Zhou et al. [38], based on the distribution of equivalent radiation dose, demonstrated high predictive ability with the AUC of 0.799 in the test set. It should be noted that Kraus et al. [39] used a predictive model with the same combination of features, but it was based on the distribution of absorbed radiation dose, which proved to be more effective. Such differences may be related to the low reproducibility and stability of dosiomics features.

Some scientific papers have compared models based on dosimetry and dosiomics features. In studies by groups led by Puttanawarut [40] and Liang [13, 41], models based on dosiomics indicators were more effective, whereas in the study by Adachi et al. [42], the combination of dosiomics and dosimetry indicators was also clinically significant. Models integrating radiomics and dosiomics indicators have demonstrated great accuracy in predicting not only post-radiation pneumonitis but also additional post-radiation damage, such as severe weight loss (by more than 5% in 2 months), which is confirmed by Lee [43] and Han [44]. Han et al. developed a medical decision support system to help healthcare providers forecast severe weight loss more accurately. These results show that it is possible to implement decisive rules based on dosiomics in clinical practice. Zheng et al. [45] created a model for predicting acute radiation esophagitis in patients with lung cancer and obtained the highest area values under the ROC curve (0.801) using a combination of radiomics, dosiomics, and clinical features.

Ren et al. [46] showed higher efficiency of dosiomics-based decision rules than dosimetric models. Authors predicted post-radiation hypothyroidism in patients with nasopharyngeal carcinoma. Yang et al. [47] indicated radiation damage to the temporal lobe in individuals with a similar diagnosis. A model based on the patient's age, dosimetric, and dosiomic features showed the best result with a C-index of 0.794 in the external test set.

Rossi et al. [29] used clinical data, dose-volume histogram indicators, and dosiomics features to improve the prediction of late radiation therapy complications of bladder and rectum radiation therapy, such as nocturia, rectal bleeding, and fecal incontinence. Monti [48] study should also be mentioned. It evaluated the relationship between dosiomics and genomics features in developing post-radiation lymphopenia in 186 patients with non-small cell lung cancer after chemoradiation therapy. The authors suggest that the discovered relationships will help develop more effective personalized radiation therapy strategies.

The reviewed studies showed that using dosiomics features in models increases the area under the ROC curve, indicating the predictive value of these parameters.

Described studies evaluating the ability to predict radiation damage to normal tissues are presented in Table 1.

Prediction of tumor recurrence/progression

These studies use the same general concepts to forecast radiation damage. Kamezawa et al. [49] and Wu et al. [14] evaluated the ability to predict local recurrence of head and neck cancer. Dosiomics-based models were the most effective. A similar study was conducted by Wang et al. [50], who built overall survival prediction models using texture indices extracted from CT, positron emission tomography CT (PET-CT), and dose distribution maps for radiation therapy planning. In terms of forecasting performance, the combined model was the most effective.

Murakami [12] and Pirrone [51] used different approaches for predicting prostate cancer recurrence. The first study predicted biochemical relapse. It was found that a model integrating clinical and dosiomic variables was the most effective for this purpose. The local recurrence prediction model in the second trial was based on radiomics and dosiomics indices generated from physiologically effective dose distribution maps, CT, and PET-CT images.

Buizza et al. [52] and Morelli et al. [53] demonstrated the effectiveness of dosiomic models in predicting the local recurrence of skull base chordomas and sacral localization. Similar decision rules also showed a high C-index in a study by Cai et al. [54] evaluating the ability to predict the recurrence and metastasis of nasopharyngeal carcinoma. Combined model by Wang et al. [55] demonstrated that machine learning with dosiomics features has the potential to predict complete remission of rectal cancer after radiotherapy.

Before treatment, Lam et al. [56] evaluated CT and MRI scans of 135 patients with nasopharyngeal carcinoma to predict the acceptability of adaptive radiation therapy. This was the first study to use the term "contouromics," which refers to a method for defining intricate geometric relationships between four pairs of volumes of interest (VOI). The most accurate model was based on radiomics, with an AUC of 0.927 (95% confidence interval, 0.905–0.948).

As in the case of predicting radiation damage, these studies show the high accuracy of dosiomics-based models. Studies indicating relapse or progression of neoplasms are presented in Table 2.

Reproducibility of dosiomics features

The statistical models and methods used in this group of studies are quite different, yet they all share the problem of

Table 1. Studies to evaluate predicting radiation damage to normal tissues

Study	Predicted radiation damage	AUC model based on dosiomics	Model with the highest AUC
Zhang et al. [35]	Post-radiation pneumonitis	0.774	R + D + C – AUC = 0.855
Li et al. [36]	Post-radiation pneumonitis	—	R + Ds – AUC = 0.885
Li et al. [37]	Post-radiation pneumonitis	0.74	R + D – AUC = 0.88
Huang et al. [2]	Post-radiation pneumonitis	0.8462	R + D – AUC = 0.90
Zhou et al. [38]	Post-radiation pneumonitis	—	R + DVH – AUC = 0.805
Kraus et al. [39]	Post-radiation pneumonitis	0.70	R + D – AUC = 0.79
Puttanawarut et al. [40]	Post-radiation pneumonitis	0.71	D – AUC = 0.71
Liang et al. [13]	Post-radiation pneumonitis	0.782	D – AUC = 0.782
Liang et al. [41]	Post-radiation pneumonitis	0.782	AUC = 0.842
Adachi et al. [42]	Post-radiation pneumonitis	0.837	Ds + D – AUC = 0.846
Lee et al. [43]	Weight loss	—	R + D – AUC = 0.710
Han et al. [44]	Weight loss	—	R + D – accuracy = 0.73, HCPs – accuracy = 0.54
Zheng et al. [45]	Acute radiation esophagitis	0.604	C + R + D – AUC = 0.801
Ren et al. [46]	Post-radiation hypothyroidism	0.7	D – AUC = 0.7
Yang et al. [47]	Radiation damage to the temporal lobe	—	Age + DVH + D – C-index = 0.794
Rossi et al. [29]	Rectal bleeding	—	C + DVH + D – AUC = 0.73
	Fecal incontinence		C + DVH + D – AUC = 0.73
	Nocturia		C + D – AUC = 0.66
	Urinary incontinence		C + DVH + D – AUC = 0.73

Note. AUC, the area under the characteristic curve; C, clinical data of patients; D, dosiomics features; Ds, dosimetry features; DVH, dose-volume histograms; R, radiomics features.

Table 2. Studies to evaluate predicting tumor progression

Study	Predicted variable	Accuracy of the dosiomics-based model	Model with the highest accuracy
Kamezawa et al. [49]	Local recurrence of head and neck cancer	AUC = 0.81	D – AUC = 0.81
Wu et al. [14]	Local recurrence of head and neck cancer	C-index = 0.66	D – C-index = 0.66
Wang et al. [50]	Local recurrence of head and neck cancer	—	R-PET + R-CT + Ds – C-index = 0.873
Murakami et al. [12]	Recurrence of prostate cancer	—	D + C – C-index = 0.67
Pirrone et al. [51]	Recurrence of prostate cancer	AUC = 0.68	D – AUC = 0.68
Buizza et al. [52]	Recurrence of skull base chordomas	C-index = 0.79	R – C-index = 0.80
Morelli et al. [53]	Recurrence of sacral chordomas	C-index = 0.86	D – C-index = 0.86
Cai et al. [54]	Relapse and metastasis of nasopharyngeal carcinoma	C-index = 0.822 for relapse, C-index = 0.786 for metastasis	D – C-index = 0.822 for relapse, D – C-index = 0.786 for metastasis
Wang et al. [55]	Remission of rectal cancer	—	AUC = 0.828
Lam et al. [56]	Grade ray therapy at carcinoma nasopharynx	AUC = 0.811	R – AUC = 0.927

Note. AUC, area under the characteristic curve; C, clinical data of patients; CT, computed tomography; D, dosiomics features; Ds, dosimetry features; PET, positron emission tomography; R, radiomics features.

low dosiomics stability and reproducibility. Two studies by Puttanawarut et al. [57, 58] were devoted to this issue. The first study assessed the general applicability of radiomics and dosiomics features derived from images of cancers of various locations. A database containing data from 101 patients with esophageal cancer patients and 93 lung cancer patients was used. Four models were developed to predict post-radiation pneumonitis in patients diagnosed with esophageal cancer and then applied to a group of patients with lung cancer. In samples of patients with esophageal cancer and lung cancer, the model based on a combination of dosiomics and radiomics features produced the best results, with AUC = 0.75 and AUC = 0.68, respectively. Such results may point to the restricted applicability of decision criteria to malignancies of various locations. The second study by Puttanawarut et al. [58] assessed the stability of dosiomics features when simulating errors in dose distribution planning. The average intraclass correlation coefficient (ICC) for the 93 dosiomics features tested was 0.9, indicating stability, with five features having values below 0.75, indicating low reproducibility. Adachi et al. [59] also assessed the reproducibility of dosiomics features when using various dose calculation algorithms. When using the Acuros XB algorithm, 34.8% of the 6,808 parameters tested exhibited good reproducibility, highlighting the limitations of dosiomics when using different types of dose calculations. Simultaneously, Sun et al. [60] reported that most dosiomic features were stable to changes in dose calculations, but DVH parameters were less variable than dosiomic features. Placidi et al. [61] identified four groups of stable dosiomics features for further research. The authors later demonstrated the significance of voxel size in dosiomics data extraction [62].

Indeed, normalization, stability, and reproducibility of features remain important aspects for such studies and require further research.

DISCUSSION

The most common predictor characteristic in the studies cited (11 studies) was post-radiation pneumonitis. In nine of them, dosiomics features without combination with other signs were used to construct the decision rule. The AUC, used as a fit measure for such models, ranged from 0.67 to 0.84. Decision rules based on dosiomics also had high accuracy when predicting relapses of tumors of various locations (C-index >0.66). The accuracy increased when combined models were constructed using dosiomics, radiomics, dosimetry features, and clinical data, indicating a good predictive ability and prospects for use in clinical practice for personalized treatment planning.

At the time of writing this article, a few studies were conducted with primarily small sample sizes, indicating the necessity for additional research into dosiomics and its possible applications. Dosiomics could be incorporated into the radiation therapy planning process. In most studies,

dosiomics was the most effective when combined with other qualitative and quantitative signs; thus, dosiomics should now be considered precisely as a direction of radiomics that allows for improving the efficiency of predictive models. The properties of dosiomics and radiomics depend on the software used and can vary significantly from study to study. Low stability and reproducibility of features are severe barriers to introducing dosiomics into clinical practice; therefore, they require further study.

CONCLUSION

Dosiomics is a new and promising area of radiomics used in texture analysis of medical images associated with radiation therapy of cancer patients. Dosiomics can contribute to developing a more personalized approach to planning radiation therapy, predicting radiation damage to normal tissues, and diagnosing relapses.

ADDITIONAL INFORMATION

Funding source. This article was not supported by any external sources of funding.

Competing interests. The authors declare that they have no competing interests.

Authors' contribution. All authors made a substantial contribution to the conception of the work, acquisition, analysis, interpretation of data for the work, drafting and revising the work, final approval of the version to be published and agree to be accountable for all aspects of the work. The major contributions were distributed as follows: V.A. Solodkiy — general concept and approval of the final version of the article; N.V. Nudnov — design and diagnostic aspects of the study; M.E. Ivannikov — data collection and analysis; E.S-A. Shakhvalieva — writing the manuscript text, preparation of illustrations; V.M. Sotnikov — radiotherapeutic aspects of the study, editing of the manuscript; A.Yu. Smyslov — dosimetric and physical aspects of the study, manuscript editing.

REFERENCES

1. Arroyo-Hernández M, Maldonado F, Lozano-Ruiz F, et al. Radiation-induced lung injury: Current evidence. *BMC Pulm Med*. 2021;21(1):9. doi: 10.1186/s12890-020-01376-4

2. Huang Y, Feng A, Lin Y, et al. Radiation pneumonitis prediction after stereotactic body radiation therapy based on 3D dose distribution: Dosiomics and/or deep learning-based radiomics features. *Radiat Oncol*. 2022;17(1):188. doi: 10.1186/s13014-022-02154-8

3. Morelli L, Parrella G, Molinelli S, et al. A dosiomics analysis based on linear energy transfer and biological dose maps to predict local recurrence in sacral chordomas after carbon-ion radiotherapy. *Cancers (Basel)*. 2022;15(1):33. doi: 10.3390/cancers15010033

4. Ryan SM, Fingerlin TE, Mroz M, et al. Radiomic measures from chest high-resolution computed tomography associated with lung function in sarcoidosis. *Eur Respir J*. 2019;54(2):1900371. doi: 10.1183/13993003.00371-2019

5. Hooda R, Mittal A, Sofat S. Segmentation of lung fields from chest radiographs: A radiomic feature-based approach. *Biomed Eng Lett*. 2018;9(1):109–117. doi: 10.1007/s13534-018-0086-z

6. Zhang B, Ni-Jia-Ti MY, Yan R, et al. CT-based radiomics for predicting the rapid progression of coronavirus disease 2019 (COVID-19) pneumonia lesions. *Br J Radiol*. 2021;94(1122):20201007. doi: 10.1259/bjr.20201007

7. Avanzo M, Stancanello J, Pirrone G, et al. Radiomics and deep learning in lung cancer. *Strahlenther Onkol*. 2020;196(10):879–887. doi: 10.1007/s00066-020-01625-9

8. Ji D, Zhang D, Xu J, et al. Prediction for progression risk in patients with COVID-19 pneumonia: The CALL score. *Clin Infect Dis*. 2020;71(6):1393–1399. doi: 10.1093/cid/ciaa414

9. Chen H, Zeng M, Wang X, et al. A CT-based radiomics nomogram for predicting prognosis of coronavirus disease 2019 (COVID-19) radiomics nomogram predicting COVID-19. *Br J Radiol*. 2021;94(1117):20200634. doi: 10.1259/bjr.20200634

10. Wang D, Huang C, Bao S, et al. Study on the prognosis predictive model of COVID-19 patients based on CT radiomics. *Sci Rep*. 2021;11(1):11591. doi: 10.1038/s41598-021-90991-0

11. Frix AN, Cousin F, Refaee T, et al. Radiomics in lung diseases imaging: State of the Art for Clinicians. *J Pers Med*. 2021;11(7):602. doi: 10.3390/jpm11070602

12. Murakami Y, Soyano T, Kozuka T, et al. Dose-Based radiomic analysis (dosiomics) for intensity modulated radiation therapy in patients with prostate cancer: Correlation between planned dose distribution and biochemical failure. *Int J Radiat Oncol Biol Phys*. 2022;112(1):247–259. doi: 10.1016/j.ijrobp.2021.07.1714

13. Liang B, Yan H, Tian Y, et al. Dosiomics: Extracting 3D spatial features from dose distribution to predict incidence of radiation pneumonitis. *Front Oncol*. 2019;(9):269. doi: 10.3389/fonc.2019.00269

14. Wu A, Li Y, Qi M, et al. Dosiomics improves prediction of locoregional recurrence for intensity modulated radiotherapy treated head and neck cancer cases. *Oral Oncol*. 2020;(104):104625. doi: 10.1016/j.oraloncology.2020.104625

15. Andreev DA, Zavyalov AA. The quality indicators to assess the prostate cancer radiotherapy performance (brief review). *Problems Social Hygiene Public Health History Med*. 2021;29(S2):1292–1297. (In Russ). doi: 10.32687/0869-866X-2021-29-s2-1292-1297

16. Chen Q, Xia T, Zhang M, et al. Radiomics in stroke neuroimaging: Techniques, applications, and challenges. *Aging Dis*. 2021;12(1):143–154. doi: 10.14336/AD.2020.0421

17. Mayerhoefer ME, Materka A, Langs G, et al. Introduction to radiomics. *J Nucl Med*. 2020;61(4):488–495. doi: 10.2967/jnumed.118.222893

18. Van Timmeren JE, Cester D, Tanadini-Lang S, et al. Radiomics in medical imaging: "How-to" guide and critical reflection. *Insights Imaging*. 2020;11(1):91. doi: 10.1186/s13244-020-00887-2

19. Radiomic Features — pyradiomics v3.0.1.post15+g2791e23 documentation [Internet]. Available from: https://pyradiomics.readthedocs.io/en/latest/features.html#. Accessed: 21.04.2023.

20. Al-Areqi F, Konyar MZ. Effectiveness evaluation of different feature extraction methods for classification of COVID-19 from computed tomography images: A high accuracy classification study. *Biomed Signal Process Control*. 2022;(76):103662. doi: 10.1016/j.bspc.2022.103662

21. Zwanenburg A, Vallières M, Abdalah MA, et al. The image biomarker standardization initiative: Standardized quantitative radiomics for high-throughput image-based phenotyping. *Radiology*. 2020;295(2):328–338. doi: 10.1148/radiol.2020191145
22. Galloway MM. Texture analysis using gray level run lengths. *Comput Graph Image Process*. 1975;4(2):172–179. doi: 10.1016/S0146-664X(75)80008-6
23. Thibault G, Angulo J, Meyer F. Advanced statistical matrices for texture characterization: Application to cell classification. *IEEE Trans Biomed Eng*. 2014;61(3):630–637. doi: 10.1109/TBME.2013.2284600
24. Chen S, Harmon S, Perk T, et al. Using neighborhood gray tone difference matrix texture features on dual time point PET/CT images to differentiate malignant from benign FDG-avid solitary pulmonary nodules. *Cancer Imaging*. 2019;19(1):56. doi: 10.1186/s40644-019-0243-3
25. He J, Ren J, Niu G, et al. Multiparametric MR radiomics in brain glioma: Models comparation to predict biomarker status. *BMC Med Imaging*. 2022;22(1):137. doi: 10.1186/s12880-022-00865-8
26. Gabryś HS, Buettner F, Sterzing F, et al. Design and selection of machine learning methods using radiomics and dosiomics for normal tissue complication probability modeling of xerostomia. *Front Oncol*. 2018;8:35. doi: 10.3389/fonc.2018.00035
27. Ledenev VV, Nudnov NV, Sotnikov VM, et al. The results of quantitative evaluation of postradiation changes in lung cancer patients, which were obtained using a new procedure for analysis of dynamic X-ray computed tomography imaging of thoracic organs. *J Radiol Nuclear Med*. 2020;101(1):30–38. (In Russ). doi: 10.20862/0042-4676-2020-101-1-30-38
28. Ledenev VV, Solodkiy VA, Nudnov NV, et al. Quantitative characteristics of radiation-induced lung damage in oncological patients during radiotherapy based on RCT data. *Med Visual*. 2022;26(4):60–74. (In Russ). doi: 10.24835/1607-0763-1182
29. Rossi L, Bijman R, Schillemans W, et al. Texture analysis of 3D dose distributions for predictive modelling of toxicity rates in radiotherapy. *Radiother Oncol*. 2018;129(3):548–553. doi: 10.1016/j.radonc.2018.07.027
30. Liu J, Guo W, Zeng P, et al. Vertebral MRI-based radiomics model to differentiate multiple myeloma from metastases: Influence of features number on logistic regression model performance. *Eur Radiol*. 2022;32(1):572–581. doi: 10.1007/s00330-021-08150-y
31. Dhir CS, Lee SY. Discriminant independent component analysis. *IEEE Trans Neural Netw*. 2011;22(6):845–857. doi: 10.1109/TNN.2011.2122266
32. Random Forest Feature Importance Computed in 3 Ways with Python | MLJAR [Internet]. Available from: https://mljar.com/blog/feature-importance-in-random-forest/. Accessed: 21.04.2023.
33. Sun R, Lerousseau M, Henry T, et al. Intelligence artificielle en radiothérapie: Radiomique, pathomique, et prédiction de la survie et de la réponse aux traitements. *Cancer Radiother*. 2021;25(6-7):630–637. doi: 10.1016/j.canrad.2021.06.027
34. Zhang X, Zhang Y, Zhang G, et al. Deep learning with radiomics for disease diagnosis and treatment: challenges and potential. *Front Oncol*. 2022;(12):773840. doi: 10.3389/fonc.2022.773840
35. Zhang Z, Wang Z, Yan M, et al. Radiomics and dosiomics signature from whole lung predicts radiation pneumonitis: A model development study with prospective external validation and decision-curve analysis. *Int J Radiat Oncol Biol Phys*. 2023;115(3):746–758. doi: 10.1016/j.ijrobp.2022.08.047
36. Li B, Ren G, Guo W, et al. Function-Wise dual-omics analysis for radiation pneumonitis prediction in lung cancer patients. *Front Pharmacol*. 2022;(13):971849. doi: 10.3389/fphar.2022.971849
37. Li B, Zheng X, Zhang J, et al. Lung subregion partitioning by incremental dose intervals improves omics-based prediction for acute radiation pneumonitis in non-small-cell lung cancer patients. *Cancers (Basel)*. 2022;14(19):4889. doi: 10.3390/cancers14194889
38. Zhou L, Wen Y, Zhang G, et al. Machine learning-based multiomics prediction model for radiation pneumonitis. *J Oncol*. 2023;2023:5328927. doi: 10.1155/2023/5328927
39. Kraus KM, Oreshko M, Bernhardt D, et al. Dosiomics and radiomics to predict pneumonitis after thoracic stereotactic body radiotherapy and immune checkpoint inhibition. *Front Oncol*. 2023;(13):1124592. doi: 10.3389/fonc.2023.1124592
40. Puttanawarut C, Sirirutbunkajorn N, Khachonkham S, et al. Biological dosiomic features for the prediction of radiation pneumonitis in esophageal cancer patients. *Radiat Oncol*. 2021;16(1):220. doi: 10.1186/s13014-021-01950-y
41. Liang B, Tian Y, Chen X, et al. Prediction of radiation pneumonitis with dose distribution: A convolutional neural network (CNN) based model. *Front Oncol*. 2020;(9):1500. doi: 10.3389/fonc.2019.01500
42. Adachi T, Nakamura M, Shintani T, et al. Multi-institutional dose-segmented dosiomic analysis for predicting radiation pneumonitis after lung stereotactic body radiation therapy. *Med Phys*. 2021;48(4):1781–1791. doi: 10.1002/mp.14769
43. Lee SH, Han P, Hales RK, et al. Multi-view radiomics and dosiomics analysis with machine learning for predicting acute-phase weight loss in lung cancer patients treated with radiotherapy. *Phys Med Biol*. 2020;65(19):195015. doi: 10.1088/1361-6560/ab8531
44. Han P, Lee SH, Noro K, et al. Improving early identification of significant weight loss using clinical decision support system in lung cancer radiation therapy. *JCO Clin Cancer Inform*. 2021;(5):944–952. doi: 10.1200/CCI.20.00189
45. Zheng X, Guo W, Wang Y, et al. Multi-omics to predict acute radiation esophagitis in patients with lung cancer treated with intensity-modulated radiation therapy. *Eur J Med Res*. 2023;28(1):126. doi: 10.1186/s40001-023-01041-6
46. Ren W, Liang B, Sun C, et al. Dosiomics-based prediction of radiation-induced hypothyroidism in nasopharyngeal carcinoma patients. *Phys Med*. 2021;(89):219–225. doi: 10.1016/j.ejmp.2021.08.009
47. Yang SS, OuYang PY, Guo JG, et al. Dosiomics risk model for predicting radiation induced temporal lobe injury and guiding individual intensity-modulated radiation therapy. *Int J Radiat Oncol Biol Phys*. 2023;115(5):1291–1300. doi: 10.1016/j.ijrobp.2022.11.036
48. Monti S, Xu T, Liao Z, et al. On the interplay between dosiomics and genomics in radiation-induced lymphopenia of lung cancer patients. *Radiother Oncol*. 2022;(167):219–225. doi: 10.1016/j.radonc.2021.12.038
49. Kamezawa H, Arimura H. Recurrence prediction with local binary pattern-based dosiomics in patients with head and neck squamous cell carcinoma. *Phys Eng Sci Med*. 2023;46(1):99–107. doi: 10.1007/s13246-022-01201-8
50. Wang B, Liu J, Zhang X, et al. Prognostic value of 18F-FDG PET/CT-based radiomics combining dosiomics and dose volume

histogram for head and neck cancer. *EJNMMI Res*. 2023;13(1):14. doi: 10.1186/s13550-023-00959-6

51. Pirrone G, Matrone F, Chiovati P, et al. Predicting local failure after partial prostate re-irradiation using a dosiomic-based machine learning model. *J Pers Med*. 2022;12(9):1491. doi: 10.3390/jpm12091491

52. Buizza G, Paganelli C, D'Ippolito E, et al. Radiomics and dosiomics for predicting local control after carbon-ion radiotherapy in skull-base chordoma. *Cancers (Basel)*. 2021;13(2):339. doi: 10.3390/cancers13020339

53. Morelli L, Parrella G, Molinelli S, et al. A dosiomics analysis based on linear energy transfer and biological dose maps to predict local recurrence in sacral chordomas after carbon-ion radiotherapy. *Cancers (Basel)*. 2022;15(1):33. doi: 10.3390/cancers15010033

54. Cai C, Lv W, Chi F, et al. Prognostic generalization of multi-level CT-dose fusion dosiomics from primary tumor and lymph node in nasopharyngeal carcinoma. *Med Phys*. 2023;50(2):922–934. doi: 10.1002/mp.16044

55. Wang D, Lee SH, Geng H, et al. Interpretable machine learning for predicting pathologic complete response in patients treated with chemoradiation therapy for rectal adenocarcinoma. *Front Artif Intell*. 2022;(5):1059033. doi: 10.3389/frai.2022.1059033

56. Lam SK, Zhang Y, Zhang J, et al. Multi-Organ omics-based prediction for adaptive radiation therapy eligibility in nasopharyngeal carcinoma patients undergoing concurrent chemoradiotherapy. *Front Oncol*. 2022;(11):792024. doi: 10.3389/fonc.2021.792024

57. Puttanawarut C, Sirirutbunkajorn N, Tawong N, et al. Radiomic and dosiomic features for the prediction of radiation pneumonitis across esophageal cancer and lung cancer. *Front Oncol*. 2022;(12):768152. doi: 10.3389/fonc.2022.768152

58. Puttanawarut C, Sirirutbunkajorn N, Tawong N, et al. Impact of interfractional error on dosiomic features. *Front Oncol*. 2022;(12):726896. doi: 10.3389/fonc.2022.726896

59. Adachi T, Nakamura M, Kakino R, et al. Dosiomic feature comparison between dose-calculation algorithms used for lung stereotactic body radiation therapy. *Radiol Phys Technol*. 2022;15(1):63–71. doi: 10.1007/s12194-022-00651-9

60. Sun L, Smith W, Kirkby C. Stability of dosiomic features against variations in dose calculation: An analysis based on a cohort of prostate external beam radiotherapy patients. *J Appl Clin Med Phys*. 2023;24(5):e13904. doi: 10.1002/acm2.13904

61. Placidi L, Gioscio E, Garibaldi C, et al. A Multicentre evaluation of dosiomics features reproducibility, stability and sensitivity. *Cancers (Basel)*. 2021;13(15):3835. doi: 10.3390/cancers13153835

62. Placidi L, Cusumano D, Lenkowicz J, et al. On dose cube pixel spacing pre-processing for features extraction stability in dosiomic studies. *Phys Med*. 2021;(90):108–114. doi: 10.1016/j.ejmp.2021.09.010

СПИСОК ЛИТЕРАТУРЫ

1. Arroyo-Hernández M., Maldonado F., Lozano-Ruiz F., et al. Radiation-induced lung injury: Current evidence // BMC Pulm Med. 2021. Vol. 21, N 1. P. 1–12. doi: 10.1186/s12890-020-01376-4

2. Huang Y., Feng A., Lin Y., et al. Radiation pneumonitis prediction after stereotactic body radiation therapy based on 3D dose distribution: Dosiomics and/or deep learning-based radiomics features // Radiat Oncol. 2022. Vol. 17, N 1. P. 188. doi: 10.1186/s13014-022-02154-8

3. Morelli L., Parrella G., Molinelli S., et al. A dosiomics analysis based on linear energy transfer and biological dose maps to predict local recurrence in sacral chordomas after carbon-ion radiotherapy // Cancers. 2023. Vol. 15, N 1. P. 33. doi: 10.3390/cancers15010033

4. Ryan S.M., Fingerlin T.E., Mroz M., et al. Radiomic measures from chest high-resolution computed tomography associated with lung function in sarcoidosis // Eur Respir J. 2021. Vol. 54, N 2. P. 1900371. doi: 10.1183/13993003.00371-2019

5. Hooda R., Mittal A., Sofat S. Segmentation of lung fields from chest radiographs: A radiomic feature-based approach // Biomed Eng Lett. 2019. Vol. 9, N 1. P. 109–117. doi: 10.1007/s13534-018-0086-z

6. Zhang B., Ni-Jia-Ti M.Y., Yan R., et al. CT-based radiomics for predicting the rapid progression of coronavirus disease 2019 (COVID-19) pneumonia lesions // Br J Radiol. 2021. Vol. 94, N 1122. P. 20201007. doi: 10.1259/bjr.20201007

7. Avanzo M., Stancanello J., Pirrone G., et al. Radiomics and deep learning in lung cancer // Strahlenther Onkol. 2020. Vol. 196, N 10. P. 879–887. doi: 10.1007/s00066-020-01625-9

8. Ji D., Zhang D., Xu J., et al. Prediction for progression risk in patients with COVID-19 pneumonia: The CALL score // Clin Infect Dis. 2020. Vol. 71, N 6. P. 1393–1399. doi: 10.1093/cid/ciaa414

9. Chen H., Zeng M., Wang X., et al. A CT-based radiomics nomogram for predicting prognosis of coronavirus disease 2019 (COVID-19) radiomics nomogram predicting COVID-19 // Br J Radiol. 2021. Vol. 94, N 1117. P. 20200634. doi: 10.1259/bjr.20200634

10. Wang D., Huang C., Bao S., et al. Study on the prognosis predictive model of COVID-19 patients based on CT radiomics // Sci Reports. 2021. Vol. 11, N 1. P. 11591. doi:10.1038/s41598-021-90991-0

11. Frix A.N., Cousin F., Refaee T., et al. Radiomics in lung diseases imaging: State of the art for clinicians // J Personal Med. 2021. Vol. 11, N 7. P. 602. doi: 10.3390/jpm11070602

12. Murakami Y., Soyano T., Kozuka T., et al. Dose-Based radiomic analysis (dosiomics) for intensity modulated radiation therapy in patients with prostate cancer: Correlation between planned dose distribution and biochemical failure // Int J Radiat Oncol Biol Phys. 2022. Vol. 112, N 1. P. 247–259. doi: 10.1016/j.ijrobp.2021.07.1714

13. Liang B., Yan H., Tian Y., et al. Dosiomics: Extracting 3D spatial features from dose distribution to predict incidence of radiation pneumonitis // Front Oncol. 2019. N 9. P. 269. doi: 10.3389/fonc.2019.00269

14. Wu A., Li Y., Qi M., et al. Dosiomics improves prediction of locoregional recurrence for intensity modulated radiotherapy treated head and neck cancer cases // Oral Oncol. 2020. N 104. P. 104625. doi: 10.1016/j.oraloncology.2020.104625

15. Андреев Д.А., Завьялов А.А. Критерии оценки качества лучевой терапии на примере рака предстательной железы (краткий обзор зарубежной литературы) // Проблемы социальной гигиены, здравоохранения и истории медицины. 2021. Т. 29, № S2. С. 1292–1297. doi: 10.32687/0869-866X-2021-29-s2-1292-1297

16. Chen Q., Xia T., Zhang M., et al. Radiomics in stroke neuroimaging: Techniques, applications, and challenges // Aging Dis. 2021. Vol. 12, N 1. P. 143–154. doi: 10.14336/AD.2020.0421

17. Mayerhoefer M.E., Materka A., Langs G., et al. Introduction to radiomics // J Nucl Med. 2020. Vol. 61, N 4. P. 488–495. doi: 10.2967/jnumed.118.222893
18. Van Timmeren J.E., Cester D., Tanadini-Lang S., et al. Radiomics in medical imaging: "How-to" guide and critical reflection // Insights Imaging. 2020. Vol. 11, N 1. P. 91. doi: 10.1186/s13244-020-00887-2
19. Radiomic Features: pyradiomics v3.0.1.post15+g2791e23 documentation [интернет]. Режим доступа: https://pyradiomics.readthedocs.io/en/latest/features.html#. Дата обращения: 21.04.2023.
20. Al-Areqi F., Konyar M.Z. Effectiveness evaluation of different feature extraction methods for classification of COVID-19 from computed tomography images: A high accuracy classification study // Biomed Signal Process Control. 2022. N 76. P. 103662. doi: 10.1016/j.bspc.2022.103662
21. Zwanenburg A., Vallières M., Abdalah M.A., et al. The image biomarker standardization initiative: Standardized quantitative radiomics for high-throughput image-based phenotyping // Radiology. 2020. Vol. 295, N 2. P. 328–338. doi: 10.1148/radiol.2020191145
22. Galloway M.M. Texture analysis using gray level run lengths // Comput Graph Image Process. 1975. Vol. 4, N 2. P. 172–179. doi:10.1016/s0146-664x(75)80008-6
23. Thibault G., Angulo J., Meyer F. Advanced statistical matrices for texture characterization: application to cell classification // IEEE Trans Biomed Eng. 2014. Vol. 61, N 3. P. 630–637. doi: 10.1109/TBME.2013.2284600
24. Chen S., Harmon S., Perk T., et al. Using neighborhood gray tone difference matrix texture features on dual time point PET/CT images to differentiate malignant from benign FDG-avid solitary pulmonary nodules // Cancer Imaging. 2019. Vol. 19, N 1. P. 56. doi: 10.1186/s40644-019-0243-3
25. He J., Ren J., Niu G., et al. Multiparametric MR radiomics in brain glioma: Models comparation to predict biomarker status // BMC Med Imaging. 2022. Vol. 22, N 1. P. 137. doi: 10.1186/s12880-022-00865-8
26. Gabryś H.S., Buettner F., Sterzing F., et al. Design and selection of machine learning methods using radiomics and dosiomics for normal tissue complication probability modeling of xerostomia // Front Oncol. 2018. N 8. P. 35. doi: 10.3389/fonc.2018.00035
27. Леденев В.В., Нуднов Н.В., Сотников В.М., и др. Результаты количественной оценки постлучевых изменений в легких у онкологических пациентов, полученные с помощью новой методики анализа динамически выполненных РКТ-исследований органов грудной клетки // Вестник рентгенологии и радиологии. 2020. Т. 101, № 1. С. 30–38. doi: 10.20862/0042-4676-2020-101-1-30-38
28. Леденев В.В., Солодкий В.А., Нуднов Н.В., и др. Количественные характеристики лучевого повреждения легочной ткани у онкологических пациентов при лучевой терапии на основании данных РКТ // Медицинская визуализация. 2022. Т. 26, № 4. С. 60–74. doi: 10.24835/1607-0763-1182
29. Rossi L., Bijman R., Schillemans W., et al. Texture analysis of 3D dose distributions for predictive modelling of toxicity rates in radiotherapy // Radiother Oncol. 2018. Vol. 129, N 3. P. 548–553. doi: 10.1016/j.radonc.2018.07.027
30. Liu J., Guo W., Zeng P., et al. Vertebral MRI-based radiomics model to differentiate multiple myeloma from metastases: Influence of features number on logistic regression model performance // Eur Radiol. 2021. Vol. 32, N 1. P. 572–581. doi: 10.1007/s00330-021-08150-y
31. Dhir C.S., Lee S.Y. Discriminant independent component analysis // IEEE Trans Neural Netw. 2011. Vol. 22, N 6. P. 845–857. doi: 10.1109/TNN.2011.2122266
32. Random Forest Feature Importance Computed in 3 Ways with Python / MLJAR [интернет]. Режим доступа: https://mljar.com/blog/feature-importance-in-random-forest/. Дата обращения: 21.04.2023.
33. Sun R., Lerousseau M., Henry T., et al. Intelligence artificielle en radiothérapie: Radiomique, pathomique, et prédiction de la survie et de la réponse aux traitements // Cancer Radiothér. 2021. Vol. 25, N 6-7. P. 630–637. doi: 10.1016/j.canrad.2021.06.027
34. Zhang X., Zhang Y., Zhang G., et al. Deep learning with radiomics for disease diagnosis and treatment: Challenges and potential // Front Oncol. 2022. N 12. P. 276. doi: 10.3389/fonc.2022.773840
35. Zhang Z., Wang Z., Yan M., et al. Radiomics and dosiomics signature from whole lung predicts radiation pneumonitis: A model development study with prospective external validation and decision-curve analysis // Int J Radiat Oncol Biol Phys. 2023. Vol. 115, N 3. P. 746–758. doi: 10.1016/j.ijrobp.2022.08.047
36. Li B., Ren G., Guo W., et al. Function-Wise Dual-Omics analysis for radiation pneumonitis prediction in lung cancer patients // Front Pharmacol. 2022. N 13. P. 3445. doi: 10.3389/fphar.2022.971849
37. Li B., Zheng X., Zhang J., et al. Lung subregion partitioning by incremental dose intervals improves omics-based prediction for acute radiation pneumonitis in non-small-cell lung cancer patients // Cancers (Basel). 2022. Vol. 14, N 19. P. 4889. doi: 10.3390/cancers14194889
38. Zhou L., Wen Y., Zhang G., et al. Machine learning-based multiomics prediction model for radiation pneumonitis // J Oncol. 2023. Vol. 2023. P. 5328927. doi: 10.1155/2023/5328927
39. Kraus K.M., Oreshko M., Bernhardt D., et al. Dosiomics and radiomics to predict pneumonitis after thoracic stereotactic body radiotherapy and immune checkpoint inhibition // Front Oncol. 2023. N 13. P. 1056. doi: 10.3389/fonc.2023.1124592
40. Puttanawarut C., Sirirutbunkajorn N., Khachonkham S., et al. Biological dosiomic features for the prediction of radiation pneumonitis in esophageal cancer patients // Radiat Oncol. 2021. Vol. 16, N 1. P. 220. doi: 10.1186/s13014-021-01950-y
41. Liang B., Tian Y., Chen X., et al. Prediction of radiation pneumonitis with dose distribution: A convolutional neural network (CNN) based model // Front Oncol. 2020. N 9. P. 1500. doi: 10.3389/fonc.2019.01500
42. Adachi T., Nakamura M., Shintani T., et al. Multi-institutional dose-segmented dosiomic analysis for predicting radiation pneumonitis after lung stereotactic body radiation therapy // Med Phys. 2021. Vol. 48, N 4. P. 1781–1791. doi: 10.1002/mp.14769
43. Lee S.H., Han P., Hales R.K., et al. Multi-view radiomics and dosiomics analysis with machine learning for predicting acute-phase weight loss in lung cancer patients treated with radiotherapy // Phys Med Biol. 2020. Vol. 65, N 19. P. 195015. doi: 10.1088/1361-6560/ab8531
44. Han P., Lee S.H., Noro K., et al. Improving early identification of significant weight loss using clinical decision support system in lung cancer radiation therapy // JCO Clin Cancer Inform. 2021. N 5. P. 944–952. doi: 10.1200/CCI.20.00189
45. Zheng X., Guo W., Wang Y., et al. Multi-omics to predict acute radiation esophagitis in patients with lung cancer treated with intensity-modulated radiation therapy // Eur J Med Res. 2023. Vol. 28, N 1. P. 126. doi: 10.1186/s40001-023-01041-6

46. Ren W., Liang B., Sun C., et al. Dosiomics-based prediction of radiation-induced hypothyroidism in nasopharyngeal carcinoma patients // Phys Medica. 2021. Vol. 89. P. 219–225. doi: 10.1016/j.ejmp.2021.08.009
47. Yang S.S., OuYang P.Y., Guo J.G., et al. Dosiomics risk model for predicting radiation induced temporal lobe injury and guiding individual intensity-modulated radiation therapy // Int J Radiat Oncol Biol Phys. 2023. Vol. 115, N 5. P. 1291–1300. doi: 10.1016/j.ijrobp.2022.11.036
48. Monti S., Xu T., Liao Z., et al. On the interplay between dosiomics and genomics in radiation-induced lymphopenia of lung cancer patients // Radiother Oncol. 2022. N 167. P. 219–225. doi: 10.1016/j.radonc.2021.12.038
49. Kamezawa H., Arimura H. Recurrence prediction with local binary pattern-based dosiomics in patients with head and neck squamous cell carcinoma // Phys Eng Sci Med. 2022. Vol. 46, N 1. P. 99–107. doi: 10.1007/s13246-022-01201-8
50. Wang B., Liu J., Zhang X., et al. Prognostic value of 18F-FDG PET/CT-based radiomics combining dosiomics and dose volume histogram for head and neck cancer // EJNMMI Res. 2023. Vol. 13, N 1. P. 14. doi: 10.1186/s13550-023-00959-6
51. Pirrone G., Matrone F., Chiovati P., et al. Predicting local failure after partial prostate re-irradiation using a dosiomic-based machine learning model // J Pers Med. 2022. Vol. 12, N 9. P. 1491. doi: 10.3390/jpm12091491
52. Buizza G., Paganelli C., D'Ippolito E., et al. Radiomics and dosiomics for predicting local control after carbon-ion radiotherapy in skull-base chordoma // Cancers. 2021. Vol. 13, N 2. P. 339. doi: 10.3390/cancers13020339
53. Morelli L., Parrella G., Molinelli S., et al. A Dosiomics analysis based on linear energy transfer and biological dose maps to predict local recurrence in sacral chordomas after carbon-ion radiotherapy // Cancers (Basel). 2023. Vol. 15, N 1. P. 33. doi: 10.3390/cancers15010033
54. Cai C., Lv W., Chi F., et al. Prognostic generalization of multi-level CT-dose fusion dosiomics from primary tumor and lymph node in nasopharyngeal carcinoma // Med Phys. 2023. Vol. 50, N 2. P. 922–934. doi: 10.1002/mp.16044
55. Wang D., Lee S.H., Geng H., et al. Interpretable machine learning for predicting pathologic complete response in patients treated with chemoradiation therapy for rectal adenocarcinoma // Front Artif Intell. 2022. N 5. P. 1059033. doi:10.3389/frai.2022.1059033
56. Lam S.K., Zhang Y., Zhang J., et al. Multi-Organ omics-based prediction for adaptive radiation therapy eligibility in nasopharyngeal carcinoma patients undergoing concurrent chemoradiotherapy // Front Oncol. 2022. N 11. P. 792024. doi: 10.3389/fonc.2021.792024
57. Puttanawarut C., Sirirutbunkajorn N., Tawong N., et al. Radiomic and dosiomic features for the prediction of radiation pneumonitis across esophageal cancer and lung cancer // Front Oncol. 2022. N 12. P. 768152. doi: 10.3389/fonc.2022.768152
58. Puttanawarut C., Sirirutbunkajorn N., Tawong N., et al. Impact of interfractional error on dosiomic features // Front Oncol. 2022. N 12. P. 726896. doi: 10.3389/fonc.2022.726896
59. Adachi T., Nakamura M., Kakino R., et al. Dosiomic feature comparison between dose-calculation algorithms used for lung stereotactic body radiation therapy // Radiol Phys Technol. 2022. Vol. 15, N 1. P. 63–71. doi: 10.1007/s12194-022-00651-9
60. Sun L., Smith W., Kirkby C. Stability of dosiomic features against variations in dose calculation: An analysis based on a cohort of prostate external beam radiotherapy patients // J Appl Clin Med Phys. 2023. Vol. 24, N 5. P. e13904 doi: 10.1002/acm2.13904
61. Placidi L., Gioscio E., Garibaldi C., et al. A multicentre evaluation of dosiomics features reproducibility, stability and sensitivity // Cancers (Basel). 2021. Vol. 13, N 15. P. 3835. doi: 10.3390/cancers13153835
62. Placidi L., Cusumano D., Lenkowicz J., et al. On dose cube pixel spacing pre-processing for features extraction stability in dosiomic studies // Phys Medica. 2021. N 90. P. 108–114. doi: 10.1016/j.ejmp.2021.09.010

AUTHORS' INFO

*** Nikolay V. Nudnov,** MD, Dr. Sci. (Med.), Professor;
address: 86 Profsoyuznaya street, 117997 Moscow, Russia;
ORCID: 0000-0001-5994-0468;
eLibrary SPIN: 3018-2527;
e-mail: nudnov@rncrr.ru

Vladimir A. Solodkiy, MD, Dr. Sci. (Med.), Professor, Academician of the Russian Academy of Sciences;
ORCID: 0000-0002-1641-6452;
eLibrary SPIN: 9556-6556;
e-mail: direktor@rncrr.ru

Mikhail E. Ivannikov;
ORCID: 0009-0007-0407-0953;
e-mail: ivannikovmichail@gmail.com

Elina S-A. Shakhvalieva;
ORCID: 0009-0000-7535-8523;
e-mail: shelina9558@gmail.com

ОБ АВТОРАХ

*** Нуднов Николай Васильевич,** д-р мед. наук, профессор;
адрес: Россия, 117997, Москва, ул. Профсоюзная, д. 86;
ORCID: 0000-0001-5994-0468;
eLibrary SPIN: 3018-2527;
e-mail: nudnov@rncrr.ru

Солодкий Владимир Алексеевич, д-р мед. наук, профессор, академик РАН;
ORCID: 0000-0002-1641-6452;
eLibrary SPIN: 9556-6556;
e-mail: direktor@rncrr.ru

Иванников Михаил Евгеньевич;
ORCID: 0009-0007-0407-0953;
e-mail: ivannikovmichail@gmail.com

Шахвалиева Элина Саид-Аминовна;
ORCID: 0009-0000-7535-8523 ;
e-mail: shelina9558@gmail.com

* Corresponding author / Автор, ответственный за переписку

Vladimir M. Sotnikov, MD, Dr. Sci. (Med.), Professor;
ORCID: 0000-0003-0498-314X;
eLibrary SPIN: 3845-0154;
e-mail: vmsotnikov@mail.ru

Aleksei Yu. Smyslov, Cand. Sci. (Engin.);
ORCID: 0000-0002-6409-6756;
eLibrary SPIN: 9341-0037;
e-mail: smyslov.ay@gmail.com

Сотников Владимир Михайлович, д-р мед. наук, профессор;
ORCID: 0000-0003-0498-314X;
eLibrary SPIN: 3845-0154;
e-mail: vmsotnikov@mail.ru

Смыслов Алексей Юрьевич, канд. тех. наук;
ORCID: 0000-0002-6409-6756;
eLibrary SPIN: 9341-0037;
e-mail: smyslov.ay@gmail.com

DOI: https://doi.org/10.17816/DD430292

Основы стандартной визуализации периферической нервной системы: МР-нейрография

С.Н. Морозова, В.В. Синькова, Д.А. Гришина, Т.А. Тумилович, А.О. Чечеткин, М.В. Кротенкова, Н.А. Супонева

Научный центр неврологии, Москва, Российская Федерация

АННОТАЦИЯ

Периферические нейропатии относятся к одним из наиболее часто встречающихся неврологических расстройств. Несмотря на наличие хорошо зарекомендовавших себя и дополняющих друг друга методов инструментальной диагностики, таких как электронейромиография и ультразвуковое исследование, диагностика и дифференциальная диагностика поражения периферических нервов различного генеза, особенно их проксимальных отделов, может быть затруднена. Магнитно-резонансная томография периферических нервов в настоящее время активно внедряется в клиническую практику в качестве ценного дополнительного диагностического инструмента.

Акцент в представленной работе делается на основных преимуществах и ограничениях упомянутых методов исследования, истории использования магнитно-резонансной томографии для визуализации структур периферической нервной системы, основных требованиях к протоколу магнитно-резонансной томографии периферических нервов различной локализации с учётом современных технических возможностей, в том числе подробно рассматриваются используемые для стандартного исследования последовательности магнитно-резонансной томографии и их диагностическое значение, рекомендации по использованию контрастирования, преимущества и недостатки различных механизмов жироподавления.

В настоящее время практически отсутствуют стандартизированные описания периферических нервов в норме и при различных патологиях, что снижает диагностическую ценность метода. Перспектива повышения его информативности и расширения использования связана, в том числе, с проведением исследований на больших группах здоровых испытуемых и пациентов с различными патологиями периферической нервной системы.

Ключевые слова: магнитно-резонансная томография; периферические нейропатии; МРТ-протокол; жироподавление; трёхмерная визуализация.

Как цитировать:

Морозова С.Н., Синькова В.В., Гришина Д.А., Тумилович Т.А., Чечеткин А.О., Кротенкова М.В., Супонева Н.А. Основы стандартной визуализации периферической нервной системы: МР-нейрография // *Digital Diagnostics.* 2023. Т. 4, № 3. С. 356–368. DOI: https://doi.org/10.17816/DD430292

Рукопись получена: 17.05.2023 **Рукопись одобрена:** 04.07.2023 **Опубликована:** 24.08.2023

DOI: https://doi.org/10.17816/DD430292

Conventional magnetic resonance imaging of peripheral nerves: MR-neurography

Sofya N. Morozova, Viktoriya V. Sinkova, Darya A. Grishina, Taisiya A. Tumilovich, Andrey O. Chechetkin, Marina V. Krotenkova, Natalya A. Suponeva

Research Center of Neurology, Moscow, Russian Federation

ABSTRACT

Peripheral neuropathy is known to be one of the most common neurological disorders. Despite the great diagnostic value of electroneuromyography and ultrasound, addressing the diagnostics and differential diagnostics of peripheral nerve diseases of different origin could be challenging. In recent years, magnetic resonance tomography has been increasingly used for evaluating cases of suspected or established peripheral neuropathy with excellent results.

This manuscript mainly deals with the advantages and limitations of the aforementioned diagnostic instruments, technical considerations according to different anatomy of peripheral nerves, along with state-of-the-art technical decisions, frequently used magnetic resonance imaging sequences and their diagnostic value based on own observation, and recommendations for contrast enhancement use and different methods of fat suppression.

Currently, there is practically no standardized description of normal magnetic resonance imaging features of peripheral nerves, as well as their changes in different diseases. The evaluation of images is mainly based on the radiologist experience, which obviously decreases method's diagnostic value. Studies of large numbers involving healthy volunteers and patients with peripheral neuropathies of different origin are required to address this issue.

Keywords: magnetic resonance imaging; peripheral nervous system diseases; MRI scans; fat suppression; imaging; three-dimensional.

To cite this article:

Morozova SN, Sinkova VV, Grishina DA, Tumilovich TA, Chechetkin AO, Krotenkova MV, Suponeva NA. Conventional magnetic resonance imaging of peripheral nerves: MR-neurography. *Digital Diagnostics.* 2023;4(3):356–368. DOI: https://doi.org/10.17816/DD430292

Received: 17.05.2023 **Accepted:** 04.07.2023 **Published:** 24.08.2023

DOI: https://doi.org/10.17816/DD430292

外周神经系统标准成像基础：磁共振神经影像学

Sofya N. Morozova, Viktoriya V. Sinkova, Darya A. Grishina, Taisiya A. Tumilovich, Andrey O. Chechetkin, Marina V. Krotenkova, Natalya A. Suponeva

Research Center of Neurology, Moscow, Russian Federation

简评

周围神经病是最常见的神经系统疾病之一。虽然已经有了完善的辅助仪器诊断方法，如神经肌电描记术和超声检查，但对各种原因引起的周围神经损坏，尤其是其近端损坏的诊断和鉴别诊断仍很困难。目前，外周神经的磁共振成像已被积极引入临床实践，成为一种宝贵的辅助诊断工具。

本文重点介绍上述检查方法的主要优点和局限性、使用磁共振成像来显示出周围神经系统结构的历史、考虑到现代技术能力的不同定位周围神经磁共振成像协议书的主要要求，包括对标准检查中使用的磁共振成像序列及其诊断价值、使用造影剂的建议以及各种脂肪抑制机制的优缺点的详细讨论。

目前，对正常和各种病变下的周围神经几乎没有标准化的描述，这降低该方法的诊断价值。为了提高该方法的信息量并扩大其应用范围，还需要对大量健康受试者和患有各种外周神经系统疾病的患者进行研究。

关键词：磁共振成像；周围神经病；磁共振成像协议书；脂肪抑制；三维成像。

引用本文：

Morozova SN, Sinkova VV, Grishina DA, Tumilovich TA, Chechetkin AO, Krotenkova MV, Suponeva NA. 外周神经系统标准成像基础：磁共振神经影像学. *Digital Diagnostics.* 2023;4(3):356–368. DOI: https://doi.org/10.17816/DD430292

收到： 17.05.2023 **接受：** 04.07.2023 **发布日期：** 24.08.2023

INTRODUCTION

Peripheral neuropathy, one of the most common neurological conditions, is an umbrella term covering peripheral nerve diseases [1]. It is classified as mononeuropathy, multiple (multifocal) mononeuropathy, or polyneuropathy based on the number of nerve fibers involved. Ischemia and compression, trauma, infections, neoplasms, dysmetabolism, disimmunity, toxicity, and insufficiency can all contribute to peripheral neuropathy [2, 3].

If peripheral neuropathy is suspected, a complete medical history and complaints, including a family history, should be obtained [4]. In most cases, the cause may be determined using laboratory tests. At present, electroneuromyography is the gold standard of research. It evaluates the conductive function of upper and lower extremity motor and sensory nerves, their proximal sections (indirectly), and innervated muscles (denervation activity) [5]. These studies can help determine the location, extent, degree, and lesion type [6, 7].

However, electrophysiology has several limitations, such as the inability to diagnose difficult-to-reach proximal areas of the peripheral nervous system [8]. Furthermore, in acute and chronic peripheral neuropathies with previously affected distal parts, they are often highly degenerated at the first visit of a patient, making diagnosis challenging (this is the so-called floor effect that occurs when a data-gathering instrument has a lower limit to the data values it can reliably specify) [3]. For the same reason, certain complications can arise when attempting to differentiate between the entirely afflicted cross-section of the distal nerve and the more proximal lesion of the peripheral fascicle [9]. Another important limiting factor is that results are operator-dependent, which refers to variations in effects caused by a healthcare professional's (HCP) levels of competence when doing an electroneuromyography.

High-resolution ultrasonography is a highly informative, supportive approach for real-time prolonged imaging of peripheral nerve conditions, identifying intraneural changes, and evaluating perineural tissues [10, 11]. Ultrasound of the peripheral nerves is now widely used to diagnose post-traumatic, compression, dysimmune, hereditary neuropathies, and nerve tumors [12]. However, the efficiency and reproducibility of this procedure largely depend on HCP experience [13], the type of ultrasound device, and the transducer frequency used. Unlike electrophysiological techniques, ultrasound does not identify the type of nerve fiber injury. Furthermore, deep-lying peripheral nerves near bone structures and internal organs may be difficult to see or inaccessible to ultrasonography [14].

Magnetic resonance imaging (MRI) is not commonly used to diagnose peripheral nervous system problems. The reasons for this are as follows: (a) the need to obtain very high-resolution 3D images to visualize morphological changes in the nerve structure, which lengthens the examination and increases the potential of artifacts, and (b) the lack of detailed description of the normal state of the peripheral nervous system visualized that complicates interpretation of the data obtained. However, with recent technological advances, MRI is now considered an alternative modality for diagnosing peripheral nerve disorders and can be recommended in cases of suspected lesions that are difficult to reach with conventional methods, surgical procedure planning, controversial electroneuromyography, ultrasound data, trauma, radiation therapy, and surgery history [15].

USE OF MRI FOR PERIPHERAL NERVOUS SYSTEM VISUALIZATION

Although even today, MRI is prescribed to patients with suspected peripheral neuropathy rather to exclude a mass lesion inside or directly adjacent to the nerve [16], as early as in the 1990s, a research group led by Filler and Howe [17, 18] developed the first MR sequences with higher spatial resolution, and increased the contrast of peripheral nerves for their optimal visualization. This procedure was known as magnetic resonance neurography (MR neurography).

Magnetic resonance neurography is used in clinical practice to diagnose traumatic nerve injuries and carpal tunnel syndromes and plan the treatment. In the first case, MR neurography distinguishes a complete nerve transection with all supporting connective tissue structures affected (neurotmesis), requiring surgical intervention and damage to the axon without its sheath destruction (axonotmesis) or local demyelination due to compression or traction with axonal structures preserved (neuropraxia), which can recover spontaneously [19]. MR neurography may also be used for nerve recovery monitoring in controversial cases. This approach is often used to locate and determine the specific location of a lesion in tunnel syndromes (compression neuropathies). If surgical treatment fails, MR neurography is also recommended.

This diagnostic area is developing more rapidly than other areas related to the peripheral nervous system [3]. Therefore, plexus MRI is now part of the confirming diagnostic criteria for chronic inflammatory demyelinating polyneuropathy and multifocal motor neuropathy [20, 21]. Noninvasiveness, low operator dependency, the specific location of pathological alterations and their clear relationship with adjacent anatomical structures, a full assessment of all anatomical structures in the area studied, and monitoring over time are all advantages.

BASIC TECHNICAL REQUIREMENTS FOR MRI PROTOCOL

Magnetic resonance neurography is a technique for optimizing peripheral nerve visualization that uses nerve-selective (imaging nerve trunks with suppressed signals from surrounding tissues and vasculature [22]) and

nerve-nonselective sequences with high-resolution and contrast augmentation.

There are also some limitations. First, because the transverse size of a nerve is typically only a few millimeters and the thickness of individual fascicles is approximately ⩽1 mm, individual nerve trunks may only be visualized using high-resolution techniques. Longer acquisition periods and lower signal-to-noise ratios are required for such images. Furthermore, adipose tissue around and inside neural systems makes qualitative and quantitative examinations of peripheral nerve structures challenging. Therefore, various fat suppression techniques are used to visualize them, which can also affect the image evaluation and the signal-to-noise ratio. Because of the intricate anatomical course of some peripheral nerves, three-dimensional sequences are required; however, images may become noisy and grainy due to overlapping vascular signals. In contrast, MRI of the peripheral nervous system is currently being intensively developed [23, 24].

To visualize individual nerve fascicles within the nerve, equipment with a magnetic field of 3 Tesla (T) [3] provides sufficient spatial resolution. They have a higher signal-to-noise ratio, allowing for stronger contrast, higher resolution in the scan plane, and the smallest slice thickness. The smallest slice thickness is required for higher end-to-end resolution in 2D sequences and higher isotropic resolution in 3D sequences [25]. However, 1.5-T MRI tomographs can be used, particularly in patients with metallic implants in the scanning field [26].

To reduce the effect of partial volume, and to visualize individual nerve structures surrounded by loose connective and fat tissues, the spatial resolution should be ⩾0.1–0.4 × 0.1–0.4 mm, and slice thickness for two-dimensional sequences should be >2.0–3.5 mm for plexuses and 4–5 mm for extremities, with minimal or no interslice gap [3, 25]. Although 2D sequences are still the gold standard for the first evaluation, 3D sequences (with the ability to reconstruct images in different planes) are critical for viewing and addressing difficulties when the anatomical nerve course is convoluted, and the available data are contentious. Slices should be designated relative to the long axes, that is, parallel or perpendicular to the nerve's extremity or course as far as feasible [25].

Optimal imaging results are achieved by using multichannel coils for specific body parts, but other solutions are possible by replacing missing coils with existing coils, provided that the patient is positioned correctly. Special multichannel coils with accelerating factors can be used with soft surface coils to increase the field of view. A combination of spinal embedded and soft surface coils is recommended for performing examinations at the trunk level [27].

Before organizing an examination, consider the broadest possible covering area, and that the more slices there are the longer the examination will last. The field of view should be restricted as much as possible to achieve improved spatial resolution, with the empty space around the area of interest being no more than 20% of its size for effective assessment of small-diameter nerves [25].

To eliminate motion artifacts, the patient should be appropriately and comfortably positioned [3]. To avoid interference with the bladder signal on maximum intensity projection reconstructions, the bladder should be emptied before studying the lumbar and sacral plexuses.

CONVENTIONAL MR NEUROGRAPHY TECHNIQUES AND THEIR CLINICAL USE

The most commonly used techniques in routine clinical practice include qualitative assessment of T1- and T2-weighted images and proton density-weighted images, which are contrasted using T1 and T2 relaxation processes and proton density localization in human tissues with spin or gradient echo sequences. Various fat suppression strategies are used (discussed in more detail below). Regardless of the area of interest, at least two scanning planes, preferably with at least one 3D sequence, are recommended.

T1-weighted images

These images are essential for neurography and can be acquired using spin echo or free fluid suppression inversion recovery sequences in the axial plane for extremity nerves and the coronal plane for plexuses. The length of the echo complex varies from three to eight for 2D images and from 33 to 68 for 3D images. A scanning plane resolution of 0.3 to 0.4 mm ensures optimal visibility of intraneural fat, epineurium thickening, and elimination of perineural fat due to mass lesion development or fibrosis (Fig. 1) [28]. Furthermore, these images are critical for determining fatty infiltration and muscular atrophy. They are also less susceptible to motion and magnetic susceptibility aberrations and can typically detect edema, tract interruption, or changes in cross-sectional nerve configuration due to compression [3].

Contrast-enhanced MR neurography

T1-weighted 3D gradient echo sequences with fat tissue signal suppression and possible subsequent image removal are recommended for pre- and post-contrast imaging. Otherwise, their use for 3D imaging can be limited due to greater artifact susceptibility and lower contrast enhancement.

After intravenous contrast agent injection, a blood–nerve barrier prevents intact nerve signals from altering [24]. Contrast enhancement has little diagnostic benefit in the case of traumatic alterations or carpal tunnel syndromes because these conditions are often investigated with MRI in the subacute period. Only denervated muscles can be increased under these conditions. However, they are well visualized on fat-suppressed images sensitive to fluid signals [25]. Contrast enhancement is related to nerve signal alterations in hereditary and demyelinating polyneuropathies; this is also unnecessary.

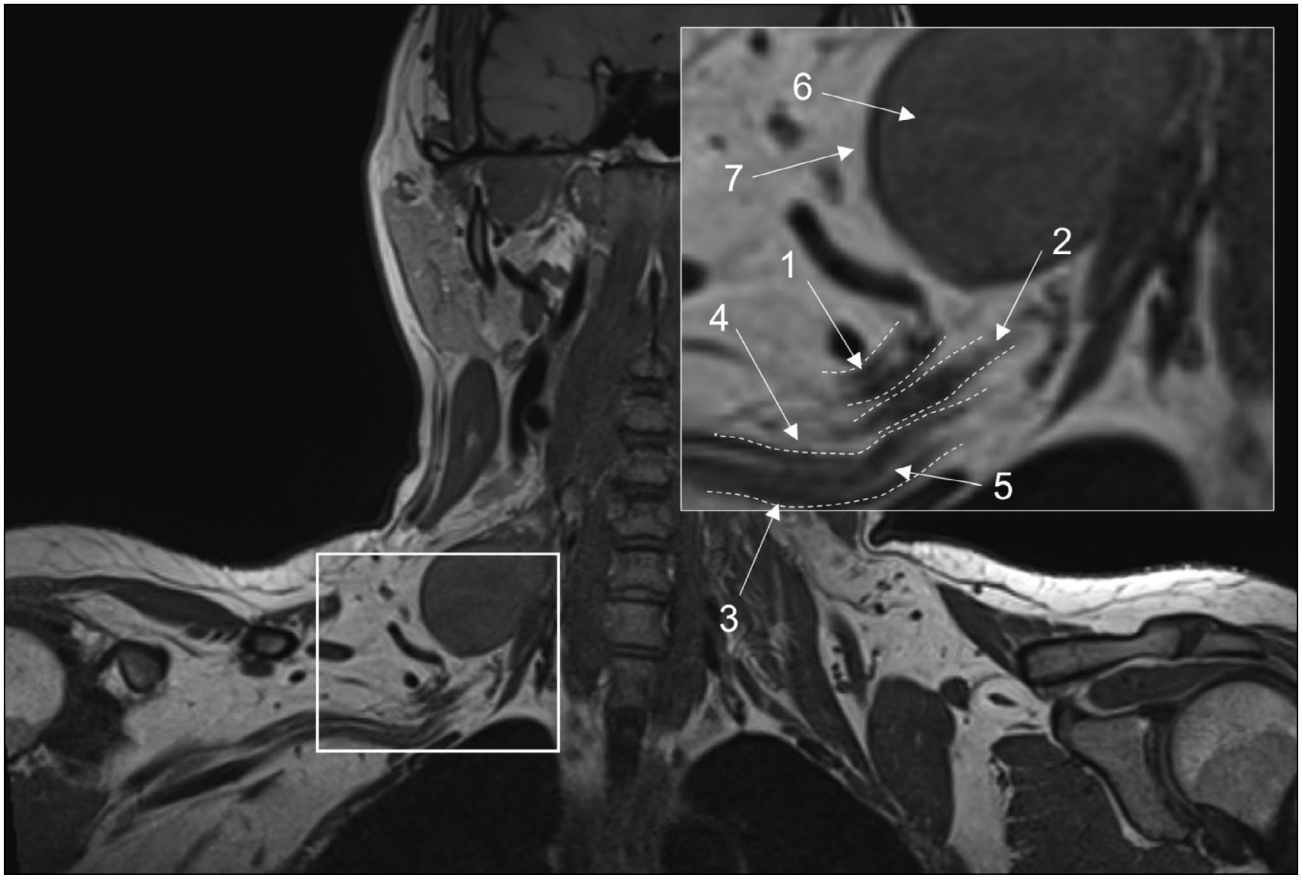

Fig. 1. Magnetic resonance imaging of the brachial plexuses in 3D-T1 mode. A coronal projection: (1) the upper trunk, (2) the middle trunk, (3) the lower trunk, (4) the perineural fatty tissue, (5) the endoneurial fat, (6) a mass lesion (schwannoma), and (7) the intact fatty tissue around the lesion.

In some circumstances, such as a suspected neural or perineural mass lesion, lymphoma, inflammatory processes related to perineural infection, and other disorders associated with damage to the blood–nerve, a contrast-enhanced examination may be recommended [29]. In addition to the disorders listed, a contrast-enhanced examination may be done following decompressive surgery to rule out the overproduction of fibrous tissue if clinical symptoms persist [30].

Nerve-specific contrast agents, such as agents with selective accumulation in areas of demyelination that gradually decreases as the fiber regenerates, are currently being developed, but related MRI techniques have not yet been approved for clinical use [24].

T2-weighted images

Early observations showed that T2 images are the most important for diagnosing peripheral nerve injuries [31]. Non-fat-suppressed sequences, typically 2D, are useful for observing the epineurium (Fig. 2). Fat suppression differentiates the relatively high nerve signal and the

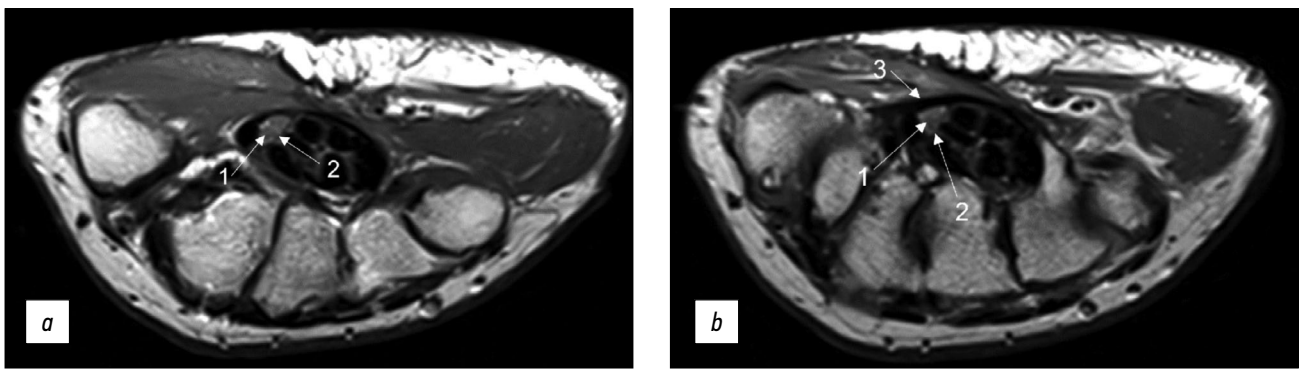

Fig. 2. Magnetic resonance imaging of the hand in T2 mode in a patient with carpal tunnel syndrome. An axial projection: (*a*) at the level of proximal epiphyses of metacarpal bonesand (*b*) at the level of distal parts of the capitate bone (1: individual fascicles as part of the median nerve, 2: epineurium, and 3: flexor retinaculum with a thickness of up to 1.29 mm).

surrounding fat tissue. For T2-weighted images without fat suppression, the recommended echo time is >90 ms (milliseconds), ideally 100–105 ms. For fat-suppressed sequences, it can be reduced to 60–80 ms. The latter, so-called fluid-sensitive images, provide ideal nerve visualization (Fig. 3) with increased signals in the area of pathological changes [32]. Fat suppression strategies are based on the difference in water–fat precession frequency and fat tissue having a longer T2 relaxation time and shorter T1 relaxation time than muscle tissue or nerve fibers [2].

The required fat suppression can be performed by spectrally selective fat suppression (FatSat) in T2-weighted spin echo sequences with high contrast, nearly no pulsation artifacts, and reduced magnetic susceptibility artifacts [33]. However, if there are metal structures in the field of vision, this technique should be avoided. The main disadvantage is poor fat suppression away from the center of the field of view or inhomogeneous fat suppression along the curves of the body [25].

Short-TI inversion recovery (STIR, where TI is the inversion time in milliseconds) provides excellent homogeneous fat suppression at various levels of magnetic induction and field homogeneity, but it is nonselective (it suppresses signal from all, not only fat, tissues with short T1). It cannot be used following intravenous contrast enhancement (as this sequence sums T2 and T1 contrast, providing only T2-weighted images). In many circumstances, it is susceptible to pulsation artifacts, erroneous nerve signal augmentation due to increased signal from intraneural fluid, and a low signal-to-noise ratio. Therefore, this sequence is more commonly used for plexus visualization, where spectrally selective fat suppression is ineffective for a variety of reasons, including the presence of metal in the field of view, using various modifications, such as shorter echo time (30–40 ms), a greater number of echo times, and a wider transmission frequency (400–500 Hz/Px).

T2 SPAIR (T2-weighted SPectral Attenuated Inversion Recovery), a combination of FatSat and STIR techniques, is the best sequence for extremity MR neurography because it suppresses fat signals similarly to STIR, but it is more selective in the center and periphery of the field of view with higher SNR and fewer pulsation artifacts. The signal from a normal nerve usually is isointense to the signal from skeletal muscle on T2-SPAIR images. Depending on the user's preferences, weak and strong contrast types are available, with the weak giving higher signal homogeneity and the strong providing greater isointensity of the nerve signal. The main disadvantage of this sequence is the possibility of poor fat suppression in some edge slices, particularly along the scanning area's boundary, and the inability to use this technique with low-field devices and significant magnetic field inhomogeneity. Although T2-SPAIR is less sensitive to metal artifacts than frequency-selective fat suppression sequences, the STIR sequence should still be used if the metal is in the scanning area.

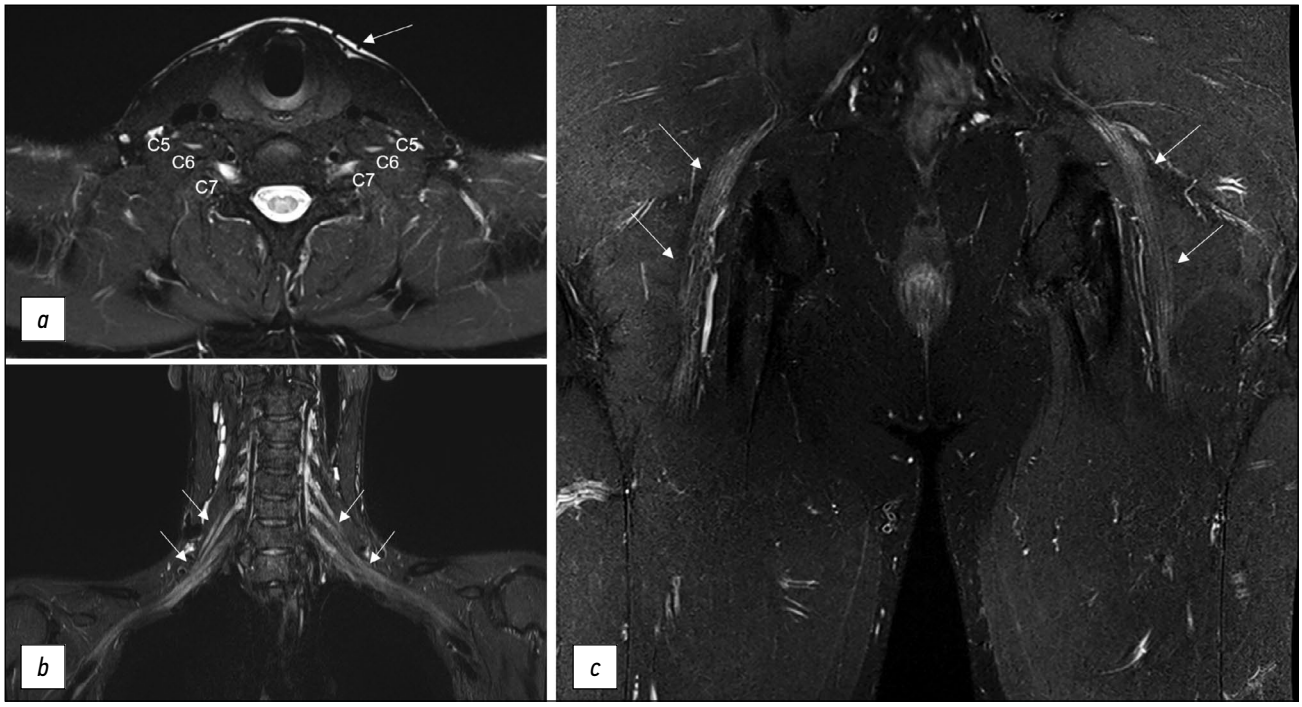

Fig. 3. Various techniques of fat suppression for magnetic resonance imaging: (*a*) brachial plexuses in T2-FatSat mode, an axial projection: the anterior branches of C5, C6, and C7 spinal nerves are noted, without abnormalities, with a slightly increased signal; heterogeneous fat suppression with unsatisfactory signal along the periphery of the area of interest (arrowed); (*b*) brachial plexuses in STIR mode, a coronal projection: homogenous fat suppression throughout the entire field of view, typical elements of brachial plexuses with a slightly increased signal (arrowed); and (*c*) sciatic nerves in T2-Dixon mode, a coronal projection: homogenous fat suppression, normal sciatic nerves with a slightly increased MR signal (arrowed).

The Dixon approach achieves optimal fat suppression, but image quality may be reduced from the central scanning area [25]. Thomas Dixon proposed this approach in 1984 [34]. The chemical shift effect was predicated on a difference in the resonance frequency of fat and water protons. A two-echo sequence is used. Water and fat signals occur in-phase and antiphase during the first and second echo times. Dixon demonstrated that additional images can be computationally created based on these images with simply the water signal (dixonW) and the fat signal (dixonF). The fat signal is suppressed in dixonW images. These images are commonly used in clinical practice because they provide homogeneous fat suppression, and the only notable artifact is a fat–water exchange caused by magnetic field inhomogeneity, which occurs frequently around the coil coverage area's border [35]. However, due to the long scanning time, the use of this neurography technique is limited to 2D imaging.

On T2-weighted images, a diseased peripheral nerve has a larger diameter and higher signal intensity, which is more visible with various fat suppression approaches. The structure and size of the nerve can be evaluated in comparison with surrounding nerves and a vascular fascicle, which can be used as an internal reference [36]. For the sciatic nerve, for example, an increase in the nerve diameter to vessel diameter ratio of >0.89 can be considered abnormal [37]. In addition to the nerve signal, special attention should be paid to signals from the adjacent muscles; increased intensity of such signals is an imaging correlate of denervation changes that can be noticed 5 days after nerve injury [3].

Some potential problems should be noted while interpreting MR neurography data. First, most healthy volunteers (approximately 60%) have locally increased signal intensity at sites of physiological constriction on fluid-sensitive images; hence, in addition to signal changes, it is necessary to evaluate their prevalence and swelling and thickening of the corresponding nerve. Another important factor is a so-called "magic angle" effect, which means the increased intensity of MR signal from structures located at the angle of 55° relative to the direction of the magnetic field B0 in short TE sequences (<32 ms) [3].

Increased signal on T2-weighted images is a sensitive but nonspecific marker of peripheral nerve injury that cannot be quantified and requires careful interpretation considering diverse patterns of lesions, including their magnitude and changes in diameter.

NS-RADS SCALE

There are guidelines for using the MRI-based Neuropathy Score Reporting and Data System (NS-RADS) scale [39]. According to the authors, it can be used for more standardized measurement of the type and severity of peripheral neuropathy using medical history and examination data. This scale is used to assess the severity of traumatic injuries (NS-RADS I1–5), compression syndromes (NS-RADS E1–3), neoplasms (NS-RADS N1–4), diffuse neuropathies (NS-RADS D1, 2), and postoperative conditions (NS-RADS PI1–3). Furthermore, it can be used in the setting of denervation changes in regional muscles (NS-RADS M0–3), insufficient data to assess changes (NS-RADS 0), and absence of changes or minor clinically insignificant changes (NS-RADS U). Furthermore, NS-RADS NOS (not otherwise specified) is a separate category for patients with clinically suspected neuropathy and contentious medical history or examination data. This classification is expected to provide the standardized assessment of MRI changes in peripheral nerves and improve interdisciplinary collaboration for optimal clinical and research outcomes. The original publication contains a more complete classification, but the authors believe that following active implementation, new categories and sections may be established to optimize its use in clinical practice [40].

CONCLUSION

Despite the possibility of greater metal artifacts, 3-T tomographs are preferable for peripheral nerve visualization due to their higher S/N ratio. It is proposed that minimum MRI protocol requirements be established. Three-dimensional sequences are indicated for plexus imaging, whereas 2D images with a small slice thickness (2.5–3.5 mm) are appropriate for extremities nerve viewing. It is important to ensure high resolution of evaluated data (0.2–0.8 mm in the scanning plane). The protocol should include fat-suppressed, fluid-sensitive imaging sequences (STIR, T2SPAIR, T2FatSat, and T2Dixon) and T1- and T2-weighted images, with at least one mode with slices perpendicular to the long axis of nerves.

Despite all the difficulties and limitations, MRI remains the highly informative method for peripheral nervous system examination, and it is increasingly being introduced into clinical practice due to its ability both to detect pathological changes in the peripheral nerves and to perform a comprehensive assessment of the surrounding structures, as well as to make a differential diagnosis in some diseases. The use of standard MR neurography techniques is related to increased informative value and wider usage of MRI, beginning with forming a population-based age normative base with a description of nerve signal sizes and characteristics. A detailed description of nerve damage patterns in various disorders is still required.

ADDITIONAL INFORMATION

Funding source. This article was not supported by any external sources of funding.

Competing interests. The authors declare that they have no competing interests.

Authors' contribution. All authors made a substantial contribution to the conception of the work, acquisition, analysis, interpretation of data for the work, drafting and revising the

work, final approval of the version to be published and agree to be accountable for all aspects of the work. S.N. Morozova — search for publications on the topic, manuscript text writing, figures preparation, V.V. Sinkova — search for publications on the topic, figures preparation, D.A. Grishina — scientific consult, manuscript text editing, T.A. Tumilovich — search for publications on the topic, figures preparation, A.O. Chechetkin — scientific consult, manuscript text editing, approval of the final version, M.V. Krotenkova, N.A. Suponeva — the concept of the study, scientific consult, approval of the final version.

REFERENCES

1. Hammi C, Yeung B. Neuropathy. [Updated 2022 Oct 15]. In: StatPearls [Internet]. Treasure Island (FL): StatPearls Publishing; 2023. Available from: https://www.ncbi.nlm.nih.gov/books/NBK542220/.

2. Chen Y, Haacke EM, Li J. Peripheral nerve magnetic resonance imaging. *F1000Research*. 2019;(8):1803. doi: 10.12688/f1000research.19695.1

3. Kollmer J, Bendszus M. Magnetic resonance neurography: Improved diagnosis of peripheral neuropathies. *Neurotherapeutics*. 2021;18(4):2368–2383. doi: 10.1007/s13311-021-01166-8

4. Thompson PD, Thomas PK. Clinical patterns of peripheral neuropathy. In: Dyck PJ, Thomas PK, editors. Peripheral neuropathy. 4th ed. Elsevier Saunders, Philadelphia: 2005. P. 1137–1161.

5. Piradov MA, Suponeva NA, Grishina DA, Pavlov YeV. Electroneuromyography: Algorithms and recommendations in polyneuropathies. Moscow: Goryachaya liniya-Telecom; 2021. 198 p. (In Russ).

6. Li J. Molecular regulators of nerve conduction: Lessons from inherited neuropathies and rodent genetic models. *Exp Neurol*. 2015;(267):209–218. doi: 10.1016/j.expneurol.2015.03.009

7. Chung T, Prasad K, Lloyd TE. Peripheral neuropathy: Clinical and electrophysiological considerations. *Neuroimaging Clin N Am*. 2014;24(1):49–65. doi: 10.1016/j.nic.2013.03.023

8. Dyck PJ, Oviatt KF, Lambert EH. Intensive evaluation of referred unclassified neuropathies yields improved diagnosis. *Ann Neurol*. 1981;10(3):222–226. doi: 10.1002/ana.410100304

9. Stewart JD. Peripheral nerve fascicles: Anatomy and clinical relevance. *Muscle Nerve*. 2003;28(5):525–541. doi: 10.1002/mus.10454

10. Mansurova AV, Chechetkin AO, Suponeva NA, et al. Possibilities of ultrasound in the diagnosis and differential diagnosis of amyotrophic lateral sclerosis: A literature review. *Neuromuscular diseases*. 2022;12(1):21–28. (In Russ). doi: 10.17650/2222-8721-2022-12-1-21-28

11. Gasparotti R, Padua L, Briani C, Lauria G. New technolo-gies for the assessment of neuropathies. *Nat Rev Neurol*. 2017;13(4):203–216. doi: 10.1038/nrneurol.2017.31

12. Deshmukh S, Sun K, Komarraju A, et al. Peripheral nerve imaging: Magnetic resonance and ultrasound correlation. *Magn Reson Imaging Clin N Am*. 2023;31(2):181–191. doi: 10.1016/j.mric.2023.01.003

13. Ohana M, Moser T, Moussaouï A, et al. Current and future imaging of the peripheral nervous system. *Diagn Interv Imaging*. 2014;95(1):17–26. doi: 10.1016/j.diii.2013.05.008

14. Muller I, Miguel M, Bong DA, et al. The peripheral nerves: Update on Ultrasound and magnetic resonance imaging. *Clin Exp Rheumatol*. 2018; 36(Suppl 114):145–58.

15. Aggarwal A, Chhabra A. Magnetic resonance neurography: Is it so complicated that it needs a touch of genius? *Eur Radiol*. 2022;32(6):3912–3914. doi: 10.1007/s00330-021-08525-1

16. Singh T, Kliot M. Imaging of peripheral nerve tumors. *Neurosurg Focus*. 2007;22(6):E6. doi: 10.3171/foc.2007.22.6.7

17. Filler AG, Howe FA, Hayes CE, et al. Magnetic resonance neurography. *Lancet*. 1993;341(8846):659–661. doi: 10.1016/0140-6736(93)90422-d

18. Howe FA, Filler AG, Bell BA, Griffiths JR. Magnetic resonance neurography. *Magn Reson Med*. 1992;28(2):328–338. doi: 10.1002/mrm.1910280215

19. Mazal AT, Faramarzalian A, Samet JD, et al. MR neurography of the brachial plexus in adult and pediatric age groups: Evolution, recent advances, and future directions. *Exp Rev Med Devices*. 2020;17(2):111–122. doi: 10.1080/17434440.2020.1719830

20. Joint Task Force of the EFNS and the PNS. European Federation of Neurological Societies/Peripheral Nerve Society guideline on management of multifocal motor neuropathy. Report of a joint task force of the European Federation of Neurological Societies and the Peripheral Nerve Society--first revision. *J Peripher Nerv Syst*. 2010;15(4):295–301. doi: 10.1111/j.1529-8027.2010.00290.x

21. Van den Bergh PY, van Doorn PA, Hadden RD, et al. European Academy of Neurology/Peripheral Nerve Society guideline on diagnosis and treatment of chronic inflammatory demyelinating polyradiculoneuropathy: Report of a joint Task Force-Second revision. *J Peripher Nerv Syst*. 2021;26(3):242–268. doi: 10.1111/jns.12455

22. Chhabra A, Madhuranthakam AJ, Andreisek G. Magnetic resonance neurography: Current perspectives and literature review. *Eur Radiol*. 2018;28(2):698–707. doi: 10.1007/s00330-017-4976-8

23. Szaro P, McGrath A, Ciszek B, Geijer M. Magnetic resonance imaging of the brachial plexus. Part 1: Anatomical considerations, magnetic resonance techniques, and non-traumatic lesions. *Eur J Radiol*. 2022;20(9):100392. doi: 10.1016/j.ejro.2021.100392

24. Holzgrefe RE, Wagner ER, Singer AD, Daly ChA. Imaging of the peripheral nerve: Concepts and future direction of magnetic resonance neurography and ultrasound. *Curr Concepts*. 2019;44(12):1066–1079. doi: 10.1016/j.jhsa.2019.06.021

25. Chhabra A, Flammang A, Padua A, et al. Magnetic resonance neurography: Technical considerations. *Neuroimaging Clin N Am*. 2014;24(1):67–78. doi: 10.1016/j.nic.2013.03.032

26. Chalian M, Chhabra A. Top-10 tips for getting started with magnetic resonance neurography. *Semin Musculoskelet Radiol*. 2019;23(4):347–360. doi: 10.1055/s-0039-1677727

27. Sneag DB, Queler S. Technological advancements in magnetic resonance neurography. *Curr Neurol Neurosci Rep*. 2019;19(10):75. doi: 10.1007/s11910-019-0996-x

28. Thakkar RS, Del Grande F, Thawait GK, et al. Spectrum of high-resolution MRI findings in diabetic neuropathy. *AJR Am J Roentgenol*. 2012;199(2):407–412. doi: 10.2214/AJR.11.7893

29. Thawait SK, Chaudhry V, Thawait GK, et al. Highresolution MR neurography of diffuse peripheral nerve lesions. *AJNR Am J Neuroradiol*. 2011;32(8):1365–1372. doi: 10.3174/ajnr.A2257

30. McDonald CM, Carter GT, Fritz RC, et al. Magnetic resonance imaging of denervated muscle: Comparison to electromyography. *Muscle Nerve*. 2000;23(9):1431–1434. doi: 10.1002/1097-4598(200009)23:9<1431::aid-mus16>3.0.co;2-p

31. Stoll G, Bendszus M, Perez J, Pham M. Magnetic resonance imaging of the peripheral nervous system. *J Neurol.* 2009;256(7):1043–1051. doi: 10.1007/s00415-009-5064-z
32. Chhabra A, Thawait GK, Soldatos T, et al. High-resolution 3T MR neurography of the brachial plexus and its branches, with emphasis on 3D imaging. *AJNR Am J Neuroradiol*. 2013;34(3):486–497. doi: 10.3174/ajnr.A3287
33. Bischoff C, Kollmer J, Schulte-Mattler W. State-of-the-art diagnosis of peripheral nerve trauma: Clinical examination, electrodiagnostic, and imaging. In: Haaster-Talini KA, Antoniadis G, editors. Modern concepts of peripheral nerve repair. 1st ed. Springer International Publishing; 2017. doi: 10.1007/978-3-319-52319-4_2
34. Dixon WT. Simple proton spectroscopic imaging. *Radiology*. 1984;153(1):189–194. doi: 10.1148/radiology.153.1.6089263
35. Grimm A, Meyer H, Nickel MD, et al. Evaluation of 2-point, 3-point, and 6-point Dixon magnetic resonance imaging with flexible echo timing for muscle fat quantification. *Eur J Radiol*. 2018;(103):57–64. doi: 10.1016/j.ejrad.2018.04.011
36. Subhawong TK, Wang KC, Thawait SK, et al. High-resolution imaging of tunnels by magnetic resonance neurography. *Skeletal Radiol*. 2012;41(1):15–31. doi: 10.1007/s00256-011-1143-1
37. Chhabra A, Chalian M, Soldatos T, et al. 3-T high-resolution MR neurography of sciatic neuropathy. *Am J Roentgenol*. 2012;198(4):357–364. doi: 10.2214/AJR.11.6981
38. Kollmer J, Bendszus M, Pham M. MR neurography: Diagnostic imaging in the PNS. *Clin Neuroradiol*. 2015;25(Suppl 2):283–289. doi: 10.1007/s00062-015-0412-0
39. Chhabra A, Deshmukh SD, Lutz AM, et al. Neuropathy score reporting and data system: A reporting guideline for MRI of peripheral neuropathy with a multicenter validation study. *AJR Am J Roentgenol*. 2022;219(2):279–291. doi: 10.2214/AJR.22.27422
40. Chhabra A, Deshmukh SD, Lutz AM, et al. Neuropathy score reporting and data system (NS-RADS): MRI reporting guideline of peripheral neuropathy explained and reviewed. *Skeletal Radiol*. 2022;51(10):1909–1922. doi: 10.1007/s00256-022-04061-1

СПИСОК ЛИТЕРАТУРЫ

1. Hammi C., Yeung B. Neuropathy. [Updated 2022 Oct 15]. In: StatPearls [Internet]. Treasure Island (FL): StatPearls Publishing; 2023. Режим доступа: https://www.ncbi.nlm.nih.gov/books/NBK542220/. Дата обращения: 15.08.2023.
2. Chen Y., Haacke E.M., Li J. Peripheral nerve magnetic resonance imaging // F1000Research. 2019. Vol. 8. P. 1803. doi: 10.12688/f1000research.19695.1
3. Kollmer J., Bendszus M. Magnetic resonance neurography: Improved diagnosis of peripheral neuropathies // Neurotherapeutics. 2021. Vol. 18. P. 2368–2383. doi: 10.1007/s13311-021-01166-8
4. Thompson P.D., Thomas P.K. Clinical patterns of peripheral neuropathy // P.J. Dyck, P.K. Thomas, editors. Peripheral neuropathy, 4th ed. Philadelphia: Elsevier Saunders, 2005. P. 1137–1161.
5. Пирадов М.А., Супонева Н.А., Гришина Д.А., Павлов Э.В. Электронейромиография: алгоритмы и рекомендации при полинейропатиях. Москва: Горячая линия-Телеком, 2021. 198 с.
6. Li J. Molecular regulators of nerve conduction: Lessons from inherited neuropathies and rodent genetic models // Exp Neurol. 2015. Vol. 267. P. 209–218. doi: 10.1016/j.expneurol.2015.03.009
7. Chung T., Prasad K., Lloyd T.E. Peripheral neuropathy: Clinical and electrophysiological considerations // Neuroimaging Clin N Am. 2014. Vol. 24, N 1. P. 49–65. doi: 10.1016/j.nic.2013.03.023
8. Dyck P.J., Oviatt K.F., Lambert E.H. Intensive evaluation of referred unclassified neuropathies yields improved diagnosis // Ann Neurol. 1981. Vol. 10, N 3. P. 222–226. doi: 10.1002/ana.410100304
9. Stewart J.D. Peripheral nerve fascicles: Anatomy and clinical relevance // Muscle Nerve. 2003. Vol. 28, N 5. P. 525–541. doi: 10.1002/mus.10454
10. Мансурова А.В., Чечёткин А.О., Супонева Н.А., и др. Возможности ультразвукового исследования в диагностике и дифференциальной диагностике бокового амиотрофического склероза: обзор литературы // Нервно-мышечные болезни. 2022. Т. 12, № 1. С. 21–28. doi: 10.17650/2222872120221212128
11. Gasparotti R., Padua L., Briani C., Lauria G. New technologies for the assessment of neuropathies // Nat Rev Neurol. 2017. Vol. 13. P. 203–216. doi: 10.1038/nrneurol.2017.31
12. Deshmukh S., Sun K., Komarraju A., et al. Peripheral nerve imaging: Magnetic resonance and ultrasound correlation // Magn Reson Imaging Clin N Am. 2023. Vol. 31, N 2. P. 181–191. doi: 10.1016/j.mric.2023.01.003
13. Ohana M., Moser T., Moussaouï A., et al. Current and future imaging of the peripheral nervous system // Diagn Interv Imaging. 2014. Vol. 95. P. 17–26. doi: 10.1016/j.diii.2013.05.008
14. Muller I., Miguel M., Bong D.A., et al. The peripheral nerves: Update on ultrasound and magnetic resonance imaging // Clin Exp Rheumatol. 2018. Vol. 36, Suppl. 114. P. 145–158.
15. Aggarwal A., Chhabra A. Magnetic resonance neurography: Is it so complicated that it needs a touch of genius? // Eur Radiol. 2022. Vol. 32, N 6. P. 3912–3914. doi: 10.1007/s00330-021-08525-1
16. Singh T., Kliot M. Imaging of peripheral nerve tumors // Neurosurg Focus. 2007. Vol. 22, N 6. P. E6. doi: 10.3171/foc.2007.22.6.7
17. Filler A.G., Howe F.A., Hayes C.E., et al. Magnetic resonance neurography // Lancet. 1993. Vol. 341, N 8846. P. 659–661. doi: 10.1016/0140-6736(93)90422-d
18. Howe F.A., Filler A.G., Bell B.A., Griffiths J.R. Magnetic resonance neurography // Magn Reson Med. 1992. Vol. 28, N 2. P. 328–338. doi: 10.1002/mrm.1910280215
19. Mazal A.T., Faramarzalian A., Jonathan D.S., et al. MR neurography of the brachial plexus in adult and pediatric age groups: Evolution, recent advances, and future directions // Expert Review of Medical Devices. 2020. doi: 10.1080/17434440.2020.1719830
20. Joint Task Force of the EFNS and the PNS. European Federation of Neurological Societies/Peripheral Nerve Society guideline on management of multifocal motor neuropathy. Report of a joint task force of the European Federation of Neurological Societies and the Peripheral Nerve Society--first

revision // J Peripher Nerv Syst. 2010. Vol. 15, N 4. P. 295–301. doi: 10.1111/j.1529-8027.2010.00290.x

21. Van den Bergh P.Y., van Doorn P.A., Hadden R.D., et al. European Academy of Neurology/Peripheral Nerve Society guideline on diagnosis and treatment of chronic inflammatory demyelinating polyradiculoneuropathy: Report of a joint Task Force-Second revision // J Peripher Nerv Syst. 2021. Vol. 26, N 3. P. 242–268. doi: 10.1111/jns.12455

22. Chhabra A., Madhuranthakam A.J., Andreisek G. Magnetic resonance neurography: Current perspectives and literature review // Eur Radiol. 2018. Vol. 28, N 2. P. 698–707. doi: 10.1007/s00330-017-4976-8

23. Szaro P., McGrath A., Ciszek B., Geijer M. Magnetic resonance imaging of the brachial plexus. Part 1: Anatomical considerations, magnetic resonance techniques, and non-traumatic lesions // Eur J Radiol. 2022. Vol. 20, N 9. P. 100392. doi: 10.1016/j.ejro.2021.100392

24. Holzgrefe R.E., Wagner E.R., Singer A.D., Daly Ch.A. Imaging of the peripheral nerve: Concepts and future direction of magnetic resonance neurography and ultrasound // Current Concepts. 2019. Vol. 44, N 12. P. 1066–1079. doi: 10.1016/j.jhsa.2019.06.021

25. Chhabra A., Flammang A., Padua A. Jr., et al. Magnetic resonance neurography: Technical considerations // Neuroimaging Clin N Am. 2014. Vol. 24, N 1. P. 67–78. doi: 10.1016/j.nic.2013.03.032

26. Chalian M., Chhabra A. Top-10 tips for getting started with magnetic resonance neurography // Semin Musculoskelet Radiol. 2019. Vol. 23, N 4. P. 347–360. doi: 10.1055/s-0039-1677727

27. Sneag D.B., Queler S. Technological advancements in magnetic resonance neurography // Curr Neurol Neurosci Rep. 2019. Vol. 19, N 10. P. 75. doi: 10.1007/s11910-019-0996-x

28. Thakkar R.S., Del Grande F., Thawait G.K., et al. Spectrum of high-resolution MRI findings in diabetic neuropathy // AJR Am J Roentgenol. 2012. Vol. 199, N 2. P. 407–412. doi: 10.2214/AJR.11.7893

29. Thawait S.K., Chaudhry V., Thawait G.K., et al. Highresolution MR neurography of diffuse peripheral nerve lesions // AJNR Am J Neuroradiol. 2011. Vol. 32, N 8. P. 1365–1372. doi: 10.3174/ajnr.A2257

30. McDonald C.M., Carter G.T., Fritz R.C., et al. Magnetic resonance imaging of denervated muscle: Comparison to electromyography // Muscle Nerve. 2000. Vol. 23, N 9. P. 1431–1434. doi: 10.1002/1097-4598(200009)23:9<1431::aid-mus16>3.0.co;2-p

31. Stoll G., Bendszus M., Perez J., Pham M. Magnetic resonance imaging of the peripheral nervous system // J Neurol. 2009. Vol. 256, N 7. P. 1043–1051. doi: 10.1007/s00415-009-5064-z

32. Chhabra A., Thawait G.K., Soldatos T., et al. High-resolution 3T MR neurography of the brachial plexus and its branches, with emphasis on 3D imaging // AJNR Am J Neuroradiol. 2013. Vol. 34, N 3. P. 486–497. doi: 10.3174/ajnr.A3287

33. Bischoff C., Kollmer J., Schulte-Mattler W. State-of-the-art diagnosis of peripheral nerve trauma: Clinical examination, electrodiagnostic, and imaging // K.A. Haaster-Talini, G. Antoniadis, editors. Modern concepts of peripheral nerve repair. 1st ed. Springer International Publishing, 2017. doi: 10.1007/978-3-319-52319-4_2

34. Dixon W.T. Simple proton spectroscopic imaging // Radiology. 1984. Vol. 153. P. 189–194. doi: 10.1148/radiology.153.1.6089263

35. Grimm A., Meyer H., Nickel M.D., et al. Evaluation of 2-point, 3-point, and 6-point Dixon magnetic resonance imaging with flexible echo timing for muscle fat quantification // Eur J Radiol. 2018. Vol. 103. P. 57–64. doi: 10.1016/j.ejrad.2018.04.011

36. Subhawong T.K., Wang K.C., Thawait S.K., et al. High-resolution imaging of tunnels by magnetic resonance neurography // Skeletal Radiol. 2012. Vol. 41. P. 15–31. doi: 10.1007/s00256-011-1143-1

37. Chhabra A., Chalian M., Soldatos T., et al. 3-T high-resolution MR neurography of sciatic neuropathy // Am J Roentgenol. 2012. Vol. 198. P. 357–364. doi: 10.2214/AJR.11.6981

38. Kollmer J., Bendszus M., Pham M. MR neurography: Diagnostic imaging in the PNS // Clin Neuroradiol. 2015. Vol. 25, Suppl. 2. P. 283–289. doi: 10.1007/s00062-015-0412-0

39. Chhabra A., Deshmukh S.D., Lutz A.M., et al. Neuropathy score reporting and data system: A reporting guideline for MRI of peripheral neuropathy with a multicenter validation study // AJR Am J Roentgenol. 2022. Vol. 219, N 2. P. 279–291. doi: 10.2214/AJR.22.27422

40. Chhabra A., Deshmukh S.D., Lutz A.M., et al. Neuropathy score reporting and data system (NS-RADS): MRI reporting guideline of peripheral neuropathy explained and reviewed // Skeletal Radiol. 2022. Vol. 51, N 10. P. 1909–1922. doi: 10.1007/s00256-022-04061-1

AUTHORS' INFO

*** Sofya N. Morozova,** MD, Cand. Sci. (Med.);
address: 80 Volokolamskoe shosse, 125637 Moscow, Russia;
ORCID: 0000-0002-9093-344X;
eLibrary SPIN: 2434-7827;
e-mail: morozova@neurology.ru

Viktoriya V. Sinkova;
ORCID: 0000-0003-2285-2725;
e-mail: 000564321@mail.ru

ОБ АВТОРАХ

*** Морозова Софья Николаевна,** канд. мед. наук;
адрес: Россия, 125637, Москва, Волоколамское шоссе, д. 80;
ORCID: 0000-0002-9093-344X;
eLibrary SPIN: 2434-7827;
e-mail: morozova@neurology.ru

Синькова Виктория Викторовна;
ORCID: 0000-0003-2285-2725;
e-mail: 000564321@mail.ru

* Corresponding author / Автор, ответственный за переписку

Darya A. Grishina, MD, Cand. Sci. (Med.);
ORCID: 0000-0002-7924-3405;
eLibrary SPIN: 6577-1799;
e-mail: dgrishina82@gmail.com

Taisiya A. Tumilovich;
ORCID: 0000-0002-9538-9690;
eLibrary SPIN: 2264-9457;
e-mail: tumilovich.taisiya@bk.ru

Andrey O. Chechetkin, MD, Dr. Sci. (Med.);
ORCID: 0000-0002-8726-8928;
eLibrary SPIN: 9394-6995;
e-mail: andreychechetkin@gmail.com

Marina V. Krotenkova, MD, Dr. Sci. (Med.);
ORCID: 0000-0003-3820-4554;
eLibrary SPIN: 9663-8828;
e-mail: krotenkova_mrt@mail.ru

Natalya A. Suponeva, MD, Dr. Sci. (Med.), Professor, Corresponding member of the Russian Academy of Sciences;
ORCID: 0000-0003-3956-6362;
eLibrary SPIN: 3223-6006;
e-mail: nasu2709@mail.ru

Гришина Дарья Александровна, канд. мед. наук;
ORCID: 0000-0002-7924-3405;
eLibrary SPIN: 6577-1799;
e-mail: dgrishina82@gmail.com

Тумилович Таисия Александровна;
ORCID: 0000-0002-9538-9690;
eLibrary SPIN: 2264-9457;
e-mail: tumilovich.taisiya@bk.ru

Чечеткин Андрей Олегович, д-р мед. наук;
ORCID: 0000-0002-8726-8928;
eLibrary SPIN: 9394-6995;
e-mail: andreychechetkin@gmail.com

Кротенкова Марина Викторовна, д-р мед. наук;
ORCID: 0000-0003-3820-4554;
eLibrary SPIN: 9663-8828;
e-mail: krotenkova_mrt@mail.ru

Супонева Наталья Александровна, д-р мед. наук, профессор, чл.-корр. РАН;
ORCID: 0000-0003-3956-6362;
eLibrary SPIN: 3223-6006;
e-mail: nasu2709@mail.ru

DOI: https://doi.org/10.17816/DD375328

Посмертные лучевые исследования в мировом и отечественном здравоохранении: анализ литературы и мнений российских специалистов

А.И. Щеголев, У.Н. Туманова

Национальный медицинский исследовательский центр акушерства, гинекологии и перинатологии имени академика В.И. Кулакова, Москва, Российская Федерация

АННОТАЦИЯ

Несмотря на особую значимость вскрытий тел умерших больных с целью определения причины смерти и эффективности проведённого лечения, во всех странах отмечается прогрессирующее снижение их количества. Одновременно с этим наблюдается активное внедрение посмертных лучевых исследований для анализа тел умерших и погибших пациентов.

Представлен анализ данных литературы, обобщающих результаты анкетирований иностранных специалистов, а также мнений российских специалистов о возможностях и особенностях проведения посмертных лучевых исследований главным образом новорождённых и младенцев. Отмечено, что посмертные лучевые исследования проводятся как в рамках патологоанатомического вскрытия, так и судебно-медицинской экспертизы. В случаях насильственной смерти чаще проводили посмертную компьютерную томографию, при смерти от болезней — посмертную магнитно-резонансную томографию. Более часто использовалось общеклиническое оборудование, находящееся в клинических отделениях лучевой диагностики, чем оборудование, расположенное в морге, патологоанатомическом отделении или судебно-медицинском учреждении. Анализ результатов посмертных лучевых исследований в большинстве наблюдений проводили врачи-рентгенологи, намного реже имел место совместный анализ рентгенолога и патологоанатома. Подчёркивается, что в Российской Федерации посмертные лучевые исследования носят в основном единичный характер. В то же время, по мнению российских исследователей, в настоящее время — время развития персонализированной медицины, лучевых методик и информационных технологий — назрела необходимость использования посмертных лучевых исследований для объективизации и повышения точности традиционных аутопсий. При этом посмертные лучевые исследования, представляющие собой объективные оператор-независимые методы исследования тел погибших, следует рассматривать как высокоэффективный этап патологоанатомического и тем более судебно-медицинского вскрытия.

Ключевые слова: аутопсия; виртопсия; посмертная магнитно-резонансная томография; посмертная компьютерная томография; КТ; танаторадиология; обзор.

Как цитировать:

Щеголев А.И., Туманова У.Н. Посмертные лучевые исследования в мировом и отечественном здравоохранении: анализ литературы и мнений российских специалистов // *Digital Diagnostics.* 2023. Т. 4, № 3. С. 369–383. DOI: https://doi.org/10.17816/DD375328

Рукопись получена: 03.05.2023 **Рукопись одобрена:** 27.05.2023 **Опубликована:** 22.08.2023

DOI: https://doi.org/10.17816/DD375328

Postmortem radiology studies in global and national healthcare: literature analysis and perspectives of Russian specialists

Aleksandr I. Shchegolev, Ulyana N. Tumanova

Research Center for Obstetrics, Gynecology and Perinatology, Moscow, Russian Federation

ABSTRACT

Despite the significant importance of autopsies for determining the cause of death and the evaluating the effectiveness of treatments, there is a progressive decrease in their number across all countries. At the same time, there is an active introduction of postmortem radiological studies to analyze the bodies of deceased patients.

The article presents literature analysis summarizing the results of surveys from foreign specialists, as well as the opinions of Russian specialists, regarding the possibilities and features of postmortem radiological studies, mainly focusing on deceased newborns and infants. It is noted that postmortem radiological studies are carried out as part of both pathoanatomical autopsy and forensic medical examination. Postmortem computed tomography in cases of violent death and postmortem magnetic resonance imaging in cases of death from diseases were performed more often. General clinical equipment located in clinical radiology departments was more frequently used than those located in the mortuary, pathology department, or forensic facility. The analysis of the results of postmortem radiological examinations was predominantly carried out by radiologists, with a joint analysis involving a radiologist and a pathologist being less common. It is emphasized that in the Russian Federation, postmortem radiological studies are mostly of a single nature. According to Russian researchers, in the current era of advancing personalized medicine, radiation techniques, and information technologies, there arises a need to use postmortem radiological studies to objectify and improve the accuracy of traditional autopsies. Postmortem radiological studies, which are objective operator-independent methods of examining the bodies of dead people, should be considered as a highly effective stage of pathology and, especially, forensic autopsy.

Keywords: autopsy; virtopsy; postmortem computed tomography; postmortem magnetic resonance imaging; thanatoradiology; review.

To cite this article:

Schegolev AI, Tumanova UN. Postmortem radiology studies in global and national healthcare: literature analysis and perspectives of Russian specialists. *Digital Diagnostics.* 2023;4(3):369–383. DOI: https://doi.org/10.17816/DD375328

Received: 03.05.2023 **Accepted:** 27.05.2023 **Published:** 22.08.2023

DOI: https://doi.org/10.17816/DD375328

全球和国内医疗保健中的放射尸检：文献分析和俄罗斯专家的观点

Aleksandr I. Shchegolev, Ulyana N. Tumanova

Research Center for Obstetrics, Gynecology and Perinatology, Moscow, Russian Federation

简评

虽然尸检对确定死因和治疗效果非常重要，但各国的尸检数量都在逐步减少。与此同时，医生正在积极引入放射尸检，以分析死亡病人的尸体。

本文介绍对文献数据的分析，这些数据总结外国专家的问卷调查结果，以及俄罗斯专家对放射尸检（主要是新生儿和婴儿）的可能性和特殊性的看法。据指出，放射尸检是在病理解剖和法医学鉴定的框架内进行的。在暴力致死的病例中，更常进行死后计算机断层扫描；在疾病致死的病例中，则进行死后磁共振成像。与停尸房、病理解剖科或法医学机构里的设备相比，临床放射诊断科的普通临床设备使用频率更高。大多数放射尸检都是由放射科医生进行分析的，而由放射科医生和病理学家共同进行分析的情况要少得多。需要强调的是，在俄罗斯联邦，放射尸检大多是零星的。同时，据俄罗斯研究人员称，在当前个性化医学、放射技术和信息技术发展的时代，有必要利用放射尸检来客观化和提高传统尸检的准确度。同时，放射尸检是独立于操作人员的客观尸体检查方法，应被视为病理解剖的高效阶段，更是法医学尸检的高效阶段。

关键词：尸检；虚拟尸检；死后磁共振成像；死后计算机断层扫描；CT；死后放射学；综述。

引用本文：

Schegolev AI, Tumanova UN. 全球和国内医疗保健中的放射尸检：文献分析和俄罗斯专家的观点. *Digital Diagnostics*. 2023;4(3):369–383. DOI: https://doi.org/10.17816/DD375328

收到：03.05.2023 **接受：**27.05.2023 **发布日期：**22.08.2023

INTRODUCTION

A conclusion about the cause of death is made by autopsy pathology specialists performing an autopsy of a deceased patient to confirm a clinical diagnosis or reveal a diagnostic error, establish the course of a disease and components of the dying process (thanatogenesis), evaluate the effectiveness of diagnostic and therapeutic measures, and generate mortality statistics [1]. Autopsies play a vital role in perinatal examinations, identification of hereditary and congenital diseases, and evaluation of subsequent pregnancy risk [2]. However, since the 1950s, in all countries where the consent of relatives is required for an autopsy, the number of these procedures has been progressively decreasing, mainly due to religious reasons, a long delay between death and burial, and the unwillingness of treating physicians to obtain information that may discredit their treatment strategy [3, 4].

In addition, the development of new medical equipment and diagnostic techniques allowed the ability to perform radiological examinations of people after death. Postmortem radiology was primarily used in forensic medicine. Therefore, in the 1990s, the Institute of Forensic Medicine at the University of Bern (Switzerland) began actively using 3D optical technologies for scanning corpses to better document external injuries and compare them with the suspected weapon of infliction. Then, postmortem computed tomography (CT) and magnetic resonance imaging (MRI) were introduced and compared with traditional autopsy [5]. In the United States, the Office of the Armed Forces Medical Examiner provided postmortem multispiral CT of dead members of the Armed Forces before autopsy to better assess combat injuries [6, 7]. Postmortem multispiral CT of people who died in the January 2020 earthquake in Haiti enabled rational body sorting for adequate subsequent autopsy [8].

Postmortem radiology is now used in many countries as part of a forensic medical examination and an autopsy, as reflected in the progressively increased number of publications [9, 10]. However, there is still no consensus on the objects (age group of patients and nature of abnormalities), type of apparatus, location, specialty, and qualifications of specialists performing postmortem radiology and analyzing results.

This information is undeniably important, particularly for those who intend to implement and perform such examinations in their institutions, cities, or regions. Because of its multinational and multireligious population, postmortem radiology is essential in the Russian Federation. Despite the relatively high level of radiology equipment in healthcare organizations, postmortem radiology is only used episodically in some institutions.

This paper aims to analyze the experience, recommendations, and proposals of foreign and Russian experts in postmortem radiology, considering potential opportunities and special aspects.

POSTMORTEM RADIOLOGY IN GLOBAL AND RUSSIAN HEALTHCARE

Conditions and stages of the study

The study is based on four surveys of members of the European Society of Pediatric Radiology (ESPR) and the International Society of Forensic Radiology and Imaging (ISFRI) from 2013 to 2021, postmortem radiology literature from eLibrary and National Center for Biotechnology Information databases (PubMed and PubMed Central), and opinions of Russian round table participants "Thanatoradiology: Real opportunities for organization and practical use in the healthcare system," which was held on October 8, 2022, in Moscow as a part of II Scientific and Practical Conference of the Interregional Thanatoradiology Society "Diagnostic radiology in pathology and forensic medicine: From antemortem to postmortem."

Due to the lack of consistent and generally accepted international guidelines on organizing and using postmortem radiology, the study analyzed literature data on surveys of foreign experts performing such examinations [11–14]. However, it should be noted that these surveys only included perinatal and pediatric medical institutions.

In the first survey (2013), questionnaires were distributed to 244 ESPR members [11]. The study included 66 questionnaires from 66 corresponding institutions, with postmortem radiological examinations performed in 47 (71%) institutions in 17 countries: Australia, Austria, Brazil, Great Britain, Hungary, Germany, Israel, Ireland, Canada, the Netherlands, New Zealand, Norway, USA, Finland, France, Switzerland, and Sweden. The largest number of responses and institutions were from the United Kingdom (11), the United States (9), and the Netherlands (5).

Three subsequent surveys included members of the ESPR and ISFRI. As a result, in the second survey (2016–2017), questionnaires were distributed to members of the aforementioned societies from 25 institutions [12]. Responses from 20 institutions in 11 countries were analyzed: Great Britain, Australia, USA, and Poland (three each); the Netherlands (2); Denmark, Italy, Switzerland, New Zealand, Canada, and Japan (one each).

In the third survey (2018–2019), questionnaires were distributed to all 14 members of the ESPR Postmortem Imaging Working Group and 17 members of the ISFRI Working Group, representing 25 different institutions [13]. The analysis included responses from 11 institutions in seven countries where postmortem radiology was used in the perinatal and pediatric practice: Australia (3), Great Britain (2), the Netherlands (2), Belgium (1), Switzerland (1), New Zealand (1), and Canada (1).

A fourth survey was conducted in 2021, with emails sent to 22 members of the ESPR Postmortem Imaging Working Group from 26 institutions. The analysis included 18 responses from 18 institutions in nine countries: Great Britain (6), Australia (3), Germany (2), the Netherlands (2), Austria (1), Belgium (1), Hungary (1), New Zealand (1), and Canada (1). Results were published by Chambers et al. [14].

Some questions were repeated in the above four surveys (questionnaires), whereas others were different. The first questions referred to objects of postmortem radiology.

Analysis of survey results

According to the first survey [11], all stillborn children were examined in 32% (15 out of 47) of institutions, whereas 26% (12/47) and 17% (8/47) examined all deceased newborns and infants, respectively. Only some stillborn children (45%), deceased newborns (49%), and infants (49%) were examined in most institutions.

According to the second survey [12], only one-third (35%) of institutions used postmortem radiology for all cases of fetal and pediatric death. In the third study [13], no institutions used postmortem radiology for all the deceased patients. According to the fourth survey [14], all institutions performed examinations on a case-by-case basis, with the majority (92.9%) performed for dead newborns (age 0–28 days), infants (1–12 months), and children (1–12 yr), followed by adolescents (age 13–18 yr; 85.7%) and fetuses (42.9%). Postmortem radiological examinations of deceased newborns and infants, children, and adolescents were less common in cases of nonviolent death: 82.4%, 58.5%, and 52.9%, respectively. However, fetal examinations were more common (76.5%) [14].

Since 2004, the Robert Kilpatrick Clinical Sciences Building Leicester Royal Infirmary in Leicester, UK, has regularly performed postmortem radiological examinations for deceased newborns and children in the radiology departments (24/7) [15].

As for the location of postmortem radiology equipment, in the first two surveys, general clinical equipment was used more frequently than in the mortuary, pathology department, or forensic institution (55% vs. 45%) [12]. According to the third survey [13], all specialists performed postmortem MRI using equipment in clinical radiology departments, and none of the centers surveyed had a special MRI scanner exclusively for postmortem imaging or a scanner located in the morgue or pathology department.

Controversial data on postmortem radiology procedures (and equipment) were obtained. The most common response in the first [11] and fourth [14] surveys was radiography (81% and 100% of cases, respectively), followed by CT (51% and 88.9%, respectively), MRI (38% and 61.1%), and ultrasound (8.5% and 27.8%). In most fatal cases, two or more different scanners (techniques) were used for radiological examination of corpses, but ultrasound was performed in all cases with radiological examination. However, in the third survey, all participants reported only postmortem MRI [13]. There are ongoing debates regarding who should conduct postmortem radiological examinations and, more importantly, who will evaluate their results. According to the second survey, radiological examinations were performed in most cases (65%) by a radiologist or a radiographer at a radiology department, considerably less frequently (15%) by morgue staff or a pathologist, and only in one institution by a forensic medical examiner [12]. According to the third survey, such examinations were performed in 90.9% of institutions by a radiologist or X-ray technician and 9.1% by an MRI specialist [13].

In terms of specialists analyzing postmortem radiology results, the first survey mentioned a radiologist in most cases (89%), including a pediatric radiologist (64%); in significantly fewer cases (17%), such an analysis was performed collaboratively by a radiologist and pathologist [11]. According to the second survey, 45% and 40% of responses mentioned radiologists and pathologists, respectively [12].

Shelmerdine et al. [12] should be cited in global literature data. This study was noteworthy because it presented a consensus protocol for postmortem CT. An important objective of Chambers et al. [14] was to evaluate funding and payment systems for postmortem radiology examinations. These aspects are undeniably important and should be the subject of separate publications on the characteristics of healthcare funding systems in different countries. However, according to most participants of the fourth survey [14], the main barrier to the widespread implementation of postmortem radiology was the lack of a special, nationally centralized (whenever possible) funding source. Therefore, in 2004, the UK Department of Health and Social Care initiated postmortem radiology of corpses, mainly deceased fetuses and newborns, as well as adults, to address the issue of possible autopsies being replaced by radiological examinations [16]. Since 2010, postmortem CT has been available in all cases of child death in the Netherlands if parents decide to perform an autopsy [17].

In our country, postmortem radiology is used episodically [18–20]. However, Academician V.I. Kulakov National Medical Research Center for Obstetrics, Gynecology, and Perinatology has conducted its research since 2011 to study and implement thanatoradiology (CT and MRI) into the practice of pathological examinations of stillborn and deceased newborns [21, 22]. Some cases of postmortem CT use in forensic medical examination have been reported in the Moscow region since 2018 [23, 24].

II SCIENTIFIC AND PRACTICAL CONFERENCE OF THE INTERREGIONAL THANATORADIOLOGY SOCIETY "DIAGNOSTIC RADIOLOGY IN PATHOLOGY AND FORENSIC MEDICINE: FROM ANTEMORTEM TO POSTMORTEM": KEY POINTS OF THE ROUND TABLE

Opportunities for organization and practical use of thanatoradiology

Due to the importance of postmortem radiology in the Russian Federation, in October 2022, a round table discussion was held as a part of II Scientific and Practical Conference of the Interregional Thanatoradiology Society "Diagnostic Radiology in Pathology and Forensic Medicine: From antemortem to postmortem" on the topic "Thanatoradiology: Real opportunities for organization and practical use in the healthcare system" [25]. The meeting was moderated by Yu. A. Vasiliev, director of the State Budgetary Institution "Research and Practical Clinical Center for Diagnostics and Telemedicine Technologies" of the Moscow Department of Health, chief freelance consultant in Radiology and Investigations of the Moscow Department of Health.

All participants noted that in the Russian Federation, in accordance with Federal Law No. 323-FZ dated November 21, 2011 (Article 67),[1] all deceased persons are subjected to a pathological autopsy, including a mandatory autopsy (despite the refusal) of stillborn children and children who died up to 28 days of life. A forensic autopsy is required if a violent death is present or suspected. Accordingly, a pathological autopsy (Article 67, paragraph 1) aims to obtain data on the cause of death and the diagnosis, and a forensic medical examination (Article 62, paragraph 1) establishes the circumstances as evidence for a specific case.

According to valid Order No. 346n of the Ministry of Health and Social Development of the Russian Federation dated May 12, 2010,[2] the type, nature, and scope of the examination are determined by the head of the forensic institution. It also determines specialists responsible for performing such an examination and involved staff of expert, scientific, educational, and other institutions. An expert should use medical technologies approved for use in the Russian Federation, primarily technologies and techniques not associated with modification, destruction, or destruction of examined objects. Moreover, paragraph 47.8 states that radiography is first performed (wherever technically possible) during an external examination of a corpse to clarify the nature and characteristics of damage or painful changes in skeletal bones. In other words, postmortem radiography is even recommended during a forensic examination; however, in accordance with the above order, only for bones. Simultaneously, according to Appendix 2 to Order No. 364n, the standard equipment for state forensic medical institutions includes an X-ray machine and a digital mobile X-ray system.

Selection of the most informative method of postmortem examination

A pathological autopsy is performed by a pathologist in accordance with Order No. 354n of the Ministry of Health of the Russian Federation dated June 6,[3] 2010, whereas histological, biochemical, microbiological, and other necessary methods of examining individual organs and tissues of the deceased people are considered an integral part of the pathological autopsy. Biological material is transferred to an appropriate structural unit of a healthcare organization to be examined. Radiology may be one of the procedures used for such mandatory examinations.

In 1969, a Soviet pathologist, I.I. Medvedev wrote about the important role of radiology, particularly X-ray, examination of a corps in guidelines for hospital anatomists *Fundamentals of pathological and anatomical technique* (Osnovy patologoanatomicheskoy tekhniki), "the X-ray method is rarely used by pathologists, although for a long time there are many reasons for its wide use, (...) therefore, it can be strongly recommended to install X-ray machines in dissecting rooms" [26]. Medvedev emphasized that X-ray examination allows the detection of even small changes in bone structure, bone tumors, osteochondropathies, calcification sites, and foreign bodies. Moreover, he stated that "the use of the X-ray method in pathology can play a great role in the development of X-ray diagnostics" [26].

Congenital abnormalities of the skeleton, which can be an independent defect or a manifestation of a syndrome, can include abnormalities of the facial skull, spine, and upper and lower extremities. In such cases, postmortem CT is the most effective and objective tool for postmortem identification of congenital abnormalities of bones, particularly small and facial bones, in stillborn and deceased newborns because of its superiority over traditional pathological autopsy [27, 28]. Accordingly, when discussing the advantages of various

[1] Federal Law No. 323-FZ dated November 21, 2011 on basics of health protection of the citizens in the Russian Federation. Link: https://base.garant.ru/12191967/.

[2] Order No. 346n of the Ministry of Health and Social Development of the Russian Federation dated May 12, 2010 on approval of the procedure for organizing and conducting forensic medical examinations in state forensic institutions of the Russian Federation. Link: https://base.garant.ru/12177987/#friends.

[3] Order No. 354n of the Ministry of Health of the Russian Federation dated June 6, 2013 on the procedure for conducting pathological autopsies. Link: https://www.garant.ru/products/ipo/prime/doc/70443162/.

DOI: https://doi.org/10.17816/DD375328

radiology methods, forensic experts named CT as a method of first choice because it provides the best visualization of injuries and fractures of bones, the degree of displacement of fragments, the course of the wound canal, hemorrhages, and foreign bodies, including bullets [29, 30]. CT also has other important advantages in forensic medicine, such as short examination duration and, accordingly, high throughput of the scanner, which is particularly important for examining bodies in cases of mass death (transport and natural disasters, military operations, or terrorist acts), as well as the availability of mobile CT modules to perform examination even directly at the place of the incident. Postmortem MRI is less popular among medical examiners than CT, although it better visualizes soft tissues and parenchymal organs.

We believe that the choice of an examination method should be based on the feasibility of obtaining maximum information in each specific case. This opinion is supported by literature data. Thus, Roberts et al. [31] found that CT is more accurate than CT in determining a cause of death in adult patients. Authors considered CT to have advantages, such as better visualization of coronary artery calcifications, hemorrhage areas, and fractures. MRI was more sensitive in acute myocardial infarction and soft tissue pathology [31]. According to Wijetunga et al. [32], a comprehensive postmortem CT and autopsy revealed more lesions in trauma deaths than either method alone, whereas Proisy et al. [33] found strong agreement between postmortem CT and autopsy data, with significant discrepancies detected primarily in lung diseases. Sieswerda-Hoogendoorn et al. [34] found a strong correlation between postmortem CT and autopsy data in cases of violent death, with no correlation in cases of natural death, and complete agreement between CT with autopsy data when the cause of death could not be determined initially. According to Krentz et al. [35], an autopsy is often superior to postmortem CT for detecting soft tissue and vascular changes, although CT is more effective for visualizing skeletal injuries.

When comparing the capabilities of postmortem CT and MRI, Arthurs et al. [36] found that MRI has higher diagnostic accuracy than CT in examining fetuses of less than 24 weeks of gestation and similar accuracy for older fetuses and newborns. Authors recommend postmortem MRI to visualize dead fetuses and children because it is the most effective method for determining brain, heart, and kidney diseases. Indeed, postmortem MRI allows one to determine the degree of brain maturity and visualize congenital abnormalities and abnormal changes [37, 38], assess the condition of lung tissue to identify those who were live-born and children with congenital pneumonia, assess the degree of pulmonary hypoplasia as a component of thanatogenesis [39–41], and determine the severity of anasarca and the volume of free fluid accumulated in serous cavities without opening cavities and tissue incisions [42, 43]. Thayyil et al. [44] reported in a large prospective study that the accuracy of postmortem MRI corresponds to the results of autopsies of dead fetuses, newborns, and infants and is lower when examining children over 1 yr of age.

To summarize, postmortem CT is the most informative method to visualize:

- traumatic, primarily mechanical, injuries, and wound channels, particularly in areas that are technically difficult for traditional dissection (bones and tissues of the facial skeleton, skull base, distal limbs, and spine);
- hemorrhages and fluid accumulations in organs, tissues, and cavities;
- air and gas accumulations in tissues, organs, lumen of blood vessels, and cavities;
- distinguishing dentition, including personal identification; and
- foreign bodies, including medical probes and catheters.

Postmortem CT is adequate for examining frozen, burned, and putrefied bodies and corpses in mummification and saponification. Limitations for postmortem CT include the low efficiency of unenhanced visualization of injuries and diseases of soft tissues, parenchymal and hollow organs, and spinal cord lesions. To assess vessels and cavities of the heart, including those with congenital abnormalities and injuries, contrast-enhanced CT should be performed [45, 46].

Postmortem MRI allows the identification of injuries and diseases of soft tissues and parenchymal organs and the examination of the brain and spinal cord, bone bruises, and hemorrhages. Compared with CT, postmortem MRI is more effective for examining dead fetuses, stillborns, and deceased newborns.

Limitations of postmortem MRI include insufficient visualization of respiratory system injuries and diseases in adult patients, as well as hollow organs, the gastrointestinal tract, and long bones. MRI images are challenging to interpret due to artifacts caused by metal elements present in the body.

Unfortunately, CT and MRI do not allow for microscopic, biochemical, toxicological, microbiological, virological, and genetic examinations of tissue and organ specimens, which are required to determine the histological picture and nature of the tumor, causative agent of the infectious process, impaired metabolic pathways, and poisonous substance. To perform this, a minimally invasive autopsy is recommended, which includes postmortem radiological examination and needle biopsy of tissue and organ specimens for the abovementioned examinations [47, 48]. This method has proven effective for postmortem diagnostics and protecting dissection staff from SARS-CoV-2 infection during autopsies of COVID-19 patients [49, 50]. Moreover, organ or tissue lesion visualization effectiveness also depends on age, body weight, and tissue condition [51].

Based on our own thanatoradiology experience [52–54], we believe that comprehensive postmortem radiology, including CT for accurate visualization of skeletal abnormalities and gas accumulations, MRI for tissue and organ assessment, and contrast-enhanced CT for assessment of blood vessels

and the heart, should be used for a complete examination of stillborn and deceased newborns. However, radiological procedures are currently selected due to the availability of the corresponding equipment or the possibility of conducting such an examination.

Selecting an institution for postmortem examination

According to Order No. 346n of the Ministry of Health and Social Development dated May 12, 2010,[4] the standard equipment of state forensic medical institutions includes an X-ray machine and a digital mobile X-ray system so such institutions can perform radiological examinations.

CT and MRI require particular premises and appropriate equipment. As for large forensic medical examination institutions that examine living persons and dead bodies, the optimal strategy would be creating a radiology office with a CT and/or MRI scanner based on such an institution. Indeed, in Switzerland, joint activities of the Institute of Forensic Medicine and the Institute of Diagnostic Radiology at the University of Bern led to conducting such postmortem CT examinations since 2000 [5]. At the Department of Forensic Medicine at the University of Copenhagen (Denmark) since 2002 and the Victorian Institute of Forensic Medicine in Melbourne (Australia) since 2005, all incoming corpses are subject to postmortem CT before autopsy [16, 55]. An interesting solution is to use mobile scanners, which are tomographs mounted on special vehicles that can be driven to the location of a corpse [56].

In Russia, any X-ray examinations are regulated by state sanitary and epidemiological rules and regulations, such as SanPiN 2.6.1.1192-03, which has been in effect since May 1, 2003.[5] These rules establish basic requirements and standards for ensuring the radiation safety of personnel, patients, and the general public when conducting diagnostic, preventive, therapeutic, or research X-ray procedures. There are no procedures to receive additional approval from Roszdravnadzor authorities for postmortem X-ray examinations. This was probably one reason pathologists participating in the above round table spoke about the need to conduct such studies in radiology departments of those healthcare institutions with pathology departments. Some proposals were made regarding using a separate room with its entrance and equipment. The above analysis of four surveys with foreign specialists shows that the same equipment is commonly used in clinical practice for living patients. However, in most of these institutions, postmortem examinations are conducted in the morning, in the evening, or at specially designated times when there are no appointments with living patients; hence, the principle of separating these flows was complied with.

Even though bodies are delivered and subjected to postmortem radiological examination in sealed plastic bags, SanPiN 2.6.1.1192-03 provides for mandatory wet cleaning of walls, washing floors, and thorough disinfection of elements and accessories of the X-ray machine, as well as monthly full-scale cleaning by wiping surfaces of the room, equipment, and accessories with a 1%–2% acetic acid.

Selecting a specialist for conducting a postmortem examination and analyzing the results obtained

As for those who should directly perform postmortem radiological examinations, all round table participants name radiologists, X-ray technicians, or radiotherapists. However, the type and extent of postmortem radiological examination before autopsy should be determined by a joint decision of a radiologist and a dissector. Because a pathological autopsy is performed after evaluating the medical history, which includes clarification of the clinical course and treatment of disease and antemortem laboratory tests and investigations, a radiologist should also be provided with available clinical information before conducting a radiological examination. This is confirmed by Fernandes et al. [57], who showed that awareness about clinical information improved the diagnostic accuracy of traditional autopsy by 8% and minimally invasive autopsy (including postmortem imaging and tissue sampling) by 12%.

In forensic medicine, the algorithm for postmortem radiological examination should be designed collaboratively based on the examination statement or decision, considering information on death circumstances, the postmortem period, and an external examination of the corpse. However, in 2010, the Republican Bureau of Forensic Medicine of the Ministry of Health of the Republic of Tatarstan began to provide special training in diagnostic radiology for internists and medical examiners [58].

During the round table, Russian experts agreed that a radiologist should also analyze and post-process images, including 3D modeling. From a legal point of view, additional certificates are not required for such activities, but a radiologist should have special knowledge of patterns of nonspecific postmortem changes in internal organs and associated radiological signs [59, 60]. When introducing postmortem radiology, a radiologist, pathologist, or medical examiner should analyze images and prepare a report [61].

Some additional questions occurred when discussing special aspects of introducing postmortem radiology in the

[4] Order No. 346n of the Ministry of Health and Social Development of the Russian Federation dated May 12, 2010 on approval of the procedure for organizing and conducting forensic medical examinations in state forensic institutions of the Russian Federation. Link: https://base.garant.ru/12177987/#friends.

[5] Resolution No. 8 of the Chief State Sanitary Inspector of the Russian Federation dated February 18, 2003 on implementation of SanPiN 2.6.1.1192-03. Link: https://base.garant.ru/4179018.

Russian Federation. For example, how much postmortem radiology data (i.e., full description or a summary conclusion) should be presented in a pathological or forensic autopsy report and whether particular combined protocols are required. Most participants agreed that a separate complete thanatoradiology report with a conclusion should be prepared even in case of discrepancies with the macroscopic and microscopic examination of a corpse. However, as with clinical guidelines, postmortem radiology reports should be unified, containing technical parameters of equipment and scanning modes.

A separate discussion is required to determine whether results of postmortem radiological examinations may or should be provided to relatives upon their request and to what extent.

CONCLUSION

Therefore, literature data and opinions of Russian specialists indicate the feasibility and urgent need to use postmortem radiology to make traditional autopsy more objective and accurate. Such examination should be considered the first stage of a pathological and forensic autopsy.

The key to effective thanatoradiological examination is close cooperation between radiologists, pathologists, or medical examiners. The collaboration of specialists and available equipment makes it possible to determine practical aspects of postmortem radiological examinations to obtain the most informative results in each case.

When determining the best place to install CT and/or MRI equipment, factual circumstances of the regional medical care and the availability of equipment and radiologists in healthcare institutions should be considered. However, for comprehensive implementation of postmortem radiology into pathological and forensic practice, a centralized solution is required for some organizational issues.

ADDITIONAL INFORMATION

Funding source. This article was not supported by any external sources of funding.

Competing interests. The authors declare that they have no competing interests.

Authors' contribution. All authors made a substantial contribution to the conception of the work, acquisition, analysis, interpretation of data for the work, drafting and revising the work, final approval of the version to be published and agree to be accountable for all aspects of the work. A.I. Shchegolev, U.N. Tumanova — concept and design of the article, data collection and analysis, drafting and revising the work, approval of the final version of the article.

REFERENCES

1. Connoly AJ, Finkbeiner WE, Ursell PC, Davis RL. Autopsy pathology: A manual and atlas. 3th ed. Elsevier Inc.; 2016. 400 p.

2. Ernst LM. A pathologist's perspective on the perinatal autopsy. *Semin Perinatol*. 2015;39(1):55–63. doi: 10.1053/j.semperi.2014.10.008

3. Oluwasola OA, Fawole OI, Otegbayo AJ, et al. The autopsy knowledge, attitude, and perceptions of doctors and relatives of the deceased. *Arch Pathol Lab Med*. 2009;133(1):78–82. doi: 10.5858/133.1.78

4. Levy B. Informatics and autopsy pathology. *Surg Pathol Clin*. 2015;8(2):159–174. doi: 10.1016/j.path.2015.02.010

5. Thali MJ, Yen K, Schweitzer W, et al. Virtopsy, a new imaging horizon in forensic pathology: virtual autopsy by postmortem multislice computed tomography (MSCT) and magnetic resonance imaging (MRI): A feasibility study. *J Forensic Sci*. 2003;48(2):386–403.

6. Eastridge BJ, Mardin M, Cantrell J, et al. Died of wounds on the battlefield: Causation and implications for improving combat casualty care. *J Trauma*. 2011;71(S.1):S4–8. doi: 10.1097/TA.0b013e318221147b

7. Eastridge BJ, Mabry RL, Seguin P, et al. Death on the battlefield (2001–2011): Implications for the future of combat casualty care. *J Trauma Acute Care Surg*. 2012;73(6 Suppl 5):S431–437. doi: 10.1097/TA.0b013e3182755dcc

8. Berran PJ, Mazuchowski EL, Marzouk A, Harcke HT. Observational case series: An algorithm incorporating multidetector computerized tomography in the medicolegal investigation of human remains after a natural disaster. *J Forensic Sci*. 2014;59(4):1121–1125. doi: 10.1111/1556-4029.12422

9. Baglivo M, Winklhofer S, Hatch GM, et al. The rise of forensic and post-mortem radiology: Analysis of the literature between the year 2000 and 2011. *J Forensic Radiol Imaging*. 2013;1(1):3–9.

10. Tumanova UN. Formation and development of postmortem radiological research in the world and in Russia. *REJR*. 2020;10(4):250–263. (In Russ). doi: 10.21569/2222-7415-2020-10-4-250-263

11. Arthurs OJ, van Rijn RR, Sebire NJ. Current status of paediatric post-mortem imaging: An ESPR questionnaire-based survey. *Pediatr Radiol*. 2014;44(3):244–251. doi: 10.1007/s00247-013-2827-6

12. Shelmerdine SC, Gerrard CY, Rao P, et al. Joint European society of paediatric radiology (ESPR) and international society for forensic radiology and imaging (ISFRI) guidelines: Paediatric postmortem computed tomography imaging protocol. *Pediatr Radiol*. 2019;49(5):694–701. doi: 10.1007/s00247-018-04340-x

13. Whitby E, Offiah AC, Shelmerdine SC, et al. Current state of perinatal postmortem magnetic resonance imaging: European society of paediatric radiology questionnaire-based survey and recommendations. *Pediatr Radiol*. 2021;51(5):792–799. doi: 10.1007/s00247-020-04905-9

14. Chambers G, Shelmerdine SC, Aertsen M, et al. Current and future funding streams for paediatric postmortem imaging: European society of paediatric radiology survey results. *Pediatr Radiol*. 2023;53(2):273–281. doi: 10.1007/s00247-022-05485-6

15. Rutty GN, Swift B. Accuracy of magnetic resonance imaging in determining cause of sudden death in adults: Comparison with conventional autopsy. *Histopathology*. 2004;44(2):187–189. doi: 10.1111/j.1365-2559.2004.01741.x

16. O'Donnell C, Rotman A, Collett S, Woodford N. Current status of routine post-mortem CT in Melbourne, Australia. *Forensic Sci Med Pathol*. 2007;3(3):226–232. doi: 10.1007/s12024-007-9006-8

17. Van Rijn RR, Beek EJ, van de Putte EM, et al. The value of postmortem computed tomography in paediatric natural cause of

death: A Dutch observational study. *Pediatr Radiol*. 2017;47(11):1514–1522. doi: 10.1007/s00247-017-3911-0

18. Halikov AD, Alexandrov DZ, Trofimova TN, et al. Virtual autopsy of a stillborn with Cantrell's pentad. *Neurosurgery Neurology Childhood*. 2009;(1):14–19. (In Russ).

19. Byval'tsev VA, Stepanov IA, Semenov AV, et al. The possibilities for diagnostics of prescription of death coming based on the changes in the lumbar intervertebral disks (the comparison of the morphological, immunohistochemical and topographical findings). *Forensic Medical Examination*. 2017;(4):4–8. (In Russ). doi: 10.17116/sudmed20176044-8

20. Borshchevskaya VN, Solonkina AD, Globa IV. Postmortem computed tomographic diagnosis of pulmonary embolism in the practice of a forensic medical expert (pilot study). In: Materials of the II Scientific and practical conference of the Interregional Thanatoradiological Society "Radiation diagnostics for pathological anatomy and forensic medical examination: from lifetime to postmortem", 7–8 October. Moscow; 2022. P. 118–121. (In Russ). doi: 10.54182/9785988117094_2022_118

21. Tumanova UN, Fedoseeva VK, Liapin VM, et al. Postmortem computed tomography of stillborn with bone pathology. *Medical imaging*. 2013;(5):110–120. (In Russ).

22. Tumanova UN, Shchegolev AI. The role and place of thanatoradiological studies in the pathological examination of fetuses and newborns. *Bull Exp Biol Med*. 2022;173(6):691–705. doi: 10.1007/s10517-022-05615-y

23. Klevno VA, Chumakova YV, Dubrova SE. Forensic medical examination and post-mortem computed tomography in case of death from mechanical asphyxia: Diagnostic difficulties. *Forensic Medicine*. 2019;(S1):54. (In Russ).

24. Klevno VA, Chumakova YV. Virtopsy: New method of research in national practice of forensic medicine. *Forensic Medicine*. 2019;5(2):27–31. (In Russ). doi: 10.19048/2411-8729-2019-5-2-27-31

25. Shchegolev AI, Tumanova UN. II Scientific and practical conference of the Interregional Thanatoradiological Society "Radiological diagnostics for pathological anatomy and forensic medicine: From lifetime to postmortem". *Forensic Medicine*. 2022;8(4):105–110. (In Russ). doi: 10.17816/fm759

26. Medvedev II. Fundamentals of pathoanatomical technology. 3nd revised and updated. Moscow: Medicine; 1969. 288 p. (In Russ).

27. Tumanova UN, Fedoseeva VK, Lyapin VM, et al. Acardiac fetus: Postmortem computed and magnetic resonance tomography imaging. *Diagnostic Int Radiol*. 2016;10(2):23–30. (In Russ).

28. Tumanova UN, Lyapin VM, Burov AA, et al. VACTERL association of newborn: Postmortem ct and mri imaging for autopsy. *REJR*. 2017;7(2):191–208. (In Russ). doi: 10.21569/2222-7415-2017-7-2-191-208

29. Kokov LS, Kinle AF, Sinitsyn VY, Filimonov BA. Possibilities of computed tomography and magnetic resonance imaging in forensic medical examination of mechanical trauma and sudden death (a literature review). *Emergency medical care. N.V. Sklifosovsky Magazine*. 2015;(2):16–26. (In Russ).

30. Kovalev AV, Kinle AF, Kokov LS, et al. Actual possibilities of postmortem imaging in forensic medicine practice. *Consilium Medicum*. 2016;18(13):9–25. (In Russ).

31. Roberts IS, Benamore RE, Benbow EW, et al. Post-mortem imaging as an alternative to autopsy in the diagnosis of adult deaths: A validation study. *Lancet*. 2012;379(9811):136–142. doi: 10.1016/S0140-6736(11)61483-9

32. Wijetunga C, O'Donnell C, So TY, et al. Injury detection in traumatic death: Postmortem computed tomography vs open autopsy. *Forensic Imaging*. 2020;(20):100349. doi: 10.1016/j.jofri.2019.100349

33. Proisy M, Marchand AJ, Loget P, et al. Whole-body post-mortem computed tomography compared with autopsy in the investigation of unexpected death in infants and children. *Eur Radiol*. 2013;23(6):1711–1719. doi: 10.1007/s00330-012-2738-1

34. Sieswerda-Hoogendoorn T, Soerdjbalie-Maikoe V, de Bakker H, van Rijn RR. Postmortem CT compared to autopsy in children; Concordance in a forensic setting. *Int J Legal Med*. 2014;128(6):957–965. doi: 10.1007/s00414-014-0964-6

35. Krentz BV, Alamo L, Grimm J, et al. Performance of post-mortem CT compared to autopsy in children. *Int J Legal Med*. 2016;130(4):1089–1099. doi: 10.1007/s00414-016-1370-z

36. Arthurs OJ, Guy A, Thayyil S, et al. Comparison of diagnostic performance for perinatal and paediatric post-mortem imaging: CT versus MRI. *Eur Radiol*. 2016;26(7):2327–2336. doi: 10.1007/s00330-015-4057-9

37. Whitby EH, Variend S, Rutter S, et al. Corroboration of in utero MRI using post-mortem MRI and autopsy in foetuses with CNS abnormalities. *Clin Radiol*. 2004;59(12):1114–1120. doi: 10.1016/j.crad.2004.04.018

38. Tumanova UN, Serova NS, Shchegolev AI. Use of the postmortem MRI for the cerebral lesions diagnosis in the fetuses and newborns. *REJR*. 2017;7(3):8–22. (In Russ). doi: 10.21569/2222-7415-2017-7-3-8-22

39. Tumanova UN, Lyapin VM, Bychenko VG, et al. Postmortem magnetic resonance imaging in the diagnosis of congenital pneumonia. *Bulletin Russ State Med University*. 2016;(4):44–50. (In Russ).

40. Tumanova UN, Serova NS, Bychenko VG, Shchegolev AI. Possibilities of postmortem radiological studies for evaluation of lung lesions. *REJR*. 2018;8(2):198–221. (In Russ). doi: 10.21569/2222-7415-2018-8-2-198-221

41. Tumanova UN, Lyapin VM, Bychenko VG, et al. Potentialities of postmortem magnetic resonance imaging for identification of live birth and stillbirth. *Bull Exp Biol Med*. 2019;167(6):823–826. doi: 10.1007/s10517-019-04631-9

42. Tumanova UN, Lyapin VM, Bychenko VG, et al. Postmortem MRI characteristics of nonimmune fetal hydrops. *REJR*. 2018;8(4):172–183. (In Russ). doi: 10.21569/2222-7415-2018-8-4-172-18

43. Tumanova UN, Lyapin VM, Bychenko VG, et al. Possibilities of postmortem magnetic resonance imaging for evaluation of anasarca in newborns. *Bull Exp Biol Med*. 2019;166(5):671–675. doi: 10.1007/s10517-019-04415-1

44. Thayyil S, Sebire NJ, Chitty LS, et al. Post-mortem MRI versus conventional autopsy in fetuses and children: A prospective validation study. *Lancet*. 2013;382(9888):223–233. doi: 10.1016/S0140-6736(13)60134-8

45. Grabherr S, Heinemann A, Vogel H, et al. Postmortem CT angiography compared with autopsy: A forensic multicenter study. *Radiology*. 2018;288(1):270–276. doi: 10.1148/radiol.2018170559

46. Tumanova UN, Lyapin VM, Bychenko VG, et al. Postmortem computed tomography angiography of newborns. *Bull Exp Biol Med*. 2020;170(2):268–274. doi: 10.1007/s10517-020-05049-4

47. Ben-Sasi K, Chitty LS, Franck LS, et al. Acceptability of a minimally invasive perinatal/paediatric autopsy: Healthcare professionals' views and implications for practice. *Prenat Diagn*. 2013;33(4):307–312. doi: 10.1002/pd.4077

48. Blokker BM, Weustink AC, Wagensveld IM, et al. Conventional autopsy versus minimally invasive autopsy with postmortem MRI, CT, and CT-guided biopsy: Comparison of diagnostic performance. *Radiology*. 2018;289(3):658–667. doi: 10.1148/radiol.2018180924
49. Shchegolev AI, Tumanova UN. Persistence of SARS-CoV-2 in deceased patients and safe handling of infected bodies. *Bulletin of RSMU*. 2021;(3):5–11. doi: 10.24075/brsmu.2021.029
50. Raviraj KG, Shobhana SS, Raviraj KG, et al. Findings and inferences from full autopsies, minimally invasive autopsies and biopsy studies in patients who died as a result of COVID19: A systematic review. *Forensic Sci Med Pathol*. 2022;18(3):369–381. doi: 10.1007/s12024-022-00494-1
51. Tumanova UN, Shchegolev AI, Kovalev AV. Technical and methodological support for postmortem radiation examinations in the pathological departments and the forensic bureau. *Forensic Medical Examination*. 2021;64(2):51–57. (In Russ). doi: 10.17116/sudmed20216402151
52. Tumanova UN, Fedoseeva VK, Lyapin VM, et al. Identification of gas accumulations in the bodies of fetuses, still-borns and dead newborns at postmortem computed tomography study. *Consilium Medicum*. 2016;18(13):26–33. (In Russ).
53. Tumanova UN, Lyapin VM, Shchegolev AI, et al. Epignatus of a newborn: Postmortem CT and MRI imaging for autopsy. *REJR*. 2017;7(4):90–107. (In Russ). doi: 10.21569/2222-7415-2017-7-4-90-107
54. Tumanova UN, Lyapin VM, Kozlova AV, et al. Galen vein aneurysm in a newborn: Postmortem MSCT with contrast enhancement of vessels within the autopsy. *REJR*. 2019;9(2):260–274. (In Russ). doi: 10.21569/2222-7415-2019-9-2-260-274
55. Poulsen K, Simonsen J. Computed tomography as routine in connection with medico-legal autopsies. *Forensic Sci Int*. 2007;171(2-3):190–197. doi: 10.1016/j.forsciint.2006.05.041
56. Fetisov VA. Advantages and disadvantages of CT scanners and their placement options for postmortem cross-sectional imaging (UK specialists experience). *Consilium Medicum*. 2016;18(13):34–37. (In Russ).
57. Fernandes F, Castillo P, Bassat Q, et al. Contribution of the clinical information to the accuracy of the minimally invasive and the complete diagnostic autopsy. *Hum Pathol*. 2019;(85):184–193. doi: 10.1016/j.humpath.2018.10.037
58. Spiridonov VA. To the question of the development of virtual autopsy in Russia, or what to do? *Forensic Medicine*. 2016;(2):93–94. (In Russ).
59. Dubrova SE, Filimonov BA. Postmortem computed tomography and its features: What should clinical radiologists know? *Consilium Medicum*. 2016;18(13):38–47. (In Russ).
60. Shchegolev AI, Tumanova UN, Lyapin VM. Pathological estimation of the time of fetal death. *Pathology Archive*. 2017;79(6):60–65. (In Russ). doi: 10.17116/patol201779660-65
61. Tumanova UN, Shchegolev AI, Kovalev AV. Organization of postmortem radiological examination in the structure of pathological departments and forensic bureaus. *Forensic Medical Examination*. 2021;64(1):57–63. (In Russ). doi: 10.17116/sudmed20216401157

СПИСОК ЛИТЕРАТУРЫ

1. Connoly A.J., Finkbeiner W.E., Ursell P.C., Davis R.L. Autopsy pathology: A manual and atlas. 3th ed. Elsevier Inc., 2016. 400 p.
2. Ernst L.M. A pathologist's perspective on the perinatal autopsy // Semin Perinatol. 2015. Vol. 39, N 1. P. 55–63. doi: 10.1053/j.semperi.2014.10.008
3. Oluwasola O.A., Fawole O.I., Otegbayo A.J., et al. The autopsy knowledge, attitude, and perceptions of doctors and relatives of the deceased // Arch Pathol Lab Med. 2009. Vol. 133, N 1. P. 78–82. doi: 10.5858/133.1.78
4. Levy B. Informatics and autopsy pathology // Surg Pathol Clin. 2015. Vol. 8, N 2. P. 159–174. doi: 10.1016/j.path.2015.02.010
5. Thali M.J., Yen K., Schweitzer W., et al. Virtopsy, a new imaging horizon in forensic pathology: Virtual autopsy by postmortem multislice computed tomography (MSCT) and magnetic resonance imaging (MRI): A feasibility study // J Forensic Sci. 2003. Vol. 48, N 2. P. 386–403.
6. Eastridge B.J., Mardin M., Cantrell J., et al. Died of wounds on the battlefield: Causation and implications for improving combat casualty care // J Trauma. 2011. Vol. 71, N S1. P. 4–8. doi: 10.1097/TA.0b013e318221147b
7. Eastridge B.J., Mabry R.L., Seguin P., et al. Death on the battlefield (2001–2011): Implications for the future of combat casualty care // J Trauma Acute Care Surg. 2012. Vol. 73, N 6, Suppl. 5. P. 431–437. doi: 10.1097/TA.0b013e3182755dcc
8. Berran P.J., Mazuchowski E.L., Marzouk A., Harcke H.T. Observational case series: an algorithm incorporating multidetector computerized tomography in the medicolegal investigation of human remains after a natural disaster // J Forensic Sci. 2014. Vol. 59, N 4. P. 1121–1125. doi: 10.1111/1556-4029.12422
9. Baglivo M., Winklhofer S., Hatch G.M., et al. The rise of forensic and post-mortem radiology: Analysis of the literature between the year 2000 and 2011 // J Forensic Radiol Imaging. 2013. Vol. 1, N 1. P. 3–9. doi: 10.1016/j.jofri.2012.10.003
10. Туманова У.Н. Становление и развитие посмертных лучевых исследований в мире и России // REJR. 2020. Т. 10, № 4. С. 250–263. doi: 10.21569/2222-7415-2020-10-4-250-263
11. Arthurs O.J., van Rijn R.R., Sebire N.J. Current status of paediatric post-mortem imaging: An ESPR questionnaire-based survey // Pediatr Radiol. 2014. Vol. 44, N 3. P. 244–251. doi: 10.1007/s00247-013-2827-6
12. Shelmerdine S.C., Gerrard C.Y., Rao P., et al. Joint European society of paediatric radiology (ESPR) and international society for forensic radiology and imaging (ISFRI) guidelines: Paediatric postmortem computed tomography imaging protocol // Pediatr Radiol. 2019. Vol. 49, N 5. P. 694–701. doi: 10.1007/s00247-018-04340-x
13. Whitby E., Offiah A.C., Shelmerdine S.C., et al. Current state of perinatal postmortem magnetic resonance imaging: European society of paediatric radiology questionnaire-based survey and recommendations // Pediatr Radiol. 2021. Vol. 51, N 5. P. 792–799. doi: 10.1007/s00247-020-04905-9
14. Chambers G., Shelmerdine S.C., Aertsen M., et al. Current and future funding streams for paediatric postmortem imaging: European society of paediatric radiology survey results // Pediatr Radiol. 2023. Vol. 53, N 2. P. 273–281. doi: 10.1007/s00247-022-05485-6
15. Rutty G.N., Swift B. Accuracy of magnetic resonance imaging in determining cause of sudden death in adults: Comparison with conventional autopsy // Histopathology. 2004. Vol. 44, N 2. P. 187–189. doi: 10.1111/j.1365-2559.2004.01741.x

16. O'Donnell C., Rotman A., Collett S., Woodford N. Current status of routine post-mortem CT in Melbourne, Australia // Forensic Sci Med Pathol. 2007. Vol. 3, N 3. P. 226–232. doi: 10.1007/s12024-007-9006-8
17. Van Rijn R.R., Beek E.J., van de Putte E.M., et al. The value of postmortem computed tomography in paediatric natural cause of death: A Dutch observational study // Pediatr Radiol. 2017. Vol. 47, N 11. P. 1514–1522. doi: 10.1007/s00247-017-3911-0
18. Халиков А.Д., Александрова З.Д., Трофимова Т.Н., и др. Виртуальная аутопсия мертворожденного с пентадой Кантрелла // Нейрохирургия и неврология детского возраста. 2009. № 1. С. 14–19.
19. Бывальцев В.А., Степанов И.А., Семенов А.В., и др. Возможности диагностики давности наступления смерти по изменениям в поясничных межпозвонковых дисках (сопоставление морфологических, иммуногистохимических и томографических результатов) // Судебно-медицинская экспертиза. 2017. № 4. С. 4–8. doi: 10.17116/sudmed20176044-8
20. Борщевская В.Н., Солонкина А.Д., Глоба И.В. Посмертная компьютерно-томографическая диагностика тромбоэмболии легочной артерии в практике судебно-медицинского эксперта (пилотное исследование) // Материалы II Научно-практической конференции Межрегионального танаторадиологического общества «Лучевая диагностика для патологической анатомии и судебно-медицинской экспертизы: от прижизненной к посмертной», 7–8 октября. Москва, 2022. С. 118–121. doi: 10.54182/9785988117094_2022_118
21. Туманова У.Н., Федосеева В.К., Ляпин В.М., и др. Посмертная компьютерная томография мертворожденных с костной патологией // Медицинская визуализация. 2013. № 5. С. 110–120.
22. Tumanova U.N., Shchegolev A.I. The role and place of thanatoradiological studies in the pathological examination of fetuses and newborns // Bull Exp Biol Med. 2022. Vol. 173, N 6. P. 691–705. doi: 10.1007/s10517-022-05615-y
23. Клевно В.А., Чумакова Ю.В., Дуброва С.Э. Судебно-медицинская экспертиза и посмертная компьютерная томография в случае смерти от механической асфиксии: сложности диагностики // Судебная медицина. 2019. № S1. С. 54.
24. Клевно В.А., Чумакова Ю.В. Виртопсия — новый метод исследования в практике отечественной судебной медицины // Судебная медицина. 2019. № 2. С. 27–31. doi: 10.19048/2411-8729-2019-5-2-27-31
25. Щеголев А.И., Туманова У.Н. II Научно-практическая конференция Межрегионального танаторадиологического общества «Лучевая диагностика для патологической анатомии и судебно-медицинской экспертизы: от прижизненной к посмертной» // Судебная медицина. 2022. № 4. С. 105–110. doi: 10.17816/fm759
26. Медведев И.И. Основы патологоанатомической техники. 3-е изд., испр. и доп. Москва: Медицина, 1969. 288 с.
27. Туманова У.Н., Федосеева В.К., Ляпин В.М., и др. Плодакардиус: посмертная компьютерная и магнитно-резонансная томография // Диагностическая и интервенционная радиология. 2016. Т. 10, № 2. С. 23–30.
28. Туманова У.Н., Ляпин В.М., Буров А.А., и др. VACTERL ассоциация у новорожденного: посмертная КТ и МРТ визуализация при патологоанатомическом исследовании // REJR. 2017. Vol. 7, N 2. P. 191–208. doi: 10.21569/2222-7415-2017-7-2-191-208
29. Коков Л.С., Кинле А.Ф., Синицын В.Е., Филимонов Б.А. Возможности компьютерной и магнитно-резонансной томографии в судебно-медицинской экспертизе механической травмы и скоропостижной смерти (обзор литературы) // Неотложная медицинская помощь. Журнал им. Н.В. Склифосовского. 2015. № 2. С. 16–26.
30. Ковалев А.В., Кинле А.Ф., Коков Л.С., и др. Реальные возможности посмертной лучевой диагностики в практике судебно-медицинского эксперта // Consilium Medicum. 2016. Т. 18, № 13. С. 9–25.
31. Roberts I.S., Benamore R.E., Benbow E.W., et al. Post-mortem imaging as an alternative to autopsy in the diagnosis of adult deaths: A validation study // Lancet. 2012. Vol. 379, N 9811. P. 136–142. doi: 10.1016/S0140-6736(11)61483-9
32. Wijetunga C., O'Donnell C., So T.Y., et al. Injury detection in traumatic death: Postmortem computed tomography vs open autopsy // Forensic Imaging. 2020. N 20. P. 100349. doi: 10.1016/j.jofri.2019.100349
33. Proisy M., Marchand A.J., Loget P., et al. Whole-body post-mortem computed tomography compared with autopsy in the investigation of unexpected death in infants and children // Eur Radiol. 2013. Vol. 23, N 6. P. 1711–1719. doi: 10.1007/s00330-012-2738-1
34. Sieswerda-Hoogendoorn T., Soerdjbalie-Maikoe V., de Bakker H., van Rijn R.R. Postmortem CT compared to autopsy in children; Concordance in a forensic setting // Int J Legal Med. 2014. Vol. 128, N 6. P. 957–965. doi: 10.1007/s00414-014-0964-6
35. Krentz B.V., Alamo L., Grimm J., et al. Performance of postmortem CT compared to autopsy in children // Int J Legal Med. 2016. Vol. 130, N 4. P. 1089–1099. doi: 10.1007/s00414-016-1370-z
36. Arthurs O.J., Guy A., Thayyil S., et al. Comparison of diagnostic performance for perinatal and paediatric post-mortem imaging: CT versus MRI // Eur Radiol. 2016. Vol. 26, N 7. P. 2327–2336. doi: 10.1007/s00330-015-4057-9
37. Whitby E.H., Variend S., Rutter S., et al. Corroboration of in utero MRI using post-mortem MRI and autopsy in foetuses with CNS abnormalities // Clin Radiol. 2004. Vol. 59, N 12. P. 1114–1120. doi: 10.1016/j.crad.2004.04.018
38. Туманова У.Н., Серова Н.С., Щеголев А.И. Применение посмертной МРТ для диагностики поражений головного мозга у плодов и новорожденных // REJR. 2017. Т. 7, № 3. С. 8–22. doi: 10.21569/2222-7415-2017-7-3-8-22
39. Tumanova U.N., Lyapin V.M., Bychenko V.G., et al. Postmortem magnetic resonance imaging in the diagnosis of congenital pneumonia // Bulletin Russ State Med University. 2016. № 4. С. 44–50.
40. Туманова У.Н., Серова Н.С., Быченко В.Г., Щеголев А.И. Возможности посмертных лучевых исследований для оценки поражений легких // REJR. 2018. Т. 8, № 2. С. 198–221. doi: 10.21569/2222-7415-2018-8-2-198-221
41. Tumanova U.N., Lyapin V.M., Bychenko V.G., et al. Potentialities of postmortem magnetic resonance imaging for identification of live birth and stillbirth // Bull Exp Biol Med. 2019. Vol. 167, N 6. P. 823–826. doi: 10.1007/s10517-019-04631-9
42. Туманова У.Н., Ляпин В.М., Быченко В.Г., и др. Посмертная МРТ-характеристика неиммунной водянки плода // Российский электронный журнал лучевой диагностики. 2018. Т. 8, № 4. С. 172–183. doi: 10.21569/2222-7415-2018-8-4-172-18
43. Tumanova U.N., Lyapin V.M., Bychenko V.G., et al. Possibilities of postmortem magnetic resonance imaging for evaluation of anasarca in newborns // Bull Exp Biol Med. 2019;166(5):671–675. doi: 10.1007/s10517-019-04415-1

44. Thayyil S., Sebire N.J., Chitty L.S., et al. Post-mortem MRI versus conventional autopsy in fetuses and children: A prospective validation study // Lancet. 2013. Vol. 382, N 9888. P. 223–233. doi: 10.1016/S0140-6736(13)60134-8
45. Grabherr S., Heinemann A., Vogel H., et al. Postmortem CT angiography compared with autopsy: A forensic multicenter study // Radiology. 2018. Vol. 288, N 1. P. 270–276. doi: 10.1148/radiol.2018170559
46. Tumanova U.N., Lyapin V.M., Bychenko V.G., et al. Postmortem computed tomography angiography of newborns // Bull Exp Biol Med. 2020. Vol. 170, N 2. P. 268–274. doi: 10.1007/s10517-020-05049-4
47. Ben-Sasi K., Chitty L.S., Franck L.S., et al. Acceptability of a minimally invasive perinatal/paediatric autopsy: Healthcare professionals' views and implications for practice // Prenat Diagn. 2013. Vol. 33, N 4. P. 307–312. doi: 10.1002/pd.4077
48. Blokker B.M., Weustink A.C., Wagensveld I.M., et al. Conventional autopsy versus minimally invasive autopsy with postmortem MRI, CT, and CT-guided biopsy: Comparison of diagnostic performance // Radiology. 2018. Vol. 289, N 3. P. 658–667. doi: 10.1148/radiol.2018180924
49. Shchegolev A.I., Tumanova U.N. Persistence of SARS-CoV-2 in deceased patients and safe handling of infected bodies // Bulletin of RSMU. 2021. N 3. P. 5–11. doi: 10.24075/brsmu.2021.029
50. Raviraj K.G., Shobhana S.S., Raviraj K.G., et al. Findings and inferences from full autopsies, minimally invasive autopsies and biopsy studies in patients who died as a result of COVID19: A systematic review // Forensic Sci Med Pathol. 2022. Vol. 18, N 3. P. 369–381. doi: 10.1007/s12024-022-00494-1
51. Туманова У.Н., Щеголев А.И., Ковалев А.В. Техническое и методическое обеспечение проведения посмертных лучевых исследований в патологоанатомических отделениях и бюро судебно-медицинской экспертизы // Судебно-медицинская экспертиза. 2021. Т. 64, № 2. С. 51–57.
52. Туманова У.Н., Федосеева В.К., Ляпин В.М., и др. Выявление скоплений газа в телах плодов, мертворожденных и умерших новорожденных при посмертном компьютерно-томографическом исследовании // Consilium Medicum. 2016. Т. 18, № 13. С. 26–33.
53. Туманова У.Н., Ляпин В.М., Щеголев А.И., и др. Эпигнатус у новорожденного: посмертная КТ- и МРТ-визуализация при патологоанатомическом исследовании // REJR. 2017. Т. 7, № 4. С. 90–107. doi: 10.21569/2222-7415-2017-7-4-90-107
54. Туманова У.Н., Ляпин В.М., Козлова А.В., и др. Аневризма вены Галена у новорожденного: посмертная КТ с контрастным усилением сосудов при патологоанатомическом исследовании // REJR. 2019. Т. 9, № 2. С. 260–274. doi: 10.21569/2222-7415-2019-9-2-260-274
55. Poulsen K., Simonsen J. Computed tomography as routine in connection with medico-legal autopsies // Forensic Sci Int. 2007. Vol. 171, N 2-3: P. 190–197. doi: 10.1016/j.forsciint.2006.05.041
56. Фетисов В.А. Преимущества и недостатки вариантов размещения компьютерных томографов для посмертной визуализации (опыт специалистов Великобритании) // Consilium Medicum. 2016. Т. 18, № 13. С. 34–37.
57. Fernandes F., Castillo P., Bassat Q., et al. Contribution of the clinical information to the accuracy of the minimally invasive and the complete diagnostic autopsy // Hum Pathol. 2019. Vol. 85. P. 184–193. doi: 10.1016/j.humpath.2018.10.037
58. Спиридонов В.А. К вопросу развития виртуальной аутопсии в России, или что делать? // Судебная медицина. 2016. № 2. С. 93–94.
59. Дуброва С.Э., Филимонов Б.А. Что должен знать клинический рентгенолог об особенностях компьютерной томографии трупа? // Consilium Medicum. 2016. Т. 18, № 13. С. 38–47.
60. Щеголев А.И., Туманова У.Н., Ляпин В.М. Патологоанатомическая оценка давности внутриутробной гибели плода // Архив патологии. 2017. Т. 79. № 6. С. 60–65.
61. Туманова У.Н., Щеголев А.И., Ковалев А.В. Организация проведения посмертных лучевых исследований в структуре патологоанатомических отделений и бюро судебно-медицинской экспертизы // Судебно-медицинская экспертиза. 2021. Т. 64, № 1. С. 57–63. doi: 10.17116/sudmed20216401157

AUTHORS' INFO

*** Aleksandr I. Shchegolev,** MD, Dr. Sci. (Med.), Professor;
address: 4 Akademika Oparina street, 117997 Moscow, Russia;
ORCID: 0000-0002-2111-1530;
eLibrary SPIN: 9061-5983;
e-mail: ashegolev@oparina4.ru

Ulyana N. Tumanova, MD, Dr. Sci. (Med.);
ORCID: 0000-0002-0924-6555;
eLibrary SPIN: 7555-0987;
e-mail: u.n.tumanova@yandex.ru

ОБ АВТОРАХ

*** Щеголев Александр Иванович,** д-р мед. наук, профессор;
адрес: Россия, 117997, Москва, ул. академика Опарина, д. 4;
ORCID: 0000-0002-2111-1530;
eLibrary SPIN: 9061-5983;
e-mail: ashegolev@oparina4.ru

Туманова Ульяна Николаевна, д-р мед. наук;
ORCID: 0000-0002-0924-6555;
eLibrary SPIN: 7555-0987;
e-mail: u.n.tumanova@yandex.ru

* Corresponding author / Автор, ответственный за переписку

DOI: https://doi.org/10.17816/DD430154

Магнитно-резонансная томография в диагностике редкого генетического заболевания — недержания пигмента (синдром Блоха–Сульцбергера) — на примере клинического случая

И.И. Ярмола[1], А.В. Аникин[1], Д.А. Ганькин[2], Л.Е. Фомина[1], Н.А. Харитонова[1], И.С. Жанин[1], А.А. Пушков[1], М.А. Басаргина[1], О.Б. Кондакова[1]

[1] Национальный медицинский исследовательский центр здоровья детей, Москва, Российская Федерация;
[2] Щёлковский перинатальный центр, Щёлково, Российская Федерация

АННОТАЦИЯ

Недержание пигмента (синдром Блоха–Сульцбергера) — редкое наследственное заболевание, проявляющееся характерными кожными высыпаниями и поражением других органов и систем. Магнитно-резонансная томография является приоритетным методом для визуализации структурной патологии головного мозга и прогноза неврологической манифестации у ребёнка.

Ключевая роль диагностики заболевания недержания пигмента принадлежит дерматологу; подтверждающая диагностика проводится путём молекулярно-генетического анализа гена *IKBKG*.

В представленном клиническом наблюдении у новорождённой девочки с высыпаниями на кожных покровах, типичными для синдрома Блоха–Сульцбергера, и выявленной делецией в гене *IKBKG* проводилась магнитно-резонансная томография головного мозга, где были обнаружены многочисленные очаги ишемии, кровоизлияния и поражение проводящих путей.

Магнитно-резонансная томография головного мозга у пациентов с синдромом Блоха–Сульцбергера используется для оценки тяжести поражения вещества мозга, что позволяет объяснить причину неврологических симптомов, скорректировать реабилитационные мероприятия, а также прогнозировать развитие ребёнка.

Ключевые слова: недержание пигмента; синдром Блоха–Сульцбергера; магнитно-резонансная томография; дегенерация проводящих путей; ген *IKBKG*.

Как цитировать:
Ярмола И.И., Аникин А.В., Ганькин Д.А., Фомина Л.Е., Харитонова Н.А., Жанин И.С., Пушков А.А., Басаргина М.А., Кондакова О.Б. Магнитно-резонансная томография в диагностике редкого генетического заболевания — недержания пигмента (синдром Блоха–Сульцбергера) — на примере клинического случая // *Digital Diagnostics*. 2023. Т. 4, № 3. С. 384–392. DOI: https://doi.org/10.17816/DD430154

Рукопись получена: 16.05.2023 **Рукопись одобрена:** 29.06.2023 **Опубликована:** 22.08.2023

DOI: https://doi.org/10.17816/DD430154

Magnetic resonance imaging for diagnosing a rare disease: incontinentia pigmenti (Bloch–Sulzberger syndrome) on the example of a clinical case

Igor I. Yarmola[1], Anatoly V. Anikin[1], Dmitry A. Gankin[2], Lyubov E. Fomina[1], Nataliya A. Kharitonova[1], Ilya S. Zhanin[1], Alexander A. Pushkov[1], Milana A. Basargina[1], Olga B. Kondakova[1]

[1] National Medical Research Center for Children's Health, Moscow, Russian Federation;
[2] Shchelkovsky Perinatal Center, Schelkovo, Russian Federation

ABSTRACT

Incontinentia pigmenti, also known as Bloch–Sulzberger syndrome, is a rare hereditary disease characterized by typical skin rashes and involvement of other organs and systems. Magnetic resonance imaging stands as the primary method for visualizing the structural pathology of the brain and predicting neurological manifestations in an affected child.

Diagnosing incontinentia pigmenti predominantly falls within the domain of dermatologists; verification is performed by molecular genetic analysis of the *IKBKG* gene. This study involved magnetic resonance imaging of the brain in a patient with skin rashes, characteristic of Bloch–Sulzberger syndrome, and deletion in the *IKBKG* gene, where numerous foci of ischemia, hemorrhages, and lesions of the tracts were detected.

Magnetic resonance imaging of the brain in patients with Bloch–Sulzberger syndrome is used to evaluate the severity of damage to the brain substance, which makes it possible to explain the cause of neurological symptoms and correct habilitation, as well as predict the development of the child.

Keywords: incontinentia pigmenti; Bloch–Sulzberger syndrome; magnetic resonance imaging; white matted tracts degeneration; *IKBKG* gene.

To cite this article:
Yarmola II, Anikin AV, Gankin DA, Fomina LE, Kharitonova NA, Zhanin IS, Pushkov AA, Basargina MA, Kondakova OB. Magnetic resonance imaging for diagnosing a rare disease: incontinentia pigmenti (Bloch–Sulzberger syndrome) on the example of a clinical case. *Digital Diagnostics.* 2023;4(3):384–392. DOI: https://doi.org/10.17816/DD430154

Received: 16.05.2023 **Accepted:** 29.06.2023 **Published:** 22.08.2023

DOI: https://doi.org/10.17816/DD430154

磁共振成像在罕见遗传性疾病（即色素失禁症，也称布洛赫-苏兹伯格综合征）诊断中的应用：临床病例

Igor I. Yarmola[1], Anatoly V. Anikin[1], Dmitry A. Gankin[2], Lyubov E. Fomina[1], Nataliya A. Kharitonova[1], Ilya S. Zhanin[1], Alexander A. Pushkov[1], Milana A. Basargina[1], Olga B. Kondakova[1]

[1] National Medical Research Center for Children›s Health, Moscow, Russian Federation;
[2] Shchelkovsky Perinatal Center, Schelkovo, Russian Federation

简评

色素失禁症（布洛克-苏兹伯格综合征，Bloch-Sulzberger Syndrome）是一种罕见的遗传性疾病，表现为特征性皮疹以及其他器官和系统的损坏。磁共振成像是显示出大脑结构病变和预测儿童神经系统表现的优先方法。

皮肤科医生在色素失禁症的诊断中起着关键作用；需要通过对IKBKG基因进行分子遗传分析，以确诊。

一名新生女婴患有典型的布洛赫-苏兹伯格综合征皮疹和IKBKG基因缺失，在进行脑磁共振成像检查后，医生发现了多处缺血、出血和传导通路病变。

布洛赫-苏兹伯格综合征患者的脑磁共振成像可用于评估脑物质损坏的严重程度，这有助于解释神经症状的原因、调整康复措施和预测患儿的发展。

关键词：色素失禁症；布洛克-苏兹伯格综合征；磁共振成像；传导通路变性；IKBKG基因。

引用本文：
Yarmola II, Anikin AV, Gankin DA, Fomina LE, Kharitonova NA, Zhanin IS, Pushkov AA, Basargina MA, Kondakova OB. 磁共振成像在罕见遗传性疾病（即色素失禁症，也称布洛赫-苏兹伯格综合征）诊断中的应用：临床病例. *Digital Diagnostics*. 2023;4(3):384–392.
DOI: https://doi.org/10.17816/DD430154

收到：16.05.2023 **接受：**29.06.2023 **发布日期：**22.08.2023

BACKGROUND

Skin, hair, teeth, nails, eyes, and the central nervous system (CNS) are all damaged by incontinentia pigmenti (OMIM 308300: Familial male-lethal type Bloch–Sulzberger syndrome; incontinentia pigmenti type II). The condition typically appears in the first few days or weeks of life.

In the global literature, 2,000 cases of incontinentia pigmenti have been described, and the number is increasing. The global prevalence of incontinentia pigmenti is estimated to be 0.7 cases per million people. The incidence in Europe is 1.2 cases per 100,000 neonates [1]. Mutations in the inhibitor of kappa B kinase gamma (*IKBKG*) gene at position Xq28 on the X chromosome's long arm cause the disorder. The gene regulates apoptosis, cell cycle, inflammation, immunology, and other processes [2–4].

The condition has a wide spectrum of clinical manifestations, ranging from a mildly reduced quality of life to deadly results. The changes in the nucleotide sequence in the gene result in structural changes in the brain [5]. Magnetic resonance imaging (MRI) can detect anomalies, which is useful in identifying various monogenic [6] and multifactorial inherited disorders [7].

Incontinentia pigmenti is inherited in an X-linked dominant trait that kills most male embryos during development. The affected girl-to-boy ratio is 20:1.

Multiple organs and systems are involved in incontinentia pigmenti, most of which emerge from the ectoderm. In 100% of cases, several skin eruptions are found. The disease is distinguished by the linear alignment of the vesicles and pustules along the lines of Blaschko. Patients with inconintentia pigmenti have been documented to have alopecia, oral development anomalies, and fingernail dystrophy. Furthermore, affected patients are more likely to develop ocular pathologies, such as retinal hypervascularization, which can lead to retinal detachment if left untreated (typically occurs during the first 6 yr of life) [8]. Strabismus, cataracts, optic atrophy, retinal pigmentation, and microphthalmia have also been reported. According to several authors, the CNS is involved in 10% to 30% of cases [9], resulting in seizures of varying severity (cases ranging from a single seizure episode to chronic epilepsy), cognitive impairment, mental retardation, and spastic paresis. Less common disorders include breast aplasia, supernumerary nipples, primary pulmonary hypertension, and leukocytosis.

Molecular genetic testing identifies *IKBKG* mutations, and histological examination of the skin tissue samples is used to diagnose the condition. There is a clinical indication [10] to suspect pigmentary incontinence.

The treatment is symptomatic to prevent skin infections, retinal detachment, and epileptic seizures. Dental implants or orthodontic correction are recommended for dental problems, whereas therapy is recommended for spastic activity or paresis.

CASE REPORT

A 14-day-old girl was taken to the Neonatal and Early Age Pathology Department of the National Medical Research Center for the Children's Health of the Ministry of Health of the Russian Federation.

Prenatal history

In the first and second trimesters of pregnancy, there was a threat of miscarriage due to cytomegalovirus infection (confirmed by polymerase chain reaction) in the first trimester; the mother had inpatient therapy. The mother experienced three episodes of acute respiratory virus infections in the third trimester and herpetic eruptions twice.

The infant was delivered at 38 weeks gestation as the second full-term spontaneous childbirth: body weight at birth, 3,470 g; body length, 53 cm; and Apgar score: 9/9.

The post-natal condition was satisfactory. Extensive exanthema covered the entire body, including the trunk, face, and limbs (Figure 1). The eruption had been removed from the scalp. The laboratory results were age-appropriate; the inflammatory indicators were not present.

The general condition began to deteriorate on Day 4: cyanotic spots appeared on the limbs; the skin was icteric, with a grayish hue; the breathing became weakened, with a tendency to tachypnea; low blood oxygen saturation (SpO_2: 81%–95%) was determined; hyperexcitability at examinations and depressed consciousness at rest were observed; upper and lower limb muscles were hypertonic; and head lag as well as seizures were demonstrated.

Fig.1. Vesicles aligned with the lines of Blaschko.

Laboratory data showed the following changes: blood pH reduced to 7.242, blood lactate increased to 6.4 mmol/L, and HCO_3 decreased to 16.7 mmol/L (metabolic acidosis).

Dermatological examination revealed that the skin lesions had receded and that linear brown-to-light pink pigmentation had appeared, which had turned to hypopigmentation during the follow-up. Bloch–Sulzberger syndrome was the preliminary diagnosis.

Molecular genetic testing was run to identify exons 4–10 deletion in *IKBKG*: multiplex allele-specific polymerase chain reaction with primers as described by Haque et al. [11] was used. The findings revealed heterozygous deletion of *IKBKG* exons 4–10 in patients with the Bloch–Sulzberger syndrome, as published in the Human Gene Mutation Database Professional. This frequent mutation in incontinentia pigmenti occurs in 65% of patients [12].

On Day 4, the girl's condition was assessed as moderately severe due to the syndrome of CNS depression. Neurosonography revealed extensive ischemia abnormalities in the brain parenchyma and numerous focal changes in the parasagittal and periventricular areas.

On Day 7, an MRI indicated large areas of tiny focal lesions in the cerebral hemispheres, with secondary involvement of the corpus callosum and the corticospinal tract. The findings were interpreted as the result of repeated ischemic strokes induced by incontinentia pigmenti (Bloch–Sulzberger syndrome).

DISCUSSION

Bloch–Sulzberger syndrome is caused by a genetic abnormality that increases the sensitivity of cells developing from ectoderm to cytokine effects, resulting in apoptosis [13]. The skin and its derivatives (nails, hair, and teeth) and the nervous system are formed from the ectoderm. Disease symptoms commonly arise within the first 10 days of life. Because the disease stage at birth varies, the previous stages are assumed to occur *in utero*.

The disease manifested in the described patient in a typical manner during the first days of life, beginning with linear skin eruptions, which later experienced incremental modifications in accordance with the disease pathomorphosis and were accompanied by neurological symptoms.

Multiple small (min. 2 mm) restricted diffusion lesions were found in the deep white matter, in and under the cortex, in the corpus callosum, posterior limb of the internal capsule, cerebral peduncles, along the corticospinal tract, and other tracts (Figure 2). Changes in the spinal pathways can be interpreted as either direct injury from incontinentia pigmenti or an early indicator of Wallerian degeneration (pre-Wallerian condition). The latter is characterized by spinal tract injury caused by neuron death and the degradation of the myelin sheath [14]. Small patches of restricted diffusion were regarded as tissue necrosis (infarctions).

There are reports in the literature of minor focal brain infarctions caused by injury to the walls of small and medium-sized arteries, resulting in microhemorrhages and thrombosis. There have also been reports of extensive bilateral hemorrhagic necrosis cases with broad brain tissue damage [15].

Among the numerous lesions in the presented instance, the brain MRI revealed single regions with hemorrhagic features compatible with ischemia (Figure 3a). This suggests that not all ischemia foci were accompanied by bleeding. Although necrotic areas eventually turn into encephalomalacia areas, some areas with minimal damage may recover entirely and even be consistent with the normal structure of brain matter in MRI [16]. The hyperintense signal was seen in the cortical area and at the gray/white matter interface in the frontal and parietal lobes in T1-weighted images (T1-WI)

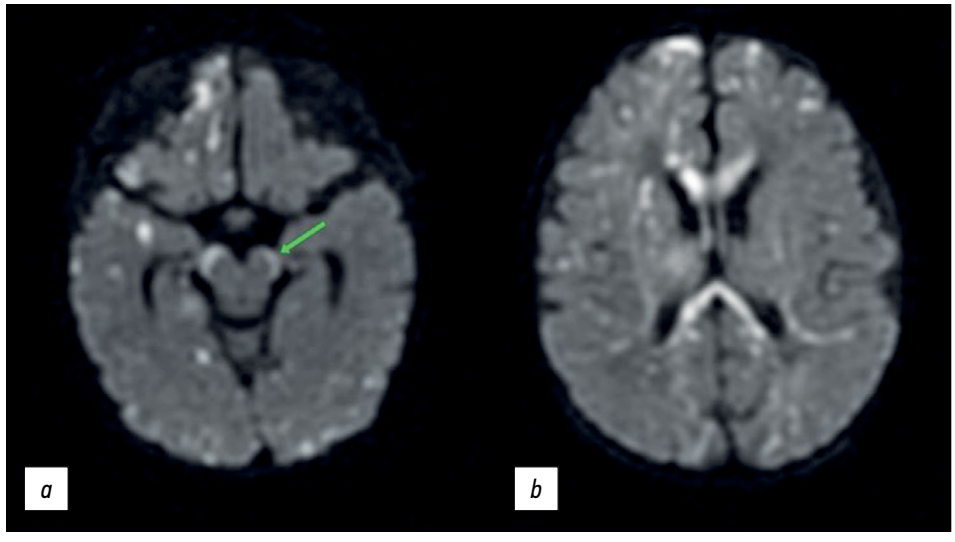

Fig. 2. Diffuse-weighted brain images in the axial plane: (*a*) the arrow shows the hyperintense signal from the spinal tracts in the brain peduncles and (*b*) multiple lesions and involvement of the corpus callosum.

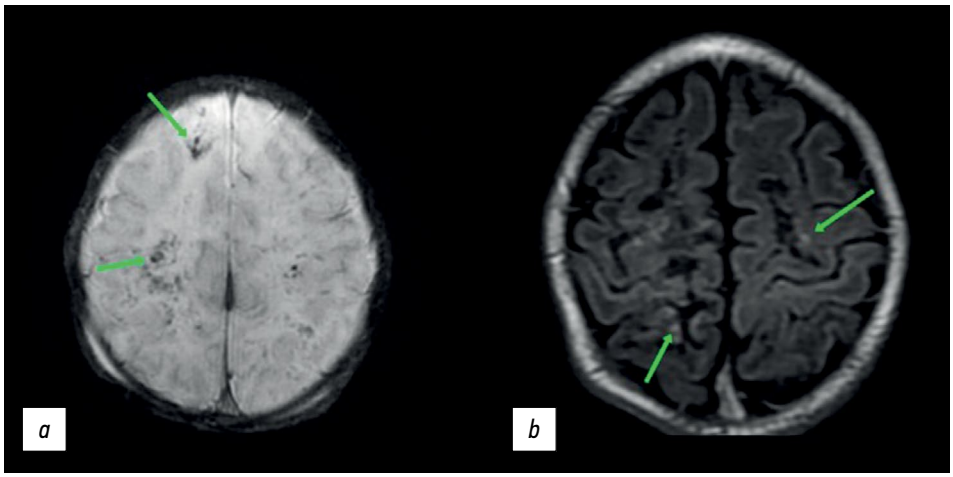

Fig. 3. Magnetic resonance imaging (MRI) of the brain: (*a*) susceptibility-weighted images (the arrows show microhemorrhages) and (*b*) T1-weighted images (the arrows indicate hyperintense areas of the cortical necrosis).

(Figure 3b). These areas resemble cortical necrosis, which occurs after ischemia damage to the cortex, resulting in monocyte infiltration and phagocytosis of cell fragments in the damaged structures. T1 images are hyperintense due to deposits of denatured protein of the dead cells and/or lipid-loaded macrophages [17].

Furthermore, histologically validated cases of inflammatory changes of the arachnoid mater and the brain with eosinophilic infiltration in patients with incontinentia pigmenti have been documented, mimicking infection-related damage without evident vascular disorders [18].

First, an MRI-based differential diagnosis is made for encephalitis and neonatal hypoxic–ischemic damage. Encephalitis is distinguished by alternating short and long areas of hyperintense signal in T2-WI with possible restricted or hyperintense diffusion, whereas incontinentia pigmenti is distinguished by chaotic small-lesion damage primarily localized in the white matter. The perinatal ischemia image corresponds to brain structural development patterns; full-term neonates generally have periventricular leukomalacia, basal ganglia damage, or violations that follow the artery patterns. Differential diagnosis of embolic stroke is complex and requires a comprehensive approach, with medical history collection and patient examination.

Vesicular rash and neurological signs may be mistaken for manifestations of herpes infection. In this case, MRI results, typical skin eruptions with evident stages of pathomorphosis, and a negative test for herpes infection should prompt clinicians to consider incontinentia pigmenti.

CONCLUSION

Because the skin eruptions are specific and follow clear stages, a dermatologist is essential in identifying incontinentia pigmenti. The molecular genetic test for *IKBKG* mutations is also important in diagnosis.

Brain MRI is the first imaging tool to assess brain matter injury when patients with Bloch–Sulzberger syndrome develop neurological symptoms. This method is safe for dynamic follow-up and enables objectively assessing rehabilitation potential, correcting the rehabilitation plan, and predicting the child's development.

ADDITIONAL INFORMATION

Funding source. This article was not supported by any external sources of funding.

Competing interests. The authors declare that they have no competing interests.

Authors' contribution. All authors made a substantial contribution to the conception of the work, acquisition, analysis, interpretation of data for the work, drafting and revising the work, final approval of the version to be published and agree to be accountable for all aspects of the work. I.I. Yarmola — writing text of the article, planning article structure, imaging analysis; A.V. Anikin — editing of the article, analytical work, discussion of the results, read and approved the direction of the manuscript for publication; D.A. Gankin — editing the text of the article, discussion of the results; L.E. Fomina — edition of the text of the article; N.A. Kharitonova — read and approved the direction of the manuscript for publication; I.S. Zhanin, A.A. Pushkov — article editing, conducting molecular genetic analysis; O.B. Kondakova — article editing, genetic counseling of the patient.

Consent for publication. Written consent was obtained from the patient's parents for publication of relevant medical information and all of accompanying images within the manuscript in Digital Diagnostics Journal.

REFERENCES

1. Scheuerle AE, Ursini MV, Adam MP, et al. Incontinentia Pigmenti. In: GeneReviews [Internet], Seattle (WA): University of Washington, Seattle; 1993.
2. Fusco F. Molecular analysis of the genetic defect in a large cohort of IP patients and identification of novel NEMO mutations interfering with NF-B activation. *Hum Mol Genet*. 2004;13(16):1763–1773. doi: 10.1093/hmg/ddh192
3. Yadlapati S, Tripathy K. Incontinentia pigmenti (Bloch Sulzberger Syndrome). In: StatPearls [Internet]. Treasure Island (FL): StatPearls Publishing; 2023.
4. Savostyanov KV. Modern algorithms of genetic diagnosis of rare hereditary diseases in Russian patients. Moscow: Polygraphist Publisher; 2022. 451 p. (In Russ).
5. Minić S, Cerovac N, Novaković I, et al. The impact of the IKBKG gene on the appearance of the corpus callosum abnormalities in incontinentia pigmenti. *Diagnostics*. 2023;13(7):1300. doi: 10.3390/diagnostics13071300
6. Chistiakov DA, Savostanov KV, Kuzenkova LM, et al. Molecular characteristics of patients with glycosaminoglycan storage disorders in Russia. *Clin Chim Acta*. 2014;(436):112–120. doi: 10.1016/j.cca.2014.05.010
7. Chistyakov DA, Savostanov KV, Nosikov VV, Turakulov RI. Genetic determinants of Graves' disease. *Mol Gen Metabol*. 2000;71(1-2):66–69. doi: 10.1006/mgme.2000.3042
8. Meuwissen ME, Mancini GM. Neurological findings in incontinentia pigmenti: A review. *Eur J Med Genet*. 2012;55(5):323–331. doi: 10.1016/j.ejmg.2012.04.007
9. Carney RG. Incontinentia pigmenti. A world statistical analysis. *Arch Dermatol*. 1976;112(4):535–542.
10. Minić S, Trpinac D, Obradović M. Incontinentia pigmenti diagnostic criteria update. *Clin Genet*. 2014;85(6):536–542. doi: 10.1111/cge.12223
11. Haque MN, Ohtsubo M, Nishina S, et al. Analysis of IKBKG/NEMO gene in five Japanese cases of incontinentia pigmenti with retinopathy: Fine genomic assay of a rare male case with mosaicism. *J Hum Genet*. 2021;66(2):645–645. doi: 10.1038/s10038-020-00836-3
12. Kawai M, Kato T, Tsutsumi M, et al. Molecular analysis of low-level mosaicism of the IKBKG mutation using the X Chromosome Inactivation pattern in Incontinentia Pigmenti. *Mol Genet Genomic Med*. 2020;8(12):e1531. doi: 10.1002/mgg3.1531
13. Tak PP, Firestein GS. NF-κB: A key role in inflammatory diseases. *J Clin Invest*. 2001;107(1):7–11. doi: 10.1172/JCI11830
14. Kleinman JT. Early Wallerian degeneration on magnetic resonance imaging: Underappreciated but highly relevant. *Dev Med Child Neurol*. 2013;55(2):104–105. doi: 10.1111/dmcn.12022
15. Salamon SA, Lichtenbelt K, Cowan FM, et al. Clinical presentation and spectrum of neuroimaging findings in newborn infants with incontinentia pigmenti. *Dev Med Child Neurol*. 2016;58(10):1076–1084. doi: 10.1111/dmcn.13140
16. Lou H, Zhang L, Xiao W, et al. Nearly completely reversible brain abnormalities in a patient with incontinentia pigmenti. *Am J Neuroradiol*. 2008;29(3):431–433. doi: 10.3174/ajnr.A0890
17. Kinoshita T, Ogawa T, Yoshida Y, et al, Curvilinear T1 hyperintense lesions representing cortical necrosis after cerebral infarction. *Neuroradiology*. 2005;47(7):647–651. doi: 10.1007/s00234-005-1398-0
18. Hauw JJ, Perié G, Bonnette J, Escourolle R. [Neuropathological study of incontinentia pigmenti. Anatomical case report (author's transl). (In French)]. *Acta Neuropathol*. 1977;38(2):159–162. doi: 10.1007/BF00688564

СПИСОК ЛИТЕРАТУРЫ

1. Scheuerle A.E., Ursini M.V., Adam M.P., et al. Incontinentia pigmenti. In: GeneReviews [Internet], Seattle (WA): University of Washington, Seattle, 1993.
2. Fusco F. Molecular analysis of the genetic defect in a large cohort of IP patients and identification of novel NEMO mutations interfering with NF-B activation // Hum Mol Genet. 2004. Vol. 13, N 16. P. 1763–1773. doi: 10.1093/hmg/ddh192
3. Yadlapati S., Tripathy K. Incontinentia pigmenti (Bloch Sulzberger Syndrome). In: StatPearls [Internet]. Treasure Island (FL): StatPearls Publishing, 2023.
4. Савостьянов К.В. Современные алгоритмы генетической диагностики редких наследственных болезней у российских пациентов. Москва: Полиграфист и издатель, 2022. 451 с.
5. Minić S., Cerovac N., Novaković I., et al. The impact of the IKBKG gene on the appearance of the corpus callosum abnormalities in incontinentia pigmenti // Diagnostics. 2023. Vol. 13, N 7. P. 1300. doi: 10.3390/diagnostics13071300
6. Chistiakov D.A., Savostanov K.V., Kuzenkova L.M., et al. Molecular characteristics of patients with glycosaminoglycan storage disorders in Russia // Clin Chim Acta. 2014. N 436. P. 112–120. doi: 10.1016/j.cca.2014.05.010
7. Chistyakov D.A., Savostanov K.V., Nosikov V.V., Turakulov R.I. Genetic determinants of Graves' disease // Mol Gen Metabol. 2000. Vol. 71, N 1-2. P. 66–69. doi: 10.1006/mgme.2000.3042
8. Meuwissen M.E., Mancini G.M. Neurological findings in incontinentia pigmenti: A review // Eur J Med Genet. 2012. Vol. 55, N 5. P. 323–331. doi: 10.1016/j.ejmg.2012.04.007
9. Carney R.G. Incontinentia pigmenti. A world statistical analysis // Arch Dermatol. 1976. Vol. 112, N 4. P. 535–542.
10. Minić S., Trpinac D., Obradović M. Incontinentia pigmenti diagnostic criteria update // Clin Genet. 2014. Vol. 85, N 6. P. 536–542. doi: 10.1111/cge.12223
11. Haque M.N., Ohtsubo M., Nishina S., et al. Analysis of IKBKG/NEMO gene in five Japanese cases of incontinentia pigmenti with retinopathy: Fine genomic assay of a rare male case with mosaicism // J Hum Genet. 2021. Vol. 66, N 2. P. 645–645. doi: 10.1038/s10038-020-00836-3
12. Kawai M., Kato T., Tsutsumi M., et al. Molecular analysis of low-level mosaicism of the IKBKG mutation using the X Chromosome Inactivation pattern in Incontinentia Pigmenti // Mol Genet Genomic Med. 2020. Vol. 8, N 12. P. e1531. doi: 10.1002/mgg3.1531
13. Tak P.P., Firestein G.S. NF-κB: A key role in inflammatory diseases // J Clin Invest. 2001. Vol. 107, N 1. P. 7–11. doi: 10.1172/JCI11830
14. Kleinman J.T. Early Wallerian degeneration on magnetic resonance imaging: Underappreciated but highly relevant // Dev Med Child Neurol. 2013. Vol. 55, N 2. P. 104–105. doi: 10.1111/dmcn.12022
15. Salamon S.A., Lichtenbelt K., Cowan F.M., et al. Clinical presentation and spectrum of neuroimaging findings in newborn

infants with incontinentia pigmenti // Dev Med Child Neurol. 2016. Vol. 58, N 10. P. 1076–1084. doi: 10.1111/dmcn.13140
16. Lou H., Zhang L., Xiao W., et al. Nearly completely reversible brain abnormalities in a patient with incontinentia pigmenti // Am J Neuroradiol. 2008. Vol. 29, N 3. P. 431–433. doi: 10.3174/ajnr.A0890
17. Kinoshita T., Ogawa T., Yoshida Y., et al, Curvilinear T1 hyperintense lesions representing cortical necrosis after cerebral infarction // Neuroradiology. 2005. Vol. 47, N 7. P. 647–651. doi: 10.1007/s00234-005-1398-0
18. Hauw J.J., Perié G., Bonnette J., Escourolle R. [Neuropathological study of incontinentia pigmenti. Anatomical case report (author's transl). (In French)] // Acta Neuropathol. 1977. Vol. 38, N 2. P. 159–162. doi: 10.1007/BF00688564

AUTHORS' INFO

*** Igor I. Yarmola;**
address: 2/1 Lomonosovsky prospekt, 119991 Moscow, Russia;
ORCID: 0000-0002-1272-5119;
eLibrary SPIN: 5591-8066;
e-mail: Lord_Dukich@bk.ru

Anatoly V. Anikin, MD, Cand. Sci. (Med.);
ORCID: 0000-0003-0362-6511;
eLibrary SPIN: 7592-1352;
e-mail: anikacor@gmail.com

Dmitry A. Gankin;
ORCID: 0009-0001-6779-8702;
e-mail: ganja-nn@yandex.ru

Lyubov E. Fomina;
ORCID: 0000-0002-3838-3284;
eLibrary SPIN: 1298-8350;
e-mail: love.fomina@mail.ru

Nataliya A. Kharitonova, MD, Cand. Sci. (Med.);
ORCID: 0000-0002-6912-1471;
eLibrary SPIN: 7379-8269;
e-mail: Kharitonova.na@nczd.ru

Ilya S. Zhanin, MD, Cand. Sci. (Med.);
ORCID: 0000-0003-1423-0379;
eLibrary SPIN: 6108-2016;
e-mail: zhanin.is@nczd.ru

Alexander A. Pushkov, Cand. Sci. (Biol.);
ORCID: 0000-0001-6648-2063;
eLibrary SPIN: 2928-5764;
e-mail: pushkov.aa@nczd.ru

Milana A. Basargina, MD, Cand. Sci. (Med.);
ORCID: 0000-0003-2075-6668;
eLibrary SPIN: 5504-7154;
e-mail: basargina.ma@nczd.ru

Olga B. Kondakova, MD, Cand. Sci. (Med.);
ORCID: 0000-0002-6316-9992;
eLibrary SPIN: 9066-3698;
e-mail: kondakova.ob@nczd.ru

ОБ АВТОРАХ

*** Ярмола Игорь Игоревич;**
адрес: Россия, 119991, Москва, Ломоносовский проспект, д. 2, стр. 1;
ORCID: 0000-0002-1272-5119;
eLibrary SPIN: 5591-8066;
e-mail: Lord_Dukich@bk.ru

Аникин Анатолий Владимирович, канд. мед. наук;
ORCID: 0000-0003-0362-6511;
eLibrary SPIN: 7592-1352;
e-mail: anikacor@gmail.com

Ганькин Дмитрий Александрович;
ORCID: 0009-0001-6779-8702;
e-mail: ganja-nn@yandex.ru

Фомина Любовь Евгеньевна;
ORCID: 0000-0002-3838-3284;
eLibrary SPIN: 1298-8350;
e-mail: love.fomina@mail.ru

Харитонова Наталья Александровна, канд. мед. наук;
ORCID: 0000-0002-6912-1471;
eLibrary SPIN: 7379-8269;
e-mail: Kharitonova.na@nczd.ru

Жанин Илья Сергеевич, канд. мед. наук.;
ORCID: 0000-0003-1423-0379;
eLibrary SPIN: 6108-2016;
e-mail: zhanin.is@nczd.ru

Пушков Александр Алексеевич, канд. биол. наук;
ORCID: 0000-0001-6648-2063;
eLibrary SPIN: 2928-5764;
e-mail: pushkov.aa@nczd.ru

Басаргина Милана Александровна, канд. мед. наук;
ORCID: 0000-0003-2075-6668;
eLibrary SPIN: 5504-7154;
e-mail: basargina.ma@nczd.ru

Кондакова Ольга Борисовна, канд. мед. наук;
ORCID: 0000-0002-6316-9992;
eLibrary SPIN: 9066-3698;
e-mail: kondakova.ob@nczd.ru

* Corresponding author / Автор, ответственный за переписку

DOI: https://doi.org/10.17816/DD472068

Компьютерная томография в диагностике лихорадки неясного генеза: описание случая

Ю.Ф. Шумская[1], Н.В. Костикова[2], Д.А. Ахмедзянова[1], М.М. Сулейманова[2], Е.В. Фоминых[2], М.Г. Мнацаканян[2], Р.В. Решетников[1]

[1] Научно-практический клинический центр диагностики и телемедицинских технологий, Москва, Российская Федерация;
[2] Первый Московский государственный медицинский университет имени И.М. Сеченова (Сеченовский Университет), Москва, Российская Федерация

АННОТАЦИЯ

Под маской лихорадки неясного генеза могут протекать более двухсот заболеваний. Позитронно-эмиссионная томография, совмещённая с компьютерной томографией, является информативным, но не всегда доступным методом диагностики причин лихорадки неясного генеза. В данной работе представлен случай пациентки с лихорадкой неясного генеза, у которой данные компьютерной томографии сыграли ключевую роль в диагностике гигантоклеточного артериита.

Пациентка, 61 год, с жалобами на повышение температуры тела в вечерние часы до 39,5°С, боли в прекардиальной и межлопаточной областях, снижение массы тела на 10 кг за 3 месяца. В рамках дифференциально-диагностического поиска исключены инфекционные и лимфопролиферативные заболевания. Как причина лихорадки неясного генеза рассматривался эрозивный колит, ранее выявленный при эндоскопическом исследовании, по поводу чего пациентка была госпитализирована в гастроэнтерологическое отделение. При повторной колоноскопии наблюдалась нормальная эндоскопическая картина. По данным компьютерной томографии органов грудной клетки и брюшной полости с внутривенным контрастированием выявлено выраженное утолщение стенок аорты и её ветвей с активным накоплением контрастного вещества, что являлось отражением высокоактивного артериита. В рамках дополнительного обследования исключён специфический артериит. Диагноз сформулирован как гигантоклеточный артериит с поражением брахиоцефального ствола, подключичных артерий, чревного ствола. Пациентке назначен преднизолон с последующим регрессом клинической симптоматики.

Несмотря на то, что компьютерная томография не является золотым стандартом в диагностике лихорадки неясного генеза, применение данного метода в рамках комплексного обследования позволило установить окончательный диагноз пациентке с неклассическим течением гигантоклеточного артериита и длительно существующей лихорадкой неясного генеза.

Ключевые слова: лихорадка неясного генеза; компьютерная томография; гигантоклеточный артериит; описание случая.

Как цитировать:
Шумская Ю.Ф., Костикова Н.В., Ахмедзянова Д.А., Сулейманова М.М., Фоминых Е.В., Мнацаканян М.Г., Решетников Р.В. Компьютерная томография в диагностике лихорадки неясного генеза: описание случая // *Digital Diagnostics.* 2023. Т. 4, № 3. С. 393–402. DOI: https://doi.org/10.17816/DD472068

Рукопись получена: 02.06.2023 **Рукопись одобрена:** 04.07.2023 **Опубликована:** 23.08.2023

DOI: https://doi.org/10.17816/DD472068

Computed tomography in the diagnosis of fever of unknown origin: A case report

Yuliya F. Shumskaya[1], Nina V. Kostikova[2], Dina A. Akhmedzyanova[1], Maria M. Suleymanova[2], Ekaterina V. Fominykh[2], Marina G. Mnatsakanyan[2], Roman V. Reshetnikov[1]

[1] Research and Practical Clinical Center for Diagnostics and Telemedicine Technologies, Moscow, Russian Federation;
[2] The First Sechenov Moscow State Medical University (Sechenov University), Moscow, Russian Federation

ABSTRACT

Fever of unknown origin can be a symptom of at least 200 diseases. Positron emission tomography-computed tomography, although highly informative, may not be readily available as an imaging tool. We present a clinical case of giant cell arteritis where computed tomography played a key role in arriving at a diagnosis.

A 61-year-old woman presented to the hospital with a nocturnal fever up to 39.5°C, accompanied by chest and scapular pain, and substantial weight loss (10 kg over 3 months). Lymphoproliferative and infectious diseases were excluded. Baseline colonoscopy had revealed erosions in the colonic mucosa, leading to a preliminary diagnosis of ulcerative colitis, and subsequently, the patient was admitted to the gastroenterology department. Follow-up colonoscopy had excluded this diagnosis. Additional imaging via chest and abdominal computed tomography scan revealed wall thickening of aorta and its branches with subtle contrast enhancement.

Conditions, such as tuberculous aortoarteritis and syphilitic aortitis, were excluded. The patient was diagnosed with giant cell arteritis involving brachiocephalic trunk, subclavian arteries, and celiac trunk. Prednisolone was administered with subsequent reduction in symptoms.

Although computed tomography may not be regarded as the gold standard for the differential diagnosis of fever of unknown origin, this case underscores its valuable contribution in establishing a definitive diagnosis.

Keywords: fever of unknown origin; tomography; X-ray computed; giant cell arteritis; case report.

To cite this article:
Shumskaya YuF, Kostikova NV, Akhmedzyanova DA, Suleymanova MM, Fominykh EV, Mnatsakanyan MG, Reshetnikov RV. Computed tomography in the diagnosis of fever of unknown origin: A case report. *Digital Diagnostics.* 2023;4(3):393–402. DOI: https://doi.org/10.17816/DD472068

Received: 02.06.2023 **Accepted:** 04.07.2023 **Published:** 23.08.2023

DOI: https://doi.org/10.17816/DD472068

电子计算机断层扫描在不明原因发热诊断中的应用：病例描述

Yuliya F. Shumskaya[1], Nina V. Kostikova[2], Dina A. Akhmedzyanova[1], Maria M. Suleymanova[2], Ekaterina V. Fominykh[2], Marina G. Mnatsakanyan[2], Roman V. Reshetnikov[1]

[1] Research and Practical Clinical Center for Diagnostics and Telemedicine Technologies, Moscow, Russian Federation;
[2] The First Sechenov Moscow State Medical University (Sechenov University), Moscow, Russian Federation

简评

有两百多种疾病可以在不明原因发热的掩盖下发生。正电子发射断层扫描结合电子计算机断层扫描是诊断不明原因发热的一种信息丰富但并非总是可用的方法。本文介绍一例不明原因发热的女性患者，CT数据在她巨细胞动脉炎的诊断中发挥了关键作用。

一名61岁的女性患者，主诉傍晚体温升高至39.5°C，心前区和肩胛间区疼痛，体重在3个月内下降了10kg。在进行鉴别诊断时，排除了感染性疾病和淋巴增生性疾病。作为不明原因发热的原因，考虑了溃疡性结肠炎，该病曾在内窥镜检查中被发现，患者因此在消化科住院治疗。再次结肠镜检查显示了，内窥镜检查结果正常。通过静脉注射造影剂对胸腔和腹腔进行了电子计算机断层扫描，发现了主动脉及其分支的管壁明显增厚，造影剂积聚活跃，这反映了高度活跃的动脉炎。其他检查排除了特异性动脉炎。诊断结果为巨细胞动脉炎，并累及头臂干、锁骨下动脉和腹腔動脈干。医生给病人开了泼尼松龙，随后临床症状有所缓解。

虽然电子计算机断层扫描不是诊断不明原因发热的金标准，但在综合检查框架内使用这种方法，最终允许了对一名患有非典型巨细胞动脉炎病程和长期不明原因发热的患者确诊。

关键词：不明原因的发热；电子计算机断层扫描；巨细胞动脉炎；病例描述。

引用本文：
Shumskaya YuF, Kostikova NV, Akhmedzyanova DA, Suleymanova MM, Fominykh EV, Mnatsakanyan MG, Reshetnikov RV. 电子计算机断层扫描在不明原因发热诊断中的应用：病例描述. *Digital Diagnostics.* 2023;4(3):393–402. DOI: https://doi.org/10.17816/DD472068

收到：02.06.2023 **接受：**04.07.2023 **发布日期：**23.08.2023

BACKGROUND

Over 200 disorders can produce fever of unknown origin (FUO) [1]. Infections, noninfectious inflammatory conditions (e.g., systemic lupus erythematosus and systemic vasculitis), and malignant disorders are the most common [2, 3]. Furthermore, up to 50% of FUO cases go untreated [4, 5]. Most clinicians find the diagnostic search challenging because the disorders that might induce FUO are so diverse. A time-consuming diagnostic search results in longer inpatient stays, which increases the risk of hospital-acquired infections and medical examination costs [6].

Diagnostic search and differential diagnosis procedures include positron emission tomography–computed tomography (PET/CT), computed tomography (CT), and ultrasound scan (US). The procedure is chosen depending on the symptoms and likely involvement of the systems and organs [7]. According to a retrospective study [4], PET/CT provided the best informative value in establishing the final diagnosis in 54% of patients with FUO. In contrast, detecting rheumatic diseases and infections with fever as the only symptom does not necessitate this costly and limited-available technology. Alternative imaging methods are more appropriate in this case.

This study presents a case of giant cell arteritis with an unusual course that did not affect the temporal artery. With a diagnosis of ulcerative colitis and a long-term fever, the patient was referred for additional diagnostics, and the decisive evidence for the final diagnosis was established with CT with intravenous contrast. This case report was prepared in line with CARE guidelines [8].

CASE REPORT

Patient

In November 2020, the 61-year-old female patient was admitted to the Gastroenterology Department of the Clinical Center at the Sechenov First Moscow State Medical University (Sechenov University UCH1) with complaints of general weakness, febrile body temperature up to 39.5°C in the evenings, pain in the pericardiac and interscapular areas, and a 10-kg weight loss over the previous 3 months.

Disease

The patient was generally well in August 2020, but she began experiencing daily elevations in body temperature to 38.5°C–39°C, followed by muscular and joint pain. Antipyretics had no effect; therefore, the patient was admitted to the Infection Department inpatient unit and received antibiotics and oral and intravenous detoxification medications. The medication improved the overall condition, although the subfebrile body temperature continued in the evenings. The thoracic CT scan revealed modest effusion in the pleural cavities, bilateral bands of peribronchovascular thickening, small subsegmental compression atelectasis in the basal regions of both lungs, and elevated hemidiaphragm (Figure 1).

Upper gastrointestinal tract esophagogastroduodenoscopy revealed no abnormalities. A colonoscopy revealed erosive lesions of the descending colon, sigmoid, and rectum mucosa. The histology of the colon biopsy samples revealed catarrhal colitis. Abdominal CT with intravenous contrast (Figure 2) showed several abdominal lymph nodes (para-aortic and superior mesenteric lymph nodes, up to 10-mm short-axis diameter) during the patient's stay in the Infection Department inpatient unit.

The findings were classified as lymphadenopathy, and the patient was referred to a hematologist in September 2020. A bone marrow trephine sample was conducted, followed by histological examination; no indication of the hematopoietic system was identified. Compared with the earlier scan in August 2020 (see Figure 1), follow-up thoracic CT (Figure 3) revealed effusion resorption from the pleural cavities and partial regress of hypoventilatory changes in the basal parts of the lungs. Otherwise, no significant changes were found.

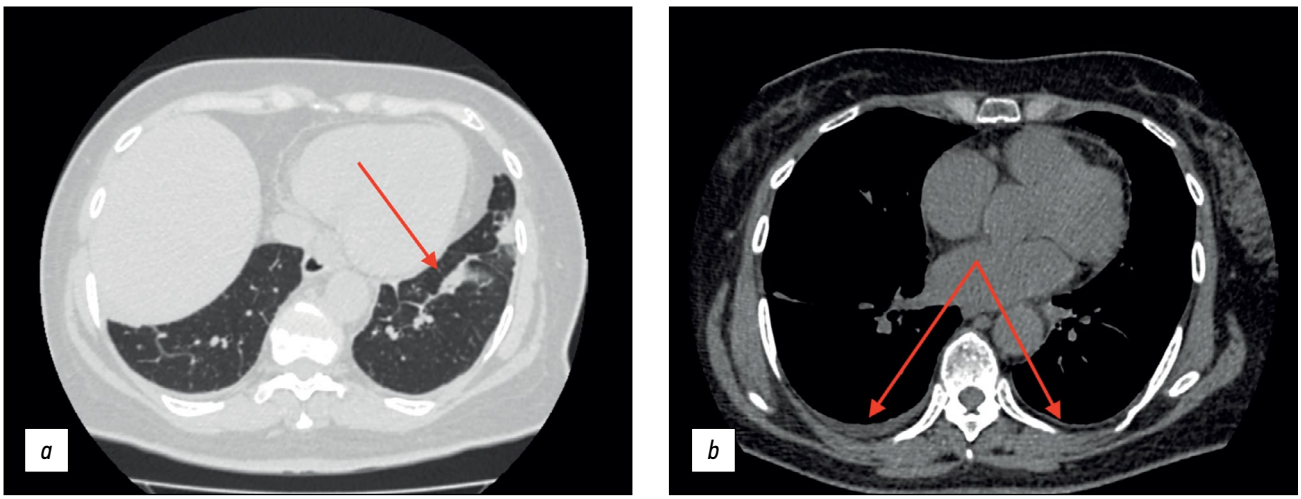

Fig. 1. Thoracic computed tomography scan (August 2020); axial plane: the red arrows show (*a*) subsegmental compression atelectasis and (*b*) mild pleural effusion.

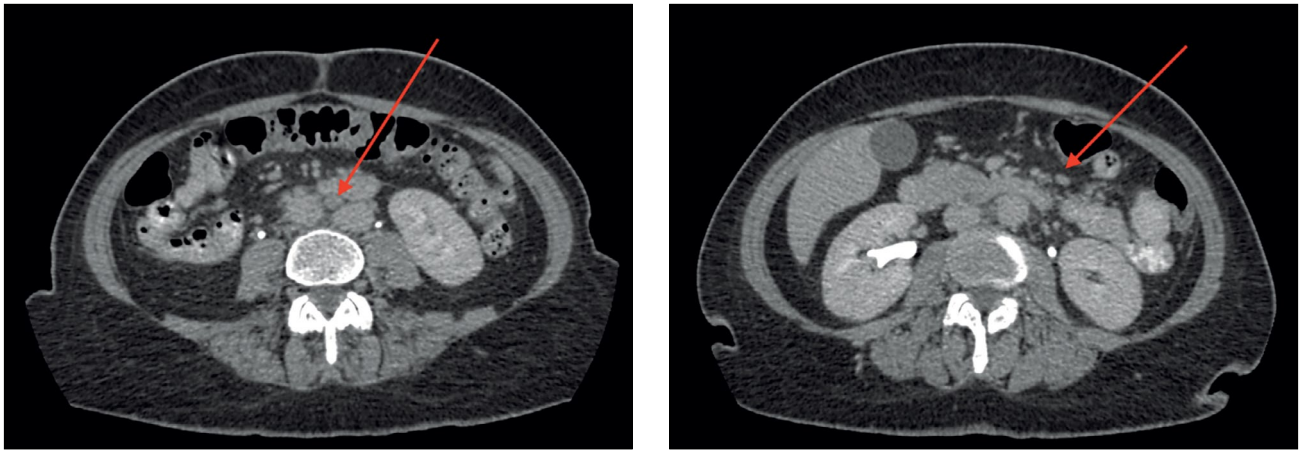

Fig. 2. Abdominal computed tomography scan with intravenous contrast (September 2020); axial plane: the red arrows show intraperitoneal lymph nodes.

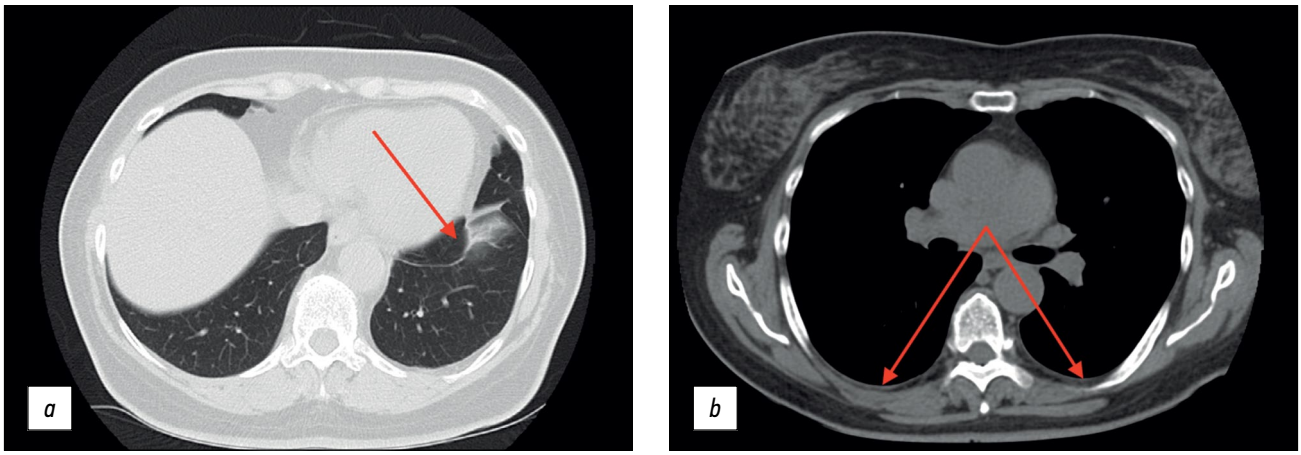

Fig. 3. Thoracic computed tomography scans (September 2020); axial plane: the red arrows show (*a*) the area with partial regression of the hypoventilation changes and (*b*) lack of pleural effusion.

The patient was hospitalized in the inpatient unit several times in November 2020 for body temperature rises to 39°C in the evenings and copious nocturnal sweating. Ulcerative colitis was suspected as a cause of fever in the context of the colonoscopy results from August 2020. Due to the positive PCR test for COVID-19, the patient was discharged from the inpatient unit and advised to continue the examinations once she was convalescent. The patient was also given a mesalazine medication at 4 g/day for ulcerative colitis, which worked well. However, after experiencing persistent fevers, the patient terminated the product without visiting a doctor.

The patient was sent to a coloprotologist in November 2020 after two consecutive negative COVID-19 swabs; the outpatient examination revealed fecal calprotectin increased to 213 μm/g (*N*: max. 50 μm/g). The patient was hospitalized in the Gastroenterology Department of Sechenov University UCH1 for examination and a decision on further treatment tactics.

Physical examination, laboratory tests, and investigations

The primary physical examination in the department showed an increased body temperature of 37.5°C, pallor of the skin and visible mucosae, rales in the posterior basal part of the left lung, tachycardia at 98 bpm, and moderate abdominal tenderness in the periumbilical area. The peripheral pulses remained intact and adequate. The rest of the show was unimpressive.

The laboratory studies revealed a significant increase in nonspecific inflammatory markers (Table 1).

The abdominal US scan revealed no lymphadenopathy or inflammation in the liver, pancreas, and biliary ducts. The patient had a follow-up fibro colonoscopy, which showed

Table 1. Pretreatment inflammatory markers measured during hospitalization

Parameter	*N*	November 24, 2020	December 01, 2020
Erythrocyte sedimentation rate (mm/h)	1–20	71	55
Fibrinogen (g/L)	1.8–4	10.16	10.97
C-reactive protein (mg/L)	0–5	119	130

that the colon and distal jejunum mucosae were in the same condition. The histological examination of the biopsy samples of the colon mucosae failed to find any evidence of structural and inflammatory changes.

Because there was no evidence of ulcerative colitis, the patient with FUO and high levels of nonspecific inflammatory markers was tested for the extractable nuclear antigens panel, which revealed no Jo-1, RNP/Sm, Scl-70, Sm, SS-A (Ro), SS-B (La), pANCA, or cANCA.

The follow-up thoracic and abdominal CT with *i.v.* contrast showed pleural thickening in the apical area of the lungs; aortic wall thickening up to 5 mm and lamellar, poorly defined contours of the aortic wall were remarkable, and they actively accumulated the contrast agent. Similar changes were visualized in the brachiocephalic trunk, subclavian arteries, and celiac artery walls. In addition, fibromuscular dysplasia of the renal arteries was discovered. The CT findings were consistent with active arteritis.

Diagnosis

Based on the findings, the differential diagnosis was carried out for giant cell arteritis or specific arteritis. Because of the patient's age and atypical aortic lesion, Takayasu's arteritis was overlooked. The syphilis serology test came out negative. The patient also consulted a tuberculosis specialist and had a T-SPOT.TB test, the result of which was consistent with functional incompetence of lymphocytes. A rheumatologist reviewed the examination results and diagnosed the patient with giant cell arteritis involving the aorta, brachiocephalic trunk, subclavian arteries, and celiac artery. Anti-inflammatory therapy was started with 60-mg/day prednisolone, which was co-administered with the antituberculosis medication of 0.3-g/day isoniazid + 0.03-g/day pyridoxine hydrochloride.

Changes over time and outcomes

The patient was advised to have 18F-FDG PET/CT to evaluate the length of arterial lesions, but she refused due to the significant clinical improvement with glucocorticoids.

A good response was noted while on therapy—the fever subsided; chest pain and overnight sweats did not return; and a trend toward normalized laboratory results was demonstrated (ESR ↓ to 42 mm/h; CRP ↓ to 16 mg/L; and fibrinogen ↓ to 6.76 g/L). Subjectively, the patient experiences improved general health and normalized appetite. At discharge, complaints of weakness and palpitations related to physical exertion or emotional distress persisted.

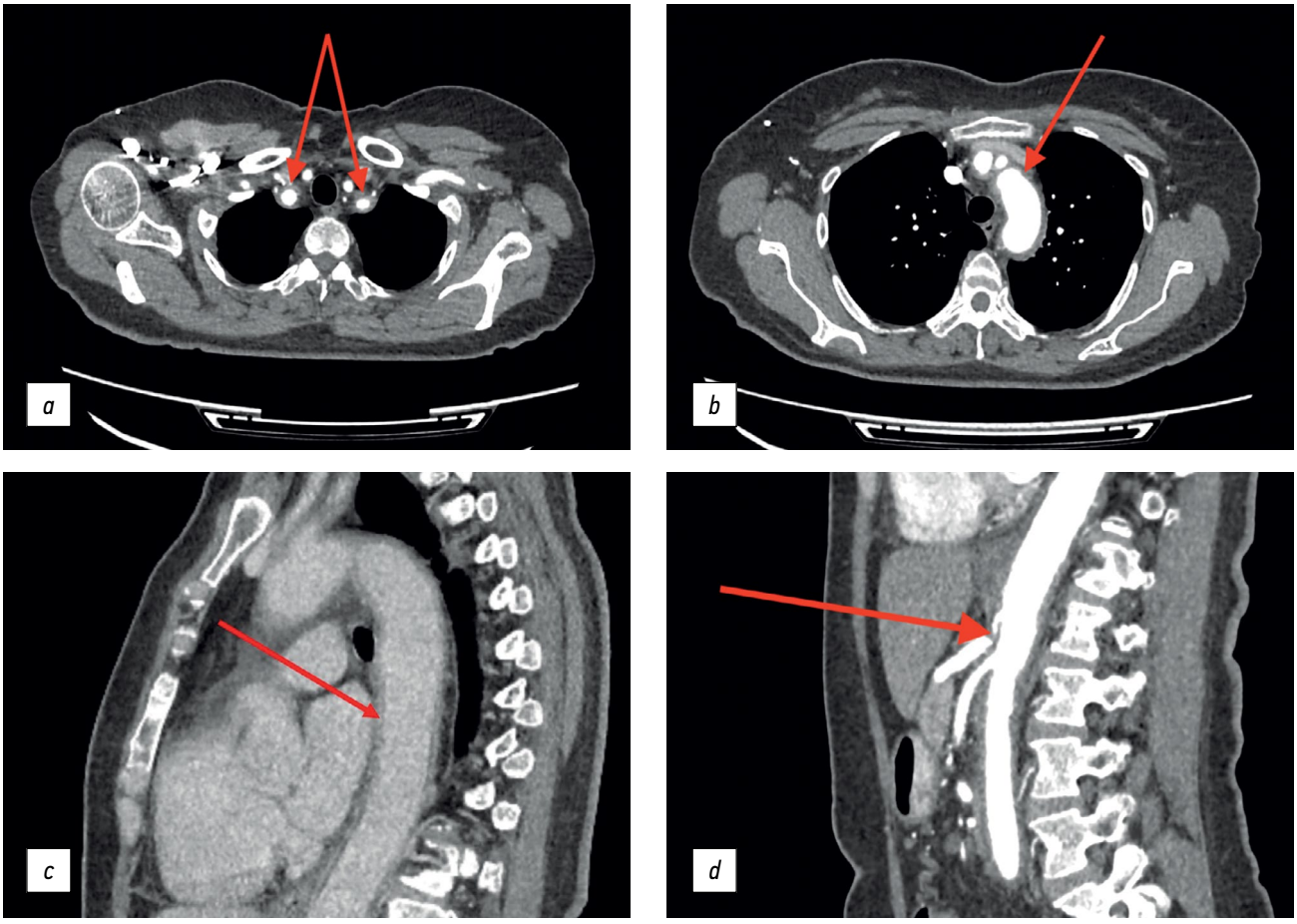

Fig. 4. Thoracic and abdominal computed tomography scan with i.v. contrast (November 2020): the red arrows show changes in the walls of the brachiocephalic trunk and subclavian arteries (*a*, axial plane); aortic wall thickening (*b*, axial plane); lamellar image if the aortic walls with contrast accumulation (*c*, sagittal plane); and occlusion of the celiac artery mouth (*d*, sagittal plane).

The patient had a follow-up appointment after 3 months. The general condition was satisfactory, with no complaints, and the therapy with 4-mg/day methylprednisolone was ongoing.

DISCUSSION

The case report highlights how challenging it is to establish the diagnosis in patients with large vessel involvement who mainly present with FUO. Our patient arrived with nonspecific symptoms, such as increased body temperature, weight loss, asthenia, autonomic nervous system problems, and pain syndrome, but she lacked characteristic temporal arteritis signs. Furthermore, the patient exhibited no signs and symptoms of vascular insufficiency, which could have suggested large vessel vasculitis, contributing to the delayed diagnosis. Moreover, abnormalities associated with ulcerative colitis were discovered during a colonoscopy and biopsy sample analysis, which was regarded as a likely cause of FUO and for which the patient was referred to a coloproctologist and was hospitalized in the Gastroenterology Department. However, the absence of gastrointestinal symptoms initially hampered the diagnosis of ulcerative colitis. Given the above, the patient had a follow-up colonoscopy, tissue samples were collected, and their analysis revealed no indication of colon inflammation.

The literature describes less than 10 cases of ulcerative colitis onset accompanied by isolated FUO without any relevant colon symptoms. A 71-year-old patient with ulcerative colitis was treated with FUO alone without any gastrointestinal problems. The final diagnosis was based on the PET/CT scan that revealed increased 18F-FDG accumulation in the colon walls, indicating active inflammation [9]. Soliman et al. [10] presented another example of Crohn's disease, an inflammatory bowel disease (IBD), in a 29-year-old patient with long-term persistent fever and mild gastrointestinal symptoms. The thickening cecum wall was visible on the abdomen CT scan; the diagnosis was later confirmed by colonoscopy and tissue biopsy.

In our case report, we interpreted historical data on colon mucosa lesions as the outcome of reactive colitis as part of a systemic inflammatory response that did not originate in the colon. It was indicated by the resolution of inflammation with short-term therapy with 5-aminosalicylic acid products. Interestingly, some patients are diagnosed with an IBD after the diagnosis of giant cell arteritis has been established. A prospective study by Yavne et al. [11] showed that patients diagnosed with giant cell arteritis often have a secondary diagnosis of an IBD, such as Crohn's disease or ulcerative colitis (hazard ratio: 2.63; $p < 0.001$). As a result, doctors should be on the lookout for the beginning of an IBD in patients with giant cell arteritis.

There were no studies that compared the value of CT with PET/CT in diagnosing FUO. CT provides several advantages, including shorter scan duration, high availability, a lower cost, and a lower radiation dose. In our case report, it was CT with *i.v.* contrast that provided decisive evidence for the final diagnosis. A similar case was described by Schäfer et al. [12]: a 79-year-old patient presenting with FUO, underweight, and elevated inflammatory markers underwent thoracic and abdominal CT with *i.v.* contrast, which showed thickened aortic walls and major aortic branch walls; the temporal artery was intact. The temporal artery remained unchanged despite thicker aortic walls and major aortic branch walls. Giant cell arteritis was diagnosed in the patient. Later, PET/CT was used to rule out cancer, and glucocorticoid medication was started, which had a beneficial effect. Al Nuaimi et al. [13] also described a 63-year-old patient with recurrent fever, rapid weight loss, and high inflammatory markers who unexpectedly developed recurrent vision loss episodes. He was referred to an inpatient care facility for a brain MRI, which revealed an MRI presentation compatible with an ischemic stroke of the right occipital area. Later, the patient had a thoracic and abdominal CT scan with *i.v.* contrast was visualized to identify the cause of FUO and diffuse thickening of the aortic walls and primary aortic branch walls with contrast accumulation. An ultrasound examination was performed, followed by a temporal artery tissue examination, because giant cell arteritis was suspected. As a result, giant cell arteritis involving the temporal artery was confirmed. The lesion length was measured by ^{18}F-FDG PET/CT, and glucocorticoid medication was started, which had a positive effect [13]. However, CT may not always entirely or partially substitute PET/CT to diagnose giant cell arteritis. For example, Grazioli-Gauthier et al. [14] described giant cell arteritis with an atypical course, with FUO as the most prominent symptom. In a 73-year-old patient with fever and increased acute inflammatory markers, thoracic and abdominal CT was inconclusive; thus, PET/CT was performed. PET/CT revealed minimally active inflammation in the ascending aorta. Metabolic activity was visualized in the ascending colon (later colonoscopy ruled out bowel diseases). The temporal artery tissue investigation was used for the final diagnosis [14].

In contrast to the examples in the literature, where the diagnosis was based on PET/CT and/or temporal artery tissue examination, we relied on CT with *i.v.* contrast to diagnose giant cell arteritis. It was feasible due to the increased activity and spread of inflammation and the disease's typical trajectory without temporal artery involvement.

CONCLUSION

Several key conclusions can be drawn from the case report. Giant cell arteritis may cause a fever of unknown origin (FUO) and have an unusual course without the temporal artery involvement, hindering the correct diagnosis. CT with intravenous contrast may aid in diagnosing arteritis, including giant cell arteritis with temporal artery involvement. In some cases, CT with intravenous contrast may be an alternative to PET/CT in the diagnostic search for the cause of a FUO.

ADDITIONAL INFORMATION

Funding source. This article was prepared by a group of authors as a part of the research and development effort titled "Opportunistic screening of high-profile and other common diseases", No. 123031400009-1 (USIS No. 123031400009-1) in accordance with the Order No. 1196 dated December 21, 2022 "On approval of state assignments funded by means of allocations from the budget of the city of Moscow to the state budgetary (autonomous) institutions subordinate to the Moscow Health Care Department, for 2023 and the planned period of 2024 and 2025" issued by the Moscow Health Care Department.

Competing interests. The authors declare that they have no competing interests.

Authors' contribution. All authors made a substantial contribution to the conception of the work, acquisition, analysis, interpretation of data for the work, drafting and revising the work, final approval of the version to be published and agree to be accountable for all aspects of the work. Y.F. Shumskaya — concept, collection and processing of material, analysis of data, writing of the manuscript; N.V. Kostikova — collection and processing of material, writing of the manuscript; D.A. Akhmedzyanova — concept, manuscript editing; M.M. Suleymanova — manuscript editing, preparation of illustrative material; E.V. Fominykh — manuscript editing, preparation of illustrative material; M.G. Mnatsakanyan — final editing of the manuscript. Suleymanova — manuscript editing, preparation of illustrativaration of illustrative material; M.G. Mnatsakanyan — final editing, manuscript approval, R.V. Reshetnikov — manuscript writing, final editing.

Consent for publication. Written consent was obtained from the patient for publication of relevant medical information and all of accompanying images within the manuscript in Digital Diagnostics Journal.

Acknowledgments. The authors would like to thank Ivan Andreevich Blokhin for his help with drafting this article.

REFERENCES

1. Unger M, Karanikas G, Kerschbaumer A, et al. Fever of unknown origin (Fuo) revised. *Wien Klin Wochenschr*. 2016;128(21-22):796–801. doi: 10.1007/s00508-016-1083-9

2. David A, Quinlan JD. Fever of unknown origin in adults. *Am Fam Physician*. 2022;105(2):137–143.

3. Fusco FM, Pisapia R, Nardiello S, et al. Fever of unknown origin (FUO): Which are the factors influencing the final diagnosis? A 2005–2015 systematic review. *BMC Infect Dis*. 2019;19(1):653. doi: 10.1186/s12879-019-4285-8

4. Weitzer F, Hooshmand T, Pernthaler B, et al. Diagnostic value of F-18 FDG PET/CT in fever or inflammation of unknown origin in a large single-center retrospective study. *Sci Rep*. 2022;12(1):1883. doi: 10.1038/s41598-022-05911-7

5. Wright WF, Auwaerter PG. Fever and fever of unknown origin: Review, recent advances, and lingering dogma. *Open Forum Infect Dis*. 2020;7(5):132. doi: 10.1093/ofid/ofaa132

6. Horowitz HW. Fever of unknown origin or fever of too many origins? *N Engl J Med*. 2013;368(3):197–199. doi: 10.1056/NEJMp1212725

7. Cunha BA, Lortholary O, Cunha CB. Fever of unknown origin: A clinical approach. *Am J Med*. 2015;128(10):1138.e1–1138.e15. doi: 10.1016/j.amjmed.2015.06.001

8. Barber MS, Aronson JK, von Schoen-Angerer T, et al. CARE guidelines for case reports: explanation and elaboration document. Translation into Russian. *Digital Diagnostics*. 2022;3(1):16–42. (In Russ). doi: 10.17816/DD105291

9. Shpilberg R, Hadjiyiannis D, Khan SA. Ulcerative colitis presenting as pyrexia of unknown origin (PUO) without bowel symptoms. *Clin Med (Lond)*. 2012;12(4):389–390. doi: 10.7861/clinmedicine.12-4-389

10. Soliman M, Shirazi-Nejad A, Bullas D, et al. An unusual case of pyrexia of unknown origin. *Cureus*. 2021;13(7):e16684. doi: 10.7759/cureus.16684

11. Yavne Y, Tiosano S, Ben-Ami D, et al. Giant cell arteritis and inflammatory bowel disease: Is there a connection? Results from a population-based study. *Autoimmun Rev*. 2018;17(11):1134–1137. doi: 10.1016/j.autrev.2018.06.003

12. Schäfer VS, Warrington KJ, Williamson EE, Kermani TA. Delayed diagnosis of biopsy-negative giant cell arteritis presenting as fever of unknown origin. *J Gen Intern Med*. 2009;24(4):532–536. doi: 10.1007/s11606-009-0925-9

13. AlNuaimi D, Ansari H, Menon R, et al. Large vessel vasculitis and the rising role of FDG PET-CT: A case report and review of literature. *Radiol Case Rep*. 2020;15(11):2246–2249. doi: 10.1016/j.radcr.2020.08.066

14. Grazioli-Gauthier L, Marcoli N, Vanini G, et al. Giant cell arteritis among fevers of unknown origin (FUO): An atypical presentation. *Eur J Case Rep Intern Med*. 2021;8(3):002254. doi: 10.12890/2021_002254

СПИСОК ЛИТЕРАТУРЫ

1. Unger M., Karanikas G., Kerschbaumer A., et al. Fever of unknown origin (Fuo) revised // Wien Klin Wochenschr. 2016. Vol. 128, N 21-22. P. 796–801. doi: 10.1007/s00508-016-1083-9

2. David A., Quinlan J.D. Fever of unknown origin in adults // Am Fam Physician. 2022. Vol. 105, N 2. P. 137–143.

3. Fusco F.M., Pisapia R., Nardiello S., et al. Fever of unknown origin (FUO): Which are the factors influencing the final diagnosis? A 2005–2015 systematic review // BMC Infect Dis. 2019. Vol. 19, N 1. P. 653. doi: 10.1186/s12879-019-4285-8

4. Weitzer F., Hooshmand T., Pernthaler B., et al. Diagnostic value of F-18 FDG PET/CT in fever or inflammation of unknown origin in a large single-center retrospective study // Sci Rep. 2022. Vol. 12, N 1. P. 1883. doi: 10.1038/s41598-022-05911-7

5. Wright W.F., Auwaerter P.G. Fever and fever of unknown origin: Review, recent advances, and lingering dogma // Open Forum Infect Dis. 2020. Vol. 7, N 5. P. 132. doi: 10.1093/ofid/ofaa132

6. Horowitz H.W. Fever of unknown origin or fever of too many origins? // N Engl J Med. 2013. Vol. 368, N 3. P. 197–199. doi: 10.1056/NEJMp1212725

7. Cunha B.A., Lortholary O., Cunha C.B. Fever of unknown origin: A clinical approach // Am J Med. 2015. Vol. 128, N 10. P. 1138.e1–1138.e15. doi: 10.1016/j.amjmed.2015.06.001

8. Barber M.S., Aronson J.K., von Schoen-Angerer T., et al. Рекомендации CARE для описания случаев: разъяснения и уточнения // Digital Diagnostics. 2022. Т. 3. № 1. С. 16–42. doi: 10.17816/DD105291

9. Shpilberg R., Hadjiyiannis D., Khan S.A. Ulcerative colitis presenting as pyrexia of unknown origin (PUO) without bowel symptoms // Clin Med (Lond). 2012. Vol. 12, N 4. P. 389–390. doi: 10.7861/clinmedicine.12-4-389

10. Soliman M., Shirazi-Nejad A., Bullas D., et al. An unusual case of pyrexia of unknown origin // Cureus. 2021. Vol. 13, N 7. P. e16684. doi: 10.7759/cureus.16684

11. Yavne Y., Tiosano S., Ben-Ami D., et al. Giant cell arteritis and inflammatory bowel disease: Is there a connection? Results from a population-based study // Autoimmun Rev. 2018. Vol. 17, N 11. P. 1134–1137. doi: 10.1016/j.autrev.2018.06.003

12. Schäfer V.S., Warrington K.J., Williamson E.E., et al. Delayed diagnosis of biopsy-negative giant cell arteritis presenting as fever of unknown origin // J Gen Intern Med. 2009. Vol. 24, N 4. P. 532–536. doi: 10.1007/s11606-009-0925-9

13. AlNuaimi D., Ansari H., Menon R., et al. Large vessel vasculitis and the rising role of FDG PET-CT: A case report and review of literature // Radiol Case Rep. 2020. Vol. 15, N 11. P. 2246–2249. doi: 10.1016/j.radcr.2020.08.066

14. Grazioli-Gauthier L., Marcoli N., Vanini G., et al. Giant cell arteritis among fevers of unknown origin (FUO): An atypical presentation // Eur J Case Rep Intern Med. 2021. Vol. 8, N 3. P. 002254. doi: 10.12890/2021_002254

AUTHORS' INFO

*** Yuliya F. Shumskaya;**
address: 24/1 Petrovka street, 127051 Moscow, Russia;
ORCID: 0000-0002-8521-4045;
eLibrary SPIN: 3164-5518;
e-mail: ShumskayaYF@zdrav.mos.ru

Nina V. Kostikova;
ORCID: 0000-0003-3509-7271;
eLibrary SPIN: 7962-4554;
e-mail: n.kostikowa@yandex.ru

Dina A. Akhmedzyanova;
ORCID: 0000-0001-7705-9754;
eLibrary SPIN: 6983-5991;
e-mail: dina_akhm@mail.ru

Maria M. Suleymanova;
ORCID: 0000-0002-5776-2693;
eLibrary SPIN: 7193-6122;
e-mail: ashe.danny.jush@gmail.com

Ekaterina V. Fominykh, MD, Cand. Sci. (Med.);
ORCID: 0000-0003-3733-4381;
e-mail: evfominykh@mail.ru

Marina G. Mnatsakanyan, MD, Dr. Sci. (Med), Professor;
ORCID: 0000-0001-9337-7453;
eLibrary SPIN: 2015-1822;
e-mail: mnatsakanyan08@mail.ru

Roman V. Reshetnikov, Cand. Sci. (Phys.-Math.);
ORCID: 0000-0002-9661-0254;
eLibrary SPIN: 8592-0558;
e-mail: reshetnikov@fbb.msu.ru

ОБ АВТОРАХ

*** Шумская Юлия Федоровна;**
адрес: Россия, 127051, Москва, ул. Петровка, д. 24, стр. 1;
ORCID: 0000-0002-8521-4045;
eLibrary SPIN: 3164-5518;
e-mail: ShumskayaYF@zdrav.mos.ru

Костикова Нина Владимировна;
ORCID: 0000-0003-3509-7271;
eLibrary SPIN: 7962-4554;
e-mail: n.kostikowa@yandex.ru

Ахмедзянова Дина Альфредовна;
ORCID: 0000-0001-7705-9754;
eLibrary SPIN: 6983-5991;
e-mail: dina_akhm@mail.ru

Сулейманова Мария Мирославовна;
ORCID: 0000-0002-5776-2693;
eLibrary SPIN: 7193-6122;
e-mail: ashe.danny.jush@gmail.com

Фоминых Екатерина Викторовна, канд. мед. наук;
ORCID: 0000-0003-3733-4381;
e-mail: evfominykh@mail.ru

Мнацаканян Марина Генриковна, д-р мед. наук, профессор;
ORCID: 0000-0001-9337-7453;
eLibrary SPIN: 2015-1822;
e-mail: mnatsakanyan08@mail.ru

Решетников Роман Владимирович, канд. физ.-мат. наук;
ORCID: 0000-0002-9661-0254;
eLibrary SPIN: 8592-0558;
e-mail: reshetnikov@fbb.msu.ru

* Corresponding author / Автор, ответственный за переписку

DOI: https://doi.org/10.17816/DD430128

Хронический пищеводный свищ как редкая причина вторичного остеомиелита грудного отдела позвоночника

В.А. Заря, П.В. Гаврилов, М.Е. Макогонова, А.Р. Козак, А.А. Вишневский

Санкт-Петербургский научно-исследовательский институт фтизиопульмонологии, Санкт-Петербург, Российская Федерация

АННОТАЦИЯ

Инфекционные заболевания позвоночника представляют собой воспалительные деструктивные заболевания органа и его структурных элементов в результате инфицирования гематогенным, лимфогенным или контактным путём, в том числе могут являться осложнением хирургического вмешательства. При постановке диагноза крайне важно оценивать в совокупности анамнез, клиническую картину, а также данные лабораторных исследований и лучевой диагностики.

В работе представлен клинический случай вторично развившегося спондилита позвонков ThVII–ThVIII вследствие пищеводного свища. При первичной диагностике спондилит связали со спинальной анестезией, которая проводилась за 6 месяцев до начала заболевания, так как имел место свищевой дефект на коже в поясничной области. По этому поводу трижды проводились оперативные вмешательства в хирургическом стационаре по месту жительства. Данные эндоскопического исследования и жалобы пациентки на связь между приёмами пищи, появлением болей и характером отделяемого из свища не были приняты врачами изначально во внимание. С помощью дополнительного обследования, включающего компьютерную томографию пищевода с пероральным контрастированием и компьютерно-томографическую фистулографию, был установлен основной диагноз «Свищ пищевода», а спондилит грудного отдела позвоночника оказался лишь вторичным осложнением.

Таким образом, окончательный диагноз при болях в спине, обусловленных не только инфицированием, но и являющихся осложнением хирургического вмешательства, должен формулироваться после проведения дифференциальной диагностики с альтернативными заболеваниями позвоночника.

Ключевые слова: остеомиелит; спондилит; свищ пищевода.

Как цитировать:

Заря В.А., Гаврилов П.В., Макогонова М.Е., Козак А.Р., Вишневский А.А. Хронический пищеводный свищ как редкая причина вторичного остеомиелита грудного отдела позвоночника // *Digital Diagnostics.* 2023. Т. 4, № 3. С. 403–410. DOI: https://doi.org/10.17816/DD430128

Рукопись получена: 16.05.2023 **Рукопись одобрена:** 22.08.2023 **Опубликована:** 30.08.2023

DOI: https://doi.org/10.17816/DD430128

Chronic esophageal fistula as a rare cause of secondary osteomyelitis of the thoracic spine

Valeriya A. Zarya, Pavel V. Gavrilov, Marina E. Makogonova, Andrey R. Kozak, Arkadiy A. Vishnevskiy

Saint-Petersburg State Research Institute of Phthisiopulmonology, Saint Petersburg, Russian Federation

ABSTRACT

Infectious diseases affecting the spine are inflammatory destructive diseases that involved the organ and its structural elements as a result of infection by hematogenic, lymphogenic, or contact pathways, including may be a complication of surgical intervention. In arriving at an accurate diagnosis, it is extremely important to evaluate the anamnesis, the clinical picture, as well as the data of laboratory studies and radiation diagnostics in the aggregate.

This article presents a clinical case with the development of secondary ThVII–ThVIII vertebral spondylitis due to esophageal fistula. At the initial diagnosis, spondylitis was associated with spinal anesthesia performed six months prior to onset of the disease, as there was a fistulous defect on the skin in the lumbar region. Consequently, surgical interventions were performed three times in a surgical hospital at the place of residence. The data from the endoscopic examination, as well as the patient's complaints regarding the relationship between meals, the appearance of pain, and the nature of the discharge from the fistula were not taken into account by doctors initially. With the help of an additional examination, including computed tomography of the esophagus with oral contrast and computed tomography fistulography, the main diagnosis was esophageal fistula. Thoracic spondylitis was only a secondary complication.

Thus, the final diagnosis of back pain and fistula in the lumbar region should be formulated after differential diagnosis with alternative diseases of the spine.

Keywords: osteomyelitis; spondylitis; esophageal fistula.

To cite this article:

Zarya VA, Gavrilov PV, Makogonova ME, Kozak AR, Vishnevskiy AA. Chronic esophageal fistula as a rare cause of secondary osteomyelitis of the thoracic spine. *Digital Diagnostics.* 2023;4(3):403–410. DOI: https://doi.org/10.17816/DD430128

Received: 16.05.2023 **Accepted:** 22.08.2023 **Published:** 30.08.2023

DOI: https://doi.org/10.17816/DD430128

慢性食管瘘作为继发性胸椎骨髓炎的罕见病因

Valeriya A. Zarya, Pavel V. Gavrilov, Marina E. Makogonova,
Andrey R. Kozak, Arkadiy A. Vishnevskiy

Saint-Petersburg State Research Institute of Phthisiopulmonology, Saint Petersburg, Russian Federation

简评

脊柱感染性疾病是由于血源性、淋巴原性或接触性感染（包括手术并发症）引起的器官及其结构元素的炎症性破坏性疾病。在进行诊断时，对病史、临床表现以及实验室检查和放射诊断数据进行评估极为重要。

本文介绍一例因食管瘘引起的ThVII-ThVIII椎骨继发性脊椎炎的临床病例。在最初诊断时，医生认为脊椎炎与脊髓麻醉有关，而脊髓麻醉是在发病前6个月进行的，因为腰部皮肤上有瘘管缺损。这次在居住地的外科医院进行了三次手术治疗。医生最初并没有考虑到内窥镜检查结果以及病人关于进食、疼痛和瘘管分泌物性质之间关系的主诉。在额外检查的帮助下，包括口服造影剂的食道CT扫描和瘘管CT造影，确定了食管瘘的主要诊断，而胸椎脊椎炎只是次要并发症。

因此，在存在背痛的原因不仅是感染，还可能是手术治疗的并发症的情况下，最终诊断应该是在与其他脊柱疾病进行鉴别诊断后再做出的。

关键词：骨髓炎；脊椎炎；食管瘘。

引用本文：

Zarya VA, Gavrilov PV, Makogonova ME, Kozak AR, Vishnevskiy AA. 慢性食管瘘作为继发性胸椎骨髓炎的罕见病因. *Digital Diagnostics*. 2023;4(3):403–410. DOI: https://doi.org/10.17816/DD430128

收到：16.05.2023 **接受：**22.08.2023 **发布日期：**30.08.2023

BACKGROUND

Spinal infections are inflammatory destructive disorders of the spine and its structural components (vertebral bodies, intervertebral discs, ligaments, and intervertebral joints). They can be caused by any bacterial agent due to a hematogenous, lymphogenous, or contact infection, or they can be surgical complications (e.g., postoperative and iatrogenic infections) [1].

Spondylitis can be infectious or non-infectious (aseptic). Infectious spondylitis is caused by bacterial, fungal, or parasitic invasions. Spondylitis can cause hematogenous (septic) or contact infections [2–4], as well as postoperative (iatrogenic) complications [5–8]. Some authors reported that spondylitis caused by esophageal perforation can spread posteriorly, resulting in secondary damage to cervical or thoracic vertebrae. For example, Janssen et al. [9] presented cervical and thoracic spondylodiscitis cases caused by esophageal perforation in patients with a history of esophageal cancer who underwent combination therapy. Some of these patients had a recurrence of esophageal fistula after previous nonsurgical and surgical treatment. The authors also reported a female patient who ingested and independently retrieved a toothpick 2 months before the onset of spondylitis, which was accompanied by an epidural and paravertebral abscess. According to Fonga-Djimi et al. [10], an esophageal perforation caused by a foreign body (a toy car wheel) was worsened by mediastinitis and spondylodiscitis. Wadie et al. [11] presented a clinical case of a child with cervical spondylodiscitis and paravertebral soft tissue phlegmon caused by pin ingestion, which resulted in perforation of the posterior pharynx at the level of the laryngeal aperture. Van Ooij et al. [12] described a female patient with cervical spondylitis caused by a fish bone trapped in the esophagus.

When an infection spreads to the chest, it causes empyema, pericarditis, and mediastinitis. As a result of spondylitis, empyema and pericarditis may reoccur. Infections of the anterior thoracolumbar and lumbar spines can result in subdiaphragmatic abscess, peritonitis, and psoas abscess.

Appropriate treatment of infectious spondylitis requires an accurate diagnosis of the etiology and pathogen. The use of X-ray diagnostics is important in the diagnosis of spondylitis. However, X-ray results do not guarantee that the nature and etiology of the infection are accurately identified. Thus, it is necessary to consider the medical history, clinical presentation, laboratory findings, and X-ray findings when diagnosing.

This study presents a rare secondary thoracic spine lesion caused by a chronic esophageal fistula.

CASE REPORT

Patient

The patient is a 42-year-old female. Back pain and lumbar fistula complaints initially appeared 3 yr ago. According to the medical history, the patient received spinal anesthesia for a cesarean section 6 months prior. The patient experienced fistula relapses approximately three to five times a year. At the presentation, a magnetic resonance imaging (MRI) revealed bony and fibrous ankylosis ThVII–ThVIII (Figure 1), which could indicate both spondylitis in remission and contact spinal infection.

At different outpatient facilities, the patient had surgery (fistulotomy and abscessotomy) three times. The surgical specimen contained hemolytic streptococcus susceptible to amoxiclav, ampicillin, cefotaxime, vancomycin, doxycycline, and meropenem. The patient received targeted antibiotic medication with no effect. Before admission to the

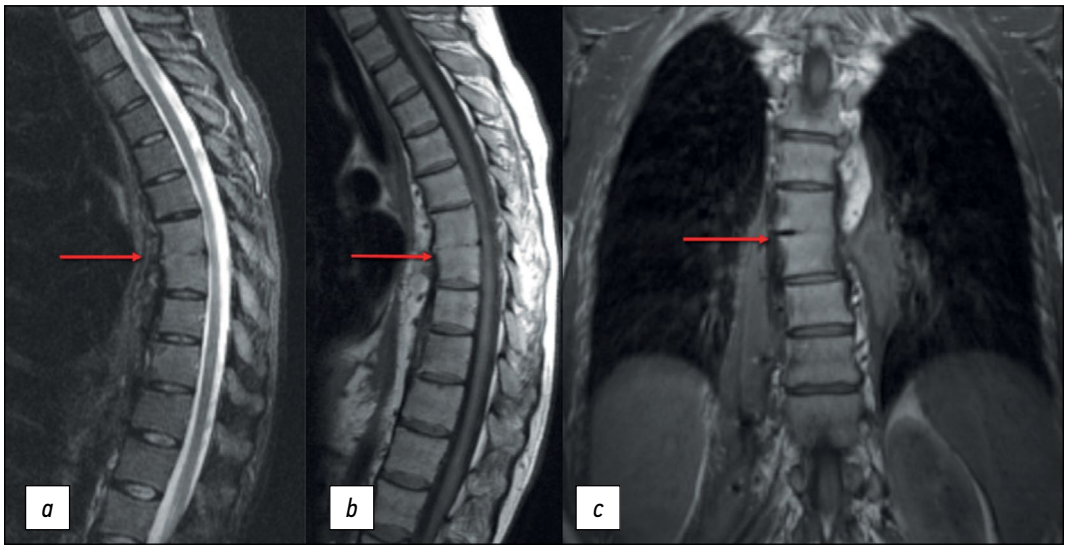

Fig. 1. Thoracic spine MRI: (*a*) STIR mode, sagittal plane; (*b*) T1WI mode, sagittal plane; and (*c*) T1WI mode, coronal plane. The arrows indicate bony and fibrous ankylosis ThVII–ThVIII.

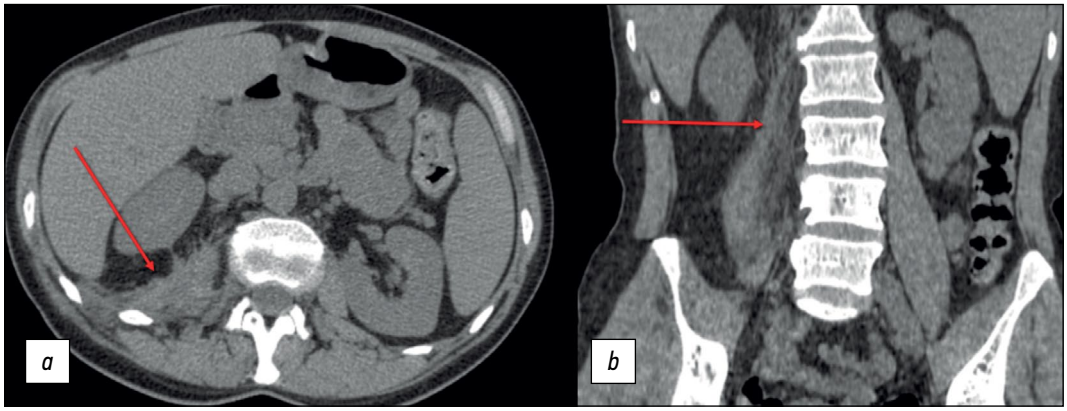

Fig. 2. Lumbar spine MRI: (*a*) soft tissue mode, axial plane, and (*b*) soft tissue mode, coronal plane. The arrows indicate the right psoas muscle abscess.

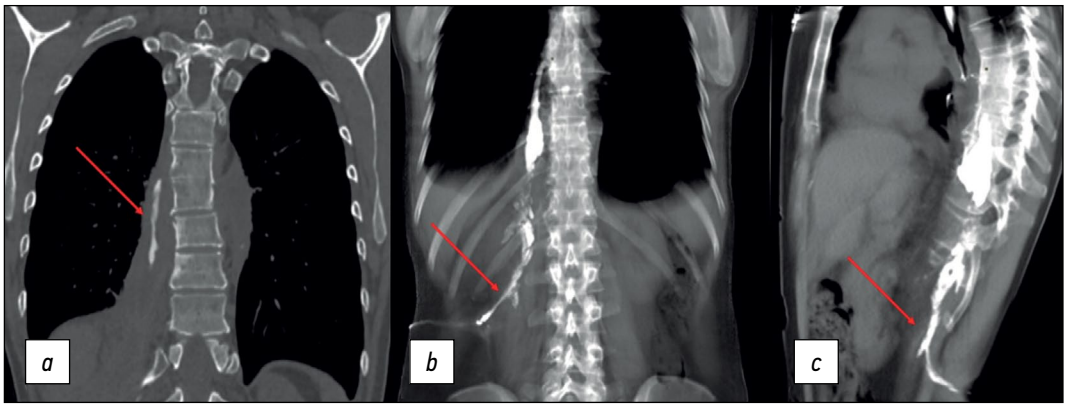

Fig. 3. (*a*) CT esophagography with oral contrast, coronal plane and (*b* and *c*) CT fistulography, multiplanar reconstruction (MPR), coronal and sagittal plane. The arrows indicate the fistula tract from the esophagus to the right paravertebral space, from the ThVII to the ThX level.

St. Petersburg Research Institute of Phthisiopulmonology, a computed tomography (CT) revealed symptoms of prior spondylitis ThVII–ThVIII and a right-sided psoas abscess (Figure 2).

During the additional history taking, the patient reported an association between his food intake (mostly liquid food), the onset of pain, and the type of discharge from the lumbar fistula tract. Due to these symptoms, a CT esophagography with oral contrast revealed a fistula tract at the ThVII level extending from the esophagus to the right paravertebral space up to the ThX level and loculated empyema on the right. An additional CT fistulography was performed to determine the length of the fistula tract, with a contract solution (iopromide 370) injected into the lumbar fistula located on the right at the LIII level. The CT fistulography revealed a fistula tract extending from the right psoas major muscle to the ThVII level. The fistula tract linked with the esophageal lumen at the same level, where the contrast agent was visible (Figure 3).

A follow-up thoracic and lumbar spine MRI performed in the hospital revealed stable changes in the ThVII–ThVIII vertebral bodies and bilateral paravertebral abscesses (Figure 4).

All laboratory findings were unremarkable, except for the erythrocyte sedimentation rate (30 mm/h). To determine further treatment strategy, an esophagogastroduodenoscopy (EGD) was performed, which revealed a fistula tract along the left posterior wall, up to 0.5 cm long, bordered with esophageal epithelium and covered by granulation tissue. The diagnosis of an esophageal fistula in the middle third was confirmed. A post hoc analysis of earlier EGD findings showed that the observed esophageal defect had previously been identified and classified as a diverticulum. However, this information was not taken into consideration in other outpatient facilities.

Thus, a multidisciplinary team made the following diagnosis based on the clinical and X-ray findings: esophagopleural fistula of the lower third of the esophagus. On the right, there is chronic loculated empyema. Chronic contiguous osteomyelitis ThVII–ThVIII with a fistula. The patient was sent to the thoracic surgery department for the excision of an esophageal fistula.

DISCUSSION

Spondylitis infections can be caused by various factors, including dental caries, ENT infections, phlegm,

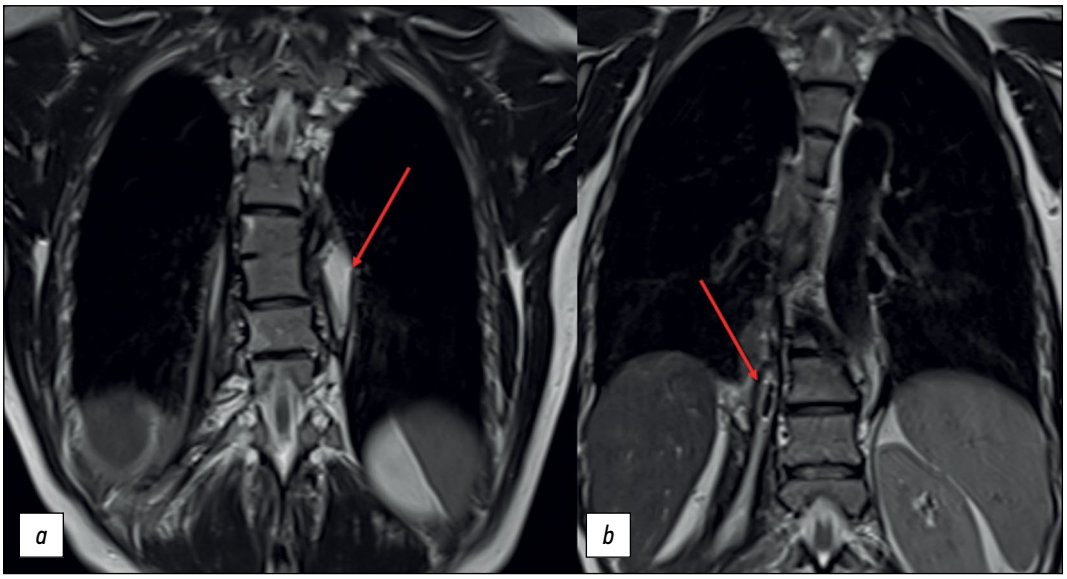

Fig. 4. Thoracic and lumbar spine MRI: T2WI mode, coronal plane. Bony and fibrous ankylosis ThVII–ThVIII and paravertebral abscesses (arrows) on the left (*a*), with air bubbles on the right (*b*).

and endocarditis. Structural damage to the spine can be caused by hematogenous or contact infections, including penetrating injuries, such as iatrogenic injury. Given the available data, the following questions arise: why was the therapy ineffective, and was the primary cause spondylitis or esophageal fistula?

A history of epidural anesthesia is the main reason supporting infectious spondylitis as the primary process. In such cases, epidural anesthesia is administered at the LIII–LV level. The affected vertebrae in our case are significantly higher. Another factor suggesting spondylitis as the causative cause is a paravertebral abscess on the left (contralateral to the esophageal fistula). Simultaneously, there was no explanation for the severe inflammatory changes in paravertebral tissues. This clinical presentation of spondylitis is not typical. In general, vertebrae are more affected than soft tissues around them. Furthermore, the patient denied any esophageal injury that may lead to a fistula.

Another factor suggesting an esophageal origin of the process was a fistulous contact between the paravertebral abscess and the esophagus (fistula tract diameter up to 5 mm). Endoscopy revealed an esophageal diverticulum and an intact esophageal wall (which was not involved in the inflammatory process); the fistula was bordered by esophageal epithelium. Moreover, the patient associated the pain syndrome with food intake, and the discharge from the lumbar fistula tract resembled previously ingested food or drink.

The long-term disease makes determining the primary process impossible. Considering all available data, esophageal perforation is proposed as the leading cause, followed by spondylitis and paravertebral abscess. Despite the patient denying any esophageal injury, the endoscopic results are most consistent with an esophageal injury caused by an ingested foreign body (such as a fish bone).

CONCLUSION

The cause of the pathological process (esophageal fistula) was unknown, and the patient was treated symptomatically (surgery and antibacterial medication) while in the hospital.

The availability of several modern imaging and surgical procedures does not eliminate the need for a thorough history taking and clinical presentation examination.

Previous diagnoses should be reviewed for compliance with diagnostic criteria in cases when appropriate therapy is ineffective.

Differential diagnosis is critical for systematically assessing possible alternative diagnoses before concluding.

The common logical fallacy of *post hoc ergo propter hoc* (a false conclusion that confuses co-occurrence with causality) should also be considered.

ADDITIONAL INFORMATION

Funding source. This article was not supported by any external sources of funding.

Competing interests. The authors declare that they have no competing interests.

Authors' contribution. All authors made a substantial contribution to the conception of the work, acquisition, analysis, interpretation of data for the work, drafting and revising the work, final approval of the version to be published and agree to be accountable for all aspects of the work. V.A. Zarya — collecting material, writing the article; P.V. Gavrilov — concept and design of the work, final editing; M.E. Makogonova — analysis of the data obtained, writing the text; A.R. Kozak — collecting material, writing the article; A.A. Vishnevskiy — concept and design of the work, final editing.

Consent for publication. Written consent was obtained from the patient for publication of relevant medical information and all of accompanying images within the manuscript in Digital Diagnostics Journal.

REFERENCES

1. Mushkin AYu, Vishnevsky AA. Clinical recommendations for the diagnosis of infectious spondylitis (draft for discussion). *Medical Alliance*. 2018;(3):65–74. (In Russ).
2. Fowler VG, Justice A, Moore C, et al. Risk factors for hematogenous complications of intravascular catheter-associated Staphylococcus aureus bacteremia. *Clin Infect Dis. 2005*;40(5):695–703. doi: 10.1086/427806
3. Lu YA, Hsu HH, Kao HK, et al. Infective spondylodiscitis in patients on maintenance hemodialysis: A case series. *Ren Fail*. 2017;39(1):179–186. doi: 10.1080/0886022X.2016.1256313
4. Choi KB, Lee CD, Lee SH. Pyogenic spondylodiscitis after percutaneous endoscopic lumbar discectomy. *J Korean Neurosurg Soc*. 2010;48(5):455–460. doi: 10.3340/jkns.2010.48.5.455
5. Hsieh MK, Chen LH, Niu CC, et al. Postoperative anterior spondylodiscitis after posterior pedicle screw instrumentation. *Spine J*. 2011;11(1):24–29. doi: 10.1016/j.spinee.2010.10.021
6. Hanci M, Toprak M, Sarioğlu AC, et al. Oesophageal perforation subsequent to anterior cervical spine screw/plate fixation. *Paraplegia*. 1995;33(10):606–609. doi: 10.1038/sc.1995.128
7. Orlando ER, Caroli E, Ferrante L. Management of the cervical esophagus and hypofarinx perforations complicating anterior cervical spine surgery. *Spine*. 2003;28:E290–E295. doi: 10.1097/00007632-200308010-00023
8. Pompili A, Canitano S, Caroli F, et al. Asymptomatic esophageal perforation caused by late screw migration after anterior cervical plating: Report of a case and review of relevant literature. *Spine*. 2002;27:E499–E502. doi: 10.1097/00007632-200212010-00016
9. Janssen I, Shiban E, Rienmüller A, et al. Treatment considerations for cervical and cervicothoracic spondylodiscitis associated with esophageal fistula due to cancer history or accidental injury: A 9-patient case series. *Acta Neurochir (Wien)*. 2019;161(9):1877–1886. doi: 10.1007/s00701-019-03985-3
10. Fonga-Djimi H, Leclerc F, Martinot A, et al. Spondylodiscitis and mediastinitis after esophageal perforation owing to a swallowed radiolucent foreign body. *J Pediatr Surg*. 1996;31(5):698–700. doi: 10.1016/s0022-3468(96)90677-6
11. Wadie GM, Konefal SH, Dias MA, McLaughlin MR. Cervical spondylodiscitis from an ingested pin: A case report. *J Pediatr Surg*. 2005;40(3):593–596. doi: 10.1016/j.jpedsurg.2004.11.023
12. Van Ooij A, Manni JJ, Beuls EA, Walenkamp GH. Cervical spondylodiscitis after removal of a fishbone. A case report. *Spine (Phila Pa 1976)*. 1999;24(6):574–577. doi: 10.1097/00007632-199903150-00015

СПИСОК ЛИТЕРАТУРЫ

1. Мушкин А.Ю., Вишневский А.А. Клинические рекомендации по диагностике инфекционных спондилитов (проект для обсуждения) // Медицинский альянс. 2018. № 3. С. 65–74.
2. Fowler V.G., Justice A., Moore C., et al. Risk factors for hematogenous complications of intravascular catheter-associated Staphylococcus aureus bacteremia // Clin Infect Dis. 2005. Vol. 40, N 5. P. 695–703. doi: 10.1086/427806
3. Lu Y.A., Hsu H.H., Kao H.K., et al. Infective spondylodiscitis in patients on maintenance hemodialysis: A case series // Ren Fail. 2017. Vol. 39, N 1. P. 179–186. doi: 10.1080/0886022X.2016.1256313
4. Choi K.B., Lee C.D., Lee S.H. Pyogenic spondylodiscitis after percutaneous endoscopic lumbar discectomy // J Korean Neurosurg Soc. 2010. Vol. 48, N 5. P. 455–460. doi: 10.3340/jkns.2010.48.5.455
5. Hsieh M.K., Chen L.H., Niu C.C., et al. Postoperative anterior spondylodiscitis after posterior pedicle screw instrumentation // Spine J. 2011. Vol. 11, N 1. P. 24–29. doi: 10.1016/j.spinee.2010.10.021
6. Hanci M., Toprak M., Sarioğlu A.C., et al. Oesophageal perforation subsequent to anterior cervical spine screw/plate fixation // Paraplegia. 1995. Vol. 33, N 10. P. 606–609. doi: 10.1038/sc.1995.128
7. Orlando E.R., Caroli E., Ferrante L. Management of the cervical esophagus and hypopharynx perforations complicating anterior cervical spine surgery // Spine. 2003. Vol. 28. P. E290–E295. doi: 10.1097/00007632-200308010-00023
8. Pompili A., Canitano S., Caroli F., et al. Asymptomatic esophageal perforation caused by late screw migration after anterior cervical plating: Report of a case and review of relevant literature // Spine. 2002. Vol. 27. P. E499–E502. doi: 10.1097/00007632-200212010-00016
9. Janssen I., Shiban E., Rienmüller A., et al. Treatment considerations for cervical and cervicothoracic spondylodiscitis associated with esophageal fistula due to cancer history or accidental injury: A 9-patient case series // Acta Neurochir (Wien). 2019. Vol. 161, N 9. P. 1877–1886. doi: 10.1007/s00701-019-03985-3
10. Fonga-Djimi H., Leclerc F., Martinot A., et al. Spondylodiscitis and mediastinitis after esophageal perforation owing to a swallowed radiolucent foreign body // J Pediatr Surg. 1996. Vol. 31, N 5. P. 698–700. doi: 10.1016/s0022-3468(96)90677-6
11. Wadie G.M., Konefal S.H., Dias M.A., McLaughlin M.R. Cervical spondylodiscitis from an ingested pin: A case report // J Pediatr Surg. 2005. Vol. 40, N 3. P. 593–596. doi: 10.1016/j.jpedsurg.2004.11.023
12. Van Ooij A., Manni J.J., Beuls E.A., Walenkamp G.H. Cervical spondylodiscitis after removal of a fishbone. A case report // Spine (Phila Pa 1976). 1999. Vol. 24, N 6. P. 574–577. doi: 10.1097/00007632-199903150-00015

AUTHORS' INFO

*** Pavel V. Gavrilov,** MD, Cand. Sci. (Med.);
address: 2-4 Ligovskiy avenue, 191036 Saint Petersburg, Russia;
ORCID: 0000-0003-3251-4084;
eLibrary SPIN: 7824-5374;
e-mail: spbniifrentgen@mail.ru

ОБ АВТОРАХ

*** Гаврилов Павел Владимирович,** канд. мед. наук;
адрес: Россия, 191036, Санкт-Петербург, Лиговский пр-т, д. 2-4;
ORCID: 0000-0003-3251-4084;
eLibrary SPIN: 7824-5374;
e-mail: spbniifrentgen@mail.ru

* Corresponding author / Автор, ответственный за переписку

Valeriya A. Zarya;
ORCID: 0000-0001-7956-3719;
e-mail: zariandra@mail.ru

Marina E. Makogonova, MD, Cand. Sci. (Med.);
ORCID: 0000-0001-6760-2426;
eLibrary SPIN: 6342-8967;
e-mail: MakogonovaME@gmail.com

Andrey R. Kozak, MD, Cand. Sci. (Med.);
ORCID: 0000-0002-3192-1430;
e-mail: andrkozak@mail.ru

Arkadiy A. Vishnevskiy, MD, Dr. Sci. (Med.);
ORCID: 0000-0002-9186-6461;
eLibrary SPIN: 4918-1046;
e-mail: vichnevsky@mail.ru

Заря Валерия Алексеевна;
ORCID: 0000-0001-7956-3719;
e-mail: zariandra@mail.ru

Макогонова Марина Евгеньевна, канд. мед. наук;
ORCID: 0000-0001-6760-2426;
eLibrary SPIN: 6342-8967;
e-mail: MakogonovaME@gmail.com

Козак Андрей Романович, канд. мед. наук;
ORCID: 0000-0002-3192-1430;
e-mail: andrkozak@mail.ru

Вишневский Аркадий Анатольевич, д-р мед. наук;
ORCID: 0000-0002-9186-6461;
eLibrary SPIN: 4918-1046;
e-mail: vichnevsky@mail.ru

DOI: https://doi.org/10.17816/DD340815

Прецизионная брахитерапия рака предстательной железы под контролем ПСМА-рецепторной молекулярной визуализации

П.В. Свиридов[1], П.О. Румянцев[2], М.В. Дегтярев[3], С.С. Серженко[3], Д.Б. Санин[1, 4], С.В. Стыров[1], Д.Ю. Агибалов[1], С.В. Коренев[5]

[1] Медицинский центр «Доктор Плюс», Обнинск, Российская Федерация;
[2] Группа клиник «Мой медицинский центр», Санкт-Петербург, Российская Федерация;
[3] Национальный медицинский исследовательский центр эндокринологии, Москва, Российская Федерация;
[4] Национальный медицинский исследовательский центр радиологии, Обнинск, Российская Федерация;
[5] Балтийский федеральный университет имени Иммануила Канта, Калининград, Российская Федерация

АННОТАЦИЯ

Одним из методов лечения локализованного рака предстательной железы без признаков прорастания капсулы железы и в отсутствии признаков метастазов (стадия cT1-T2N0M0) является брахитерапия с имплантацией микроисточников на основе изотопа ^{125}I. Методы структурной визуализации (ультразвуковое исследование; компьютерная томография, КТ; магнитно-резонансная томография, МРТ) не обладают высокой специфичностью в дифференциальной диагностике рака предстательной железы. Гибридные технологии лучевой визуализации (однофотонная эмиссионная компьютерная томография + компьютерная томография, ОФЭКТ/КТ; позитронно-эмиссионная томография + компьютерная томография, ПЭТ-КТ; позитронно-эмиссионная томография + магнитно-резонансная томография, ПЭТ/МРТ) сочетают в себе достоинства высокой чувствительности кросс-секционных методов структурной визуализации (КТ и МРТ) и высокой специфичности методов молекулярной визуализации (ОФЭКТ, ПЭТ) с туморотропными радиофармацевтическими лекарственными препаратами.

В данной работе на 7 клинических наблюдениях локализованного рака предстательной железы (шкала Глисона 6–7) показано, что прецизионность низкодозной брахитерапии микроисточниками ^{125}I локализованных карцином предстательной железы, равно как и прицельной биопсии, может быть повышена при использовании гибридных методов ПСМА-рецепторной (простатспецифический мембранный антиген) молекулярной визуализации (ОФЭКТ/КТ, ПЭТ/КТ). Метод ОФЭКТ/КТ более доступен, чем ПЭТ/КТ, и при наличии холодных наборов (HYNIC-PSMA) позволяет выполнять исследование в любой лаборатории радиоизотопной диагностики, располагающей соответствующими сканерами.

Инновационная технология ПСМА-навигационной биопсии и брахитерапии под контролем гибридной молекулярной визуализации может применяться при первичных и рецидивных случаях локализованного рака предстательной железы, увеличивает точность и снижает травматичность процедур, повышает медико-экономическую эффективность низкодозной брахитерапии микроисточниками ^{125}I.

Необходимы дальнейшие исследования для совершенствования технологии и оценки отдалённых результатов лечения на многочисленной группе пациентов.

Ключевые слова: брахитерапия низкодозная прецизионная; йод-125; простатспецифический мембранный антиген; ПСМА; однофотонная эмиссионная компьютерная томография, совмещённая с компьютерной томографией; ОФЭКТ/КТ; позитронно-эмиссионная томография, совмещённая с компьютерной томографией; ПЭТ/КТ.

Как цитировать:
Свиридов П.В., Румянцев П.О., Дегтярев М.В., Серженко С.С., Санин Д.Б., Стыров С.В., Агибалов Д.Ю., Коренев С.В. Прецизионная брахитерапия рака предстательной железы под контролем ПСМА-рецепторной молекулярной визуализации // *Digital Diagnostics*. 2023. Т. 4, № 3. С. 411–426. DOI: https://doi.org/10.17816/DD340815

Рукопись получена: 18.04.2023 **Рукопись одобрена:** 20.07.2023 **Опубликована:** 25.08.2023

DOI: https://doi.org/10.17816/DD340815

Precision low-dose brachytherapy of prostate cancer under PSMA-receptor molecular visualization

Pavel V. Sviridov[1], Pavel O. Rumiantsev[2], Mikhail V. Degtyarev[3], Sergey S. Serzhenko[3], Dmitry B. Sanin[1, 4], Sergey V. Styrov[1], Dmitry Yu. Agibalov[1], Sergey V. Korenev[5]

[1] Medical center "Doctor Plus", Obninsk, Russian Federation;
[2] Clinics group "My Medical Center", Saint Peterburg, Russian Federation;
[3] Endocrinology Research Centre, Moscow, Russian Federation;
[4] National Medical Research Radiological Center, Obninsk, Russian Federation;
[5] I. Kant Baltic Federal University, Kaliningrad, Russian Federation

ABSTRACT

Brachytherapy with implantation of micro sources based on isotope ^{125}I is a preferred treatment for localized prostate cancer without signs of germination of the gland capsule and in the absence of signs of metastases (stage cT1-T23aN0M0). Structural imaging methods (ultrasound, computed tomography, and magnetic resonance imaging) do not have high specificity in the differential diagnosis of prostate cancer. Hybrid technologies of radiation imaging (single-photon emission computed tomography/computed tomography, positron emission tomography/computed tomography, and positron emission tomography/magnetic resonance imaging) combine the advantages of high sensitivity of cross-sectional structural imaging methods (computed tomography and magnetic resonance imaging) and high specificity of molecular imaging methods (single-photon emission computed tomography and positron emission tomography) with tumorotropic radiopharmaceuticals. In this original clinical study, based on seven observations of localized prostate cancer (Gleason 6–7), it was shown that the precision of low-dose brachytherapy using ^{125}I micro sources of localized prostate carcinomas, along with targeted biopsy, can be increased using hybrid methods of PSMA-receptor molecular imaging (single-photon emission computed tomography/ computed tomography, positron emission tomography/ computed tomography). The single-photon emission computed tomography/ computed tomography method is more accessible than positron emission tomography/ computed tomography. Moreover, when coupled with cold kits (HYNIC-PSMA), it allows research within any radioisotope diagnostics laboratory equipped with single-photon emission computed tomography/ computed tomography. The innovative technology of PSMA-navigation biopsy and brachytherapy, under the control of hybrid molecular imaging, can be used in primary and recurrent cases of localized prostate cancer, increases the accuracy and reduces the traumatic nature of procedures, and increases the medical and economic efficiency of low-dose brachytherapy with ^{125}I micro sources. Further research is needed to improve the technology and evaluate its long-term results.

Keywords: brachytherapy low-dose rate precision; ^{125}I; prostate-specific membrane antigen; PSMA; single-photon emission computed tomography / computed tomography; positron emission tomography / computed tomography.

To cite this article:
Sviridov PV, Rumiantsev PO, Degtyarev MV, Serzhenko SS, Sanin DB, Styrov SV, Agibalov DYu, Korenev SV. Precision low-dose brachytherapy of prostate cancer under PSMA-receptor molecular visualization. *Digital Diagnostics.* 2023;4(3):411–426. DOI: https://doi.org/10.17816/DD340815

Received: 18.04.2023 **Accepted:** 20.07.2023 **Published:** 25.08.2023

DOI: https://doi.org/10.17816/DD340815

在PSMA受体分子成像控制下的前列腺癌精确近距离照射

Pavel V. Sviridov[1], Pavel O. Rumiantsev[2], Mikhail V. Degtyarev[3], Sergey S. Serzhenko[3], Dmitry B. Sanin[1, 4], Sergey V. Styrov[1], Dmitry Yu. Agibalov[1], Sergey V. Korenev[5]

[1] Medical center "Doctor Plus", Obninsk, Russian Federation;
[2] Clinics group "My Medical Center", Saint Peterburg, Russian Federation;
[3] Endocrinology Research Centre, Moscow, Russian Federation;
[4] National Medical Research Radiological Center, Obninsk, Russian Federation;
[5] I. Kant Baltic Federal University, Kaliningrad, Russian Federation

简评

治疗无腺囊萌发迹象和无转移迹象（cT1-T2N0M0期）的局部前列腺癌的方法之一是植入基于同位素^{125}I的微源近距离照射。结构成像方法（超声检查、电子计算机断层扫描（CT）、磁共振成像（MRI））在前列腺癌的鉴别诊断中特异性不高。混合放射成像技术（单光子发射计算机断层扫描+电子计算机断层扫描，SPECT/CT；正电子发射计算机断层扫描+电子计算机断层扫描，PET/CT；正电子发射断层扫描+磁共振成像，PET/MRI）结合了结构成像的横断面方法（CT和MRI）的高灵敏度和分子成像方法（SPECT、PET）的高特异性与肿瘤放射治疗物的优点。

在这项研究中，7例局部前列腺癌（格里森评分为6-7分）的临床观察结果表明了，通过使用PSMA受体（前列腺特异性膜抗原）分子成像（SPECT/CT、PET/CT）的混合方法，可以提高使用微源^{125}I对局部前列腺癌进行低剂量近距离照射以及靶向活检的精确度。SPECT/CT比PET/CT更经济实惠，而且在存在冷试剂盒（HYNIC-PSMA）的情况下，允许在任何拥有适当扫描仪的放射性同位素诊断实验室进行检查。

混合分子成像控制下的PSMA引导活检和近距离照射创新技术可用于原发性和复发性的局部前列腺癌病例，提高准确度，减少检查创伤性，提高微源^{125}I低剂量近距离照射的医疗和经济效益。

还需要进一步的研究来改进这种技术，并对大量患者的长期治疗效果进行评估。

关键词：精确低剂量近距离照射；碘125；前列腺特异性膜抗原；PSMA；联合电子计算机断层扫描的单光子发射计算机断层扫描；SPECT/CT；联合电子计算机断层扫描的正电子发射计算机断层扫描；PET/CT。

引用本文：
Sviridov PV, Rumiantsev PO, Degtyarev MV, Serzhenko SS, Sanin DB, Styrov SV, Agibalov DYu, Korenev SV. 在PSMA受体分子成像控制下的前列腺癌精确近距离照射. *Digital Diagnostics*. 2023;4(3):411–426. DOI: https://doi.org/10.17816/DD340815

收到：18.04.2023 **接受：**20.07.2023 **发布日期：**25.08.2023

BACKGROUND

Prostate cancer is the second most common malignant neoplasm in males and the fifth most common cause of death in the world [1]. Screening for prostate cancer based on the level of prostate-specific antigen (PSA) in the blood increases the number of prostate carcinomas detected at an early stage, significantly improving the prognosis of patient survival [2].

One method for treating localized prostate cancer without signs of capsule germination and without metastases (cT1-T2N0M0) is brachytherapy with implantation of ^{125}I-based microsources [3–8].

In brachytherapy, the radiation dose is achieved by spatial distribution of microsources during implantation in the projection of primary prostate carcinoma guided by computed tomography (CT) or ultrasound (US). Implanted microsources are fixed in the tissue, protecting surrounding healthy tissue from irradiation. Simultaneously, safe irradiation borders (2–3 mm) along the periphery of microsources do not lead to side irradiation of risk organs, such as the urethra, bladder, and rectum, which are inevitably affected during prostatectomy, external beam radiation therapy, and high-dose brachytherapy. Some studies of prostate cancer patients at low and moderate risk of tumor recurrence showed better tumor ablation than external beam radiotherapy [4, 5]. The effectiveness of low-dose brachytherapy in patients with localized prostate cancer (pT1-2N0M0) is at least noninferior compared with any other current treatment method, whereas patient tolerability and quality of life are significantly higher [9]. While in the early 2000s, low-dose brachytherapy was combined with external beam radiation therapy for boosting in a moderate risk group, in recent decades, this method has been used more frequently [10].

The brachytherapy method has several advantages, including its low invasiveness (puncture technology), the ability to control the process of installing microsources using structural imaging methods (ultrasound and CT), and the low frequency and low severity of adverse effects [11].

Hybrid radiation imaging technologies, such as single photon emission CT combined with CT (SPECT/CT), positron emission tomography combined with CT (PET/CT), and positron emission tomography combined with magnetic resonance imaging (PET/MRI), combine the high sensitivity of cross-sectional structural imaging methods (CT and MRI) and high specificity of molecular imaging methods (SPECT and PET) with tumor tropic radiopharmaceuticals (RPs).

Prostate-specific membrane antigen (PSMA) in humans is encoded by the *FOLH1* gene, which is involved in folate metabolism. It is a zinc-containing transmembrane glycoprotein produced in prostate epithelial cells and known as N-acetyl-L-aspartyl-L-glutamate peptidase or glutamate carboxypeptidase II. Its expression is significantly higher in malignant cells and closely related to tumor aggressiveness, particularly in castration-resistant and metastatic prostate cancer [12].

PSMA-receptor molecular imaging techniques (SPECT and PET) provide additional advantages in determining tumor stage and selecting targets for precision biopsy and brachytherapy of prostate carcinoma [13]. PET/CT with ^{68}Ga-PSMA-11 and ^{18}F-PSMA-1007 and SPECT/CT with ^{99m}Tc-HYNIC-PSMA (small-molecule PSMA inhibitors) are accessible in Russian clinical practice. The latter appears highly promising because of its greater availability (significantly more SPECT/CT scanners than PET/CT scanners), easy operation, lower cost, and technological advantages to ensure high precision in biopsy and brachytherapy of localized prostate cancer.

CASE REPORTS

Patients

The study examines treatment outcomes in seven patients aged 65–84 yr (mean: 73 yr; 95% confidence interval [95% CI], 66.8–79.2]) with histologically diagnosed prostate cancer who underwent brachytherapy using ^{125}I-based microsources at the Doctor-Plus clinic in Obninsk, Kaluga region, Russia. All patients had histologically confirmed prostate carcinoma with no signs of regional and/or distant metastases. Five patients had primary tumors. Another two patients had local tumor recurrence in 21 and 28 months after receiving brachytherapy with ^{125}I-based microsources. The tumor stage in two patients was T1N0M0, whereas the stage in four patients was T2N0M0. The stage in one patient was T3aN0M0. In the other case, the patient refused the proposed surgical treatment, which included combined external beam radiation and androgen deprivation therapy.

The Gleason score was 6 (3 + 3) in five cases and 7 (3 + 4) in two cases. Before brachytherapy, blood PSA levels ranged from 2.8 to 12 ng/mL (mean: 8.2 ng/mL).

Methods

Patients with local tumor recurrence were treated with interstitial radiation therapy using ^{125}I-based microsources in the first stage. The time to progression ranged from 12 to 29 months (24.2 [95% CI, 17.8–30.5]).

Clinical examination included standard measurement of serum PSA levels. A venous blood sample was collected in the morning under fasting conditions and prepared in accordance with study protocols. Serum PSA levels were measured using a chemiluminescent immunoassay (sensitivity limits: 0.008–30.0 ng/mL).

Transrectal ultrasound diagnostics was performed using a B/K Medical scanner (USA) to determine the prostate volume and residual urine. Uroflowmetry was performed to assess the maximum volumetric urine flow rate.

In the excretory phase, a pelvic CT with intravenous contrast enhancement (Omnipaque 350 mg/mL, 30 mL) was performed to better visualize the anatomy of organs at risk using a Somatom Scope multidetector (32 slices) CT scanner (Siemens, Germany) with subsequent data transfer for planning interstitial radiation therapy.

A radionuclide study with ^{99m}Tc-HYNIC-PSMA was performed using a General Electric Discovery NM/CT 670 hybrid scanner. The finished RP was administered intravenously with a vent visor (intranasal control) at a 6.3 MBq/kg b.w rate. A pelvic area was scanned 2 h after RP administration using a SPECT/CT gamma camera; 60 projections with 30-s exposures per projection, matrix 256 × 256. CT data acquisition parameters were as follows: tube voltage, 120 kV; current (modulated), 80–400 mA; slice thickness, 3.75 mm with 1.25-mm reconstruction; and couch increment, 1 mm. The resulting 3D SPECT/CT image was analyzed using the General Electric Xeleris 4DR data workstation. The identified prostate lesions of focal RP accumulation were indicated on a schematic PI-RADS prostate sector map.

Without anesthesia, a US-guided biopsy was performed transperineally (using SPECT/CT data with ^{99m}Tc-HYNIC-PSMA) with a Promag 2.0 biopsy needle and gun. If required, a CT-guided biopsy of the prostate gland and seminal vesicles was performed under spinal anesthesia through pararectal access. Histological biopsy specimens were examined in pathological laboratories with Gleason score determination.

Planning and conducting brachytherapy with ^{125}I sources

Topometry and dosimetry planning were performed for pre-implantation planning using a VariSpeed dosimetry planning system (Varian, USA). That system allowed the DICOM format images of different modalities to be combined.

^{125}I-based microsources were implanted under a CT guide using a Siemens Somatom Scope (Germany) using a 3D stereotactic machine with a hole increment of 2.5 mm to perform targeted brachytherapy. Under spinal anesthesia, the procedure was performed via pararectal access.

Figure 1 shows an example of pre-implantation brachytherapy planning using ^{125}I sources. Crosses indicate virtual holes in the stereotactic array, which fully corresponds to the array implanted in a patient. Red dots indicate microsources, whereas colored lines indicate isodose distribution.

^{125}I microsources in the form of grains (BEBIG LLC, Russia) were used for interstitial implantation. Each source measured 4.5 mm in length and 0.8 mm in diameter. According to the comprehensive examination results and dosimetry planning, the number of sources was ordered individually for each patient (Table 1).

Brachytherapy requires bowel preparation and antibiotic therapy. Spinal anesthesia with lidocaine/bupivacaine was administered to relieve pain.

The implantation was performed in accordance with 2014 recommendations [12]. During control scans and

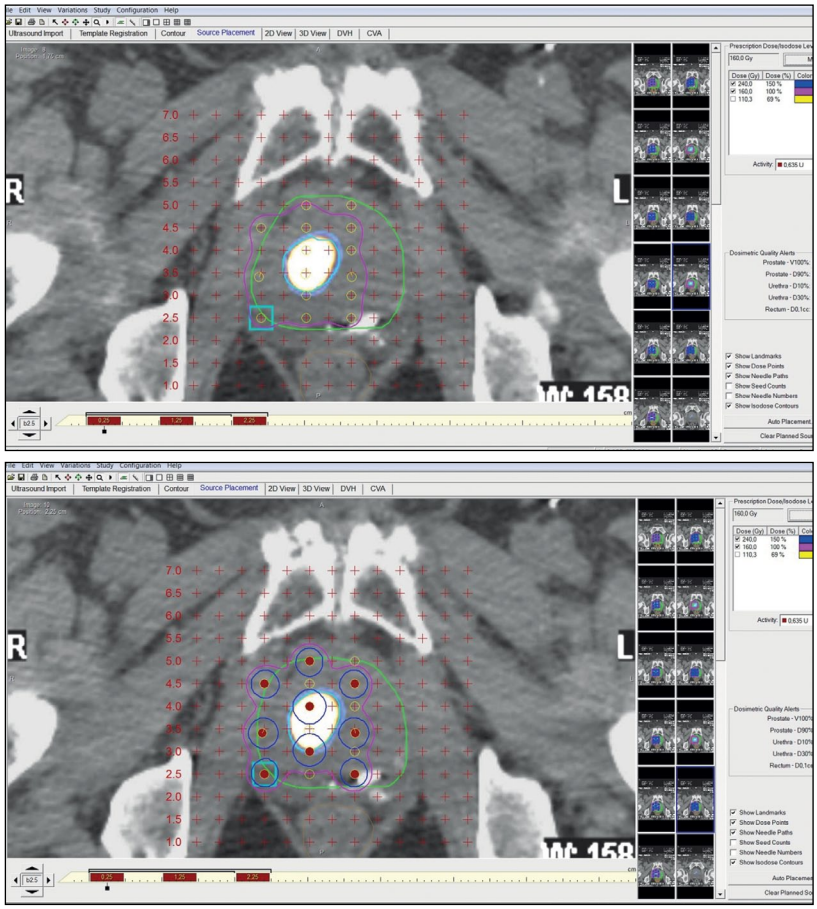

Fig. 1. Stages of dosimetry planning of brachytherapy localized prostate cancer using ^{125}I microsources considering SPECT/CT with ^{99m}Tc-HYNIC-PSMA: (*a*) topometric marking and (*b*) topometric marking and dosimetry planning of brachytherapy.

Table 1. Demographic data and clinical and morphological characteristics of patients

Age[a], yr	Tumor			Prostate volume/ prostate tumor volume, mL	Localization in pancreas[d]	Planned number of ^{125}I microsources/length of procedure[e]	Planned number of ^{125}I microsources/length of procedure[f]
	Stage, TNM[b]	Primary case or relapse[c]	Gleason score				
Patient 1 84 years old	T2N0M0	Primary	7 (4 + 3)	40/40	Right lobe TZa (mid)	60 75 min	60 75 min
Patient 2 79 years old	T2N0M0	Primary	6 (3 + 3)	38/15	Right lobe TZa (apex), Left lobe TZp (mid)	60 75 min	20 25 min
Patient 3 73 years old	T1N0M0	Primary	6 (3 + 3)	36/14	Right lobe TZa (apex), Left lobe PZpl (base) PZpl (mid)	70 87 min	32 45 min
Patient 4 68 years old	T3N0M0	Relapse	7 (4 + 3)	38/15	Right lobe TZp, PZpl (base)	60 75 min	20 25 min
Patient 5 70 years old	T2N0M0	Relapse	6 (3 + 3)	30/15	Right lobe PZpl (mid)	70 87 min	30 40 min
Patient 6 65 years old	T1N0M0	Primary	7 (4 + 3)	60/15	Right lobe TZa (mid)	90 112 min	30 40 min
Patient 7 69 years old	T2N0M0	Primary	6 (3 + 3)	78/78	Right lobe TZa (apex), Left lobe PZpl (base) PZpl (mid)	32 45 min	90 112 min

Note. PSMA, prostate-specific membrane antigen; PZpl (mid/base), posterior zone (middle/basal part); SPECT/CT, single photon emission computed tomography combined with computed tomography; TZa (mid/apex), anterior transition zone (middle/apical part); TZp (mid), posterior transition zone (middle part).

[a]Age of patients at the time of treatment.

[b]UICC, 8th ed. (https://oncology.ru/specialist/treatment/tnm/tnm8_summary.pdf).

[c]Method of primary treatment.

[d]International standard.

[e]Without tumor visualization using SPECT/CT.

[f]Under PSMA/SPECT/CT guide.

reconstruction of the resulting images, the placement of ^{125}I microsources was visually monitored.

Patients were discharged 1 day after brachytherapy and were able to return to normal activities within 3–5 days. None of the patients required bladder catheterization or epicystostomy. Mild difficulty urinating was relieved using alpha-blockers in generally accepted doses. There were no reports of early or late radiation effects.

The duration of the brachytherapy procedure depended on the number of implanted ^{125}I microsources and ranged from 25 to 112 min (mean: 51.7 min), which was 34.8% less than the average estimated time (79.4 min) using a standard procedure (without PSMA-SPECT/CT guide).

No severe complications were observed in the early and long-term post-procedure periods (mean: 24.5 months). Mild dysuric symptoms were reported in two patients for several post-procedure days, but they did not require catheterization or drug therapy and resolved spontaneously.

Case report 1

Patient Zh., 84 years old, was admitted with prostate cancer (PSA of 20 ng/mL; adenocarcinoma, Gleason 7 [4 + 3]). On October 9, 2020, CT-guided interstitial radiation therapy with ^{125}I microsources and pararectal access was performed using SPECT/CT data. PSA levels were 0.16 ng/mL 2 yr later, indicating tumor remission. PSA was 0.1 ng/mL on January 14, 2023.

Figure 2 shows SPECT/CT data with ^{99m}Tc-HYNIC-PSMA.

Case report 2

Patient Z., 79 years old, was admitted with diffuse prostatic hyperplasia. PSA level was 4.5 ng/mL. No abnormal lesions were found in the prostate tissue using ultrasound, TRUS, and contrast-enhanced MRI. SPECT/CT with ^{99m}Tc-HYNIC-PSMA revealed 15-mm^3 sites of RP accumulation in the prostate tissue (Figure 3). Because rectal amputation made US-guided prostate biopsy impossible, a targeted CT-guided biopsy

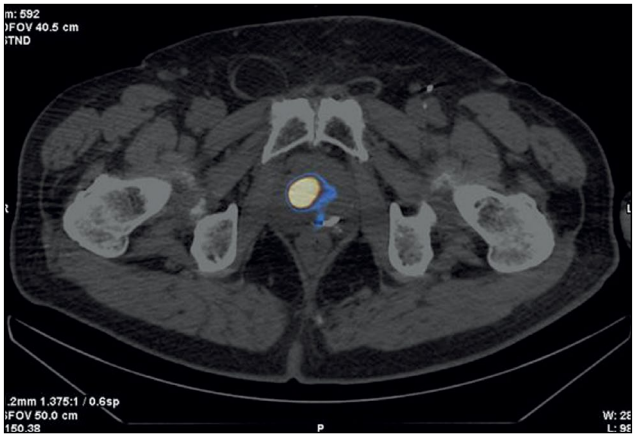

Fig. 2. Patient Zh., 8 years old, SPECT/CT with ^{99m}Tc-HYNIC-PSMA, axial projection: Site of radiopharmaceutical accumulation in the transition zone of the middle part of the right prostate lobe.

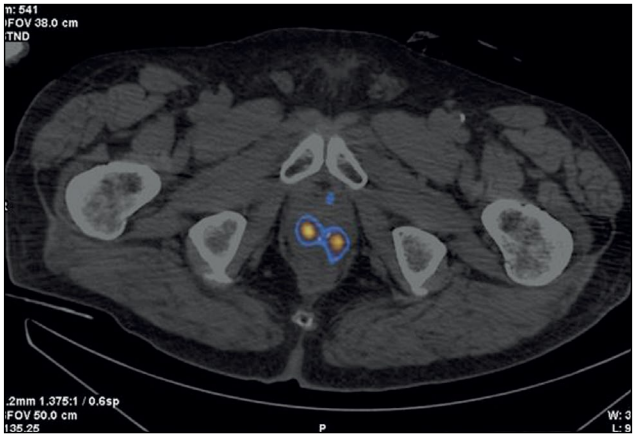

Fig. 3. Patient Z., 7 years old, SPECT/CT with ^{99m}Tc-HYNIC-PSMA: Sites of radiopharmaceutical accumulation in transitory zones of both lobes at the border of the middle third and the apex of the prostate gland.

was performed pararectally. A morphological diagnosis was adenocarcinoma, Gleason 6 (3 + 3).

On January 28, 2021, ^{125}I sources were implanted pararectally under a CT guide. In the follow-up examination, PSA levels were 0.2 ng/mL (September 2022) and 0.1 ng/mL (January 14, 2023).

In this case, two problems were revealed: an unknown cause of increased PSA over time and the inability to perform a targeted prostate carcinoma biopsy under US guide. Both problems were successfully resolved using hybrid SPECT/CT with ^{99m}Tc-HYNIC-PSMA followed by CT-guided RP accumulation site biopsy, and precision brachytherapy was performed with a smaller number of ^{125}I microsources due to the SPECT/CT pattern.

Case report 3

Patient K., 73 years old, was admitted with diffuse prostatic hyperplasia, urinary retention, an epicystostomy, and a 12.7-ng/mL PSA. A multisite biopsy performed under US guide revealed no evidence of malignant development. SPECT/CT data with ^{99m}Tc-HYNIC-PSMA are shown in Figure 4. SPECT/CT revealed a 14-mm^3 site of RP accumulation in the prostate tissue. A CT-guided targeted biopsy was performed using pararectal access. A morphological diagnosis was adenocarcinoma, Gleason 6 (3 + 3).

On November 28, 2020, CT-guided focal implantation of ^{125}I sources was performed pararectally. Transurethral resection of the intravesical component was performed, and the epicystostomy was removed. The follow-up examination (November 28, 2022) showed a PSA level of 0.13 ng/mL, spontaneous urination, and 15-cm^3 residual urine.

In this case, problems were as follows: inability to identify the cause of elevated PSA, a "large" volume of the prostate gland, and epicystostomy. Considering data on RP accumulation patterns and biopsy results, we were unable to successfully solve these problems and perform successful focal brachytherapy using a hybrid diagnostic use of RP CT-guided biopsy.

Fig. 4. Patient K., 73 years old, SPECT /CT with ^{99m}Tc-HYNIC-PSMA, (*a*) frontal and (*b*) axial sections: Sites of radiopharmaceutical accumulation in the anterior part of the transition zone in the apex of the right lobe, posterolateral part of the peripheral zone at the level of the base of the left lobe, and posterolateral part of the peripheral zones at the level of the base and middle third of the left lobe of the prostate gland; physiological accumulation of radiopharmaceuticals in the bladder.

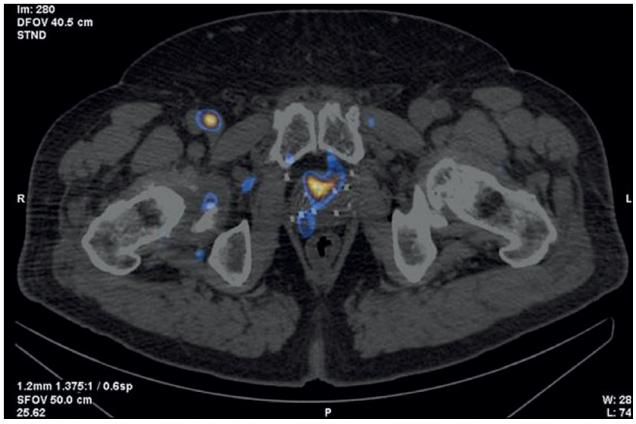

Fig. 5. Patient F., 68 years old, SPECT/CT with ^{99m}Tc-HYNIC-PSMA: Sites of radiopharmaceutical accumulation at the border of the central zone and the posterolateral part of the peripheral zone on the right side at the level of the base of the right prostate lobe. The scan visualizes multiple rods in the prostate gland, implanted during previous brachytherapy.

Case report 4

Patient F., 68 years old, was admitted with prostate cancer, T3a, which had spread to the prostate gland capsule. In 2013, ^{125}I sources were implanted into the prostate tissue and the extracapsular area. PSA has increased since the end of 2020. SPECT/CT was performed using ^{99m}Tc-HYNIC-PSMA due to an increased PSA level of 0.95–2.8 ng/mL after the previous treatment (Figure 5). SPECT/CT revealed a 15-mm^3 site of tumor tropic RP accumulation, which was biopsied under the CT guide. A histological diagnosis was prostate adenocarcinoma, Gleason 6 (3 + 3). Dosimetry planning for low-dose brachytherapy was performed using SPECT/CT. On November 03, 2021, ^{125}I microsources were re-implanted according to topometric markings to implement the dosimetry plan. The PSA level was 0.05 ng/mL during the follow-up examination (January 23, 2023).

In this case, SPECT/CT with ^{99m}Tc-HYNIC-PSMA allowed for a precision biopsy, which confirmed the local recurrence of prostate cancer and subsequently enabled brachytherapy to be repeated (salvage) under the CT guide.

Case report 5

Patient G., 70 years old, was admitted with prostate cancer (diagnosed in 2005), T2a, adenocarcinoma, Gleason 6 (3 + 3). CT-guided brachytherapy was successfully performed in 2005. The PSA level has increased (1.94–2.31 ng/mL) since 2017. Because of this growth, ultrasound, TRUS, CT, and contrast-enhanced MRI were performed; no data for a local recurrence or another cause of PSA growth were obtained. When the PSA level reached 2.63 ng/mL, SPECT/CT with ^{99m}Tc-HYNI-PSMA was performed (Figure 6). Results showed a 15-mm^3 site of RP accumulation, and a targeted biopsy of a recurrent prostate carcinoma lesion was performed based on its SPECT/CT location. Adenocarcinoma was confirmed histologically, Gleason 6 (3 + 3). On March 10, 2020, a brachytherapy with reimplantation of ^{125}I microsources was performed. The follow-up examination (December 2022) showed a PSA level of 0.21 ng/mL.

In this case, SPECT/CT with ^{99m}Tc-HYNIC-PSMA enabled prostate carcinoma–targeted biopsy and precision brachytherapy.

Case report 6

Patient M., 65 years old, was diagnosed with benign prostatic hyperplasia. Due to an increased PSA level of 4.5 ng/mL, a US-guided multifocal biopsy was performed with no histological evidence of cancer. A repeat biopsy was performed 3 months later and revealed no malignant tumor. SPECT/CT with ^{99m}Tc-HYNIC-PSMA revealed a site of RP accumulation in the prostate tissue (Figure 7). A CT-guided targeted biopsy was performed, and the following diagnosis was morphologically confirmed: adenocarcinoma,

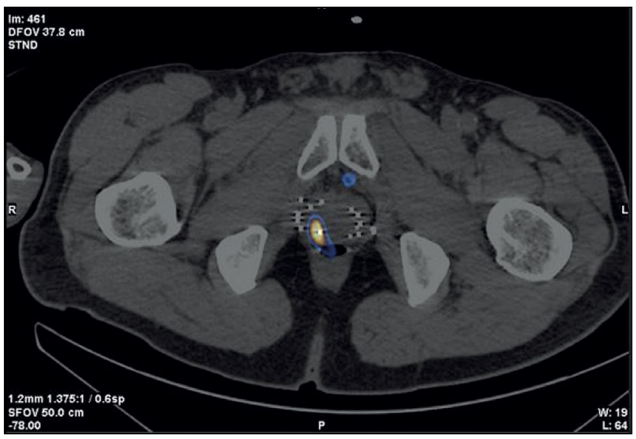

Fig. 6. Patient G., 70 years old, SPECT/CT with ^{99m}Tc-HYNIC-PSMA: Site of radiopharmaceutical accumulation in the posterolateral part of the peripheral zone of the middle part of the right prostate lobe. Multiple rods in the prostate gland were implanted during previous brachytherapy.

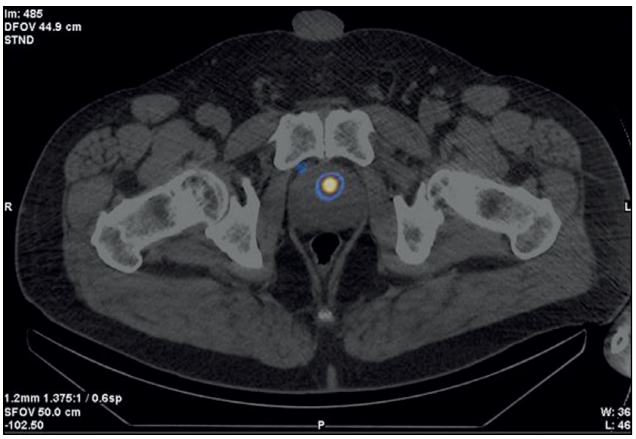

Fig. 7. Patient M., 65 years old, SPECT/CT with ^{99m}Tc-HYNIC-PSMA: Site of radiopharmaceutical accumulation in the transition zone (at the border of the middle third and the base) of the left prostate lobe.

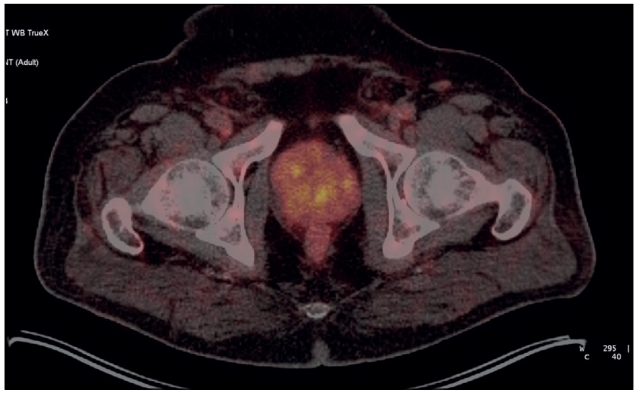

Fig. 8. Patient M., 69 years old, PET/CT with 68Ga-PSMA-11: Sites of radiopharmaceutical accumulation in the prostate gland, multifocal tumor.

Gleason 7 (4 + 3). When planning low-dose brachytherapy using ^{125}I microsources, SPECT/CT data were entered into the dosimetry planning system. On October 4, 2020, the focal implantation of ^{125}I microsources was performed under a CT guide using pararectal access based on data on local isotope accumulation in the prostate tissue. The follow-up examination (January 2023) showed a 0.11-ng/mL PSA level.

Case report 7

Patient M., 6 years old, had an increased PSA level of 6.8 ng/mL and underwent a multifocal prostate biopsy at a local clinic. The diagnosis was confirmed morphologically as adenocarcinoma, Gleason 6 (3 + 3), based on data from the transitory zone of the right prostate lobe. Adenocarcinoma elements were not found in other prostate biopsy specimens. Considering MRI evidence of changes in the same zone, implantation with 30 ^{125}I sources with a 32-cm^3 volume was proposed.

SPECT/CT with ^{99m}Tc-HYNIC-PSMA revealed diffuse focal RP accumulation under the base of the bladder. PET/CT with 68Ga-PSMA-11 was additionally performed to more accurately visualize prostate lesions. PET/CT revealed multiple sites of RP accumulation in the prostate gland, indicating that the tumor was multifocal (Figure 8). Implantation planning was adjusted to include the total volume of the prostate gland (78 cm^3) using 90 ^{125}I microsources (instead of preliminary 30 microsources).

On February 25, 2022, implantation was performed for the total volume of the prostate gland. The initial prostate volume for brachytherapy was 32 cm^3. PET/CT revealed a volume of 72 cm^3 for implantation. The PSA level decreased to 0.31 ng/mL within a year after brachytherapy.

Changes in PSA levels in all patients included are shown in Figure 9.

All patients are under clinical supervision and have regular follow-up examinations.

DISCUSSION

A biopsy of prostate lesions is required to confirm the diagnosis and select a management strategy. This procedure is often performed under a US or MRI guide [14-15]. Because radiological structural diagnostics methods (ultrasound, CT, and MRI) do not always visualize lesions of the primary tumor, traumatic multifocal biopsies are often required [15]. False-negative biopsy results are reported in up to 49% of cases. If blood PSA levels increase, a biopsy is repeated [16]. A repeat biopsy is typically performed within 3 months after the initial [16]. Conventional diagnostic methods (ultrasound, CT, and MRI), particularly multiparametric MRI, visualize structural abnormalities but do not differentiate between benign and malignant tumors or assess the borders of a malignant tumor and its multifocal nature [15–17].

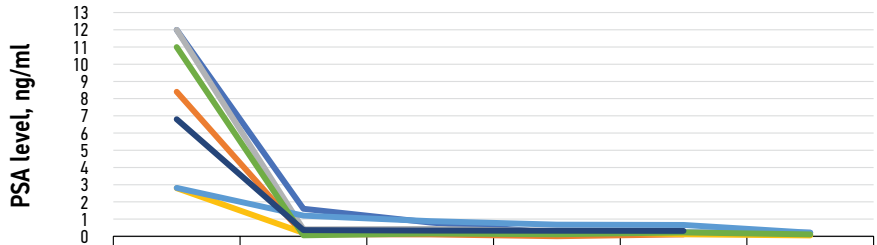

	Before brachytherapy	Month 3	Month 6	Month 9	Month 12	Month 24
1	12	1,6	0,8	0,18	0,23	0,21
2	8,4	0,12	0,11	0	0,11	-
3	12	0,4	0,43	0,3	0,2	0,1
4	2,8	0,2	0,3	0,3	0,12	0,05
5	2,81	1,2	0,88	0,68	0,66	0,21
6	11	0,06	0,16	0,12	0,23	0,11
7	6,8	0,36	0,33	0,32	0,31	-

Fig. 9. Changes in prostate-specific antigen levels in individual patients.

The morbidity and false-negative results of conventional prostate biopsy can be reduced with PSMA-receptor imaging guidance using SPECT/CT and/or PET/CT [18–21].

For prostate carcinomas with a low and moderate risk of recurrence (Gleason ⩽7), no growth beyond the organ capsule, and evidence of metastases, brachytherapy with ^{125}I microsources is the least traumatic of all recommended treatment options, demonstrating not only high effectivity but also high quality of life [22].

Molecular imaging methods (SPECT and PET) combined with cross-sectional imaging (CT and MRI) differentiates between lesions of malignant prostate tumors with high expression of PSMA receptors and benign structural lesions. As a result, it is possible to perform a US-guided targeted biopsy of positive lesions (considering molecular imaging data) and accurately plan and provide CT-guided brachytherapy.

The paper presents original clinical experience proving the feasibility of precision biopsy and brachytherapy of localized nonmetastatic prostate cancer (pT1-3N0M0) guided by PSMA-receptor molecular imaging (SPECT/CT with ^{99m}Tc-HYNIC-PSMA and PET/CT with ^{68}Ga-PSMA-11). Topometric marking and dosimetry planning of brachytherapy of tumor lesions using ^{125}I microsources was also based on the above hybrid molecular imaging data. As a result, topometric imaging of prostate carcinoma lesions enabled us to accurately plan and perform brachytherapy while reducing radiation exposure to healthy tissue and surrounding adjacent organs at risk, hence improving the patient's quality of life after treatment.

Due to the selective overexpression in prostate cancer tumor cells, PSMA-receptor molecular imaging using positron emission tomography (PET) has been used effectively in clinical practice. If PET/CT with ^{68}Ga-PSMA-11, ^{18}F-DCFPyL (piflufolastat F-18), and ^{18}F-PSMA-1007 is not achievable, SPECT/CT with ^{99m}Tc-HYNIC-PSMA may be performed. There are no significant differences in the specificity of PSMA-receptor imaging using PET/CT and SPECT/CT, but the sensitivity of PET/CT is significantly higher; therefore, this method is recommended when results of PSMA-receptor SPECT/CT are negative or questionable [23–25]. However, a valuable advantage of SPECT/CT with ^{99m}Tc-HYNIC-PSMA is the ability to improve molecular imaging of tumor lesions in the second phase (delayed, ⩾15 h after RP administration) [26].

At the current stage of personalized and precision oncology development, molecular imaging (SPECT and PET), particularly when combined with structural cross-sectional pictures (CT and MRI), enables the detection of tumor lesions based on receptor characteristics or intracellular metabolism. This is especially true for increased precision of external beam radiation therapy, which includes brachytherapy [27].

In our patients, the average implantation time was reduced by one-third (34.8%), proportionally to decreased implanted microsources. Approximately 15–20 min was spent positioning the patient on the tomograph table after spinal anesthesia and installing and positioning the stereotactic attachment to the CT scanner. The length of this process is determined by the patient's weight and general condition rather than the number of implanted sources. On average, it takes about one and a half minutes to install one needle, position it under CT control, remove styles, load sources, and remove the needles with a control scan. Decreased implantation time is also associated with greater preparedness of the implantation plan due to more accurate visualization of the affected area and its configuration. Therefore, in most cases, there was a significant decrease in the number of microsources, procedure time, personnel radiation exposure, CT scanner occupancy, and rate of injury and subsequent prostate gland swelling (six out of seven). In another case, there were indications for increasing the number of implanted microsources based on PET/CT data using ^{68}Ga-PSMA-11, which was considered when planning and performing the procedure.

Brachytherapy can provide high doses of radiation at tumor sites (average: 160 Gray) and is associated with minimal irradiation of surrounding healthy prostate tissue, including the urethra. It does not irradiate adjacent organs at risk (bladder and rectum).

When SPECT/CT with ^{99m}Tc-HYNIC-PSMA and PET/CT with ^{68}Ga-PSMA-11 were used in a clinical population of seven patients with primary (n = 5) and recurrent (n = 2) prostate carcinomas of low and moderate risk, a total number ^{125}I microsources implanted were less (by 36%; 404/282) than the potential number of microsources implanted using standard technique without PSMA-receptor hybrid molecular imaging methods. Simultaneously, as previously reported, molecular imaging reduced the number of sources in six cases while increasing the number of microsources in one case (multifocal tumor). We are not discussing the willingness to "save" microsources; instead, we are talking about the priority of precise diagnostic and treatment processes and personalized increases in the effectiveness and safety of treatment.

A positive biochemical response was achieved in all clinical cases, with PSA levels decreasing to low values and a tendency to decrease further.

ALGORITHM FOR PSMA-PRECISION BRACHYTHERAPY FOR LOCALIZED PROSTATE CANCER

In our cases, the use of hybrid molecular PSMA-receptor imaging (SPECT/CT and PET/CT) methods enabled us to:

- personalize and increase the precision of diagnostic (biopsy) and therapeutic (brachytherapy) procedures in patients with prostate cancer;
- reduce time, increase accuracy, and reduce injury rate associated with morphological verification of the primary tumor: in three of seven cases, a biopsy (previously unsuccessful and traumatic multifocal one)

of the tumor was performed using SPECT/CT from the site of accumulation of ^{99m}Tc-HYNIC-PSMA, and in all three cases, the presence the tumor was confirmed by histological examination;
- determine the stage of the tumor and exclude regional and distant metastases;
- increase precision of dosimetry and topometric location of ^{12}I microsources to reduce the risk of radiation reactions and improve patient quality of life;
- increase accuracy of microsource implantation due to tumor-targeted planning of interstitial radiation therapy of the tumor lesions with morphological confirmation;
- distribute radioactive sources using a hybrid molecular imaging guide (SPECT/CT, PET/CT, and PET/MRI) and approve the dosimetry plan;
- reduce the waiting time by targeted biopsy of the tumor lesion, considering PSMA-receptor hybrid scintigraphy (SPECT/CT and PET/CT) data on its location; and
- increase the number and topometric plan of placement of ^{125}I microsources during brachytherapy (in this series of cases, the number of microsources was 36% lower, and the procedure time was 34.8% less than the standard treatment plan).

Based on the data given, an algorithm for PSMA-precision brachytherapy for localized prostate cancer was developed and used in the clinical practice of our clinic (Figure 10).

The strength of the study is the use of the original, innovative technology of precision brachytherapy under molecular PSMA-receptor imaging guide using SPECT/CT with ^{99m}Tc-HYNIC-PSMA. The half-life of ^{99m}Tc is 6 h, allowing for delayed (next day) SPECT/CT of areas of interest and more clearly visualize sites of accumulation of ^{99m}Tcwith virtually no background half-lives of ^{18}F and ^{68}Ga are 110 and 68 min, respectively)The limitations of our study are a small clinical sample (seven patients), a short period of follow-up (up to 2 yr), and a lack of MRI disk revision (only conclusions were analyzed, which in all cases were negative regarding tumor lesion localization), as well as the inability to evaluate and compare the diagnostic value of methods. All these aspects should be considered while designing further studies.

We found no reports on the use of such technology in the Russian or foreign literature; therefore, on January 25, 2023, invention patent No. 2788859, "Method of targeted brachytherapy for prostate cancer under hybrid PSMA-receptor scintigraphy guide" was obtained [28].

CONCLUSION

The study suggests that the precision of targeted biopsy and low-dose brachytherapy with ^{125}I microsources for localized prostate carcinomas can be improved using hybrid methods of PSMA-receptor molecular imaging (SPECT/CT and PET/CT). The methods are complementary in terms of diagnostic and therapeutic guides; however, SPECT/CT is more accessible than PET/CT. The availability of cold kits (HYNIC-PSMA) enables one to examine any radioisotope diagnostic laboratory with appropriate equipment.

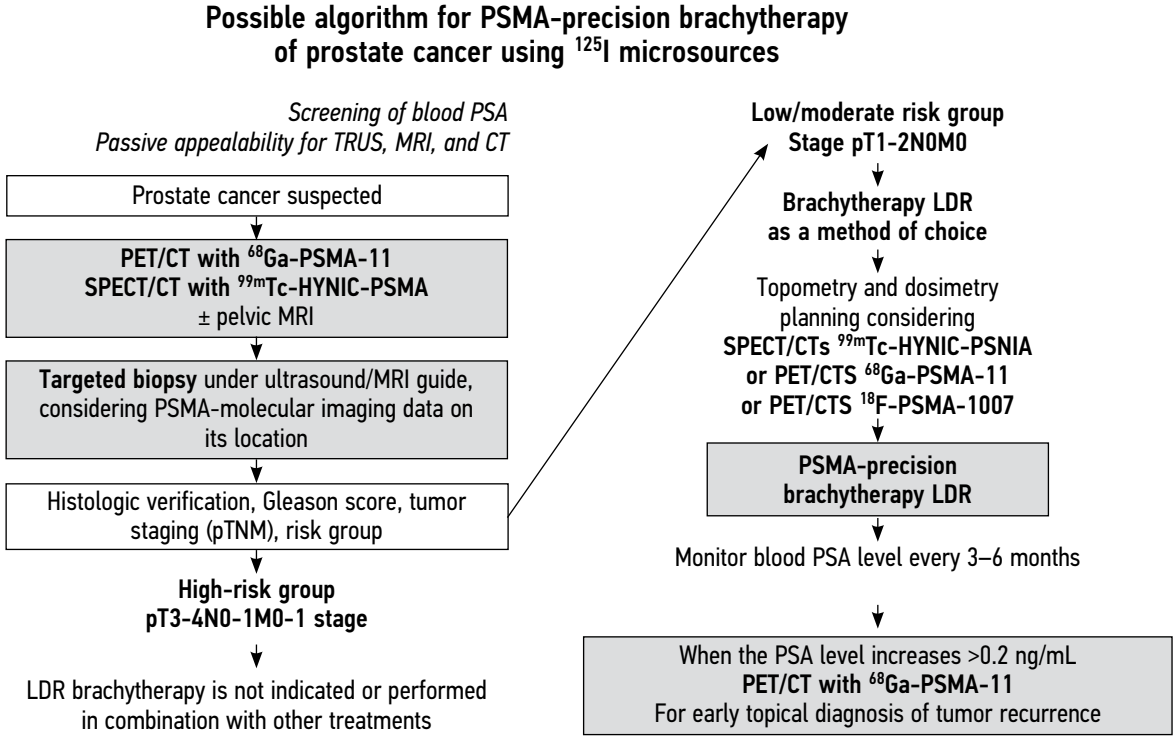

Fig. 10. Algorithm for selecting patients for low-dose brachytherapy, emphasizing increasing precision under PSMA-receptor molecular imaging guide. ku, contrast enhancement; LDR, low-dose rate; PSMA, prostate-specific membrane antigen.

The innovative technology of PSMA-precision biopsy brachytherapy guided by hybrid molecular imaging can be used for primary and recurrent localized prostate cancer, improving accuracy, reducing invasiveness of procedures, and increasing the medical and economic efficiency of low-dose brachytherapy with ^{125}I microsources.

Further research is required to develop the technology and evaluate long-term treatment outcomes in a larger group of patients.

ADDITIONAL INFORMATION

Funding source. This article was not supported by any external sources of funding.

Competing interests. The authors declare that they have no competing interests.

Authors' contribution. All authors made a substantial contribution to the conception of the work, acquisition, analysis, interpretation of data for the work, drafting and revising the work, final approval of the version to be published and agree to be accountable for all aspects of the work. P.V. Sviridov — management of patients, brachytherapy procedure conduction, test writing and preparing of images, P.O. Rumiantsev — paper idea, design, coordination, paper writing and edition; M.V. Degtyarev — introduction and interpretation of SPECT/CT and PET/CT, writing of corresponding parts of the paper; S.S. Serzhenko — introduction and interpretation of SPECT/CT, writing of corresponding parts of the paper; D.B. Sanin — dosimetry planning of brachytherapy, writing of corresponding parts of the paper; S.V. Styrov — execution of computed tomography, writing of corresponding parts of the paper; D.Yu. Agibalov — data elaboration, paper edition; S.V. Korenev — assistance in obtaining diagnostic information about treated patients, helping in paper edition.

Consent for publication. Written consent was obtained from all patients for publication of relevant medical information and all of accompanying images within the manuscript in Digital Diagnostics Journal.

REFERENCES

1. Sung H, Ferlay J, Siegel RL, et al. Global cancer statistics 2020: Globocan estimates of incidence and mortality worldwide for 36 cancers in 185 countries. *CA Cancer J Clin*. 2021;71(3):209–249. doi: 10.3322/caac.21660

2. Nyame YA, Gulati R, Tsodikov A, et al. Prostate-Specific antigen screening and recent increases in advanced prostate cancer. *JNCI Cancer Spectr*. 2021;5(1):pkaa098. doi: 10.1093/jncics/pkaa098

3. Pommier P, Ferré M, Blanchard P, et al. Prostate cancer brachytherapy: SFRO guidelines 2021. *Cancer Radiotherap*. 2022;26(1-2):344–355. doi: 10.1016/j.canrad.2021.11.019

4. Parker C, Castro E, Fizazi K, et al. Prostate cancer: ESMO clinical practice guidelines for diagnosis, treatment and follow-up. *Ann Oncol*. 2020;31(9):1119–1134. doi: 10.1016/j.annonc.2020.06.011

5. Mottet N, van der Berg R, Briers E, et al. EAU-eanm-estro-esur-siog guidelines on prostate cancer-2020 update. Part 1: Screening, diagnosis, and local treatment with curative intent. *Eur Urol*. 2021;79(2):243–262. doi: 10.1016/j.eururo.2020.09.042

6. Nosov DA, Volkova MI, Gladkov OA, et al. Practical recommendations for the treatment of prostate cancer. *Malignant Tumors. Practical recommendations RUSSCO*. 2022;12(#3s2):607–626. (In Russ). doi: 10.18027/2224-5057-2022-12-3s2-607-626

7. Tsumura H, Tanaka N, Oguchi T, et al. Comparative effectiveness of low-dose-rate brachytherapy with or without external beam radiotherapy in favorable and unfavorable intermediate-risk prostate cancer. *Sci Rep*. 2022;12(1):11023. doi: 10.1038/s41598-022-15028-6

8. Tanaka N, Asakawa I, Hasegawa M, Fujimoto K. Low-dose-rate brachytherapy for prostate cancer: A 15-year experience in Japan. *Int J Urol*. 2020;27(1):17–23. doi: 10.1111/iju.14098

9. Fellin G, Mirri MA, Santoro L, et al. Low dose rate brachytherapy (LDR-BT) as monotherapy for early stage prostate cancer in Italy: Practice and outcome analysis in a series of 2237 patients from 11 institutions. *Br J Radiol*. 2016;89(1065):20150981. doi: 10.1259/bjr.20150981

10. Okamoto K, Okuyama K, Kohno N, Tsugawa T. Clinical outcomes of low-dose-rate brachytherapy based radiotherapy for intermediate risk prostate cancer. *J Contemp Brachytherapy*. 2020;12(1):6–11. doi: 10.5114/jcb.2020.92405

11. Cunha JA, Flynn R, Bélanger C, et al. Brachytherapy future directions. *Semin Radiat Oncol*. 2020;30(1):94–106. doi: 10.1016/j.semradonc.2019.09.001

12. Afshar-Oromieh A. PSMA-ligand imaging in the diagnosis of prostate cancer. In: Clinical Nuclear Medicine: Second Edition. Springer International Publishing; 2020. P. 755–763. doi: 10.1007/978-3-030-39457-8_25

13. Zippel C, Ronski SC, Bohnet-Joschko S, et al. Current status of PSMA-radiotracers for prostate cancer: Data analysis of prospective trials listed on clinicaltrials.gov. *Pharmaceuticals*. 2020;13(1):12. doi: 10.3390/ph13010012

14. Zyryanov AV, Oshchepkov VN, Sviridov PV, et al. Recommendations for the treatment of prostate cancer with low-dose permanent interstitial radiation therapy (brachytherapy). Expert meeting of the Association of Brachytherapists of Russia (OBR), October 4, 2014, Moscow. *Experimental Clin Urol*. 2015;(2):37–46. (In Russ).

15. Kasivisvanathan V, Rannikko AS, Borghi M, et al. MRI-targeted or standard biopsy for prostate-cancer diagnosis. *N Engl J Med*. 2018;378(19):1767–1777 doi: 10.1056/nejmoa1801993

16. Sazuka T, Imamoto T, Namekawa T, et al. Analysis of preoperative detection for apex prostate cancer by transrectal biopsy. *Prostate Cancer*. 2013;2013:705865. doi: 10.1155/2013/705865

17. Tewes S, Peters I, Tiemeyer A, et al. Evaluation of MRI/Ultrasound fusion-guided prostate biopsy using transrectal and transperineal approaches. *Biomed Res Int*. 2017;2017:2176471. doi: 10.1155/2017/2176471

18. Qiu DX, Li J, Zhang JW, et al. Dual-tracer PET/CT-targeted, mpMRI-targeted, systematic biopsy, and combined biopsy for the diagnosis of prostate cancer: A pilot study. *Eur J Nucl Med Mol Imaging*. 2022;49(8):2821–2832. doi: 10.1007/s00259-021-05636-1

19. Donato P, Morton A, Yaxley J, et al. 68Ga-PSMA PET/CT better characterizes localised prostate cancer after MRI and transperineal prostate biopsy: Is 68Ga-PSMA PET/CT guided biopsy the future? *Eur J Nucl Med Mol Imaging*. 2020;47(8):1843–1851. doi: 10.1007/s00259-019-04620-0

20. Zhang LL, Li WC, Xu Z, et al. 68Ga-PSMA PET/CT targeted biopsy for the diagnosis of clinically significant prostate cancer compared with transrectal ultrasound guided biopsy: A prospective randomized single-centre study. *Eur J Nucl Med Mol Imaging*. 2021;48(2):483–492. doi: 10.1007/s00259-020-04863-2

21. Duan H, Ghanouni P, Daniel B, et al. A pilot study of 68Ga-PSMA11 and 68Ga-RM2 PET/MRI for biopsy guidance in patients with suspected prostate cancer. *J Nuclear Med*. 2022;64(5):744–750. doi: 10.2967/jnumed.122.264448

22. Chin J, Rumble RB, Kollmeier M, et al. Brachytherapy for patients with prostate cancer: American Society of Clinical Oncology / Cancer Care Ontario joint guideline update. *J Clin Oncol*. 2017;35(15):1737–1745. doi: 10.1200/JCO.2016.72.0466

23. Basu S, Alavi A. SPECT-CT and PET-CT in oncology: An overview. *Curr Med Imaging Rev*. 2011;7(3):202–209. doi: 10.2174/157340511796411168

24. Soldatov A, von Klot CA, Walacides D, et al. Patterns of progression after 68Ga-PSMA-Ligand PET/CT-Guided radiation therapy for recurrent prostate cancer. *Int J Radiat Oncol Biol Phys*. 2019;103(1):95–104. doi: 10.1016/j.ijrobp.2018.08.066

25. Werner P, Neumann C, Eiber M, et al. [99cmTc]Tc-PSMA-I&S-SPECT/CT: experience in prostate cancer imaging in an outpatient center. *EJNMMI Res*. 2020;10(1):45. doi: 10.1186/s13550-020-00635-z

26. Berliner C, Steinhelfer L, Chantadisai M, et al. Delayed imaging improves lesion detectability in [99mTc]Tc-PSMA-I&S SPECT/CT in recurrentprostate cancer. *J Nucl Med*. 2023;64(7):1036–1042. doi: 10.2967/jnumed.122.265252

27. Rumyantsev PO. The increasing role of functional imaging methods for navigation of remote radiotherapy and brachytherapy on the example of prostate cancer. *Digital Diagnostics*. 2022;2(4):488–497. (In Russ). doi: 10.17816/DD96197

28. Patent RUS № RU 2788859 C2. Agibalov DYu, Degtyarev MV, Rumyantsev PO, et al. Method of targeted brachytherapy of prostate cancer under the navigation of hybrid PSMA-receptor scintigraphy. Available from: https://yandex.ru/patents/doc/RU2788859C2_20230125. Accessed: 15.08.2023.

СПИСОК ЛИТЕРАТУРЫ

1. Sung H., Ferlay J., Siegel R.L., et al. Global Cancer Statistics 2020: GLOBOCAN Estimates of Incidence and Mortality Worldwide for 36 Cancers in 185 Countries // CA Cancer J Clin. 2021. Vol. 71, N 3. P. 209–249. doi: 10.3322/caac.21660

2. Nyame Y.A., Gulati R., Tsodikov A., et al. Prostate-Specific antigen screening and recent increases in advanced prostate cancer // JNCI Cancer Spectr. 2021. Vol. 5, N 1. P. pkaa. 098 doi: 10.1093/jncics/pkaa098

3. Pommier P., Ferré M., Blanchard P., et al. Prostate cancer brachytherapy: SFRO guidelines 2021 // Cancer Radiotherap. 2022. Vol. 26, N 1-2. P. 344–355. doi: 10.1016/j.canrad.2021.11.019

4. Parker C., Castro E., Fizazi K., et al. Prostate cancer: ESMO Clinical Practice Guidelines for diagnosis, treatment and follow-up // Ann Oncol. 2020. Vol. 31, N 9. P. 1119–1134. doi: 10.1016/j.annonc.2020.06.011

5. Mottet N., van der Berg R., Briers E., et al. EAU-eanm-estro-esur-siog guidelines on prostate cancer-2020 update. Part 1: Screening, diagnosis, and local treatment with curative intent // Eur Urol. 2021. Vol. 79, N 2. P. 243–262. doi: 10.1016/j.eururo.2020.09.042

6. Носов Д.А., Волкова М.И., Гладков О.А., и др. Практические рекомендации по лечению рака предстательной железы // Злокачественные опухоли. Практические рекомендации RUSSCO. 2022. Т. 12, № #3s2. С. 607–626. doi: 10.18027/2224-5057-2022-12-3s2-607-626

7. Tsumura H., Tanaka N., Oguchi T., et al. Comparative effectiveness of low-dose-rate brachytherapy with or without external beam radiotherapy in favorable and unfavorable intermediate-risk prostate cancer // Sci Rep. 2022. Vol. 12, N 1. P. 11023. doi: 10.1038/s41598-022-15028-6

8. Tanaka N., Asakawa I., Hasegawa M., Fujimoto K. Low-dose-rate brachytherapy for prostate cancer: A 15-year experience in Japan // Int J Urol. 2020. Vol. 27, N 1. P. 17–23. doi: 10.1111/iju.14098

9. Fellin G., Mirri M.A., Santoro L., et al. Low dose rate brachytherapy (LDR-BT) as monotherapy for early stage prostate cancer in Italy: Practice and outcome analysis in a series of 2237 patients from 11 institutions // Br J Radiol. 2016. Vol. 89, N 1065. P. 20150981. doi: 10.1259/bjr.20150981

10. Okamoto K., Okuyama K., Kohno N., Tsugawa T. Clinical outcomes of low-dose-rate brachytherapy based radiotherapy for intermediate risk prostate cancer // J Contemp Brachytherapy. 2020. Vol. 12, N 1. P. 6–11. doi: 10.5114/jcb.2020.92405

11. Cunha J.A., Flynn R., Bélanger C., et al. Brachytherapy future directions // Semin Radiat Oncol. 2020. Vol. 30, N 1. P. 94–106. doi: 10.1016/j.semradonc.2019.09.001

12. Afshar-Oromieh A. PSMA-ligand imaging in the diagnosis of prostate cancer // Clinical Nuclear Medicine: Second Edition. Springer International Publishing, 2020. P. 755–763. doi: 10.1007/978-3-030-39457-8_25

13. Zippel C., Ronski S.C., Bohnet-Joschko S., et al. Current status of PSMA-radiotracers for prostate cancer: Data analysis of prospective trials listed on clinicaltrials.gov // Pharmaceuticals. 2020. Vol. 13, N 1. P. 12. doi: 10.3390/ph13010012

14. Зырянов А.В., Ощепков В.Н., Свиридов П.В., и др. Рекомендации по лечению рака предстательной железы с помощью низкодозной перманентной внутритканевой лучевой терапии (брахитерапии). Экспертное совещание Объединения брахитерапевтов России (ОБР), 4 октября 2014, Москва // Экспериментальная и клиническая урология. 2015. № 2. С. 37–46.

15. Kasivisvanathan V., Rannikko A.S., Borghi M., et al. MRI-Targeted or standard biopsy for prostate-cancer diagnosis // N Engl J Med. 2018. Vol. 378, N 19. P. 1767–1777. doi: 10.1056/nejmoa1801993

16. Sazuka T., Imamoto T., Namekawa T., et al. Analysis of preoperative detection for apex prostate cancer by transrectal biopsy // Prostate Cancer. 2013. Vol. 2013. P. 705865. doi: 10.1155/2013/705865

17. Tewes S., Peters I., Tiemeyer A., et al. Evaluation of MRI/Ultrasound fusion-guided prostate biopsy using transrectal and transperineal approaches // Biomed Res Int. 2017. Vol. 2017. P. 2176471. doi: 10.1155/2017/2176471

18. Qiu D.X., Li J., Zhang J.W., et al. Dual-tracer PET/CT-targeted, mpMRI-targeted, systematic biopsy, and combined biopsy for the diagnosis of prostate cancer: A pilot study // Eur J Nucl Med Mol Imaging. 2022. Vol. 49, N 8. P. 2821–2832. doi: 10.1007/s00259-021-05636-1

19. Donato P., Morton A., Yaxley J., et al. 68Ga-PSMA PET/CT better characterizes localised prostate cancer after MRI and transperineal prostate biopsy: Is 68Ga-PSMA PET/CT guided biopsy the future? // Eur J Nucl Med Mol Imaging. 2020. Vol. 47, N 8. P. 1843–1851. doi: 10.1007/s00259-019-04620-0

20. Zhang L.L., Li W.C., Xu Z., et al. 68Ga-PSMA PET/CT targeted biopsy for the diagnosis of clinically significant prostate cancer compared with transrectal ultrasound guided biopsy: A prospective randomized single-centre study // Eur J Nucl Med Mol Imaging. 2021. Vol. 48, N 2. P. 483–492 doi: 10.1007/s00259-020-04863-2

21. Duan H., Ghanouni P., Daniel B., et al. A pilot study of 68Ga-PSMA11 and 68Ga-RM2 PET/MRI for biopsy guidance in patients with suspected prostate cancer // J Med. 2022. Vol. 64, N 5. P. 744–750. doi: 10.2967/jnumed.122.264448

22. Chin J., Rumble R.B., Kollmeier M., et al. Brachytherapy for patients with prostate cancer: American Society of Clinical Oncology / Cancer Care Ontario joint guideline update // J Clin Oncol. 2017. Vol. 35, N 15. P. 1737–1745. doi: 10.1200/JCO.2016.72.0466

23. Basu S., Alavi A. SPECT-CT and PET-CT in oncology: An overview // Curr Med Imaging Rev. 2011. Vol. 7, N 3. P. 202–209. doi: 10.2174/157340511796411168

24. Soldatov A., von Klot C.A., Walacides D., et al. Patterns of progression after 68Ga-PSMA-ligand PET/CT-guided radiation therapy for recurrent prostate cancer // Int J Radiat Oncol Biol Phys. 2019. Vol. 103, N 1. P. 95–104. doi: 10.1016/j.ijrobp.2018.08.066

25. Werner P., Neumann C., Eiber M., et al. [99cmTc]Tc-PSMA-I&S-SPECT/CT: experience in prostate cancer imaging in an outpatient center // EJNMMI Res. 2020. Vol. 10, N 1. P. 45. doi: 10.1186/s13550-020-00635-z

26. Berliner C., Steinhelfer L., Chantadisai M., et al. Delayed imaging improves lesion detectability in [99mTc]Tc-PSMA-I&S SPECT/CT in recurrentprostate cancer // J Nucl Med. 2023. Vol. 64, N 7. P. 1036–1042. doi: 10.2967/jnumed.122.265252

27. Румянцев П.О. Возрастающая роль методов функциональной визуализации для навигации дистанционной радиотерапии и брахитерапии на примере рака предстательной железы // Digital Diagnostics. 2022. Т. 2, № 4. С. 488–497. doi: 10.17816/DD96197

28. Патент РФ на изобретение № RU 2788859 C2. Агибалов Д.Ю., Дегтярев М.В., Румянцев П.О., и др. Способ прицельной брахитерапии рака предстательной железы под навигацией гибридной ПСМА-рецепторной сцинтиграфии. Режим доступа: https://yandex.ru/patents/doc/RU2788859C2_20230125. Дата обращения: 15.08.2023.

AUTHORS' INFO

*** Pavel O. Rumiantsev,** MD, Dr. Sci. (Med.);
address: 8 Malaya Konyushennaya street, 191186 Saints Peterburg, Russia;
ORCID: 0000-0002-7721-634X;
eLibrary SPIN: 7085-7976;
e-mail: pavelrum@gmail.com

Pavel V. Sviridov;
ORCID: 0009-0008-3362-8255;
eLibrary SPIN: 4702-3067;
e-mail: p_sviridov73@mail.ru

Mikhail V. Degtyarev;
ORCID: 0000-0001-5652-2607;
eLibrary SPIN: 7725-7831 ;
e-mail: germed@mail.ru

Sergei S. Serzhenko;
ORCID: 0000-0003-2326-1396;
eLibrary SPIN: 4713-8986;
e-mail: vv1ld@yandex.ru

Dmitry B. Sanin, Cand. Sci. (Biol.);
ORCID: 0009-0004-2047-4921;
eLibrary SPIN: 8939-9101;
e-mail: dimitresko82@yandex.ru

Sergey V. Styrov;
ORCID: 0000-0003-4315-8855;
eLibrary SPIN: 9019-8520;
e-mail: rizost@yandex.ru

ОБ АВТОРАХ

*** Румянцев Павел Олегович,** д-р мед. наук;
адрес: Россия, 191186, Санкт-Петербург, ул. Малая Конюшенная, д. 8;
ORCID: 0000-0002-7721-634X;
eLibrary SPIN: 7085-7976;
e-mail: pavelrum@gmail.com

Свиридов Павел Владимирович;
ORCID: 0009-0008-3362-8255;
eLibrary SPIN: 4702-3067;
e-mail: p_sviridov73@mail.ru

Дегтярев Михаил Владимирович;
ORCID: 0000-0001-5652-2607;
eLibrary SPIN: 7725-7831;
e-mail: germed@mail.ru

Серженко Сергей Сергеевич;
ORCID: 0000-0003-2326-1396;
eLibrary SPIN: 4713-8986;
e-mail: vv1ld@yandex.ru

Санин Дмитрий Борисович, канд. биол. наук;
ORCID: 0009-0004-2047-4921;
eLibrary SPIN: 8939-9101;
e-mail: dimitresko82@yandex.ru

Стыров Сергей Викторович;
ORCID: 0000-0003-4315-8855;
eLibrary SPIN: 9019-8520;
e-mail: rizost@yandex.ru

* Corresponding author / Автор, ответственный за переписку

Dmitry Yu. Agibalov;
ORCID: 0000-0003-2995-7140;
eLibrary SPIN: 6938-5804;
e-mail: agibalovd@bk.ru

Sergey V. Korenev, MD, Dr. Sci. (Med.), Professor;
ORCID: 0000-0003-2310-0576;
eLibrary SPIN: 5257-4476;
e-mail: korenevsv@mail.ru

Агибалов Дмитрий Юрьевич;
ORCID: 0000-0003-2995-7140;
eLibrary SPIN: 6938-5804;
e-mail: agibalovd@bk.ru

Коренев Сергей Владимирович, д-р мед. наук, профессор;
ORCID: 0000-0003-2310-0576;
eLibrary SPIN: 5257-4476;
e-mail: korenevsv@mail.ru

DOI: https://doi.org/10.17816/DD321670

Опыт применения мобильного компьютерного томографа в резервном госпитале для лечения пациентов с новой коронавирусной инфекцией COVID-19

Н.Д. Кудрявцев[1], А.В. Петряйкин[1], Е.С. Ахмад[1], Ф.А. Киселев[1], В.В. Бурашов[1], А.Н. Мухортова[1], И.В. Солдатов[1], А.С. Шкода[2]

[1] Научно-практический клинический центр диагностики и телемедицинских технологий, Москва, Российская Федерация;
[2] Городская клиническая больница № 67 имени Л.А. Ворохобова, Москва, Российская Федерация

АННОТАЦИЯ

Пандемия новой коронавирусной инфекции COVID-19 бросила вызов системам здравоохранения практически всех стран мира. От организаторов здравоохранения требовалось принятие оперативных и эффективных решений для обеспечения высокого качества оказания медицинской помощи в новых условиях. Потребность в формировании резервного коечного фонда при пандемии была обусловлена высокой нагрузкой на городские больницы в Москве, в связи с чем в непрофильных сооружениях (ледовые арены, торговые центры, выставочные павильоны) были организованы временные резервные госпитали для лечения пациентов с COVID-19. Это потребовало поиска решений для обеспечения необходимого уровня диагностики и лечения, соответствующего профильному медицинскому учреждению. С учётом технических и временных ограничений, связанных с установкой стационарного компьютерного томографа, одним из решений была установка мобильного компьютерного томографа.

Целью работы было поделиться опытом использования мобильного компьютерного томографа в условиях временного резервного госпиталя для лечения пациентов с коронавирусной инфекцией COVID-19. В работе представлена информация о характеристиках мобильного компьютерного томографа; отмечены его преимущества и недостатки; представлен вариант планировки аппаратной, пультовой комнат и вариант размещения томографа; представлены результаты дозиметрических исследований; дана клиническая оценка применимости подобного типа диагностических устройств.

Ключевые слова: мобильный компьютерный томограф; пандемия коронавирусной инфекции; COVID-19; отделение лучевой диагностики.

Как цитировать:

Кудрявцев Н.Д., Петряйкин А.В., Ахмад Е.С., Киселев Ф.А., Бурашов В.В., Мухортова А.Н., Солдатов И.В., Шкода А.С. Опыт применения мобильного компьютерного томографа в резервном госпитале для лечения пациентов с новой коронавирусной инфекцией COVID-19 // *Digital Diagnostics.* 2023. Т. 4, № 3. С. 427–438. DOI: https://doi.org/10.17816/DD321670

Рукопись получена: 11.04.2023 **Рукопись одобрена:** 17.04.2023 **Опубликована:** 25.05.2023

DOI: https://doi.org/10.17816/DD321670

Using a mobile computer tomography scanner in a field hospital setting to manage patients with COVID-19

Nikita D. Kudryavtsev[1], Alexey V. Petraikin[1], Ekaterina S. Akhmad[1], Fyodor A. Kiselev[1], Vyacheslav V. Burashov[1], Anna N. Mukhortova[1], Ilya V. Soldatov[1], Andrey S. Shkoda[2]

[1] Moscow Center for Diagnostics and Telemedicine, Moscow, Russian Federation;
[2] City Clinical Hospital No. 67 named after L.A. Vorokhobov, Moscow, Russian Federation

ABSTRACT

The global outbreak of COVID-19 has posed unprecedented challenges to healthcare systems worldwide. Healthcare administrators had to make quick and effective decisions to ensure high quality of medical care standards in new conditions. The need to form a reserve bed fund during the pandemic was due to the high load on city hospitals in Moscow. Due to this fact, temporary reserved hospitals for COVID-19 patients were organized in non-core facilities, such as ice arenas, shopping malls, and exhibition pavilions. This urgency prompted a search for solutions that could provide the necessary level of diagnosis and treatment appropriate to specialized medical facility. Given the technical and time constraints associated with the installation of a fixed computer tomographic scanner, the deployment of mobile computer tomographic scanners emerged as a viable option. The study aims to share insights gained from using a mobile computer tomographic scanner within a temporary backup hospital setting to treating patients with COVID-19 coronavirus infection. The paper discusses the features, advantages, and disadvantages of mobile computer tomography. It also presents hardware and control room layouts, along with the placement options for the computer tomography device. The research includes the results of dosimetry studies and provides a clinical assessment of the applicability of this type of diagnostic devices.

Keywords: computer tomographic scanner; COVID-19 pandemics; radiology departments.

To cite this article:
Kudryavtsev ND, Petraikin AV, Akhmad ES, Kiselev FA, Burashov VV, Mukhortova AN, Soldatov IV, Shkoda AS. Using a mobile computer tomography scanner in a field hospital setting to manage patients with COVID-19. *Digital Diagnostics.* 2023;4(3):427–438. DOI: https://doi.org/10.17816/DD321670

Received: 11.04.2023 **Accepted:** 17.04.2023 **Published:** 25.05.2023

DOI: https://doi.org/10.17816/DD321670

在备用医院使用移动式电脑断层扫描仪治疗新型冠状病毒感染（COVID-19）患者的经验

Nikita D. Kudryavtsev[1], Alexey V. Petraikin[1], Ekaterina S. Akhmad[1], Fyodor A. Kiselev[1], Vyacheslav V. Burashov[1], Anna N. Mukhortova[1], Ilya V. Soldatov[1], Andrey S. Shkoda[2]

[1] Moscow Center for Diagnostics and Telemedicine, Moscow, Russian Federation
[2] City Clinical Hospital No. 67 named after L.A. Vorokhobov, Moscow, Russian Federation

简评

新型冠状病毒感染（COVID-19）的大流行给世界上几乎所有国家的卫生系统带来了挑战。医疗保健组织者需要做出迅速有效的决定，以确保在新的条件下提供高质量的医疗保健服务。在大流行期间，由于莫斯科的城市医院负担格外沉重，因此需要建立一个备用床基金，并在非核心建筑物（冰上运动场、购物中心、展览馆）中建立临时备用医院，以治疗COVID-19患者。这就需要寻找解决方案，以在专业医疗机构中提供必要水平的诊断和治疗。考虑到安装固定式电脑断层扫描仪的技术和时间限制，解决方案之一是安装移动式电脑断层扫描仪。

本文旨在分享在临时备用医院使用移动式电脑断层扫描仪治疗冠状病毒感染COVID-19病人的经验。该文章介绍移动式电脑断层扫描仪的特性；指出其优缺点；介绍设备室、控制室的布局变式和电脑断层扫描仪的摆放变式；介绍剂量测定研究的结果；对此类诊断设备的适用性进行了临床评估。

关键词：移动式电脑断层扫描仪；冠状病毒大流行；COVID-19；放射诊断科。

引用本文：
Kudryavtsev ND, Petraikin AV, Akhmad ES, Kiselev FA, Burashov VV, Mukhortova AN, Soldatov IV, Shkoda AS. 在备用医院使用移动式电脑断层扫描仪治疗新型冠状病毒感染（COVID-19）患者的经验. *Digital Diagnostics*. 2023;4(3):427–438. DOI: https://doi.org/10.17816/DD321670

收到：11.04.2023 **接受：**17.04.2023 **发布日期：**25.05.2023

INTRODUCTION

During the COVID-19 pandemic, in Moscow, a reserve bed capacity was required due to the high load on city hospitals. Field COVID-19 hospitals were deployed in noncore buildings (ice arenas, shopping centers, and exhibition halls), and special solutions were required to provide the necessary level of diagnosis and treatment comparable with a specialist healthcare institution [1]. One field hospital was located at the Krylatskoye Ice Palace (State Budgetary Healthcare Institution "L.A. Vorokhobov City Clinical Hospital No. 67," Department of Healthcare of Moscow Fig. 1).

Diagnostic radiology techniques (particularly computed tomography [CT]) are recommended for detecting signs of COVID-19 pneumonia and to establishing a differential diagnosis for other lung diseases and assessing disease severity, changes in a patient's condition, and treatment effectiveness [2–4]. A mobile Airo TruCT tomograph (Stryker, USA) was deployed due to technical and time constraints of employing a stationary computed tomograph.

The purpose of this study was to assess the efficacy of mobile CT in a field hospital for COVID-19 patients.

A MOBILE COMPUTED TOMOGRAPHER: EFFECTIVENESS IN SETTING OF A FIELD HOSPITAL FOR COVID-19 PATIENTS

General characteristics of a mobile CT

The Airo TruCT is designed for use in neurosurgery operating rooms, but the manufacturer claims that it can also be used to diagnose urgent conditions in other anatomical areas.[1] Airo TruCT has a compact size (Fig. 2), making it simple to install and transport. A moveable base, a gantry with a 107-cm aperture, and 32 rows of 1-mm detectors comprise this CT system. CT is controlled by a hard-wired console connected by a 5-m wire (Fig. 3). The mobile CT is adaptable to a variety of power supply conditions and is linked to a 1.5-kW network. A power supply system, on the other hand, permits scanning at 120 kV and 250 mA, which corresponds to a power of 30 kW.

Location and dosimetry

In accordance with current rules and measurement methods, a CT room was certified for compliance with technical requirements during technical equipment testing (monitoring of operating parameters) and radiation monitoring at the workplace and adjacent rooms.

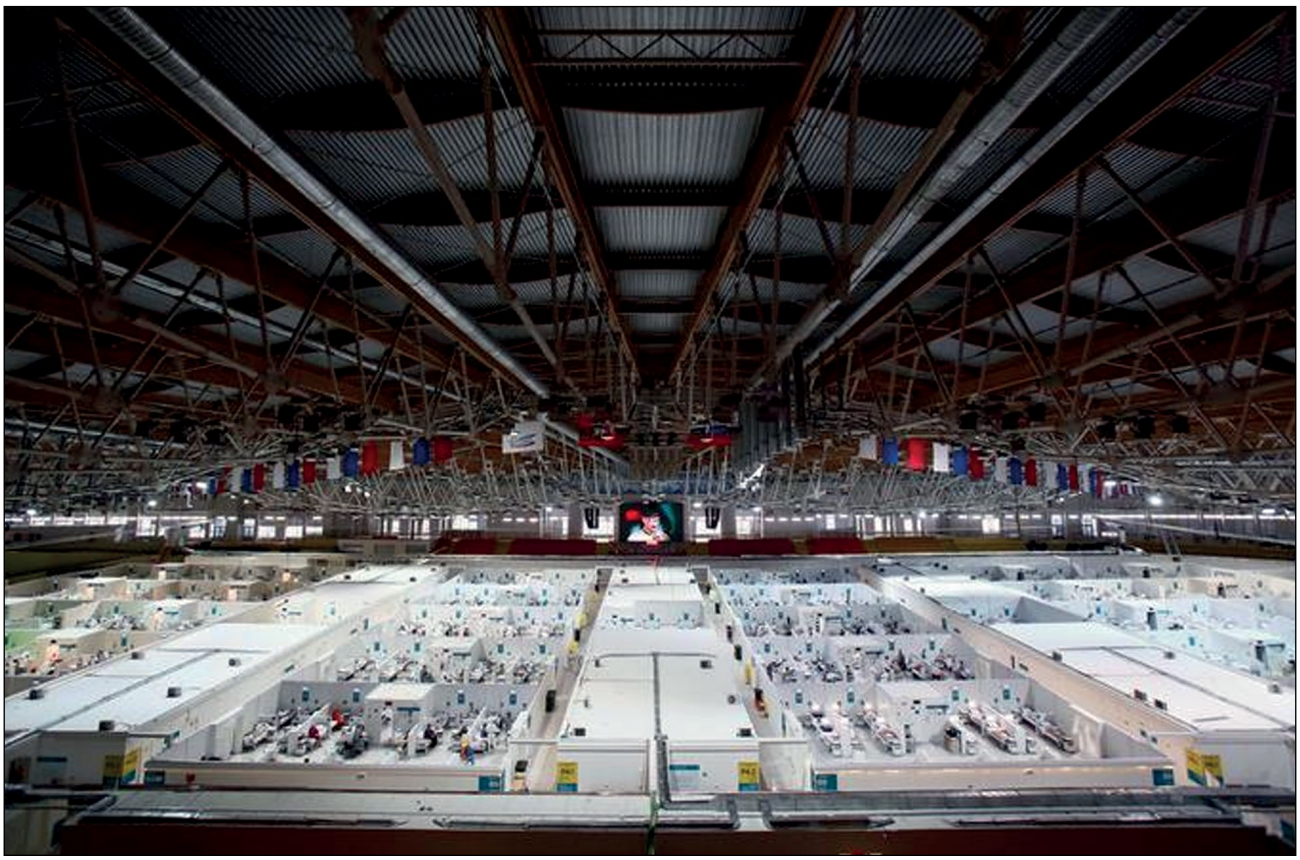

Fig. 1. A field hospital for COVID-19 patients in Krylatskoye Ice Palace (Moscow, Russia). Reuters (https://pictures.reuters.com/).

[1] Stryker.com [Internet]. Neurosurgery (https://www.stryker.com/us/en/spine/products/airo-truct/imaging/clinical/neurosurgery.html); Airo Truct Mobile Imaging System (https://www.stryker.com/us/en/spine/products/airo-truct/imaging.html).

DOI: https://doi.org/10.17816/DD321670

Fig. 2. A mobile computed tomograph ready for scanning.

Fig. 3. Airo TruCT control console.

The CT room is located on the first floor of Krylatskoye Ice Palace, in the Emergency Department (Fig. 4). Due to the increased patient flow and off label use of this device, some technical solutions were required:

1. The CT console was relocated to the control room to ensure technicians' radiation safety.
2. A video system was constructed to monitor the patient's status and the progress of the scanning because there was no viewing in the control room.
3. Baofeng portable radios were used for communicating with patients during scanning due to the lack of built-in voice commands for holding breath.

Radiation protection in adjacent rooms complied with Russian requirements for design and operation of X-ray rooms, considering operating parameters of Airo TruCT (during scanning, the gantry moves, whereas the patient table is fixed). Sheets of X-ray protective plasterboard from Knauf (Iphofen, Germany) were used to safeguard stationary building envelops.

Dosimetry monitoring at workplaces, in adjacent rooms, and in adjacent regions revealed that exposure levels did not exceed values defined in current regulatory regulations at the observed spots (see Fig. 4).

Technical quality control

In accordance with current norms, a standard assessment of the CT system's operational parameters was performed[2]. Sum filtering, half-value layer, anode voltage ripple, anode

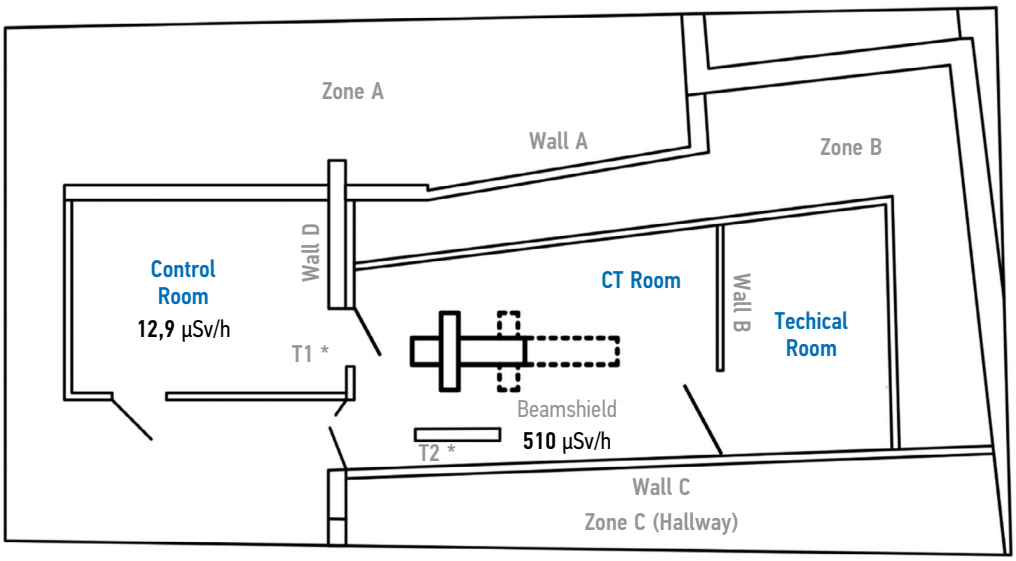

Fig. 4. The project of a computed tomography room, control room, and radiologist's office: Zone A—pavilion; Zone B—technical area; Zone C—hallway (zones A to C are areas without permanent presence of personnel).

[2] Electronic base of legal and regulatory technical documents of Codex JSC [Internet]. GOST R IEC 61223-2-6-2001 Evaluation and routine testing in medical imaging departments. Parts 2-6. Constancy tests. X-ray equipment for computed tomography(https://docs.cntd.ru/document/1200029048); GOST R 51746-2001 Evaluation and routine testing in medical imaging departments. Part 1. General requirements. (https://docs.cntd.ru/document/1200012982); GOST R IEC 61223-3-5-2008 Evaluation and routine testing in medical imaging departments. Parts 3-5. Acceptance tests. Imaging performance of computed tomography X-ray equipment. (https://docs.cntd.ru/document/1200071695); GOST R IEC 60601-2-44-2013 Medical electrical equipment. Parts 2-44. Special requirements for the basic safety and essential performance of X-ray equipment for computed tomography (https://docs.cntd.ru/document/1200105919).

Table 1. Standardized scanning protocols for different anatomical regions

Anatomic region parameter	Chest	Brain	Abdomen
Scanning direction	Craniocaudal	Craniocaudal	Craniocaudal
Scan type	Spiral	Spiral	Spiral
Electric voltage (kV)	120	120	120
Electric current (mA)	38	155	69
Slice thickness (mm)	1.0	1.0	1.0
Pitch factor	1.415	1.415	1.415
X-ray tube rotation time (s)	1.92	1.92	1.92
Reconstruction matrix (px)	512 × 512	512 × 512	512 × 512
Duration of scan (s)	12	8	16
Absorbed radiation dose (mGy*cm)	230.7	1,186.8	564
Scan length (cm)	30	20	40

voltage, exposure time, radiation dose linearity, radiation dose repeatability, and image quality characteristics were evaluated.

According to the test results, the CT system meets performance and standard requirements.

Clinical use

A field hospital accepted patients with mild and moderate COVID-19 [2] with CT-1 and CT-2 lung parenchyma damage, requiring hospital treatment and observation. The chest CT was performed on all hospitalized patients. The only exception was for patients who had a recent CT (4 days). CT data revealed that 155 (31.0%) of 500 randomly selected patients had CT-1, 202 (40.4%) had CT-2, 109 (21.8%) had CT-3, and 34 (6.8%) had CT-4. Due to the high-power consumption and possibility of X-ray tube overheating during multiphase scanning, contrast-enhanced CT was not performed. The relative duration of scanning was a limitation of that technique.

Computed tomography scans of the brain and head, abdomen and retroperitoneum, pelvic organs, spine, and extremities were conducted when clinically required (scanning parameters are listed in Table 1).

The system's wide (107 cm) gantry aperture was an apparent advantage.

Chest CT was conducted in the majority of cases to obtain a diagnosis or to provide continuing observation for patients with COVID-19 pneumonia. The scanning parameters (Table 1) enable us to obtain images of adequate quality to differentiate between viral pneumonia, cardiogenic pulmonary edema, and bacterial pneumonia. Fig. 5 shows CT data for COVID-19-associated viral pneumonia patients.

Long-term (15–25 s) scanning was too long for patients with respiratory insufficiency to remain their breath for the entire examination compared with stationary CT (3–5 s). As a result, motion artifacts (Fig. 6*a*) and steps (Fig. 6b) were

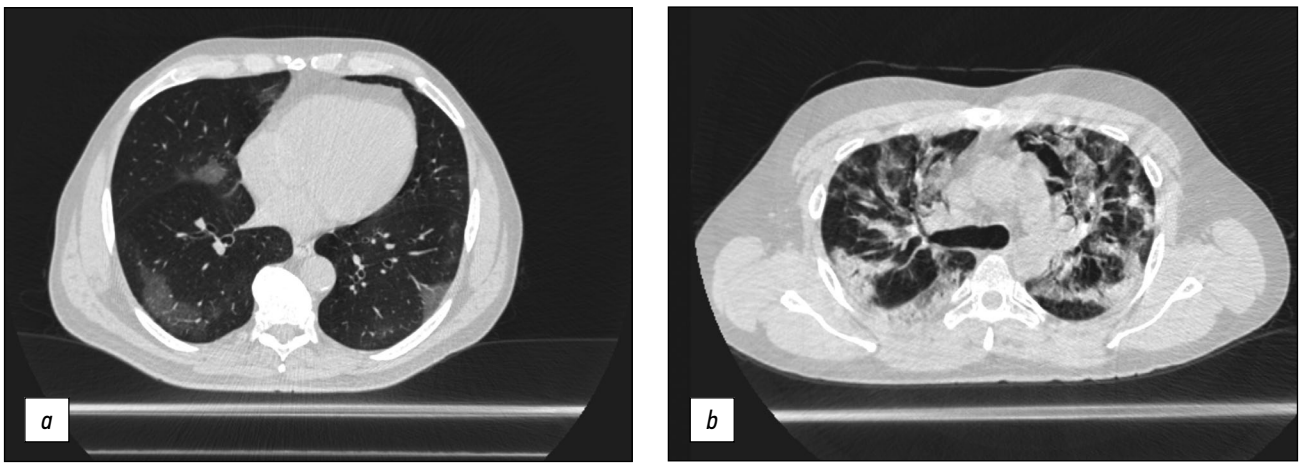

Fig. 5. Axial computed tomographic slices of chest organs in the lung window: (*a*) polymorphic, predominantly subpleural areas of ground-glass opacity, corresponding to the CT image of viral pneumonia (including COVID-19), CT-1, and (*b*) multiple polymorphic areas of parenchyma compaction with a tendency to merge, with ground-glass opacity areas and mild reticular changes, CT-3.

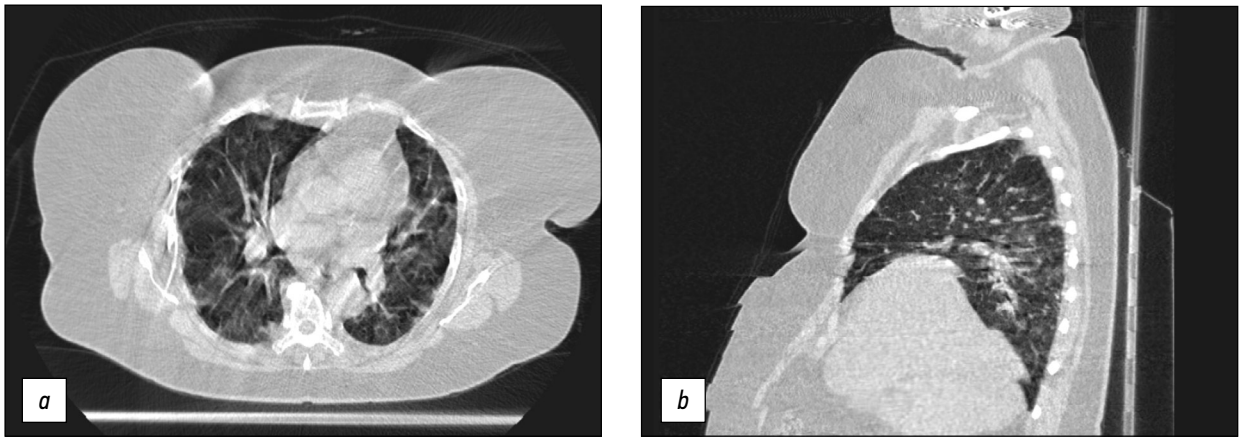

Fig. 6. Axial and sagittal computed tomographic slices of chest organs in the lung window: (*a*) motion artifacts and (*b*) step artifacts caused by respiratory chest movements during scanning.

present in CT images produced by breathing motions of the chest (Fig. 6).

Brain CT was used to diagnose acute cerebrovascular accident, intracranial hematomas, brain tumors, and traumatic skull injuries (Fig. 7).

Windmill artifacts (Fig. 8a) were mixed with strike artifacts and helical scanning [5], and artifacts intensified at the level of skull base, where significant beam hardening and scattering artifacts occurred (Fig. 8, *b*). Therefore, subtentorial brain areas were challenging to assess.

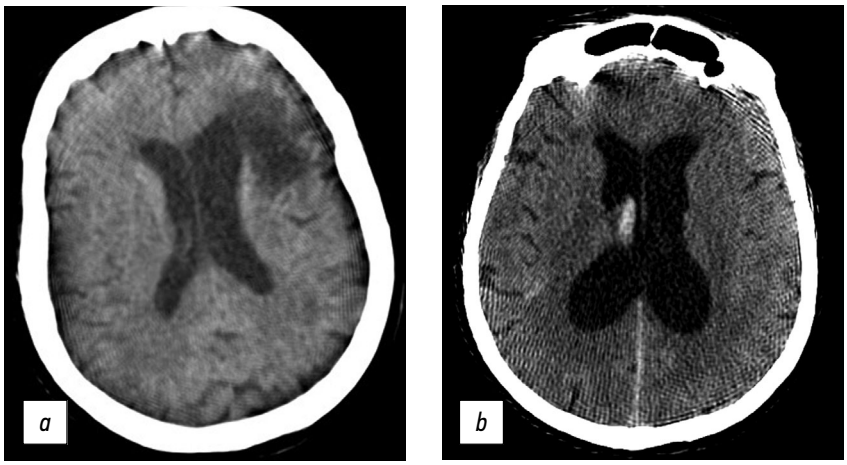

Fig. 7. Axial computed tomographic images of the brain: (*a*) reconstruction of a 3-mm low-density area at the anterior horn of the left lateral ventricle, in the periventricular, subcortical direction (CT image of subacute cerebrovascular accident of the left middle cerebral artery), and (*b*) a 1-mm site of subarachnoid hemorrhage with blood breakthrough into the ventricular system (vicarious hydrocephalus).

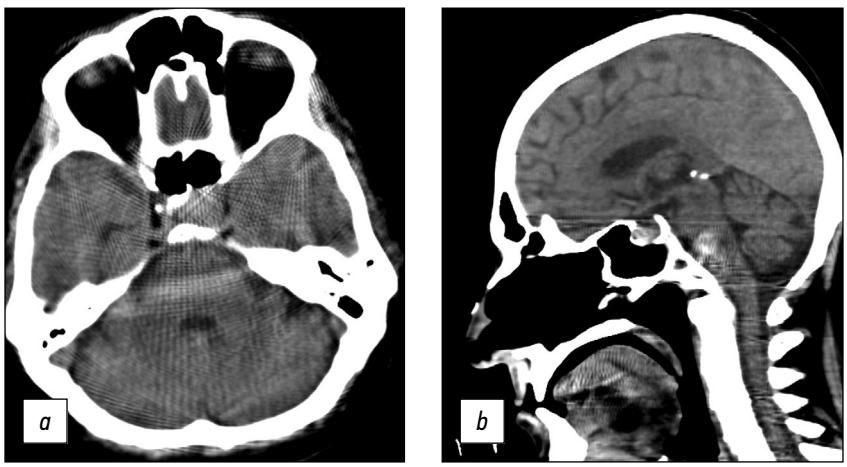

Fig. 8. Axial (*a*) and sagittal (*b*) computed tomographic images of the head in the region of the posterior cranial fossa and base of skull showed windmill, strike, beam hardening, and scattering artifacts. Area of bone structures and the posterior fossa is hard to evaluate.

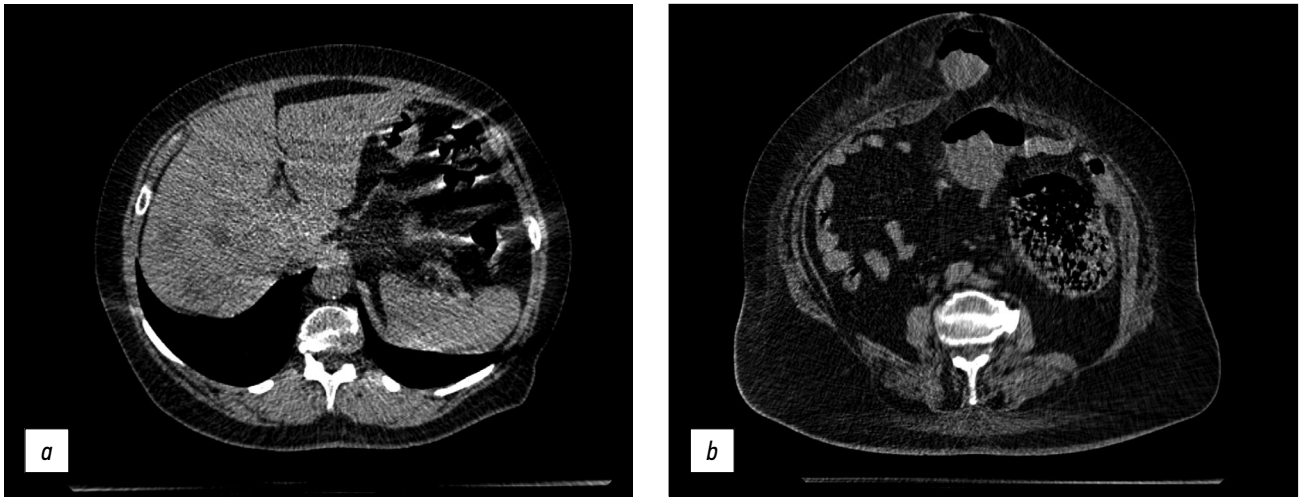

Fig. 9. Axial computed tomographic images of the abdomen: (*a*) CT image of multiple hypodense lesions of both liver lobes, helical artifacts, and gas interface artifacts in the intestinal area and (*b*) CT image of a strangulated umbilical hernia.

Abdomen CT was used to assess acute abdominal problems, such as suspected intestinal blockage, and detect free liquid or gas (Fig. 9).

Artifacts were also identified during abdomen CT at the point of contact of various density media, such as intestine gas and surrounding soft tissue (gas-interface artifact) and helical scanning artifacts.

The scanning parameters (Table 1) enable the acquisition of images of sufficient quality for the diagnosis of abdominal and retroperitoneal disorders (liver steatosis, gallstone disease, adrenal hyperplasia and incidentaloma, kidney cysts and urolithiasis, focal liver lesions, and other conditions).

Evaluation of a mobile CT effectiveness

From the start of the field hospital operation (August 11, 2020) to January 31, 2021, 6,264 CT scans were performed, including 6,126 (97.80%) chest CTs, 98 (1.56%) brain CTs, 31 (0.49%) abdomen CTs, and nine (0.14%) other CTs. The average radiation exposure was 3.22 mSv for chest CT, 2.49 mSv for brain CT, and 8.46 mSv for abdomen CT.

To assess CT effectiveness, a load equal to the ratio of the average number of CT scans per day to the Moscow standard (41 scans per day for three-shift work) was determined. The average number of scans performed in such case was 44 a day (ranging 14 scans at the start of the temporary hospital operation to >110 scans per day in days with the highest inpatient flow). This amounted to 106% of the recommended load. When Airo TruCT was compared with stationary Aquilion Prime or Revolution EVO tomographs, the utilization levels were equivalent. The average level of utilization for stationary CT in two hospitals was 113%, according to data. As previously stated, no contrast-enhanced CT scans were conducted.

Such a load validated excellent efficacy of using a mobile CT in temporary hospitals. However, technical difficulties were recorded during periods of extensive mobile CT use, which could result in the tomograph being shut down for maintenance. The manufacturer suggests conducting six scans per hour to extend the operational time of a mobile CT and avoid technical concerns.

DISCUSSION

The COVID-19 pandemic has raised various challenges regarding inpatient care organization, such as how to enhance bed capacity, organize field hospitals, and provide logistics for such solutions [6].

One method for ensuring CT availability in field hospitals is to use tiny transportable computed tomographs. This paper summarizes experience of using an Airo TruCT mobile CT. Apparent advantages of this CT system include compatibility with various power supply parameters, ease of installation and transportation, and the ability to quickly design a room for a mobile CT scan and put this equipment into operation.

A mobile CT generated acceptable quality chest CT images detecting viral pneumonia (see Fig. 5 *a*), and the patient capacity was sufficient for a temporary hospital with 1,300 beds in overload circumstances. The peak load was 110 scans per day, with an average of 44. This system differs from modular and mobile CTs mounted on trailers [7], mostly due to the use different types of CT.

However, some limitations were observed, indicating that the present modification's usage of a mobile CT was a forced solution. Some motion artifacts developed as a result of low scanning speed compared with stationary CT scanners. The caudal–cranial direction was proposed for chest CT scanning to limit the amount of respiratory artifacts [8]. Due to the configuration of the CT room (gantry movement was limited due to insufficient console wire length) in our situation of using Airo TruCT, such a solution proved unacceptable. The problem was fixed by postponing the command to hold the breath for 3–4 s after the scan began. Although the apical lung segment exhibited significant motion abnormalities and steps, the basal portions were clearly visible. This observation

is significant because patches of ground-glass opacity or consolidation are precisely situated in the dorsal sections of the lower lobes in COVID-19 pneumonia [9]. Simple technical solutions, such as handheld transceivers and video communication, were also used to adopt off-label use of Airo TruCT. Due to the significant number of artifacts detected, additional scanning, reconstruction, and postprocessing algorithms should be developed, and scanning parameters should be optimized [10].

Despite the mobility and easy installation of mobile CTs, design of an equipment room should comply with all radiation safety requirements (see Fig. 2).

In addition to field COVID-19 hospitals, mobile CTs can be used efficiently in healthcare institutions where there are no conditions for fixed CT installation or when the main CT scanner has failed. Mobile CT scanners can be used in remote communities and temporary mobile hospitals for emergency recovery.

The use of mobile CT also opens up new avenues for scientific research; for example, in our case, the mobile CT was used to investigate the influence of COVID-19 on the cardiovascular system [11]. When preforming chest, brain, abdomen, and retroperitoneum CT at temporary hospital for COVID-19 patients, the use of Airo TruCT provide requisite diagnostic effectiveness.

Based on the identified disadvantages, a list of requirements for mobile CT systems was prepared, and the need to develop a new type of CT was demonstrated, including high compatibility with various power supply sources, the ability to quickly design rooms for CT deployment in temporary hospitals, and the ability of use in emergency situations and remote areas with unprepared infrastructure.

CONCLUSION

The installation of mobile CT in a field COVID-19 hospital was a forced solution due to the rapid development of the pandemic. The Airo TruCT is intended for use in neurosurgical operating rooms. Despite the off-label use, the mobile CT produced images of satisfactory quality. A fixed CT situated on a trailer or a separate module is an alternative to mobile CT, although this type of equipment has its disadvantages (e.g., difficult transport and placement outside the healthcare institution and problems with scanning in severe patients). In turn, the Airo TruCT has excellent mobility and reduced space and power requirements, allowing it to be transported by a single person. However, the high mobility of this tomograph affects the quality of images.

ADDITIONAL INFORMATION

Funding source. This article was prepared by a group of authors as a part of the research and development effort titled "Theoretical and methodological framework for digital transformation in radiology", (USIS No. 123031400118-0) in accordance with the Order No. 1196 dated December 21, 2022 "On approval of state assignments funded by means of allocations from the budget of the city of Moscow to the state budgetary (autonomous) institutions subordinate to the Moscow Health Care Department, for 2023 and the planned period of 2024 and 2025" issued by the Moscow Health Care Department.

Competing interests. The authors declare that they have no competing interests.

Authors' contribution. All authors made a substantial contribution to the conception of the work, acquisition, analysis, interpretation of data for the work, drafting and revising the work, final approval of the version to be published and agree to be accountable for all aspects of the work. N.D. Kudryavtsev — the concept of publication, text writing, clinical analysis of mobile CT; A.V. Petraikin — clinical analysis of mobile CT; E.S. Akhmad — technical quality control of mobile CT, text writing; F.A. Kiselev, V.V. Burashov — technical quality control of mobile CT; A.N. Mukhortova — evaluation of the effectiveness of the use of mobile CT; I.V. Soldatov — design of the radiology department, text editing; A.S. Shkoda — organization of the work in the radiology department, text editing.

REFERENCES

1. Morozov SP, Kuzmina ES, Ledikhova NV, et al. Mobilizing the academic and practical potential of diagnostic radiology during the COVID-19 pandemic in Moscow. *Digital Diagnostics*. 2020;1(1):5–12. (In Russ). doi: 10.17816/DD51043

2. Prevention, diagnosis and treatment of new coronavirus infection (2019-nCoV): temporary guidelines. Version 17 (12/14/2022). (In Russ). Available from: https://static-0.minzdrav.gov.ru/system/attachments/attaches/000/061/254/original/%D0%92%D0%9C%D0%A0_COVID-19_V17.pdf?1671088207. Accessed: 15.03.2023. (

3. De Smet K, De Smet D, Ryckaert T, et al. Diagnostic performance of chest CT for SARS-CoV-2 infection in individuals with or without COVID-19 symptoms. *Radiology*. 2021;298(1):E30–E37. doi: 10.1148/radiol.2020202708

4. Huang Y, Cheng W, Zhao N, et al. CT screening for early diagnosis of SARS-CoV-2 infection. *Lancet Inf Dis*. 2020;20(9):1010–1011. doi: 10.1016/S1473-3099(20)30241-3

5. Barrett JF, Keat N. Artifacts in CT: Recognition and avoidance. *RadioGraphics*. 2004;24(6):1679–1691. doi: 10.1148/rg.246045065

6. Samorodskaja IV, Larina VN, Nazimkin KE, Larin VG. Organizational and clinical problems of outpatient COVID-19 diagnostics. *Vrach*. 2020;31(5):23–30. (In Russ). doi: 10.29296/25877305-2020-05-05

7. Cester G, Giraudo C, Causin F, et al. Retrospective analysis of a modified organizational model to guarantee CT workflow during the COVID-19 outbreak in the Tertiary Hospital of Padova, Italy. *J Clin Med*. 2020;9(9):3042. doi: 10.3390/jcm9093042

8. Bates DD, Vintonyak A, Mohabir R, et al. Use of a portable computed tomography scanner for chest imaging of COVID-19 patients in the urgent care at a tertiary cancer center. *Emerg Radiol*. 2020;27(6):597–600. doi: 10.1007/s10140-020-01801-5

9. Khristenko EA, von Stackelberg O, Kautsor HU, et al. CT patterns in COVID-19 associated pneumonia: Standardization of research descriptions based on the Fleischner Society Glossary. *Rejr*. 2020;10(1):16–26. (In Russ). doi: 10.21569/2222-7415-2020-10-1-16-26

10. Kyriakou Y, Meyer E, Prell D, Kachelriess M. Empirical beam hardening correction (EBHC) for CT. *Med Phys*. 2010;37(10):5179–5187. doi: 10.1118/1.3477088

11. Aliev AF, Kudryavtsev ND, Petryaykin AV, et al. Changing of pulmonary artery diameter in accordance with severity of COVID-19 (assessment based on non-contrast computer tomography). *Digital Diagnostics*. 2021;2(3):249–260. (In Russ). doi: 10.17816/DD76726

СПИСОК ЛИТЕРАТУРЫ

1. Morozov S.P., Kuzmina E.S., Ledikhova N.V., et al. Mobilizing the academic and practical potential of diagnostic radiology during the COVID-19 pandemic in Moscow // Digital Diagnostics. 2020. Vol. 1, N 1. P. 5–12. doi: 10.17816/DD51043

2. Профилактика, диагностика и лечение новой коронавирусной инфекции (2019-nCoV): временные методические рекомендации. Версия 17 (14.12.2022). Режим доступа: https://static-0.minzdrav.gov.ru/system/attachments/attaches/000/061/254/original/%D0%92%D0%9C%D0%A0_COVID-19_V17.pdf?1671088207. Дата обращения: 15.03.2023.

3. De Smet K., De Smet D., Ryckaert T., et al. Diagnostic performance of chest CT for SARS-CoV-2 infection in individuals with or without COVID-19 symptoms // Radiology. 2021. Vol. 298, N 1. P. E30–E37. doi: 10.1148/radiol.2020202708

4. Huang Y., Cheng W., Zhao N., et al. CT screening for early diagnosis of SARS-CoV-2 infection // Lancet Infect Dis. 2020. Vol. 20, N 9. P. 1010–1011. doi: 10.1016/S1473-3099(20)30241-3

5. Barrett J.F., Keat N. Artifacts in CT: Recognition and avoidance // RadioGraphics. 2004. Vol. 24, N 6. P. 1679–1691. doi: 10.1148/rg.246045065

6. Самородская И.В., Ларина В.Н., Назимкин К.Е., Ларин В.Г. Организационные и клинические проблемы диагностики COVID-19 на амбулаторном этапе // Врач. 2020. Т. 31, № 5. С. 23–30. doi: 10.29296/25877305-2020-05-05

7. Cester G., Giraudo C., Causin F., et al. Retrospective analysis of a modified organizational model to guarantee CT workflow during the COVID-19 outbreak in the Tertiary Hospital of Padova, Italy // J Clin Med. 2020. Vol. 9, N 9. P. 3042. doi: 10.3390/jcm9093042

8. Bates D.D., Vintonyak A., Mohabir R., et al. Use of a portable computed tomography scanner for chest imaging of COVID-19 patients in the urgent care at a tertiary cancer center // Emerg Radiol. 2020. Vol. 27, N 6. P. 597–600. doi: 10.1007/s10140-020-01801-5

9. Христенко Е.А., фон Стакельберг О., Кауцор Х.У., et al. КТ-паттерны при COVID-19-ассоциированных пневмониях: стандартизация описания исследований на основе глоссария общества Флейшнера // Rejr. 2020. Т. 10, № 1. С. 16–26. doi: 10.21569/2222-7415-2020-10-1-16-26

10. Kyriakou Y., Meyer E., Prell D., Kachelriess M. Empirical beam hardening correction (EBHC) for CT // Med Phys. 2010. Vol. 37, N 10. P. 5179–5187. doi: 10.1118/1.3477088

11. Aliev A.F., Kudryavtsev N.D., Petryaykin A.V., et al. Changing of pulmonary artery diameter in accordance with severity of COVID-19 (assessment based on non-contrast computer tomography) // Digital Diagnostics. 2021. Vol. 2, N 3. P. 249–260. doi: 10.17816/DD76726

AUTHORS' INFO

*** Nikita D. Kudryavtsev;**
address: 24/1 Petrovka street, 127051 Moscow, Russia;
ORCID: 0000-0003-4203-0630;
eLibrary SPIN: 1125-8637;
e-mail: KudryavtsevND@zdrav.mos.ru

Alexey V. Petraikin, MD, Dr. Sci. (Med.), Associate Professor;
ORCID: 0000-0003-1694-4682;
eLibrary SPIN: 6193-1656;
e-mail: PetryajkinAV@zdrav.mos.ru

Ekaterina S. Akhmad;
ORCID: 0000-0002-8235-9361;
eLibrary SPIN: 5891-4384;
e-mail AkhmadES@zdrav.mos.ru

Fyodor A. Kiselev;
ORCID: 0009-0006-6472-8940;
e-mail: KiselevFA@zdrav.mos.ru

ОБ АВТОРАХ

*** Кудрявцев Никита Дмитриевич;**
адрес: Россия, 127051, Москва, ул. Петровка, д. 24, стр. 1;
ORCID: 0000-0003-4203-0630;
eLibrary SPIN: 1125-8637;
e-mail: KudryavtsevND@zdrav.mos.ru

Петряйкин Алексей Владимирович, д-р мед. наук, доцент;
ORCID: 0000-0003-1694-4682;
eLibrary SPIN: 6193-1656;
e-mail: PetryajkinAV@zdrav.mos.ru

Ахмад Екатерина Сергеевна;
ORCID: 0000-0002-8235-9361;
eLibrary SPIN: 5891-4384;
e-mail AkhmadES@zdrav.mos.ru

Киселев Федор Алексеевич;
ORCID: 0009-0006-6472-8940;
e-mail: KiselevFA@zdrav.mos.ru

* Автор, ответственный за переписку / Corresponding author

Vyacheslav V. Burashov;
ORCID: 0000-0001-9250-0667;
eLibrary SPIN: 4308-0912;
e-mail: BurashovVV@zdrav.mos.ru

Anna N. Mukhortova;
ORCID: 0000-0001-9814-3533;
eLibrary SPIN: 9051-1130;
e-mail: MukhortovaAN@zdrav.mos.ru

Ilya V. Soldatov;
ORCID: 0000-0002-4867-0746;
eLibrary SPIN: 4065-6048;
e-mail: SoldatovIV2@zdrav.mos.ru

Andrey S. Shkoda, MD, Dr. Sci. (Med), Professor;
ORCID: 0000-0002-9783-1796;
eLibrary SPIN: 4520-2141;
e-mail: gkb67@zdrav.mos.ru

Бурашов Вячеслав Владимирович;
ORCID: 0000-0001-9250-0667;
eLibrary SPIN: 4308-0912;
e-mail: BurashovVV@zdrav.mos.ru

Мухортова Анна Николаевна;
ORCID: 0000-0001-9814-3533;
eLibrary SPIN: 9051-1130;
e-mail: MukhortovaAN@zdrav.mos.ru

Солдатов Илья Владимирович;
ORCID: 0000-0002-4867-0746;
eLibrary SPIN: 4065-6048;
e-mail: SoldatovIV2@zdrav.mos.ru

Шкода Андрей Сергеевич, д-р мед. наук, профессор;
ORCID: 0000-0002-9783-1796;
eLibrary SPIN: 4520-2141;
e-mail: gkb67@zdrav.mos.ru

DOI: https://doi.org/10.17816/DD514629

Система менеджмента качества: инструмент развития организации или дополнительная нагрузка?

С.Ю. Заюнчковский, С.А. Коновалов, В.В. Зинченко, Д.Е. Шарова, Е.С. Ахмад, А.В. Владзимирский

Научно-практический клинический центр диагностики и телемедицинских технологий, Москва, Российская Федерация

АННОТАЦИЯ

Система менеджмента качества представляет собой основную систему управления организацией, которая направлена на обеспечение главного свойства выпускаемой продукции — качества. Основу поддержки качества на производстве выполняет система менеджмента качества с главной целью — быть готовыми к удовлетворению меняющейся потребительской ценности, а также всегда учитывать удовлетворённость самих потребителей. Говоря о производстве медицинских изделий, систему менеджмента качества в данной отрасли можно определить как организационную структуру, её функции, процедуры, процессы и ресурсы, необходимые для руководства и управления относительно качества медицинской продукции.

В статье отражены принципы системы менеджмента качества и процессы управления. Основное внимание уделено особенностям системы менеджмента качества медицинских изделий, в том числе особенностям системы менеджмента качества программного обеспечения, являющего медицинским изделием. Отмечены условия, при которых система менеджмента качества становится инструментом для обеспечения устойчивого развития организации и не представляется дополнительной нагрузкой, не имеющей необходимости. Представлены результаты опроса организаций, выпускающих медицинские программные изделия, связанные с опытом внедрения системы менеджмента качества, а также готовности к изменениям в организации.

Ключевые слова: система менеджмента качества; медицинское изделие; программное обеспечение; искусственный интеллект.

Как цитировать:

Заюнчковский С.Ю., Коновалов С.А., Зинченко В.В., Шарова Д.Е., Ахмад Е.С., Владзимирский А.В. Система менеджмента качества: инструмент развития организации или дополнительная нагрузка? // *Digital Diagnostics*. 2023. Т. 4, № 3. С. 439–447. DOI: https://doi.org/10.17816/DD514629

Рукопись получена: 27.06.2023 **Рукопись одобрена:** 06.07.2023 **Опубликована:** 30.08.2023

DOI: https://doi.org/10.17816/DD514629

Quality management system: A tool for the development of the organization or an additional burden?

Sergey Yu. Zayunchkovsky, Sergey A. Konovalov, Viktoria V. Zinchenko, Daria E. Sharova, Ekaterina S. Akhmad, Anton V. Vladzymyrskyy

Moscow Center for Diagnostics and Telemedicine, Moscow, Russian Federation

ABSTRACT

A quality management system constitutes one of the organization's management systems that provides for the selection of a set of processes in the organization's activities designed to ensure the stable quality of products and services provided.

The growth of global industrial production has underscored the need for the creation of such production and management systems. These systems are designed to ensure that enterprises remains prepared to meet the constantly changing consumer value of manufactured products in accordance with consumer requirements, as well as the satisfaction of consumers themselves. As a result, attention began to focus on the production processes implemented within the organization when creating products. Regarding the production of medical devices, a quality management system can be defined as an organizational structure encompassing its functions, procedures, processes, and resources necessary for the coordinated direction and management of a manufacturing organization with respect to the quality of medical products.

The article reflects the principles of the quality management system and management processes. Noteworthy emphasis is placed on the features of quality management systems for medical devices, including the features of the quality management system for software that is a medical device. Furthermore, the conditions under which the quality management system becomes a tool for ensuring the sustainable development of the organization are noted.

Keywords: quality management system; medical device; software; artificial intelligence.

To cite this article:

Zayunchkovsky SYu, Konovalov SA, Zinchenko VV, Sharova DE, Akhmad ES, Vladzymyrskyy AV. Quality management system: A tool for the development of the organization or an additional burden? *Digital Diagnostics.* 2023;4(3):439–447. DOI: https://doi.org/10.17816/DD514629

Received: 27.06.2023 **Accepted:** 06.07.2023 **Published:** 30.08.2023

DOI: https://doi.org/10.17816/DD514629

质量管理体系：组织发展的工具还是额外负担？

Sergey Yu. Zayunchkovsky, Sergey A. Konovalov, Viktoria V. Zinchenko, Daria E. Sharova, Ekaterina S. Akhmad, Anton V. Vladzymyrskyy

Moscow Center for Diagnostics and Telemedicine, Moscow, Russian Federation

简评

质量管理体系是组织的管理体系之一，它规定了组织活动中的一系列流程，旨在确保产品和服务的稳定质量。

随着全球工业生产的增长，有必要建立特殊的生产和管理系统，以确保企业能够根据消费者的要求随时满足制成品不断变化的客户价值，并使消费者本身感到满意。在这方面，人们开始关注组织内部在创造产品时实施的生产流程。就医疗器械生产而言，质量管理体系可定义为：与医疗产品质量有关的生产组织的协调领导和管理所需的组织结构、职能、程序、流程和资源。

该文章介绍质量管理体系的原则和管理流程。主要关注医疗器械质量管理体系的特殊性，包括作为医疗器械的软件质量管理体系的特殊性。本文指出质量管理体系成为确保组织可持续发展工具的条件。

关键词：质量管理体系；医疗器械；软件；人工智能。

引用本文：

Zayunchkovsky SYu, Konovalov SA, Zinchenko VV, Sharova DE, Akhmad ES, Vladzymyrskyy AV. 质量管理体系：组织发展的工具还是额外负担？ *Digital Diagnostics.* 2023;4(3):439–447. DOI: https://doi.org/10.17816/DD514629

收到：27.06.2023 **接受：**06.07.2023 **发布日期：**30.08.2023

INTRODUCTION

General applicability of quality management system principles

A quality management system (QMS) is one of the organization's management systems. A QMS identifies organizations' processes to ensure the consistent quality of products and services. A QMS is designed to improve these processes as a set of interrelated and interacting activities and develop a management style for an organization that involves managers, engineers, and technical as well as support personnel in improving product quality. Following the implementation of a QMS changes aimed to provide technological transparency of all types of activities. Such standards enable tracking of a product's whole life cycle in which the organization is involved, from the decision to develop a product to its final stage of disposal. Such an approach helps systematize an organization's activities, create conditions for the self-fulfillment of process participants, improve product quality, and become more competitive.

According to ISO 9001,[1] the scheme of QMS development is universal for any organization; hence, it is important to highlight special aspects of its activities and properly divide them into key processes.

Basic processes of a Russian organization

For a long time, corporate management in Russia was exclusively "functional." Such an approach was quite viable. It was mainly limited to delegating responsibility for individual functions in specific activity areas (design, production, supply, sales, business and infrastructure maintenance, and after-sales service) to the corresponding functions as well as their managers and employees. Simultaneously, the aim of such functional management (heads of services, departments, and higher-level units) was to ensure compliance of specific (highly specialized) functional activities with internal quality criteria, which were established by corporate standards [1]. However, the functional management approach failed as global industrial production developed. This required the development of production and management systems capable of ensuring both customer satisfaction through providing the highest consumer values and the organization's capacity to be prepared for constantly changing consumer value of their products in compliance with consumer requirements. Processes related to product development and manufacturing received special attention.

A QMS in the manufacturing of medical devices is defined as the organizational structure, functions, procedures, processes, and resources required for coordinated activities to manage the quality of healthcare products manufactured by an organization. A medical device QMS should ensure compliance of released medical devices with relevant general safety and effectiveness criteria, labeling, and technical as well as operational documentation requirements. The need to implement and comply with a QMS is not absolute in healthcare; not everyone must implement and maintain a QMS for healthcare products, but everyone has the right to do so.

A MEDICAL DEVICE QMS

A new trend is emerging to ensure the quality and safety of medical devices at all stages of their life cycle. Medical device regulators are shifting their focus from product design and development to the whole life cycle of a medical device, including steps from production to decommissioning. This approach is reflected in ISO 13485.[2]

Effective medical device life cycle management is crucial for ensuring end-user safety [2]. Therefore, in accordance with Regulation (EU) 2017/745 of the European Parliament and of the Council on Medical Devices [3], CE certification of medical devices is based on an assessment of procedures regulating product development and manufacturing. At one stage of medical device CE certification, the QMS should be confirmed to conform with ISO 13485.

Manufacturers of medical devices (except for Class 1 medical devices and nonsterile Class 2a medical devices due to potential harm to users) must implement a QMS depending on medical device class[3, 4] before submitting approval documents as part of medical device regulation in the Eurasian Economic Union. Figure 1 demonstrates a scheme of requirements for medical device QMS implementation based on potential harm to users. Suppose a manufacturer of medical devices has implemented a QMS in accordance with standards equivalent to ISO 13485. In that case, the QMS's compliance with such standards should be confirmed (certificate of compliance and audit report) to ensure compliance with Decision No. 106 of the Council of the Eurasian Economic Commission dated November 10, 2017, regarding processes and procedures for using a medical device QMS .[5]

---

[1] ISO 9001:2015 Quality management systems — —Requirements. This standard was last reviewed and confirmed in 2021. Therefore, this version remains valid. Link: https://www.iso.org/standard/62085.html.

[2] ISO 13485:2016 Medical devices. Quality management systems. Requirements for regulatory purposes. This standard was last reviewed and confirmed in 2020. Therefore this version remains current. Link: https://www.iso.org/standard/59752.html.

[3] Decree N 136 of the Government of the Russian Federation dated February 9, 2022 on approval of requirements for the implementation, maintenance and evaluation of the medical device quality management system depending on potential risk of their use. Link: https://base.garant.ru/403517950/.

[4] Decision No. 106 of the Council of the Eurasian Economic Commission dated November 10, 2017 on approval of requirements for implementation, maintenance and evaluation of a medical device quality management system depending on potential harm to users. Link: https://pharmvestnik.ru/documents/reshenie-soveta-evrazijskoj-ekonomicheskoj-komissii-ot-10-11-2017-g-106.html.

[5] Ibid.

DOI: https://doi.org/10.17816/DD514629

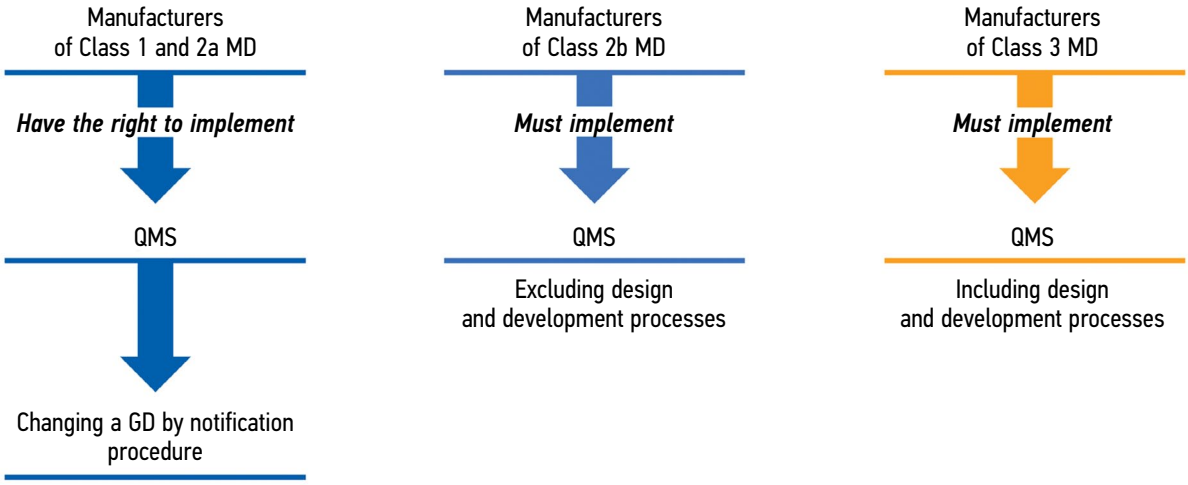

Fig. 1. Requirements for implementing a medical device quality management system depend on the potential risk of their use. GD, governing document; MD, medical devices; QMS, quality management system.

Special aspects of a medical device QMS

Special aspects of a medical device QMS are related to some requirements for products (medical devices) and their properties associated with such requirements. These properties should be distinct or require special attention compared with other types of industrial products. They are included in basic documents that govern the design, development, and distribution of medical devices. Medical device requirements include safety, effectiveness, and quality. A medical device QMS should ensure compliance with these requirements. In general, an organization must meet the following criteria (in accordance with ISO 13485):

- to identify current risks and risk situations
- to perform risk monitoring/analysis and explore parameters regularly
- to provide internal control of an organization's activities
- to ensure necessary adjustments to be made
- to improve a medical device QMS, including its components, and
- to develop supporting documentation and comply with other conditions specified in ISO 13485.

A medical device QMS should be designed to encourage compliance with the key requirement to ensure that the benefit outweighs possible adverse effects. Medical devices should be safe. Medical device effectiveness is another important QMS function. If the effectiveness of a medical device is not mandatory, there is no point in developing and manufacturing such a product. Quality is an umbrella term for a set of such properties and characteristics of a medical device that affect its ability to function as intended in accordance with the manufacturer's requirements.

Special attention should be given to QMS processes for evaluating the quality, effectiveness, and safety of medical devices, primarily performed as part of state registration, a procedure developed to ensure product market circulation. The deliverable is a marketing authorization, a document confirming medical device compliance with established requirements and medical device approval in Russia. A marketing authorization is mandatory for medical device circulation on the market. Therefore, state registration processes should be included in the overall QMS of an organization manufacturing medical devices. This is another important aspect of a Russian organization's QMS.

To summarize, a medical device QMS is primarily related to life cycle processes, and medical device circulation is an integral part of these processes.

Special aspects of medical device software QMS

Regarding medical device software, some additional aspects of a QMS that are relevant to the manufacturing process may be highlighted. In contrast to physical products, software manufacturing does not require assembly and manufacturing sites. However, manufacturing medical device software requires strict quality and safety control at all stages of the product life cycle.

Software, unlike physical products, may be constantly updated, requiring quality management, including design, performance, and risk reviews. Otherwise, product failure may lead to incorrect conclusions, potentially harming patient health. To prevent such situations, medical device software should be controlled at the design, development, risk management, and manufacturing stages. Corrective and preventive actions should be implemented in accordance with the QMS.

Moreover, security and privacy risks should be managed because many software systems rely on communication technologies and are vulnerable to cyber-attacks that could lead to failures or leaks of patient information. The Korea Ministry of Food and Drug Safety has published application

methods, cybersecurity cases, and cybersecurity risk management guidelines [4].

A software QMS should include design, development, testing, verification and validation, documentation, and personnel training. A QMS should be in place to ensure the software's safety, reliability, and performance. To ensure the safety and performance of their software, healthcare organizations must adhere to all aspects of their QMS.

Special characteristics of an artificial intelligence–based medical device software QMS: National standard

In general, an artificial intelligence (AI)–based medical device software QMS should adhere to ISO 13485 while considering special aspects of using AI technologies in healthcare.

Requirements for the development, testing, and operation of AI-based healthcare technologies should be unified and standardized by the Artificial Intelligence in Healthcare subcommittee of the Technical Artificial Intelligence Standards Committee (PK 01/TK 164). PK 01/TK 164 is based on the Center for Diagnostics and Telemedicine Technologies of the Moscow Healthcare Department [5]. As part of the PK 01/TK 164 activities, a series of national AI Systems in Clinical Medicine standards was developed.

GOST R 59921.8-2022 is one of these standards.[6] The document includes recommendations for interpreting all sections of GOST ISO 13485-2017, as well as cases, descriptions, and options that may be used by organizations in developing and implementing a QMS in compliance with these standards.

Therefore, when developing and implementing a QMS, manufacturers of AI technologies should consider the above aspects. Industry QMS requirements have changed from ISO 9001 to GOST R 59921.8; some requirements about special aspects of medical devices have been added or clarified, and guidelines for applying ISO 13485 to processes of ordering, supply, development, use, and maintenance of AI systems have been developed (Figure 2).

An AI-based software QMS and its impact on the competitiveness and potential of an organization

A QMS for AI technology directly impacts an organization's competitiveness and potential. Users will be more confident in a product, promoting an organization on the market if tasks are performed correctly, the safety and effectiveness of AI technologies are provided, and their risks are managed.

For this paper, a brief survey of AI technology manufacturers was conducted. Respondents were asked to answer questions on implementing a QMS that complied with ISO 13485. The list of questions is presented in Table 1. The survey included 10 AI technology manufacturers. The number of employees in the organizations surveyed ranged from 10 to 600 people. When asked about the QMS implementation, 60% of respondents answered positively. Of the remaining 40% of companies, 75% planned to develop and implement a QMS. Changes in business processes after QMS implementation were rated 3 to 9 points on a 10-point scale. It should be noted that the QMS implementation may encounter resistance from the part of the team; therefore, at the stage of QMS implementation, it is necessary to ensure that each team member understands the significance of this process. The level of team resistance to QMS implementation was 40%. All surveyed organizations with certified ISO 13485 QMS compliance used the services of a consulting company for QMS development as well as implementation and appointed a person responsible for QMS. When developing and implementing a QMS, 33% of surveyed companies used the national standard GOST R 59921.8-2022.

CONCLUSION

The main objective of a medical device QMS is to provide benefits without creating additional burdens on the organization during the life cycle. However, it is challenging to integrate a medical device QMS into the ongoing activities of an organization, especially if a medical device QMS is not mandatory. In this case, stimulating factors for ISO 13485 certification may include an organization's higher status as a tender participant, wider opportunities for supplying products outside of the Russian Federation, increased trust of end users, and improved internal business processes. A decision to integrate a medical device QMS should not be formal to simply obtain a certificate of compliance but instead, be driven by an organization's conscious internal requirements to use a medical device QMS as a sustainability tool.

Fig. 2. Development of industry requirements for an AI-based medical device quality management system.

[6] ГОСТ Р 59921.8-2022. Artificial Intelligence Systems in Clinical Medicine: national standard of the Russian Federation. Part 8. Guidelines for the application of GOST ISO 13485-2017 Link: https://docs.cntd.ru/document/1200193729.

Table 1. Survey of AI technology manufacturers on the availability, use, and implementation of a quality management system

No.	Question
1	Number of employees
2	Has your organization implemented a quality management system (QMS)?
3	If not, do you plan to develop and implement a QMS?
4	Do you have a certificate of QMS compliance with ISO 13485:2016 or GOST ISO 13485-2017?
5	Which certification system was used to obtain a certificate?
6	How much have your business processes changed after the QMS implementation? Rate on a scale of 0 to 10.
7	Rate your team's resistance to the QMS implementation on a scale of 0 to 10.
8	Did you use the services of a consulting company when developing and implementing a QMS?
9	Do you have a person responsible for QMS?
10	Did you use national standard GOST R 59921.8-2022 Artificial Intelligence Systems in Clinical Medicine? Part 8. Guidelines for application of GOST ISO 13485-2017 when developing and implementing a QMS?
11	Does your QMS comply with Decree No. 136 of the Government of the Russian Federation, dated February 9, 2022, on approval of requirements for implementing, maintaining, and evaluating the medical device QMS, depending on the potential risk of their use?
12	Does your QMS comply with Decision No. 106 of the Council of the Eurasian Economic Commission dated November 10, 2017, on approval of requirements for implementation, maintenance, and evaluation of a medical device quality management system depending on potential harm to users?

ADDITIONAL INFORMATION

Funding source. This article was prepared by a group of authors as a part of the research and development effort titled "Theoretical and methodological framework for digital transformation in radiology" (USIS No. 123031400118-0) in accordance with the Order No. 1196 by the Moscow Health Care Department dated December 21, 2022 "On approval of state assignments funded by means of allocations from the budget of the city of Moscow to the state budgetary (autonomous) institutions subordinate to the Moscow Health Care Department, for 2023 and the planned period of 2024 and 2025".

Competing interests. The authors declare that they have no competing interests.

Authors' contribution. All authors made a substantial contribution to the conception of the work, acquisition, analysis, interpretation of data for the work, drafting and revising the work, final approval of the version to be published and agree to be accountable for all aspects of the work. S.Yu. Zayunchkovsky — writing the manuscript, structuring and analyzing the obtained results, a bibliography; S.A. Konovalov — writing the manuscript, analyzing the survey results; V.V. Zinchenko — structuring and analyzing the obtained results, writing the manuscript; D.E. Sharova — generating a research hypothesis, developing a questionnaire; E.S. Ahmad — analyzing the obtained results, reviewing the manuscript; A.V. Vladzimirsky — reviewing the manuscript, the overall guidance.

REFERENCES

1. Mikhailov Yul. Process management in the quality management system of the enterprise. *Discourse*. 2017;(6):51–57. (In Russ).

2. Zinovieva EV, Sapunova AV, Ivanov IV. Safety of circulation of medical devices at all stages of their life cycle. *Public health*. 2022;2(3):16–24. (In Russ). doi: l0.21045/2782-1676-202l-2-3-16-24

3. Regulation (EU) 2017/745 of the European Parliament and of the Council of 5 April 2017 on medical devices, amending Directive 2001/83/EC, Regulation (EC) No 178/2002 and Regulation (EC) No 1223/2009 and repealing Council Directives 90/385/EEC and 93/42/EEC // Official J Eur Union. Available from: https://eur-lex.europa.eu/legal-content/EN/TXT/PDF/?uri=CELEX:32017R0745. Accessed: 15.07.2023.

4. Lim K, Heo TY, Yun J. Trends in the approval and quality management of artificial intelligence medical devices in the Republic of Korea. *Diagnostics (Basel)*. 2022;12(2):355. doi: 10.3390/diagnostics12020355

5. Gusev AV, Vladzimirsky AV, Sharova DE, et al. Development of research and development in the field of artificial intelligence technologies for healthcare in the Russian Federation: Results of 2021. *Digital Diagnostics*. 2022;3(3):178–194. (In Russ). doi: 10.17816/DD107367

СПИСОК ЛИТЕРАТУРЫ

1. Михайлов Ю.И. Управление процессами в системе менеджмента качества предприятия // Дискурс. 2017. № 6. С. 51–57.

2. Зиновьева Е.В., Сапунова А.В., Иванов И.В. Безопасность обращения медицинских изделий на всех этапах их жизненно-

го цикла // Общественное здоровье. 2022. Т. 2, № 3. С. 16–24. doi: l0.21045/2782-1676-202l-2-3-16-24

3. Regulation (EU) 2017/745 of the European Parliament and of the Council of 5 April 2017 on medical devices, amending Directive 2001/83/EC, Regulation (EC) No 178/2002 and Regulation (EC) No 1223/2009 and repealing Council Directives 90/385/EEC and 93/42/EEC // Official J Eur Union. Режим доступа: https://eur-lex.europa.eu/legal-content/EN/TXT/PDF/?uri=CELEX:32017R0745. Дата обращения: 15.07.2023.

4. Lim K., Heo T.Y., Yun J. Trends in the approval and quality management of artificial intelligence medical devices in the Republic of Korea // Diagnostics (Basel). 2022. Vol. 12, N 2. P. 355. doi: 10.3390/diagnostics12020355

5. Гусев А.В., Владзимирский А.В., Шарова Д.Е., и др. Развитие исследований и разработок в сфере технологий искусственного интеллекта для здравоохранения в Российской Федерации: итоги 2021 года // Digital Diagnostics. 2022. Т. 3, № 3. С. 178–194. doi: 10.17816/DD107367

AUTHORS' INFO

*** Viktoria V. Zinchenko;**
address: 24/1 Petrovka street, 127051 Moscow, Russia;
ORCID: 0000-0002-2307-725X;
eLibrary SPIN: 4188-0635;
e-mail: ZinchenkoVV1@zdrav.mos.ru

Sergey Yu. Zayunchkovskiy;
ORCID: 0009-0002-7463-7699;
e-mail: ZayunchkovskijSY@zdrav.mos.ru

Sergey A. Konovalov;
ORCID: 0009-0003-0011-3371;
e-mail: KonovalovSA4@zdrav.mos.ru

Daria E. Sharova;
ORCID: 0000-0001-5792-3912;
eLibrary SPIN: 1811-7595;
e-mail: SharovaDE@zdrav.mos.ru

Ekaterina S. Akhmad;
ORCID: 0000-0002-8235-9361;
eLibrary SPIN: 5891-4384;
e-mail AkhmadES@zdrav.mos.ru

Anton V. Vladzymyrskyy, MD, Dr. Sci. (Med.);
ORCID: 0000-0002-2990-7736;
eLibrary SPIN: 3602-7120;
e-mail: npcmr@zdrav.mos.ru

ОБ АВТОРАХ

*** Зинченко Виктория Валерьевна;**
адрес: Россия, 127051, Москва, ул. Петровка, д. 24, стр. 1;
ORCID: 0000-0002-2307-725X;
eLibrary SPIN: 4188-0635;
e-mail: ZinchenkoVV1@zdrav.mos.ru

Заюнчковский Сергей Юрьевич;
ORCID: 0009-0002-7463-7699;
e-mail: ZayunchkovskijSY@zdrav.mos.ru

Коновалов Сергей Анатольевич;
ORCID: 0009-0003-0011-3371;
e-mail: KonovalovSA4@zdrav.mos.ru

Шарова Дарья Евгеньевна;
ORCID: 0000-0001-5792-3912;
eLibrary SPIN: 1811-7595;
e-mail: SharovaDE@zdrav.mos.ru

Ахмад Екатерина Сергеевна;
ORCID: 0000-0002-8235-9361;
eLibrary SPIN: 5891-4384;
e-mail AkhmadES@zdrav.mos.ru

Владзимирский Антон Вячеславович, д-р мед. наук;
ORCID: 0000-0002-2990-7736;
eLibrary SPIN: 3602-7120;
e-mail: npcmr@zdrav.mos.ru

* Corresponding author / Автор, ответственный за переписку

DOI: https://doi.org/10.17816/DD569112

Ошибка в статье «Сравнение измерения линейного размера и объёма лёгочных очагов по данным скрининга рака лёгких с помощью низкодозной компьютерной томографии» (doi: 10.17816/DD117481)

М.М. Сучилова[1], И.А. Блохин[1], О.О. Алешина[2], В.А. Гомболевский[3], Р.В. Решетников[1], В.Ю. Босин[1], О.В. Омелянская[1], А.В. Владзимирский[1, 4]

[1] Научно-практический клинический центр диагностики и телемедицинских технологий, Москва, Российская Федерация;
[2] Государственная клиническая больница № 13, Москва, Российская Федерация;
[3] Институт искусственного интеллекта, Москва, Российская Федерация;
[4] Первый Московский государственный медицинский университет имени И.М. Сеченова (Сеченовский Университет), Москва, Российская Федерация

В статье «Сравнение измерения линейного размера и объёма лёгочных очагов по данным скрининга рака лёгких с помощью низкодозной компьютерной томографии», опубликованной в Т. 4, № 1 журнала Digital Diagnostics за 2023 год (doi: 10.17816/DD117481), была допущена ошибка в указании источника финансирования проведенного исследования. По просьбе авторского коллектива ошибка в указании источника финансирования была устранена, исходная версия опубликованной статьи заменена издательством на исправленную, информация на сайте также была скорректирована. Верный текст раздела об источниках финансирования проведенного исследования: Данная статья подготовлена авторским коллективом в рамках научно-исследовательской работы (№ ЕГИСУ: 123031400009-1) в соответствии с Приказом Департамента здравоохранения города Москвы от 21.12.2022 г. № 1196.

Авторы и издатель приносят извинения читателям за допущенную ошибку и выражают уверенность в том, что эта ошибка не могла существенно повлиять на восприятие и интерпретацию результатов исследования, описываемого в тексте произведения.

Ключевые слова: ошибка, erratum, corrigendum, компьютерная томография; скрининг рака лёгкого; лёгочные узлы.

Как цитировать:
Сучилова М.М., Блохин И.А., Алешина О.О., Гомболевский В.А., Решетников Р.В., Босин В.Ю., Омелянская О.В., Владзимирский А.В. Ошибка в статье «Сравнение измерения линейного размера и объёма лёгочных очагов по данным скрининга рака лёгких с помощью низкодозной компьютерной томографии» (doi: 10.17816/DD117481) // *Digital Diagnostics*. 2023. Т. 4, № 3. С. 448–450. DOI: https://doi.org/10.17816/DD569112

Рукопись получена: 06.09.2023 **Рукопись одобрена:** 11.09.2023 **Опубликована:** 12.09.2023

DOI: https://doi.org/10.17816/DD569112

Erratum in “Volumetry versus linear diameter lung nodule measurement: an ultra-low-dose computed tomography lung cancer screening study” (doi: 10.17816/DD117481)

Maria M. Suchilova[1], Ivan A. Blokhin[1], Olga O. Aleshina[2], Victor A. Gombolevskiy[3], Roman V. Reshetnikov[1], Viktor Yu. Bosin[1], Olga V. Omelyanskaya[1], Anton V. Vladzymyrskyy[1, 4]

[1] Moscow Center for Diagnostics and Telemedicine, Moscow, Russian Federation;
[2] City Clinical Hospital No 13, Moscow, Russian Federation;
[3] Artificial Intelligence Research Institute, Moscow, Russian Federation;
[4] The First Sechenov Moscow State Medical University (Sechenov University), Moscow, Russian Federation

In the article "Volumetry versus linear diameter lung nodule measurement: an ultra-low-dose computed tomography lung cancer screening study" published in Digital Diagnostics journal Volume 4 Issue 1 in 2023 (doi: 10.17816/DD117481) contained an error in the paragraph with data of funding sources for the study.
At the request of the authors' team, the error was eliminated, the original version of the published article and the information on the journal's site was replaced with the corrected one.
Correct text of the changed: This paper was prepared by a group of authors as part of the research work (USIS No. 123031400009-1) in accordance with the Order issued by the Moscow Health Care Department No. 1196 dated December 21, 2022.
The authors and the publisher apologize to readers for the published error and express their confidence that this mistake could not significantly affect the perception and interpretation of the results of the study described in the text of the article.

Keywords: erratum; tomography X-Ray compute; early detection of cancer; lung neoplasms.

To cite this article:
Suchilova MM, Blokhin IA, Aleshina OO, Gombolevskiy VA, Reshetnikov RV, Bosin VYu, Omelyanskaya OV, Vladzymyrskyy AV. Erratum in “Volumetry versus linear diameter lung nodule measurement: an ultra-low-dose computed tomography lung cancer screening study” (doi: 10.17816/DD117481). *Digital Diagnostics.* 2023;4(3):448–450. DOI: https://doi.org/10.17816/DD569112

Received: 06.09.2023 **Accepted:** 11.09.2023 **Published:** 12.09.2023

AUTHORS' INFO

*** Maria M. Suchilova,** MD;
address: 24 Bld. 1, Petrovka st., 127051, Moscow, Russia;
ORCID: 0000-0003-1117-0294;
eLibrary SPIN: 4922-1894;
e-mail: m.suchilova@npcmr.ru

Ivan A. Blokhin, MD;
ORCID: 0000-0002-2681-9378;
eLibrary SPIN: 3306-1387;
e-mail: i.blokhin@npcmr.ru

Olga O. Aleshina, MD;
ORCID: 0000-0001-9924-0204;
eLibrary SPIN: 6004-2422;
e-mail: olya.aleshina.tula@gmail.com

Victor A. Gombolevskiy, MD, Cand. Sci. (Med);
ORCID: 0000-0003-1816-1315;
eLibrary SPIN: 6810-3279;
e-mail: gombolevskiy@npcmr.ru

Roman V. Reshetnikov, Cand. Sci. (Phys.-Math.);
ORCID: 0000-0002-9661-0254;
eLibrary SPIN: 8592-0558;
e-mail: reshetnikov@fbb.msu.ru

Viktor Yu. Bosin, MD, Dr. Sci. (Med.);
ORCID: 0000-0002-4619-2744;
eLibrary SPIN: 3380-7889;
e-mail: bosin@npcmr.ru

Olga V. Omelyanskaya;
ORCID: 0000-0002-0245-4431;
eLibrary SPIN: 8948-6152;
e-mail: o.omelyanskaya@npcmr.ru

Anton V. Vladzymyrskyy, MD, Dr. Sci (Med.);
ORCID: 0000-0002-2990-7736;
eLibrary SPIN: 3602-7120;
e-mail: a.vladzimirskiy@npcmr.ru

ОБ АВТОРАХ

*** Сучилова Мария Максимовна;**
адрес: Россия, 127051, Москва, ул. Петровка, д. 24, стр. 1;
ORCID: 0000-0003-1117-0294;
eLibrary SPIN: 4922-1894;
e-mail: m.suchilova@npcmr.ru

Блохин Иван Андреевич;
ORCID: 0000-0002-2681-9378;
eLibrary SPIN: 3306-1387;
e-mail: i.blokhin@npcmr.ru

Алёшина Ольга Олеговна;
ORCID: 0000-0001-9924-0204;
eLibrary SPIN: 6004-2422;
e-mail: olya.aleshina.tula@gmail.com

Гомболевский Виктор Александрович, канд. мед. наук;
ORCID: 0000-0003-1816-1315;
eLibrary SPIN: 6810-3279;
e-mail: gombolevskiy@npcmr.ru

Решетников Роман Владимирович, канд. физ.-мат. наук;
ORCID: 0000-0002-9661-0254;
eLibrary SPIN: 8592-0558;
e-mail: reshetnikov@fbb.msu.ru

Босин Виктор Юрьевич, докт. мед. наук;
ORCID: 0000-0002-4619-2744;
eLibrary SPIN: 3380-7889;
e-mail: bosin@npcmr.ru

Омелянская Ольга Васильевна;
ORCID: 0000-0002-0245-4431;
eLibrary SPIN: 8948-6152;
e-mail: o.omelyanskaya@npcmr.ru

Владзимирский Антон Вячеславович, докт. мед. наук;
ORCID: 0000-0002-2990-7736;
eLibrary SPIN: 3602-7120;
e-mail: a.vladzimirskiy@npcmr.ru

* Corresponding author / Автор, ответственный за переписку